

Hyphenated Analytical Techniques for Studying the Speciation and Fate of Contaminants and Nanoparticles in Waste Treatment and Bioenergy Processes

Thèse N° 7184

Présentée le 22 février 2019

**à la Faculté de l'environnement naturel, architectural et construit
Groupe Ludwig
Programme doctoral en génie civil et environnement**

pour l'obtention du grade de Docteur ès Sciences

par

Debora FOPPIANO

Acceptée sur proposition du jury

**Prof. A. J. Wüest, président du jury
Prof. C. Ludwig, Dr M. Tarik, directeurs de thèse
Prof. J. Wang, rapporteur
Dr P. Krystek, rapporteuse
Prof. S. Takahama, rapporteur**

2019

Acknowledgements

At the end of this very long journey, it is almost a duty but it is most of all my pleasure to thank all the people that somehow have contributed to this work. We are always the result of the people we have met in our lives, with no exception for these last four years. I apologize in advance if some names are not reported here, I am sure that I will remember all of you. It has been an amazing adventure absolutely worth to start.

First of all, I would like to thank my professor Christian Ludwig and my thesis co-director Dr. Mohamed Tarik for giving me the opportunity of joining the CPM group as a doctoral student.

Dear Chrigu, you gave me the chance to start a unique experience in my life, the chance to discover. I have worked hard and pushed my limits; I have tried to do my best to repay back your expectations. Thank you for trusting me and for the flexibility and freedom you gave me in shaping this project and my schedule, these are the main reasons why I have learned so much, not only about science but also about myself. I know now how to handle a stressful moment and how to process my emotions in a more rational way, as well as how to make my voice heard without being disrespectful. I have challenged myself on so many aspects; I have grown up. Nothing, not even one of those things, would have been possible without that initial leap of faith. Thank you.

Dear Mohamed, your professionalism and respect for your co-workers will always set a standard; you have been an example for me since the beginning. I have tried to learn from you as much as possible. We all know how important it is to find a like-minded person, especially when you work so closely; I have been very lucky with you. It was never difficult to understand each other and it felt every day like an enriching experience. I had my set-back during this project but you were always there to support me, without being intrusive but showing me the way to set the right path by myself. If now I can feel self-confident and able to proceed alone, it is also thanks to what you have taught me along the way. It has been a pleasure to work with you.

I am also very grateful to Prof. Alfred Johnny Wüest (EPFL/EAWAG), Prof. Jing Wang (ETHZ/EMPA), Prof. Satoshi Takahama (EPFL) and Dr. Petra Krystek (TNO and visiting fellow at University of Amsterdam) for agreeing to be members of my PhD examination committee. I have highly appreciated your feedback on the thesis and your questions, as well as the very respectful attitude during the exam, resulting in the perfect closure for this very nice experience.

I would like to acknowledge all the co-authors in our publications that made this work possible with their support, in particular, Elisabeth Müller, Adrian Hess, Serge Biollaz, Jörg Schneebeili, and Adelaide Calbry- Muzyka.

My gratitude goes also to all the people of the CPM group, Ajay Patil, Agnese Carino, Florentina Maxim, Marica Giordano, Reza Andalibi, Frank Pilger, Bhavish Patel, Rudolf Struis, Andrea Testino, Albert Schuler, Nicole Hippenmeyer, Silvia Vita, Carla Pausta, Annalise Annoscia and Sonya Barzgar, for their support, useful comments, and for those pearls of wisdom during the coffee breaks (Ajay in particular, the book is on the way).

Over these years, it has been extremely helpful the technical support received from other members of our laboratory (LBK, The Bioenergy and Catalysis Laboratory) and co-workers here at PSI. I would like to thank in particular, Erich De Boni, Jörg Schneebeil, Alwin Frei, Peter Hottinger, Marcel Hottiger (for building the particle collection cell) and Albert Schuler (for taking care of the initial installation and calibration of the TGA). Special thanks also to all the rest of the laboratory members for the nice excursions and time spent together. Dear Gisela, I have a special place for you in my memories. I would like to thank you for your smile, for your calm, for the incredible support in the administrative requests in which we too often get lost, and for your delicious cakes.

My sincere gratitude goes to my friends who have been like a big family here in Switzerland, I want to thank you all for the beautiful things we have shared. You have made this time unforgettable.

Dear Ilona, you have been my closest friend since my arrival, you have never left me even in my darkest moments and you have enjoyed with me the happiest too, it is not ordinary and I am well aware of how lucky I am. I wish us a lot of travels around the world.

Dear Flori and Marica, you were my first strong core here and we were there for each other at the most important turning point of our lives. I wish all your dreams will come true, also for you Angelo.

Dear “Abuelas” (Daniela, Marc, Vicky, Irene, Simon, Pablito, Samy, Franky) you have adopted me and together with the rest of the Franz-family (Joanna, Anne, Valentyn, Mike, Chris) you have organized the most awesome parties, Catan days, barbecues, brunches and so many other things in these years. I’m going to miss you all. Let’s keep alive our habit of one travel together per year (Italy is waiting for you this summer!).

I also feel grateful for all the new people I met along the way, thank you for being there to celebrate, to laugh, to dance, to share with me hiking and camping activities, beers and dinners. Among them, I would like to thank my former flatmates (Michele and Laura), the “Spanish mafia” (Henar, Pablo, Laurita y su hija Namrata, Marina, and Paula), all the “Mammoth Hunters” (Jan among the recent members, plus Dario, Muriel and Mateusz as invited guest), my colleagues in the corridor (especially Laura and Marta for the good mood they always bring along), the “best groupie ever” (Damaris and Paola), the “Germans” (Christoph, Paul, Max, and Fabian), and Andrea (Caro Muolo, pensavi che mi sarei dimenticata, e invece no!! Quante risate che ci aspettano ancora!).

Dear PSIchedelics, Peter, Patryk, Sierra, Florian, Makis, Marc, Pablito, Samy, Mateusz, Bhavish, Eric, Joe, Jing, and Laso, it has been a pleasure to sing with you. Most importantly, we always had so much fun. My gratitude also goes to the Jam Addicts (Micha, Tomaz, Maxime, Arthur) for including me in part of their last show.

My dear Italian friends, grazie per essermi rimasti vicino nonostante la lontananza e per aver trovato il modo di vederci anche se solo qualche volta all'anno (Federica, Francesca, Martina, Serena, Alice, Alby, Sere, Marti). A te Agne in particolare, per avermi segnalato questa posizione...te ne sarò sempre grata, mi ha cambiato la vita.

Saretta, che dire, mia cara compagna di avventure, te la sei vissuta con me questa Svizzera. Sei quella che più di tutti è stata l'anello di congiunzione tra i miei due mondi, è stato bellissimo averti qui e farti conoscere tutti i miei nuovi amici... è stato come se pezzi di un puzzle trovassero il loro posto da soli. Grazie di tutto. Come per Ilona, ci auguro una miriade di altri viaggi insieme (Cuba nel cuore), come ben sai il miglior regalo di sempre.

My biggest gratitude goes to my family, without them and their love I would have never pushed myself so far away, you were the first believing in me and encouraging me to start this new chapter of my life.

Alla mia mamma, per la sua forza incredibile, per aver combattuto e non essersi mai arresa contro un male che non puoi controllare, sei il pilastro della nostra famiglia.

A mia sorella Marilena e mio cognato Fabio, per esserci stati anche quando io non potevo, senza di voi forse non avrei mai finito questo dottorato. Ho sempre saputo di lasciarli in ottime mani.

Al mio papa, per quel rapporto tutto speciale che abbiamo solo noi due, quanto mi sono mancate le nostre scampagnate insieme...lo faremo questo cammino Gio'!

Al mio nipotino Alessio, per avermi rubato il cuore e averlo riempito di una gioia immensa. Il tuo amore è la medicina migliore per risentirmi subito a casa, anche quando non sono più tanto sicura di dove sia veramente "casa".

A tutto il resto della mia allargata e bellissima famiglia, zii, cugini, e nonni, è sempre bello trovare il modo di vedersi e stare insieme. Grazie di tutto.

Dear Panamanian family, muchas gracias por todo el cariño, el amor y la alegría que siempre compartimos en la distancia tambien. De verdad me siento parte de vuestra linda familia y siempre los tengo en mis pensamientos. Rosa, tu sabes, no pude encontrar suegrita mejor que tú, porque nos unes este amor tan grande por él pero tambien la payasada.

Last but not least....

...dear Eibar, this experience would have not been the same without you. You were there always for all the beautiful and for all the difficult things. You never stopped believing in me, also when I could not. Little by little, your positive attitude has made me believe that I could do everything. You know that this achievement is also yours. It is very difficult to describe in words what we are to each other, but you know how I feel... you are my home, wherever we will be. Thank you for all the life waiting for us.

Villigen PSI, February 2019

Debora

Abstract

The widespread use of nanoparticles (NPs) and other potentially ecotoxic chemical compounds to enhance the quality of consumer products has raised concern about their fate in the environment. Indeed, those products have to be ultimately disposed of and along with them also NPs and contaminants could end up in landfills or in facilities where waste and nano-waste, as well as biomass products, are stored and/or treated. Among the possible pathways involving their release in the environment, this thesis' focus is in particular on gaseous emissions during two main applications, namely waste treatment and bioenergy generation. In this frame, the effect of contaminants is considered not only in terms of their toxicity but also in terms of their effect on energy efficiency or potential damages caused to the facilities along the process chain. For this purpose, new online and offline methods were developed by using hyphenated analytical techniques to achieve complementary and superior power of investigation.

Firstly, the speciation of siloxane compounds were studied during bio-methane production from manure and agricultural waste. The samples were collected using a liquid quench (LQ) sampling system that concentrates condensable and non-condensable compounds in a liquid solvent in continuous contact with the gas probed, for an improved time resolution. The offline investigation required a complete method development for the combination of a separation technique, such as gas chromatography (GC), and detectors able to provide chemical information. The novelty was represented by the simultaneous use of GC with a flame ionization detector (FID) and inductively coupled plasma mass spectrometry (ICP-MS), which could fulfill the requirements of recent regulations for the specific application, with lower detection limits compared to existing methods.

Secondly, the fate of zinc oxide (ZnO) NPs were investigated during the combustion of impregnated wood, as a model of nano-waste. ZnO was specifically considered because of its use in paints and waterproofing agents. The potential release of NPs during nano-waste treatment was investigated with an online method that combines an RDD (rotating disk diluter) used as conditioning and dilution unit, an SMPS (scanning mobility particle sizer) providing the particle size distribution and ICP-MS used as a multi-elemental analytical technique. An initial assessment of the performances of the RDD-SMPS-ICP-MS was required, to correct some major assumptions used in the SMPS data treatment. The technique was successfully applied even to heterogeneous matrices. The particular capability of performing online sampling and simultaneous size-resolved and elemental analysis on the off-gases produced during wood combustion was providing the needed insights to verify the predicted mechanism of reduction and further re-oxidation of ZnO nano-objects. Thanks to the calibration strategy coupling a TGA (thermogravimetric analyzer) with RDD-ICP-MS, a successful determination of their concentration was also possible.

In conclusion, the development of specific hyphenated techniques was proven to be crucial to improve the capabilities of the already existent state-of-the-art methods and to develop new ones that could give more insight on the two main scientific questions that were the driving force of this thesis.

Keywords

Nanoparticles, nano-objects, nano-waste, contaminants, hyphenated analytical techniques, waste treatment, bioenergy processes, wood combustion, biogas, siloxanes, ZnO NPs, GC-ICP-MS/FID, RDD-SMPS-ICP-MS, TGA, speciation analysis, size-resolved measurement.

Riassunto

L'uso sempre più diffuso di nanoparticelle (NP) e di altri composti chimici potenzialmente ecotossici per migliorare la qualità di prodotti di consumo ha suscitato preoccupazione in particolar modo riguardo il loro rilascio nell'ambiente. Una volta terminato il loro uso, questi prodotti tendono a finire in discariche o in strutture dove i rifiuti e i nano-rifiuti, così come i residui di biomasse, vengono immagazzinati e/o trattati. Tra le varie possibilità di rilascio e diffusione di agenti inquinanti a livello ambientale, questa tesi si concentra in particolare sulle emissioni gassose durante due processi energetici, ossia il trattamento dei rifiuti e la generazione di energia dall'uso di biomasse. In questo contesto, l'effetto dei contaminanti è considerato non solo in termini di tossicità ma anche in termini di efficienza energetica o dei potenziali danni causati alla struttura lungo la catena di processo. Per questo motivo, si è reso necessario lo sviluppo di nuovi metodi diretti ("online") e indiretti ("offline") in cui tecniche analitiche accoppiate vengono utilizzate per ottenere informazioni complementari e un superiore potere investigativo.

In primo luogo, la speciazione di silossani è stata studiata durante la produzione di biometano da letame e rifiuti agricoli. I campioni sono stati raccolti utilizzando un sistema di campionamento di liquido di raffreddamento (LQ) in cui i composti condensabili e non condensabili vengono concentrati in un solvente liquido in contatto continuo con il gas campionato, per una migliore risoluzione temporale. I campioni vengono così analizzati in un secondo tempo per mezzo di un metodo "offline" che combina una tecnica di separazione, come la gascromatografia (GC), a rivelatori in grado di fornire informazioni chimiche. L'innovazione in questo caso è rappresentata da un completo sviluppo del metodo nonché dall'uso simultaneo di GC con un rivelatore a ionizzazione di fiamma (FID) e spettrometria di massa al plasma accoppiato induttivamente (ICP-MS), quest'ultimo in grado di soddisfare i requisiti delle recenti normative europee, con limiti di rilevazione inferiori rispetto a quelli di metodi esistenti.

In secondo luogo, l'emissione NP di ossido di zinco (ZnO) è stato studiato durante la combustione di legno trattato con NP, come modello di "nano-rifiuto". ZnO è stato specificamente considerato a causa del suo uso in vernici e agenti impermeabilizzanti. Il potenziale rilascio di NP durante il trattamento di "nano-rifiuti" è stato studiato con un metodo "online" che combina un RDD (Rotating Disk Diluter) usato come unità di condizionamento e diluizione, un SMPS (Scanning Mobility Particle Sizer) che fornisce la distribuzione delle dimensioni delle particelle e ICP-MS utilizzato come tecnica analitica multi-elementare. In seguito ad una valutazione iniziale delle prestazioni del RDD-SMPS-ICP-MS, resa necessaria da alcune delle principali ipotesi utilizzate nel trattamento dei dati, questa tecnica accoppiata è stata applicata con successo anche a matrici eterogenee. La particolare capacità di eseguire il campionamento "online" e l'analisi simultanea delle

dimensioni e degli elementi sulle emissioni prodotte durante la combustione del legno ha fornito le informazioni necessarie per verificare il meccanismo previsto di riduzione e ulteriore riossidazione di nano-oggetti di ZnO. Grazie ad una particolare strategia di calibrazione per RDD-ICP-MS, ottenuta accoppiando ulteriormente un TGA (analizzatore termo-gravimetrico), è stato anche possibile determinare con successo anche la loro concentrazione.

In conclusione, lo sviluppo di specifiche tecniche accoppiate è risultato cruciale per migliorare le capacità di metodi avanzati già esistenti e per svilupparne di nuovi in grado di fornire maggiori informazioni sulle due principali questioni scientifiche alla base di questa tesi.

Parole chiave

Nanoparticelle, nano-oggetti, “nano-rifiuti”, contaminanti, tecniche analitiche accoppiate, trattamento dei rifiuti, processi bioenergetici, combustione del legno, biogas, silossani, ZnO NPs, GC-ICP-MS / FID, RDD-SMPS-ICP-MS, TGA, analisi di speciazione, misura con alto potere di risoluzione.

Contents

Acknowledgements	iii
Abstract	vi
Riassunto	viii
Glossary	xv
Chapter 1 Introduction	1
1.1 Motivation	2
1.1.1 Waste to energy	2
1.1.2 Valorization of biomass with high calorific value	3
1.1.3 Valorization of biomass with low calorific value	8
1.2 Goals and scope of the thesis.....	10
1.2.1 NPs emission in combustion processes: on-line characterization	11
1.2.2 Method development for the analysis of siloxanes in biogas	14
1.3 Structure of the thesis.....	14
Chapter 2 Methods and experimental.....	17
2.1 Instruments.....	18
2.1.1 Aerosol sources.....	18
2.1.2 Conditioning and sampling unit.....	20
2.1.3 Characterization techniques	22
2.2 Hyphenated techniques for the different applications.....	23
2.2.1 GC-ICP-MS/FID	23
2.2.2 RDD-SMPS-ICP-MS	25
2.2.3 Different aerosol sources coupled with RDD-SMPS-ICP-MS	29
2.3 Materials.....	32

2.3.1	Speciation study with GC-ICP-MS/FID	32
2.3.2	Preliminary studies with RDD-SMPS-ICP-MS	33
2.3.3	RDD-SMPS-ICP-MS calibration strategy and resolving power in heterogeneous matrices.....	33
2.3.4	Combustion experiments	34
2.4	Additional off-line characterization techniques.....	34
2.4.1	Nanozetasizer	34
2.4.2	X-ray disc centrifuge	35
2.4.3	Scanning Electron Microscopy (SEM) and Transmission Electron Microscopy (TEM).....	35
Chapter 3	Speciation analysis with GC-ICP-MS/FID of siloxane compounds in biogas	39
3.1	Experimental and Results.....	40
3.1.1	Method development for the speciation analysis of siloxanes.....	40
3.1.2	Simultaneous speciation analysis using GC-ICP-MS/FID.....	47
3.1.3	Additional characterization of the biogas samples	49
Chapter 4	Preliminary studies with RDD-SMPS-ICP-MS.....	51
4.1	Abstract.....	52
4.2	Experimental and results.....	52
4.2.1	NaCl solution	52
4.2.2	ZnO suspension	53
4.2.3	Powders thermal treatment.....	57
Chapter 5	RDD-SMPS-ICP-MS calibration strategy and resolving power for heterogeneous matrices.....	61
5.1	Experimental section	62
5.1.1	Instrumentation.....	62
5.1.2	Calibration experiment with ZnCl ₂ powder	63
5.1.3	Calibration experiment with CdCl ₂ powder	64
5.1.4	ZnCl ₂ particle analysis	65
5.1.5	Mixture of different metal chlorides particles analysis	65
5.1.6	TEM analysis: experimental procedure	66
5.1.7	Data evaluation.....	66

5.2	Results and discussion	68
5.2.1	ICP-MS calibration	68
5.2.2	SMPS and ICP-MS data comparison	69
5.2.3	Mixture of different metal chlorides particles analysis	72
Chapter 6	Emissions of secondary formed nano-objects from the combustion of	
	impregnated wood.	75
6.1	Experimental section	76
6.1.1	Instrumental Arrangement	76
6.1.2	Temperature program of the lab-scale incinerator.	77
6.1.3	Size-Selected Particles Collection and Sample Preparation for TEM.....	78
6.2	Results and discussion	78
6.2.1	ZnO injected particles during sawdust thermal treatment.....	78
6.2.2	ZnO impregnated sawdust thermal treatment.	81
6.2.3	ZnO impregnated sawdust incineration.....	83
6.2.4	ZnO nano-object from impregnated wood combustion: estimation of Zn content in emissions.	86
6.2.5	Wood fly ashes.	87
Chapter 7	Concluding remarks and outlook	89
7.1	Speciation of siloxanes in biogas production process	90
7.1.1	Outlook	91
7.2	Fate of NPs during combustion of impregnated wood, used as a model nano- waste	91
7.2.1	Outlook	92
7.3	Final remarks	93
Bibliography	95
Appendix A	Additional data sets	109
A.1	Siloxanes in biogas.....	109
A.1.1	Stock and standard solution concentrations.....	109
A.1.2	7700x ICP-MS (Agilent Technologies) additional operating conditions.....	110
A.1.3	D5 stock solutions and calibration standards for gas composition optimization in ORS.....	110

A.1.4 GC-ICP-MS figures of merit when only one column is connected to the GC inlet ...	110
A.2 Preliminary studies with RDD-SMPS-ICP-MS	111
A.2.1 Zinc oxide nanopowder characterization	111
A.2.2 ZnO suspension characterization.....	112
A.3 RDD-SMPS-ICP-MS calibration strategy and resolving power for heterogenous matrices	113
A.3.1 TGA temperature program during ZnCl ₂ calibration experiment.....	113
A.3.2 HSC thermochemical calculation on CdCl ₂	113
A.3.3 TGA temperature program during CdCl ₂ calibration experiment	114
A.3.4 TGA temperature program during metal oxides and CaCl ₂ ·2H ₂ O experiments.....	114
A.3.5 CdCl ₂ calibration curve.....	115
A.3.6 Reproducibility of analysis for ZnO and CaCl ₂ ·2H ₂ O experiment.....	115
A.3.7 TEM analysis on Mixed oxide powders and CaCl ₂ ·2H ₂ O experiment	115
A.4 Emissions of secondary formed nano-objects from the combustion of impregnated wood.	116
A.4.1 Sawdust multi-element analysis in ICP-MS	116
A.4.2 ZnO impregnated sawdust multi-element analysis in ICP-MS.....	117
A.4.3 Efficiency of sawdust impregnation with ZnO nanopowder	117
A.4.4 Thermochemical calculations	118
Appendix B Co-authorship	119
List of figures	121
List of tables	128
List of publications	130
Curriculum vitae	131

Glossary

AED atomic emission detector

AG aerosol generator

AMS aerosol mass spectrometer

APC air pollution control system

APS aerodynamic particle sizer,

BIOSWEET “Biomass for Swiss Energy future”

CI condensation interface

CPC condensation particle counter

CPM Chemical Processes and Materials group

CV-AAS cold vapour atomic absorption spectroscopy

DLS dynamic light scattering

DMA differential mobility analyzer

DSF dynamic shape factor

ECD electron-capture detector

ECHA European Chemical Agency

EDXS energy dispersive X-ray spectroscopy

ELPI electrical low-pressure impactor

EMPIR European Metrology Program for Innovation and Research

ENPs engineered nanoparticles

EURAMET European Association of National Metrology Institutes

FID flame ionization detector

FMPS fast mobility particle sizer

FT-IR Fourier Transform Infrared spectroscopy

GC gas chromatography

GC-MS gas chromatography mass spectrometry

GCV gross calorific value

HEPA high-efficiency particulate air filter

HR-AMS high-resolution aerosol mass spectrometry

HRLPI high-resolution low-pressure cascade impactor

HR-TOF-AMS high-resolution time-of-flight aerosol mass spectrometry

HSC thermochemical calculation software (Outotech)

ICP-MS inductively coupled plasma mass spectrometry

ICP-OES inductively coupled plasma optical emission spectrometry

ISO International Organisation for Standardisation

LOD limit of detection

LOQ limit of quantification

LQ liquid quench sampling system

MFC mass flow controller

NO nano-objects

NPs nanoparticles

PAA poly acrylic acid

PID photoionization detector

PIXE proton-induced X-ray emission

PM particulate matter

POA primary organic aerosols

PSD particle size distributions

PSD_n number-weighted PSD of classified aerosol

PSD_v volume-weighted PSD

PSI Paul Scherrer Institut

PTR-MS proton transfer reaction mass spectrometer

PTR-ToF-MS proton transfer reaction time of flight mass spectrometer

RDD rotating disk diluter

REACH Registration, Evaluation, and Authorisation of Chemicals

SCCER Swiss Competence Centers for Energy Research

SCR selective catalytic reduction technology

SEM Scanning Electron Microscopy

SMPS scanning mobility particle sizer

SOFCs solid oxide fuel cells

SP-AMS soot particle aerosol mass spectrometry

SPI-TOF-AMS single photon ionization time-of-flight aerosol mass spectrometry

TCD thermal conductivity detector

TCP Thermochemical Processes group

TEM transmission electron microscopy

TGA thermogravimetric analyzer

VOC volatile organic compounds

WIP waste incinerator plant

XRF x-ray fluorescence

Chapter 1 Introduction

This doctoral thesis combines aspects of analytical chemistry and environmental engineering for energy applications, in particular for Waste and Bioenergy Technology development. All the activities were developed in the facilities of the Chemical Processes and Materials (CPM) group at Paul Scherrer Institut (PSI). The general subject of the research group revolves around sustainable resources management but the main contribution regards the development of new materials, the fate of valuable or potentially harmful materials in the environment, and the recovery and the reuse of waste.

The **motivation** of this work is summarized in section 1.1, where the waste to energy concept is explained as well as the different processes applied for the valorization of biomass. Waste incinerators and biogas production plants were particularly considered as two examples of technologies where still a gap remained in terms of analytical solutions to understand the fate of nanoparticles emissions and the presence of contaminants throughout the process.

In sections 1.2 (**Goal and Scope**), the state-of-the-art characterization methods for those applications are introduced as well as the concept of coupling of different instruments, so called hyphenated techniques, is considered to develop new methods or to improve the performance of already existent methods to study the speciation and fate of nanoparticles and contaminants during waste treatment and bioenergy processes. Ultimately, this information would be useful to develop environmentally clean technologies.

Finally, the general **structure of the thesis** is presented in section 1.3, where also the author's contribution is enlisted together with the different original publications (reported as superscript notation in roman numbers and in full bibliographic reference here below) on which the chapters and some section of this introduction are based.

Material from this chapter has been partially published in:

- (I) [Debora Foppiano](#), Mohamed Tarik, Jörg Schneebeil, Adelaide Calbry- Muzyka, Serge Biollaz and Christian Ludwig, Siloxanes compounds in biogas from manure and agricultural waste: Method development and Speciation analysis with GC-ICP-MS/FID., **2018**, *in peer-review*.
- (II) Mohamed Tarik, [Debora Foppiano](#), Adrian Hess, and Christian Ludwig, A Practical Guide on Coupling a Scanning Mobility Particle Sizer and Inductively Coupled Plasma Mass Spectrometer (SMPS-ICPMS), *J. Vis. Exp.*, **2017**, (125), e55487, doi:10.3791/55487.
- (III) [Debora Foppiano](#), Mohamed Tarik, Elisabeth Müller Gubler, and Christian Ludwig, Combustion generated nanomaterials: online characterization *via* an ICP-MS-based technique. Part I: calibration strategy with a TGA, *J. Anal. At. Spectrom.*, **2018**, 33, 1493-1499.
- (IV) [Debora Foppiano](#), Mohamed Tarik, Elisabeth Müller Gubler, and Christian Ludwig, Combustion generated nanomaterials: online characterization *via* an ICP-MS-based technique. Part II: resolving power for heterogeneous matrices, *J. Anal. At. Spectrom.*, **2018**, 33, 1500-1505.
- (V) [Debora Foppiano](#), Mohamed Tarik, Elisabeth Müller Gubler, and Christian Ludwig, Emissions of Secondary Formed Nano-Objects from the Combustion of Impregnated Wood. An Online Size-Resolved Elemental Investigation, *Environ. Sci. Technol.*, **2018**, 52, 895-903.

1.1 Motivation

The Paris agreement was an unprecedented moment in human history regarding climate change and the promotion of clean energy technologies. More than 110 countries, which count for almost 75% of global emissions, agreed on equally investing in ambitious climate policies. Supporting this vision, Barack Obama reported in a policy forum on Science: *«analysis of countries' individual contributions suggests that meeting medium-term respective targets and increasing their ambition in the years ahead—coupled with scaled-up investment in clean energy technologies—could increase the international community's probability of limiting warming to 2°C by as much as 50% »* [1].

In light of this event, European countries promoted the use of renewable sources and envisioned a change in the future energy supply. The Swiss government decided not only to implement the use of renewables but also to aim to an increased bioenergy share in the final energy consumption by 2050.[2] In this frame, the communication and the collaboration among higher education institutions was fostered by creating the Swiss Competence Centers for Energy Research (SCCERs).

Among them, SCCER BIOSWEET (which stands for “BIOmass for SWiss EnErgy fuTure”) focuses on the implementation of biomass valorization processes with high technological readiness level by exploring the limit of existing technologies and by designing better-integrated energy system for the use of the different feedstocks. Not only dry biomass conversion but also anaerobic digestion and hydrothermal gasification were taken into account. Regarding feedstocks, the use of waste from households, food industry, agriculture, and manure was also considered for the production of biogas.[2]

1.1.1 Waste to energy

Although largely considered as intrinsically with low value and at the end of its life cycle, waste can be a source of energy if properly treated. *“Ideally, waste management will ultimately turn waste into a valuable product (e. g. appropriately treated residue which can be left in a safe landfill for indefinite durations) or recycle it by transforming it physically and/or chemically so that it becomes valuable again as a raw material for new products.”* [3]

The waste and the biomass valorization usually starts with pre-treatment methods, such as mechanical separation, and it is followed very often by a thermal treatment, which has to be optimized according to the solid fuel's physical and chemical characteristics, such as gross calorific value (GCV), moisture content, ash content, bulk density, and particle size. [4]

Waste can be classified into two main categories according to their GCV:

- i. High calorific value (e.g. wood, paper, cardboard, plastic foils, and packaging)
- ii. Low calorific value (e.g. humid organic waste, minerals, and metals)

1.1.2 Valorization of biomass with high calorific value ^V

Wood or waste wood is a good example of biomass with high GCV. Value added-chemicals can be efficiently obtained from its main constituents (i.e. hemicellulose, cellulose and lignin) by discrete degasification. As shown in figure 1.1-1, the thermal degradation starts at 200°C for hemicellulose, between 300 and 400°C for cellulose and reaches 500°C for lignin, the most stable. Since their thermal stabilities overlap and significantly differ in decomposition rates - especially between hemicellulose/cellulose and lignin- the process has to be controlled by carefully selecting temperature (possibly in different steps), heating rates and gas-solid residence times.[5] After an initial drying step to homogenize the fuel and get rid of moisture, the biomass thermochemical conversion can be generally divided into low-temperature and high-temperature treatments.

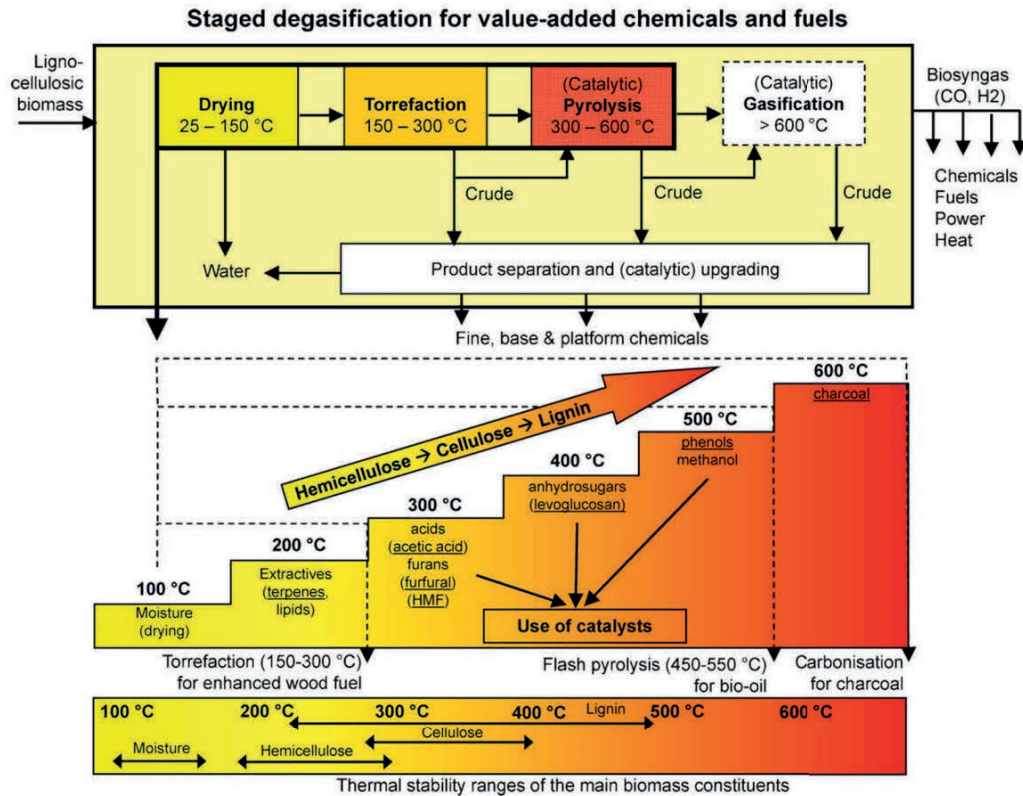


Figure 1.1-1 Fuels and value-added chemicals in staged degasification. Source : [5]

The torrefaction is one example of the first kind; it is normally carried out under atmospheric conditions in absence of oxygen, around 150 and 300°C. The main purpose is the removal of oxygen-containing compounds out of the biomass, not only to destruct the fibrous structure but also to increase the calorific value. Pyrolysis, instead, is operated between 300 and 600°C and it is the first stage of solid degradation, in which condensable volatiles, permanent gases, and char are produced. Often it is followed by a secondary pyrolysis in which thermal cracking, re-polymerization, and re-

condensation between the products occur. The gasification is a partial oxidation of the carbonaceous feedstock above 800°C. The syngas (i.e. CO, H₂) obtained can be used to produce methanol and hydrocarbons or directly used for many applications, such as turbines and engines.

The combustion includes the main oxidation step, where the bio-syngas is the result of former processes prior to oxidation. The most important parameter to control during the process is λ , the oxygen equivalent ratio added, which must be sufficient to ensure a full conversion of the combustible parts of the fuels, even though other options are possible, e.g. purification using H₂O. Ideally, each step should be optimized for a specific solid fuel and a specific technology employed for its valorization.

The technologies widespread employed in industrial combustion are bubbling and circulating fluidized bed furnaces, fixed-bed (grate) furnaces, and dust burners. [4] During disintegration of the organic fraction, not only tars, gases and chars are generated, but also inorganic volatile fraction, including alkali metals and chlorides while heavy metals are normally emitted at higher temperatures. Upon precipitation, from the inorganic volatile fraction, the ashes are formed. The most common techniques used for ashes removal are *settling chambers, cyclones/ multi-cyclones, electrostatic precipitators, baghouse filters, scrubbers, and panel bed filters, as well as flue gas condensation units*. [4] In nowadays waste incinerator plant (WIP) the emissions are significantly reduced thanks to air pollution control (APC) that includes normally not only the ashes separators mentioned beforehand, but also DeNOx system based on the selective catalytic reduction (SCR) technology for the removal of nitrogen oxides as well as other gaseous species (e. g. dioxins, furans, mercury, acidic gases, volatile organic compounds). In woody biomass combustion plant normally pre-separator, such as a cyclone, are installed before the final dust separator, as shown in Figure 1.1-2, where a schematic of a large burner with moving grate is represented. Ashes can be divided into three different types:

- i. Bottom ashes, which are immediately lost in the primary chamber;
- ii. Fly ashes, collected in the APC;
- iii. Fugitive ashes, which deposit in the stack after passing the APC.

The APC residues often present enrichment in volatile compounds and in nutrients as well as toxic heavy metals, which might pose a treat for their disposal. For this reason, their chemical composition and physical properties must be determined. [6] Regarding physical properties, such as grain size, a detailed schematic of the mechanism involving ash formation is reported in figure 1.1-3, where it is shown that particles between 0.01 and 200 μm are generated.

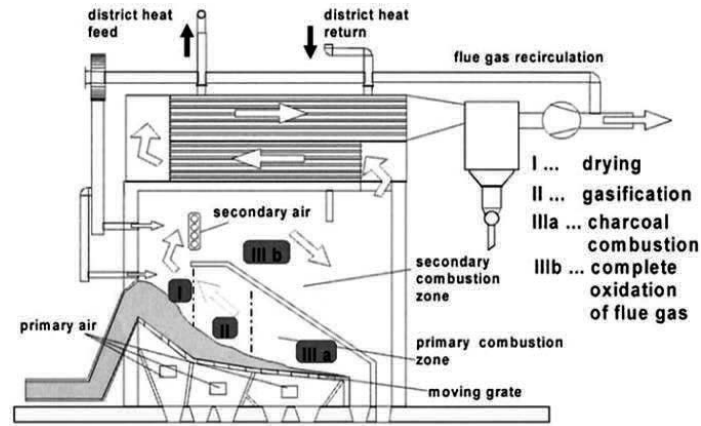


Figure 1.1-2 Schematic of a moving grate furnace [4]

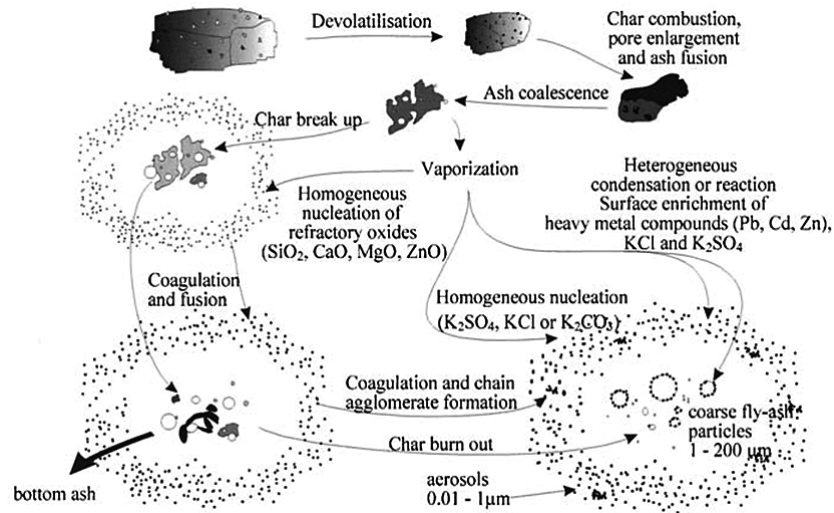


Figure 1.1-3 Schematic of ash formation from biomass during combustion, adapted from reference [7]

Particles are typically classified according to their aerodynamic diameter, which is defined as «the diameter of a sphere of density 1000 kg m^{-3} with the same settling velocity as the particle of interest».[8] Figures 1.1.-4 represent the main classes of atmospheric particles and their formation and coagulation mechanism, which we assumed here similar in the case of combustion generated particles. Coarse particles generally include particulate matter with an aerodynamic diameter between 2.5 and $10 \text{ }\mu\text{m}$ ($\text{PM}_{2.5-10}$), while fine particles have diameters below $2.5 \text{ }\mu\text{m}$ ($\text{PM}_{2.5}$). UFP (ultrafine particles) which are normally generated during combustion of fossil-fuels or by condensation of gas phase species into nucleation and Aitken modes. The first mode normally indicates newly formed particles with

a limited growth, which can often act as « seeds » for coagulation of other gas species. The Aitken mode instead includes recently formed particles actively coagulating among each other. The life-time of such a particle can be shorter than coarse particles and it is regulated not by the particle mass but by the particle number. [9] The International Organisation for Standardisation (ISO) additionally defines particle with size range between 1 and 100 nm as nanoparticles (NPs) or more generally as «*nano-object with all three external dimensions in the nanoscale*»[10]

In the early 2000s, a survey was published on the health impact of the average $PM_{2.5}$, showing how particles in this size range have a direct connection with lung cancer and respiratory mortality.[11] Another study reported that even within the same size class the transport of NPs to human lung fibroblast can anyway vary a lot.[12] In the case of particles between 25 and 50 nm, the tendency to rapidly form larger agglomerates can limit the diffusion through the organism, while particles between 250-500 nm are mostly unagglomerated. Furthermore, not only the size but also the chemical composition and morphology of NPs or nano-objects affect the inflammatory response. For example, Dandley et al. showed that reduced fibrosis is associated with Al_2O_3 coated carbon nanotubes when compared to an acute pulmonary response that is visible for in-vitro human cells and mice after exposure of carbon nanotubes, if they are coated with ZnO.[13]

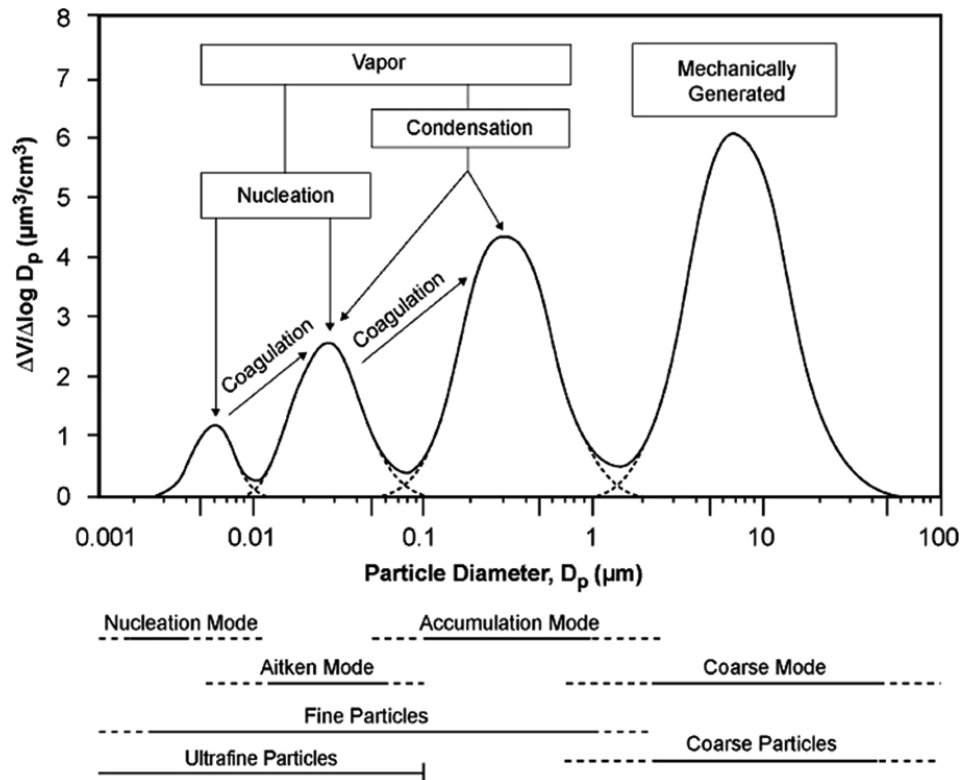


Figure 1.1-4 Main classes of atmospheric particles; the major formation and growth mechanisms are also reported. The four main modes are shown for particles with different particle size: nucleation, Aitken, accumulation and coarse mode for ambient particles. V = volume, D_p = particle diameter. [9]

1.1.2.1 Emissions from waste incinerator plants

Engineered nanoparticles (ENPs) and nano-objects (NO) are widely used in many applications such as motor- or vehicle- related products, electronics, paints, coatings and adhesives, household products, and personal care and cosmetic products. Therefore, the release of such nanoparticles from waste incineration and combustion processes has grown in importance. During waste combustion, metallic ultrafine particle emissions have been reported (dominated by K, Ca, Mg, Na, Fe, and Zn)[14] but their fate in waste treatment processes is poorly understood and not well investigated.

The implementation in the last decades of APC in modern WIPs has been crucial to significantly reduce the release of ultrafine particle in the atmosphere. A study carried out by various institutions in Switzerland focused on the fate of NPs intentionally added to the feedstocks in WIPs., where a large part of NPs added (in form of CeO_2) was remaining in the bottom ashes.[15] This observation was considered a sufficient prove of the non- significant occurrence of NPs in emissions from WIPs, which is any case not considering either the fact that for sludge and wood incineration mainly fly ashes are produced[16] or the fact that decisions for the ashes disposal are required[6]. More importantly, the occurrence of unintentionally produced nanomaterials cannot be excluded. The so-called incidental nanoparticles may volatilize in the incinerator during incomplete combustion processes and they can re-form after filtration of the flue gas, as represented in Figure 1.1-5.[17] Moreover, new nano-objects can be formed also as result of disaggregation of the already present nano-object and re-formation of new nano-sized compounds and materials.[18] Therefore, it is more accurate to consider not only the presence of ENPs but also two other main sources of nano-objects in the feedstocks, namely “*bulk-derived nano-objects and combustion-generated nano-objects. Bulk-derived-NO are defined as the nanosized fraction of bulk materials (e.g., pigments), while combustion-generated-NO are nanosized particles unintentionally produced in incineration processes*”.[16]

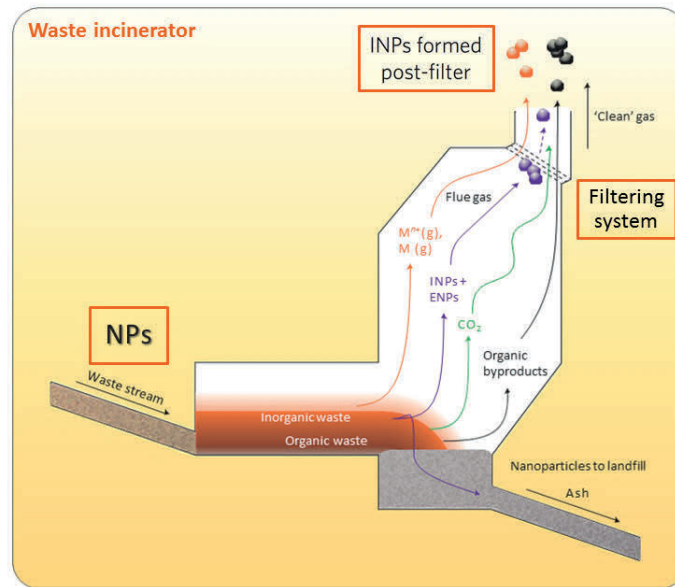


Figure 1.1-5 Schematic of unintentionally produced nanomaterials or so-called incidental nanoparticles (INPs) in a waste incinerator. Adapted from reference [17]

Depending on their surface area, the evaporation temperature of metal ENPs is significantly lower than that of the respective bulk material. However, when heterogeneous reactions and agglomeration occur during combustion, a generally decreased surface area of nanoparticles allows lower temperatures of evaporation. Moreover, the stability of metal ENPs is enhanced for the oxidized form, known to be less soluble and with a higher flash point than the corresponding metal. Therefore, certain metal oxide ENPs such as cerium oxide have a higher tendency to remain in the bottom ashes without being volatilized during incineration.[19]

Regarding the matrix effect, Jakob et al. showed how thermal treatment of fly ashes, involving thermochemical reactions of the heavy metals with other constituents (e.g. alumino-silicates, alkali metals chlorides and carbon species), provoke their evaporation.[20]

Zinc oxide is one of the relevant metal oxide NPs regarding significant exposures [21,22] and it is often contained in paints and impregnation or waterproofing sprays, which are used for wood preservation. Particular redox conditions could influence the evaporation of zinc since it can be reduced in the presence of carbon from its oxide to its metallic state, which evaporates at a much lower temperature.[23] Thus, zinc represents an interesting example of unintentionally produced nanomaterials during the combustion process, in which a large amount of carbon is present. Generally, the volatility of Zn decreased in the presence of oxygen and water but is strongly enhanced in presence of C contained in the feedstock, leading to the increase in volatility from 20% at 750 °C to 100% at about 950-1130 °C.[24] The presence of Zn in waste wood combustion off-gases was measured by an online elemental analysis of process gases, performed with ICP-OES (inductively coupled plasma optical emission spectrometer).[25] Furthermore, data from several studies have been identifying a Zn-enrichment in the fraction of fine particles;[26] while in these studies the particle size distribution was measured on-line, the chemical composition of the collected fly ashes was determined off-line.

1.1.3 Valorization of biomass with low calorific value ¹

The organic fraction from municipal solid waste or agricultural waste and manure are examples of biomass with low calorific value, which can be mixed to solid fuel with high GCV to control the combustion process or more often require a different type of treatment rather than combustion. Composting techniques have been widely used for centuries and they gradually evolved from aerobic to anaerobic digestion to recover biogas.

Biogas production in Europe has been consistently increasing up to 18 billion m³ methane (654 PJ) in 2015, in the frame of renewable energy policies. With 127 TJ of heat and 61 TWh of electricity delivered in 2015 and 17'400 biogas plants installed, the EU is currently the world leader for biogas production for generation of heat and electricity.[27] According to a recent estimation, a profitable investment would be reached only if administrations (at governmental level) would provide about 20–50 €MWh_e⁻¹ in biogas for power generation, and 15–25 € MWh⁻¹ for the production of purified biomethane, that can be directly introduced in the gas grid.[28]

As mentioned before, biogas can be recovered through anaerobic digestion of different biomass sources and waste, such as sewage, municipal, agricultural, food waste, and manure. Even if tradi-

tionally used as fertilizer, manure digestion is beneficial not only to the environment by lowering methane (CH_4) and carbon dioxide (CO_2) emissions to the atmosphere, but also to humans and animals by removing pathogens, avoiding water contamination, and mitigating odors. With the further advantage that, since the level of nutrients in the digestate remains the same, it can still be used as fertilizer.[29] Numerous studies have also shown that the use of food waste and in general biomass with high content in proteins, fat, and carbohydrates lead to higher biogas yields. [30]

1.1.3.1 Siloxane compounds in biogas

Although mostly composed of CH_4 (60-70%) and CO_2 (30-40%), the remaining constituents of biogas are often the cause of corrosion damages to the industrial plants and facilities. The most relevant impurities are nitrogen, oxygen, hydrogen, aromatic hydrocarbons, alkanes and alkenes, halogenated compounds, and volatile organic carbon (VOC) including sulfur compounds and organic silicon compounds (or siloxanes).[31] Siloxane compounds are employed in hygiene products, shampoos, cosmetics, detergents, and lotions. They can be linear or cyclic, in which case they are indicated with either the letter L or D, respectively. The number following the letter indicates the amount of Si atoms contained in the molecule.[32,33] While normally non-reactive or corrosive, these semi-volatile compounds can turn into abrasive silica (SiO_2) at high temperature and pressure conditions in an engine's combustion chamber. Solid oxide fuel cells (SOFCs) are also highly susceptible to the presence of siloxanes, even in trace level (ppb_v).[34-36] The mechanism, suggested by post-mortem analysis on the cell, consist of silica deposition at the inlet of the fuel channel and on the anode side, creating an insulating layer that leads to higher ohmic resistance and rapid degradation.[37] Such a deposition occurs also on engines surfaces or in microturbines, which are increasingly used in Europe thanks to small exhaust quantities and perfect suitability to methane. Maintenance time for removal can reduce the normal operating hours from 20'000-40'000 to 14'000 only.[38] Silica deposition can affect also domestic appliances by increasing the flow resistance in heat exchangers. In gas-fired flow-through hot water heat exchanger, higher flow resistance means lower air intake, hence a potential threat for users due to higher emissions of CO with time.[39]

Although siloxanes are largely considered non-toxic for humans and environment, an extensive survey by Mojsiewicz-Pieńkowska and Krenczkowska presents the evolution of consciousness on siloxanes exposure over the last 70 years. Because of their physicochemical properties, these compounds can be hardly replaced. However, properties such as the degree of polymerization, molecular weight, volatility, and lipophilicity are precisely the ones allowing migration into and accumulation in the organism. The effects caused upon absorption should be analyzed for each specific compound and not for the overall class.[40] Although concerns on siloxanes toxicity were raised only 20 years ago, the REACH (Registration, Evaluation, and Authorisation of Chemicals) has already defined D4 as “*a persistent, bio-accumulative, and toxic (PBT) and very persistent and very bioaccumulative (vPvB) substance*” , while D5 “*meets the Annex XIII criteria for both a persistent (P) and a very persistent (vP) substance in water and sediment, and a bioaccumulative (B) and very bioaccumulative (vB) substance*”.[41] Regarding gaseous emissions, rather than their persistence in the atmosphere, the

effect on the environment is prominently faced as deposition on the lithosphere and hydrosphere. Almost 200 tonnes of siloxanes are released every year in the environment, only in the United States. On the matter, most of EU Member States adhered to the ECHA (European Chemical Agency) report banishing from the markets personal care product with D4 “*concentrations equal to or greater than 0.1% by weight*,”[42] EURAMET (the European Association of National Metrology Institutes) set the maximum level of total silicon content to 0.5 mg m^{-3} , under normal conditions, while recommended levels are between 0.1 mg m^{-3} and 0.3 mg m^{-3} , levels which are often not reached by available methods. [43] In the frame of the European Metrology Program for Innovation and Research (EM-PIR), several institutions among Europe have been investing “*for the development and drafting of standardized test methods for biomethane and upgraded biogas to fill this void*,”.

1.2 Goals and scope of the thesis

This thesis is focused on the need of developing new analytical methods for online and offline analysis of gases produced during biomass valorization. Figure 1.2-1 is summarizing the different operational steps involving the reuse of waste/nano-waste and biomass, already explained in the **motivation** (section 1.1) of this thesis.

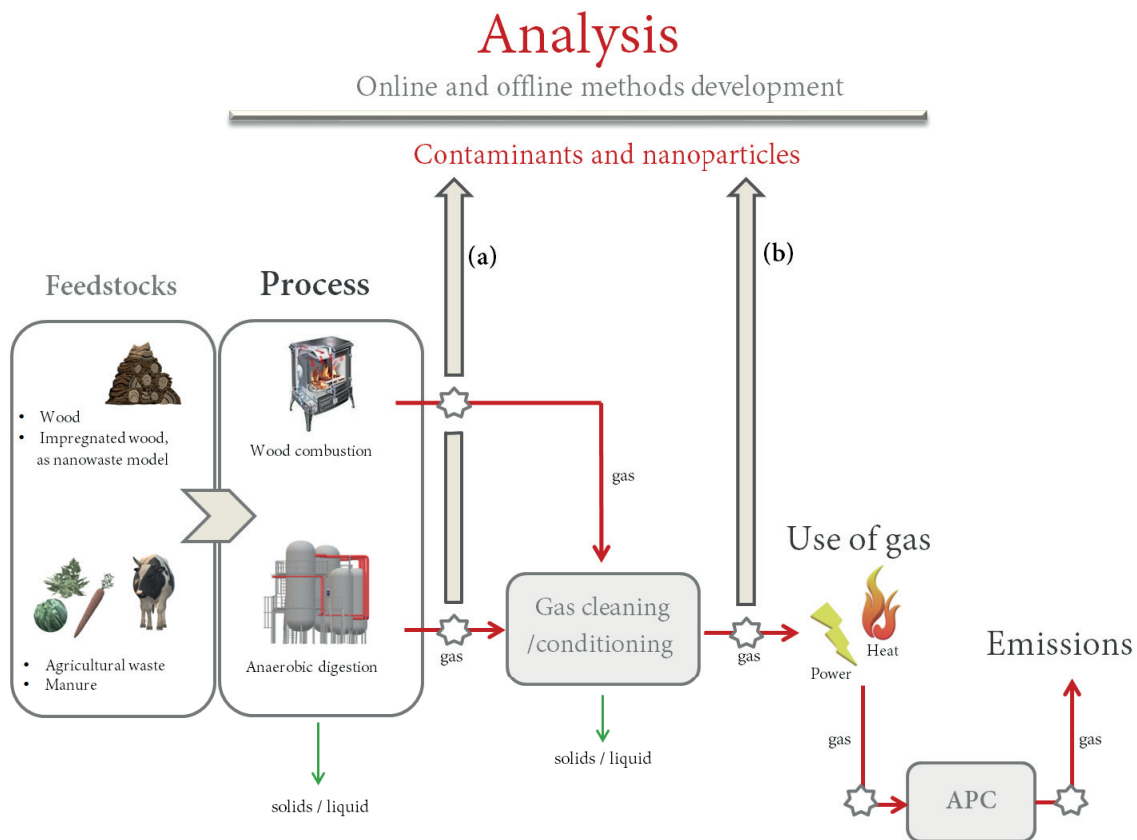


Figure 1.2-1 Graphical concept summarizing goals and scope of the thesis.

(☆ = potential sampling point of interest, APC=air pollution control system)

Two different types of feedstocks were considered, namely ZnO impregnated wood (as a model of nanowaste) and a mixture of agricultural waste and manure. Their valorization processes were chosen according to their calorific properties, so in the first case, a combustion treatment was applied while in the second, the most suitable process was anaerobic digestion for the production of biogas. The potential sampling points of interest are indicated in Figure 1.2-1 with a 7-point star. Among them, only the three corresponding to the following gas fractions were selected:

- a) Gas emitted after processing, before the gas cleaning and conditioning unit;
- b) Gas emitted after processing, after the gas cleaning and conditioning unit;

The online and offline analysis on these two fractions can be crucial to understand the fate of contaminants and improve the existent technologies. Therefore, the goal and scope of this thesis are divided into two main subsections regarding, first, the online measurement of NPs emissions from combustion processes of waste wood (a), and second, the method development for the analysis of siloxane compounds in biogas (a and b). For a better understanding of the novelty in this study, the main analytical methods and techniques commonly used for the two applications are also introduced and compared.

1.2.1 NPs emission in combustion processes: on-line characterization

1.2.1.1 Characterization of particles in aerosols^{II, III}

In numerous fields, the characterization of particles in aerosols - including the determination of chemical composition and size distribution - is an important issue. A variety of analytical techniques to determine particle properties is used in different environmental, industrial and research applications, such as measuring/monitoring air-borne or combustion-emitted particles, characterizing synthesized engineered nano-objects, and studying their health and environmental effects.

On one hand, the size information of gas-borne particles and particles in suspensions is conventionally gained by using different particle sizers, such as Aerodynamic Particle Sizer (APS), Dynamic Light Scattering devices (DLS), electrical low-pressure impactor (ELPI) or a Scanning Mobility Particle Sizer (SMPS).^[44–50] The latter - well- established aerosol measurement tool - consists of two parts, a Differential Mobility Analyzer (DMA) and a Condensation Particle Counter (CPC), mounted in series. The first one allows the classification of the aerosol particles according to their mobility diameters by varying the voltage between two electrodes in an air stream. In the CPC, entering nanoparticles act as condensation nuclei to form "large" droplets that are then optically counted.^[51] The SMPS output data represent size-resolved number information about the measured particles and are given as Particle Size Distributions (PSD). On the other hand, the chemical characterization of gas-borne particles and particles in suspensions is usually performed offline.^[52] An appropriate collection and sample preparation procedure is required prior to the analysis. Such offline investigations usually include the application of a spectroscopic technique, such as Inductively Coupled Plasma Mass Spec-

trometry (ICP-MS). This is an established method in element and trace- element analysis of liquid samples with very high sensitivity and low detection limits.[53] Other surface and/or bulk analytical techniques are used either to achieve a complete characterization and/or to gain more information about the particle characteristics. Imaging techniques, such as Scanning Electron Microscopy (SEM) and Transmission Electron Microscopy (TEM), are widely used for this purpose.[54,55]

In the last decades, online studies had prevalently preferred a mass spectrometry-based techniques, such as the aerosol mass spectrometer (AMS), which provides information about size class and molecular composition for the characterization of mainly organic compounds.[56,57] However, the complexity of those mass spectra often requires accurate molecular databases and high-resolution MS or tandem MS-MS. The use of ICP-MS, instead, is significantly improving the determination of ENPs[58], particularly as single particle measurement (sp-ICP-MS) on monodisperse particles in suspensions[59,60] or environmental liquid samples with very low particle concentration, which has become possible thanks to pre-concentration methods (like cloud-point extraction) or separation techniques in combination with the new ICP-MS generations, in which the dwell time is in the order of few tens of microseconds.[61–63] To simultaneously gain time-resolved chemical and size information, two different analytical techniques, such as SMPS and a plasma spectrometric technique, can be combined in one setup. [64] This online measurement concept can avoid problems related to sample collection, preparation, and offline analysis procedure. A short overview of previous attempts to develop such a combined setup was reported by Hess et al.[65] In this specific case, the use of ICP-MS for aerosol application can ease the detection of inorganic particles and their discrimination during multi-component system analysis.[65] In order to obtain information not only about the chemical composition but in term of concentrations of the analyzed species, a calibration of the setup is required.

An appropriate calibration strategy of the SMPS -ICP-MS could be the coupling with a TGA (thermogravimetric analyzer) to correlate linearly the weights loss measured by TGA with the ICP-MS intensities. The previous attempt of this sort of calibration was applied to ICP-OES signals by Ludwig et al. in a study which mainly focused on “inorganic high-boiling-temperature substances”, otherwise not easily measurable with a simple TGA-MS (mostly used to detect gaseous organic products).[66] The particles generated into the TGA were transferred to the detector with the use of a condensation interface (CI). The CI was making it possible to analyze heavy metals present as a vapor compounds in a hot gas with a detector operating at room temperature, by quenching and diluting a representative fraction of the analytes into the carrier gas (argon).[67] In our case this function can be performed with an RDD (rotating disk diluter), that not only allows adjusting finely the dilution factor applied but also acts as a reliable sampling unit for the diluted gases into the setup, avoiding possible condensation phenomena and losses.[68]

1.2.1.2 On-line time resolved elemental analysis (RDD-SMPS-ICP-MS) for combustion studies (IV, V)

Quantification and characterization of nanomaterials are becoming crucial to determine the fate and concentration of ENPs in environmental samples. As mentioned before, the possibility of using ICP-

MS for that purpose has so far been extensively exploited, leading to its prevalent use in single particle mode for the determination of ENPs in concentration levels close to part-per-trillion (ppt).[69] The detection of particles is performed by acquiring transient signals with millisecond dwell times or even microsecond for an improved resolution and working range.[70] Certainly, the possibility of acquiring multiple isotopes in a short time represents one of the main points of interest, in particular in the determination of complex particle structure, e.g. with core-shell structure. Multiple elements detection is possible thanks to an improved nebulization efficiency using a micro-droplet generator or by employing a modified ICP-MS, like the prototype of ICP-Time-of-Flight spectrometer (ICP-TOF-MS) presented by Borovinskaya et al.[71–74]. Some limitations arise for the presence of naturally-occurring-nano-materials or if the concentration of dissolved analytes lie above the (ppt) level, for which different fractionation or separation techniques have been combined in the past (e.g. asymmetric flow field-flow fractionation, filtration, coupling with ion-exchange resin cloud point extraction, or capillary electrophoresis, etc.).[62,63,75–77] Although initially conceived for atmospheric chemistry and detection of aerosol particles, sp-ICP-MS is moving towards becoming the leading routine analysis for the characterization of metal-containing nanomaterials principally in aqueous dispersion[78], with size detection limits down to few nanometers estimated for more than 40 elements.[79]

Other online techniques normally employed in aerosol research for the analysis of nanoparticles are either specifically optimized for atmospheric metal detection in a very low concentration range[80], or particularly focused on organic gaseous emissions employing soft ionization techniques like HR-AMS (High-Resolution Aerosol Mass Spectrometry) or HR-TOF-AMS (High-Resolution Time-of-Flight Aerosol Mass Spectrometry)[81], which can only be applied to non-refractory materials (only for boiling points below 600°C due to instrumental limitations). The use of SP-AMS (Soot- Particle Aerosol Mass Spectrometry) or SPI-TOF-AMS (Single-Photon Ionization Time-of-Flight Mass Spectrometry) presents major advantages in case of combustion emissions, such as the possibility to follow the transformation of primary organic aerosols (POA) occurring in the atmosphere and their impact on cloud formation. Also, studying in detail the change in composition and concentration of primary and secondary volatile organic compounds (VOC) could help to assess improvements in stoves design.[82] SP-AMS allows characterizing with high time resolution also metallic compounds even when linked to refractory materials, e.g. black carbon (rBC), although a drop in sensitivity for some trace metals occur if they are not contained in rBC-aerosol particles.[56] Nevertheless, for all these systems an extensive data treatment and availability of fragmentation tables and datasets are required. For relatively high concentration ranges of the analytes of interest and complex heterogenous matrixes, such as in combustion emission measurements, the use of an online method focused on metallic or metal oxides particles analysis is of particular interest, even more if it involves a faster data treatment. Alternatively, the RDD-SMPS-ICP-MS technique is proposed as a robust online analytical tool having high ability to provide simultaneously size-resolved elemental and quantitative information with a good time resolution.

1.2.2 Method development for the analysis of siloxanes in biogas¹

The most widespread sampling methods for siloxanes can be divided into two subclasses if they a) include or b) not include analytes enrichment during the process. In the first case, the enrichment of analytes occurs through adsorption on a solid (adsorbent tubes) or a solution (impingers). In the second case, cylinders, canisters or gasbags are the containers most used for sampling. Sampling methods should take into account the selection of a representative fraction, short/long-term stabilities, and minimization of the losses. Arrhenius et al. suggested that only a combination of different sampling techniques could help to obtain a representative fraction of the biogas, depending on the impurities of interest. In addition, recoveries assessment is always advisable.[83]

Among offline analytical techniques, GC-MS (gas chromatography-mass spectrometry) has been widely used for siloxanes analysis. Cortada et al. compared several methods using GC-MS, from which can be noticed a trend towards low limits of detection (LOD) relative to other techniques. A few attempts with GC-FID (gas chromatography-flame ionization detector) were also done, resulting though in much higher LODs than methods using GC-MS.[84–86] Even though GC-MS has high performance and provides structural information, the chromatogram often suffers from high levels of interferences. The combination of GC with element-specific techniques, such as ICP-MS could result in a cleaner chromatogram with improved detection limits and sensitivities, that depend mainly on ionization efficiency, isotopic abundance of the element, and reduced/absent interferences.[87] Nevertheless, not many methods using GC-ICP-MS for Siloxane analyses were developed. [88] The use of atomic emission detectors (AED) has been reported more often in literature.[43,89]

The resolution of single compounds is still possible with online techniques, such as PTR-MS (proton transfer reaction- mass spectrometer) or PTR-TOF-MS (proton transfer reaction- time of flight- mass spectrometer). As the name suggests, hydronium ions (H_3O^+) are used to chemically ionize each compound, which will have its experimental and expected m/z value. Tables can be consulted to compare those values for tentative identification. The main limitation of PTR-MS and PTR-TOF-MS is linked, though, to post-processing data analysis of large data sets (giga-bite h^{-1}).[90–92]

Semi-online techniques such as FT-IR (Fourier Transform Infrared spectroscopy) and other commercially available online instruments monitor the total Si content, but their detection limits are close to or above the maximum level recommended for Si.[93,94]

1.3 Structure of the thesis

This thesis is composed of seven chapters and two appendices. In this first chapter (**Chapter 1**) the general motivation and the broad context of this work together with the state-of-the-art techniques are reported. The superscript notation with roman numbers in brackets indicate the original publication on which the chapter or a particular section of a chapter is based and they were already introduced with their full bibliographic reference in the beginning of the thesis and in the first page of this chapter. Here below the content of the remaining chapters of the thesis is briefly summarized, as well as the author's contribution.

Chapter 2: Methods and experimental ^{I, II, III, IV, V}

The instrumental arrangements and methodologies employed during this thesis are summarized in this chapter, together with detailed information about samples and materials used. The instruments are singularly explained in their basic theory and also shown in the different couplings used for the experiments reported in this thesis. Among them, the most relevant in this work are GC, SMPS, TGA, ICP-MS, and the RDD conditioning sampling unit. Additionally, other off-line techniques specifically used for NPs suspensions characterization, such as DLS (dynamic light scattering), X-ray disc centrifuge, and SEM/ TEM, are briefly introduced and explained.

Chapter 3: Speciation analysis with GC-ICP-MS/FID of siloxane compounds in biogas ^I

The purpose of this study was to develop and optimize a method to analyze, simultaneously with GC-ICP-MS and GC-FID, the siloxanes concentration in biogas samples from anaerobic digestion of manure and mixed organic sources (food, agricultural, manure, and green wastes). The samples were collected in a biogas production plant in Switzerland with a liquid quench sampling system (LQSS), which concentrates condensable trace compounds from the biogas into a liquid solvent. While GC-ICP-MS is suitable to reach the specifications required from EURAMET[43], GC-FID can provide complementary information on other impurities present in the biogas. The figures of merit and performance of the two methods are compared to each other and with analytical techniques reported in literature.

- The author carried out the method development and the speciation analysis with GC-ICP-MS, and performed the biogas analyses, the evaluation of the GC-FID method, and the coordination of the research project, as well as taking the lead in the compilation of the first draft of the manuscript.

Chapter 4: Preliminary studies with RDD-SMPS-ICP-MS ^{II, V}

The versatility of RDD-SMPS-ICP-MS coupling is demonstrated in example measurements on three different aerosols generated out of *a)* a salt solution, *b)* a suspension, and *c)* emitted by a thermal process with three different aerosol generator sources. Particular interest is given to the preparation and characterization of NPs suspension, together with initial assessing of the thermochemical behavior in different redox and thermal conditions.

- The author planned and executed the NPs suspension preparation and characterization as well as the experiments on salt solution, suspension, and powders (except for the CuCl₂ powder experiment made by M. Tarik).

Chapter 5: RDD-SMPS-ICP-MS calibration strategy and resolving power for heterogeneous matrices ^{III, IV}

This chapter describes the calibration strategy of the RDD-SMPS-ICP-MS, the figure of merit of the method and the comparison between SMPS and ICP-MS data sets. An application assessing the resolving power of the RDD-SMPS-ICP-MS setup in the determination of nanomaterial is also presented, in evaporation experiments from a complex mixture of different oxides.

- The author performed the experiments with the TGA and the RDD-SMPS-ICP-MS measurements, as well as the data treatment and evaluation, and took the lead in compiling the first draft of the manuscripts.

Chapter 6: Emission of secondary formed ZnO nano-objects from combustion of impregnated wood ^{IV, V}

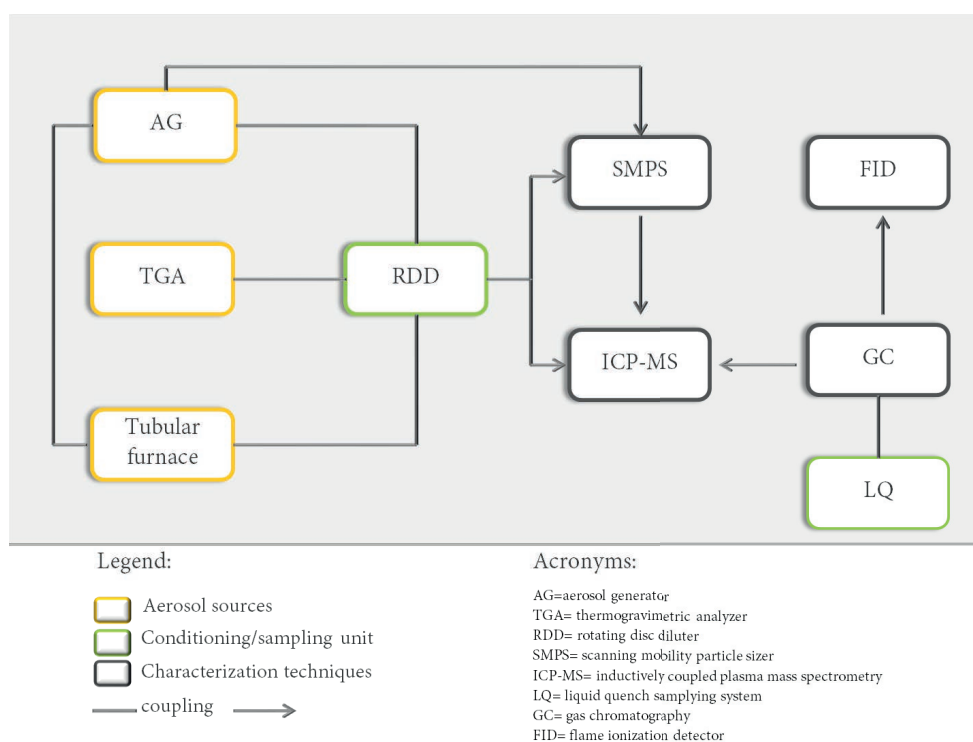
ZnO dried particles, beech wood sawdust and, ZnO impregnated sawdust were combusted following two different temperature profiles in a lab-scale incinerator. The potential release of ZnO nanoparticles in sawdust samples formed in the reducing process gases was of particular interest. Upon verification of secondary formed ZnO nano-objects emissions, the calibration strategy explained in chapter 5 was employed to obtain quantitative information.

- The author carried out the incineration experiments and the RDD-SMPS-ICP-MS measurements, as well as the indexation of the electron diffraction pattern (under the supervision of E. G. Müller), the data treatment and evaluation, and took the lead in compiling the first draft of the manuscript.

Chapter 7: Concluding remarks and outlook ^{I, II, III, IV, V}

In this last chapter, the concluding remarks and possible outlook are presented for all the different topics discussed in the previous chapters.

Chapter 2 Methods and experimental



Material from this chapter has been partially published in :

- (I) Debora Foppiano, Mohamed Tarik, Jörg Schneebeli, Adelaide Calbry- Muzyka, Serge Biollaz and Christian Ludwig, Siloxanes compounds in biogas from manure and agricultural waste: Method development and Speciation analysis with GC-ICP-MS/FID., **2018**, in peer-review.
- (II) Mohamed Tarik, Debora Foppiano, Adrian Hess, and Christian Ludwig, A Practical Guide on Coupling a Scanning Mobility Particle Sizer and Inductively Coupled Plasma Mass Spectrometer (SMPS-ICPMS), *J. Vis. Exp.*, **2017**, (125), e55487, doi:10.3791/55487.
- (III) Debora Foppiano, Mohamed Tarik, Elisabeth Müller Gubler, and Christian Ludwig, Combustion generated nanomaterials: online characterization via an ICP-MS-based technique. Part I: calibration strategy with a TGA, *J. Anal. At. Spectrom.*, **2018**, 33, 1493-1499.
- (IV) Debora Foppiano, Mohamed Tarik, Elisabeth Müller Gubler, and Christian Ludwig, Combustion generated nanomaterials: online characterization via an ICP-MS-based technique. Part II: resolving power for heterogenous matrices, *J. Anal. At. Spectrom.*, **2018**, 33, 1500-1505.
- (V) Debora Foppiano, Mohamed Tarik, Elisabeth Müller Gubler, and Christian Ludwig, Emissions of Secondary Formed Nano-Objects from the Combustion of Impregnated Wood. An Online Size-Resolved Elemental Investigation, *Environ. Sci. Technol.*, **2018**, 52, 895-903..

In this chapter, all the methods and materials used during the thesis are summarized. Each instrument is briefly introduced separately in section 2.1, while section 2.2 explains how they were hyphenated for the different applications reported in this thesis. The corresponding materials used are listed in section 2.3, whereas additional off-line characterization techniques are described in section 2.4. The roman number reported as superscript notation indicates the original publications (in full bibliographic reference in the first page of this chapter) on which certain sections of this chapter were based.

2.1 Instruments

2.1.1 Aerosol sources

2.1.1.1 Aerosol generator (AG)

An aerosol generator was used to generate NPs in a gas media (in this case argon) starting from liquid solutions or suspensions. The peculiarity of the used atomizer is the injection principle based on a two-stream nozzle, placed close by the spray outlet (wall of the glass vessel). This design allows only smaller droplets to proceed their way up to the aerosol outlet, while the larger particles impact with the wall and ultimately are recovered again in the liquid reservoir. For a better understanding, a schematic of the working principle is also shown in Figure 2.1-1. A silica gel dryer is often coupled to the outlet of aerosol generator to reduce and control as much as possible the content of water, more correctly to lower relative humidity (RH%).

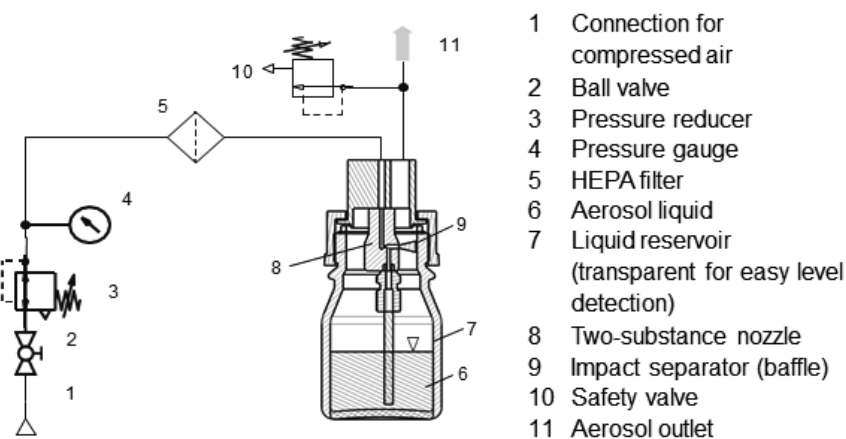


Figure 2.1-1 Schematic of aerosol generator ATM 221 representing the nozzle working principle. Courtesy of Topas GmbH (Germany).

2.1.1.2 Thermogravimetric analyzer (TGA)

In thermogravimetric analysis (TGA) information on the mass of a sample and the loss rate are obtained with high time-resolution during a thermal treatment at defined heating rate or/and at isothermal regime. [95] The further coupling of a TGA with other analytical techniques grants chemical

information also on the emitted gas or particles. Ultimately, this acquired knowledge is used to determine specific characteristic of the material or to better understand the decomposition mechanisms occurring at a certain temperature, as well as information on the kinetics of a certain reaction. The mass of the sample is measured by a highly sensitive balance, while the temperature is carefully monitored with thermo-elements placed in close proximity of the sample, in a protected atmosphere (generally Ar or N₂). For the applications later presented, the TGA was considered as an aerosol source used to generate particles during the thermal treatment of solid samples and to obtain precise information on their weight loss over time. The TGA/DSC 1, (Mettler-Toledo, CH) presents some advantages in its design, in particular, an efficient transport of the particles takes place thanks to an alumina tube installed in proximity of the sample and directing the exhaust to the outlet of the furnace. Its relative small length and the presence of the alumina disks around it not only prevent heat dissipation but also avoid the transfer of aerosol and deposition phenomena by reducing the dead volume of the furnace, especially in the area adjacent to the tube, as it is shown in the Figure 2.1-2 below.

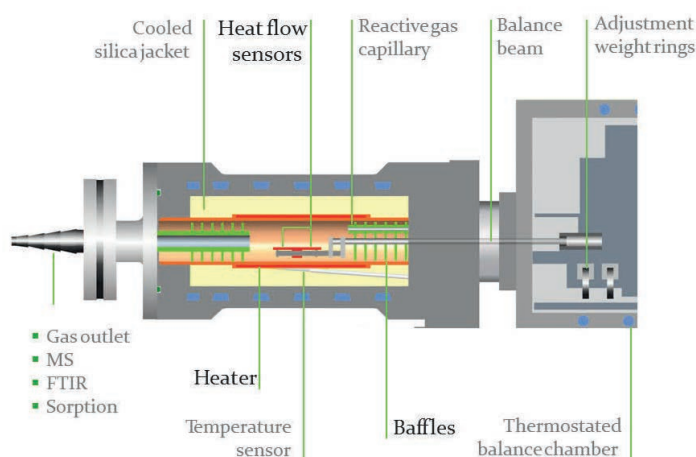


Figure 2.1-2 Schematic of the TGA/DCS 1. Courtesy of Mettler Toledo (CH).

2.1.1.3 Tubular furnace

A tubular furnace (Heraeus, RE 1.1) was used as a lab-scale incinerator. The samples were introduced in the furnace either already as an aerosol or as a solid sample in the quartz tube using a boat-shaped alumina crucible. The tube was kept under argon atmosphere with a defined flow controlled by an MFC (mass flow controller). The tubular furnace is considered as a potential source of gas-borne particles, if they are generated during thermal treatment of a solid sample. The temperature gradient into the furnace was monitored with a thermo-couple, measuring the temperature in close proximity with the sample every 10 seconds. Temperatures higher than 950°C were never set to avoid deterioration of the quartz tube. Nevertheless, this temperature was sufficient to study the application of interest (i.e. the combustion of wood). Additionally, this particular design allowed a rapid and

efficient cleaning after each measurement, with very low background signals in term of particle concentrations.

2.1.2 Conditioning and sampling unit

2.1.2.1 RDD (rotating disk diluter) ^v

The RDD consists of two main parts, namely a dilution head and a control unit. The dilution head is further divided in two units, a rotating disk with several cavities (8 or 10 cavities) and a steel block with two gas channels that can be heated up from 80 to 120°C. Regarding the gas channels, one of them is used to sample the raw gas while the other is used to provide the dilution gas (A and B, respectively, in the schematic in figure 2.1-3). The dilution argon flow provided to the dilution head has to be defined by an MFC, because it determines also the flow rate of the diluted aerosol directed to the coupled analytical instruments. The working principle is based on the transport of only small fraction of volume from the sampled gas (A) to the measurement channel (B) by the disk cavities. The dilution ratio of the raw gas is dependent on the disk rotation frequency, a calibration factor inherently depending on the instruments design and it is inversely dependent on the dilution flow rate. The diluted gas is directed first to the control unit and from there eventually to an evaporation tube (with maximum temperature 400°C), which is normally used either to avoid condensation and/or further dilute the particles or to evaporate volatile organic compounds present in the processed gas. This last step can be quite useful to maintain reproducible operating conditions throughout different experiments.

To summarize, the RDD was used as sampling and conditioning system allowing to adjust precisely a wide range of dilution (over several orders of magnitude, between 15x and 1500x), thus it represents an optimal choice for different aerosol sources and applications.

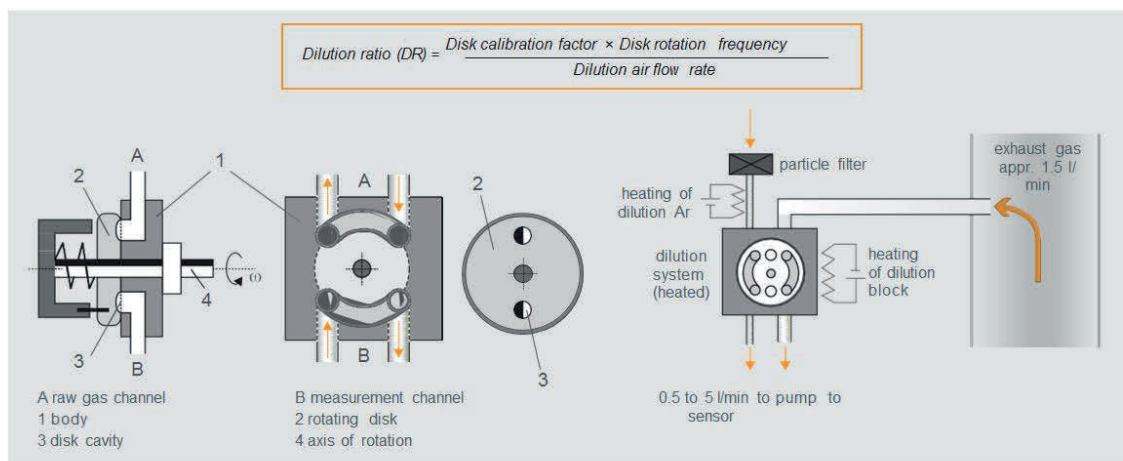


Figure 2.1-3 Rotating disc diluter (RDD) working principle side views. Courtesy of Testo GmbH (Germany)

2.1.2.2 Liquid quench sampling system (LQ)¹

The liquid quench (LQ) is a sampling system used to examine condensable trace compounds from biogas by concentrating them into a liquid solvent (in this study, 2-propanol). The system had been developed in-house at PSI in collaboration with the “Thermochemical Processes” (TCP) research group and it was used in this thesis to sample condensable and non-condensable compounds in biogas. A detailed description can be found in previous works [96,97], whereas a brief introduction is given in Figure 2.1-4 and in the following paragraph.

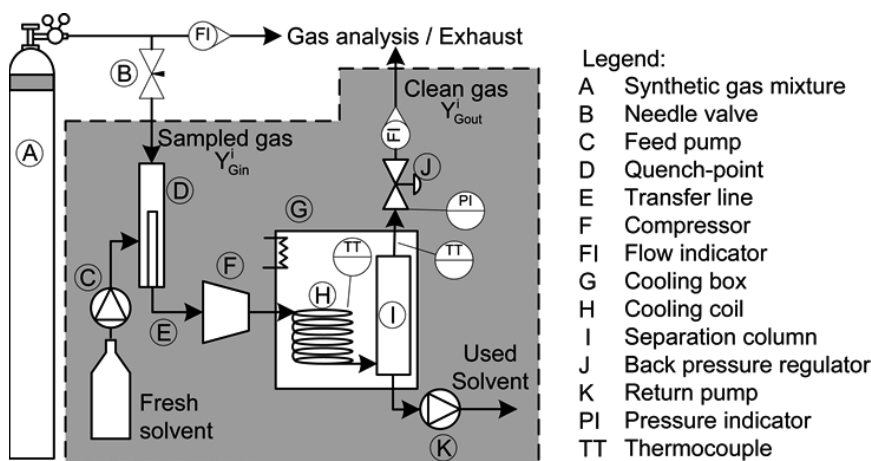


Figure 2.1-4 Schematic of the liquid quench sampling system, adapted from reference [96]. A, in the case of this dissertation, indicates not a synthetic gas mixture but biogas sampled in a methane production plant.

The biogas sampling section of the LQ consists of two co-axially positioned stainless steel tubes, of 2 mm ID and 0.8 mm ID, respectively. These are inserted directly into the center of biogas flows through pre-existing sampling points at biogas production sites. The solvent is first fed towards the biogas source through the smaller stainless steel tube, and it is then immediately pulled back with a membrane pump into the 2 mm ID outer tube along with a slipstream of biogas. The two-phase mixture of biogas and solvent is compressed to 2.5 bar and cooled to -20°C (point D in Figure 2.1-4), after which the resulting liquid solution of isopropanol and condensable biogas trace compounds is collected in sample tubes. The distinct attribute of this system is the continuous flow of gas and liquid through the system that allows time-resolved sampling of both condensable and non-condensable compounds, depending on the chosen experimental conditions the time resolution can vary from 10 to 20 minutes. Different gas-to-liquid ratios can be tuned by varying the sampled biogas flow rate or the liquid solvent flow rate. The set gas-to-liquid ratio and the trace compound concentration found in the solvent samples allow calculating back the concentration of this compound in biogas form.

2.1.3 Characterization techniques

2.1.3.1 SMPS (*Scanning Mobility Particle Sizer*)

The SMPS is a characterization technique used to obtain information on the size distribution and concentration of particles in an aerosol fraction. It consists of two main units, the DMA (differential mobility analyzer) and the CPC (condensation particle counter). The particles are classified according to their mobility diameter by varying the voltage at given DMA sheath and aerosol gas flows. The number concentration of the classified particles is determined afterwards by the CPC. In the CPC particles pass through a super saturated chamber where they act like “seeds” for the condensation of a used solvent (butanol or water) to reach the critical volume needed to be optically counted. Before entering the DMA, the diluted aerosol passes a radioactive source, i.e. an aerosol neutralizer, in order to establish a known charge equilibrium (assuming a Boltzmann charge distribution).[51]

The SMPS used in this work had been developed in the CPM research group at PSI in the four years previous to the start of this dissertation and it presents some modification compared to a commercial instrument. It consists of a DMA tube internally built at Paul Scherrer Institute (similar to a TSI commercial long DMA) working with Ar instead of air, and a commercial CPC (TSI, model 3010). A more detailed description is reported in section 2.2.2 and in the schematic in figure 2.2-3.

2.1.3.2 ICP-MS (*Inductively Coupled Plasma Mass Spectrometry*)

The ICP-MS is a versatile technique for trace and ultra-trace elemental analysis that can be applied to almost all the elements in the periodic table in ranges of concentration going from pg mL^{-1} to $\mu\text{g mL}^{-1}$. In ICP-MS, the argon plasma serves to dry, atomize and ionize the introduced liquid samples.[98] The atomic ions are then directed and focused with ion lenses through a mass analyzer where positive ions are classified according to their mass to charge ratio (m/z). Most of the mass analyzers used requires high vacuum ($>10^{-4}$ mbar) that is maintained by using turbomolecular pumps. The pressure is firstly significantly reduced by passing through two sampling cones placed in close proximity to the sampling area of the plasma, first the sampling cone (aperture size < 0.5 mm), then the skimmer (aperture size: 0.05 -1 mm). After being selected according to their m/z , the ions are finally counted in analog or pulsed mode in Faraday cup detector, or electron multiplier detector. An important feature of electron multipliers is the quite wide range of current in which they can operate linearly.[98] A schematic of all these parts is reported in both figures 2.2-1 and 2.2-3.

Besides liquid samples, ICP-MS is also used for gas and particle analysis. For example, gas can be directly introduced into the ICP-MS and analyzed.[25,99,100] Therefore, in this thesis a commercial ICP-MS instrument (Agilent 7700x), was used to determine the elemental composition of the aerosol-laden particles and gaseous contaminants.

2.1.3.3 Gas Chromatography

Gas chromatography is properly defined as a separation technique of the individual components in a mixture of different compounds at specific temperature and pressure. The sample can be introduced either as a liquid or a gas. In the first case a calibrated microsyringe is used to introduce the sample

through a septum into a heated port close to the column; by applying a selective temperature program, each compound will elute at a specific retention time, normally closely related to their boiling points. Details on the mobile phase and on the capillary column are reported in section 2.2.1. The combination of the GC with different detectors makes it also a very powerful characterization technique. The FID (flame ionization detector) is the most widely used detector for GC because of its low noise, high sensitivity and large linear response range. The current produced by ions and electrons during the pyrolysis of the sample (using air and O₂) is monitored with high impedance picoammeter and provides an indication of the number of atoms entering the detector that can be reduced, so it is generally considered *“a mass-sensitive rather than a concentration-sensitive device”*.^[101] Other detectors normally coupled with GC are the thermal conductivity detector (TCD), the electron-capture detector (ECD)- selectively responding to halogen containing organic compounds-, the thermionic detector - selective toward organic compounds containing phosphorus and nitrogen-, the photoionization detector (PID), the atomic emission detector (AED), and other analytical techniques such as mass spectrometry (MS) and Fourier transform infrared spectroscopy (FTIR).^[101]

2.2 Hyphenated techniques for the different applications

In this section the instrumental arrangements for the different applications investigated are presented. According to the need of each topic of interest, the instruments reported in section 2.1 were coupled together. Speciation studies for siloxanes in biogas were performed by hyphenating GC and ICP-MS in comparison with other classical detectors, such as GC-FID. An initial introduction of the main features of these techniques is hereby presented. It follows an extensive explanation on the RDD-SMPS-ICP-MS coupling and their operating conditions, with a particular care on the combination with the three different aerosol sources already introduced, i.e. an aerosol generator, a thermogravimetric analyzer and a tubular furnace. The coupling with the TGA is considered not only in the frame of aerosol generation during thermal processes but especially as calibration strategy of the RDD-SMPS-ICP-MS. Once the quantification strategy was proven to be successful, the same combination of instruments was employed to test the resolving power of the technique in heterogeneous matrices and to quantify the emitted metal compounds.

Combustion studies were performed using a tubular furnace as a lab-scale incinerator. In some experiments the aerosol generator was connected to the furnace in order to study the behavior of the generated particles during combustion processes. The analysis focused in particular on the release of primary and secondary nanoparticles during combustion of waste wood. The resolving power of RDD-SMPS-ICP-MS was therefore tested also in real combustion experiment and the calibration strategy applied to obtain not only qualitative but also quantitative information.

2.2.1 GC-ICP-MS/FID¹

In speciation analysis, a GC can be coupled to ICP-MS to separate and detect volatile compounds.^[102] A single organic compound of a class with similar properties is first separated in

the chromatographic column (based on their retention time) and later introduce into ICP-MS for the elemental determination of a specific isotope of interest.

2.2.1.1 Coupling concept

The GC-ICP-MS/FID experimental setup used in this thesis consists of a gas chromatograph GC 7890A with an FID, additionally hyphenated to an ICP-MS 7700x series. All instruments were provided by Agilent Technology (Germany). The GC 7890A was equipped with a 7693A automatic sampler, a split/splitless injector at the front inlet, and an FID detector operating with a mixture of air and hydrogen. The interface connecting the GC with the ICP-MS is a heated line providing an efficient transport of the high-boiling compounds thanks to passivation of the transfer line material (using Sulfinert™) and to the elevated heating temperatures, up to 300°C till the tip of the ICP-MS injector. A schematic of the setup is presented in Figure 2.2-1. The 7700x ICP-MS is equipped with an Octopole Reaction System (ORS, 3rd generation) with an improved design for increased ion focusing and collision efficiency, and the possibility of using a mixture of different collision and reactive gases (later proven to be fundamental to achieve lower LOD and LOQ and a stable background). In the case of ICP-MS, the sensitivity is rather linked to the Si content in the siloxane compound, while that of the FID, instead, varies based on the combustion efficiency of the organic compound, which depends on the chemical structure and bonding characteristic of the compound itself. The optimization of the oven temperature program for GC-FID and the GC-ICP-MS method development was performed by connecting only a single column to the respective detector. For the analysis of biogas samples, the two detectors (FID and ICP-MS) were run in parallel by connecting two 5% phenyl methyl siloxane stationary phase columns (HP-5, 19091J-413, 30 m × 0.320 mm, 0.25 µm film thickness, J&W Agilent column) through the same inlet with a 2-holes ferrule (G/V ferrule, 1/16" × 0.4 mm, GV1624, 382438, BGB Analytik AG). The instruments were controlled by means of the software provided by the producer: OPENLAB for GC-FID and Mass Hunter for ICP-MS.

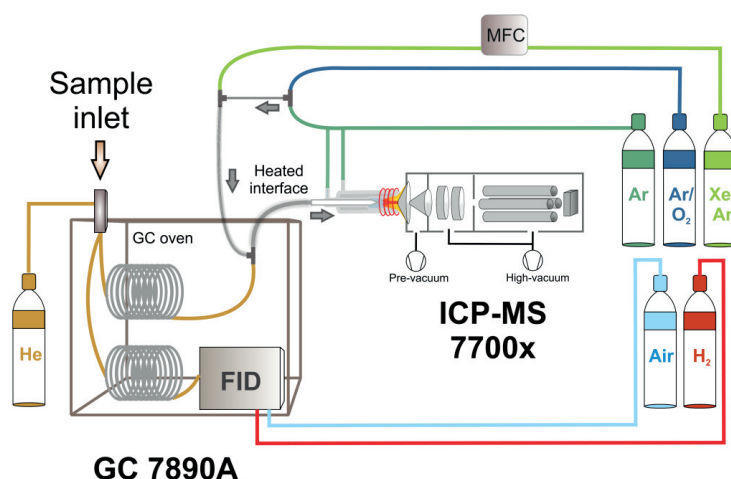


Figure 2.2-1 Schematic of the experimental setup combining GC-FID and GC-ICP-MS, each connected to a separate column from the same inlet (split 50:50). Legend: GC = gas chromatographer; FID = flame ionization detector; MFC = mass flow controller; ICP-MS= inductively coupled plasma mass spectrometry.

2.2.1.2 Data analysis

The data of GC-ICP-MS and GC-FID were treated using two different integration methods, represented in Figure 2.2-2. Calculations on GC-ICP-MS peaks were done with *Method 1*, following the same principles of MassHunter software (Agilent Technologies). The peak is initially refined using a smoothing function; once the peak apex has been defined, an average of n points around the peak height is calculated. The computation done with MassHunter is considering only 3 points, while in this thesis an average of 9 points was considered. *Method 2* is based, instead, on the OPENLAB software normally used for FID peak integration. In this second case over 68 points are selected starting from the two baseline points. The two methods will be discussed and compared more in detail in chapter 3, where the analytical challenges linked to the coupling and simultaneous use of GC-FID and GC-ICP-MS are also addressed.

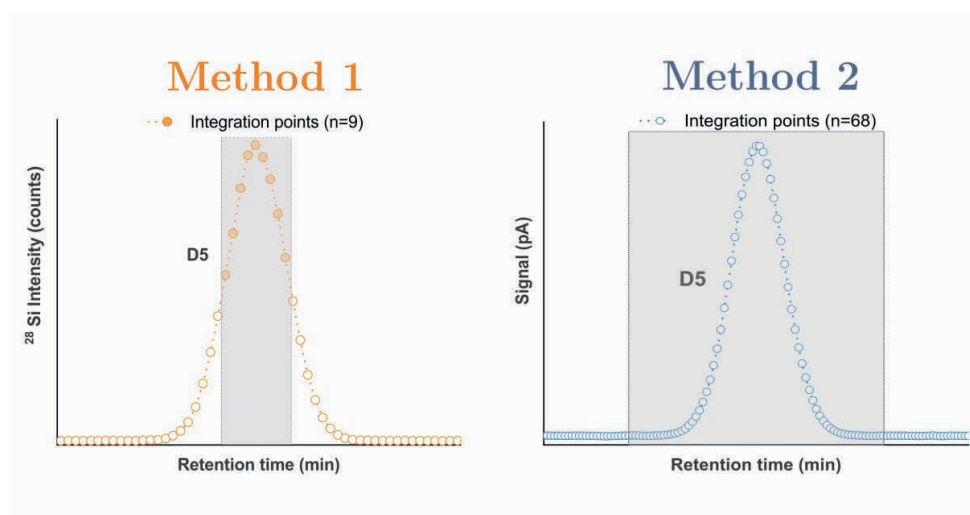


Figure 2.2-2 Integration methods used for the measured ^{28}Si peak of D5 (siloxane compound).

2.2.2 RDD-SMPS-ICP-MS ^{II}

The hyphenation of RDD-SMPS-ICP-MS allowed performing online sampling with simultaneous size-resolved and elemental analysis on the aerosol generated. The working principle of the three different units was separately explained in the section 2.1, thus this section focuses only on the technical details related to their coupling.

2.2.2.1 Coupling concept

In order to couple RDD, SMPS and ICP-MS some modifications in the instrumental arrangements are needed. The coupling concept was already presented first by Hess et al.[103] Nevertheless, it is relevant to briefly summarize the main coupling steps in this section.

The different instrumental parts are connected as shown in Figure 2.2-3, using conductive tubing with inner/outer diameters 6.0/12.0 mm (carbon impregnated silicone tubing), particularly suitable to minimize deposition and losses of the particles.

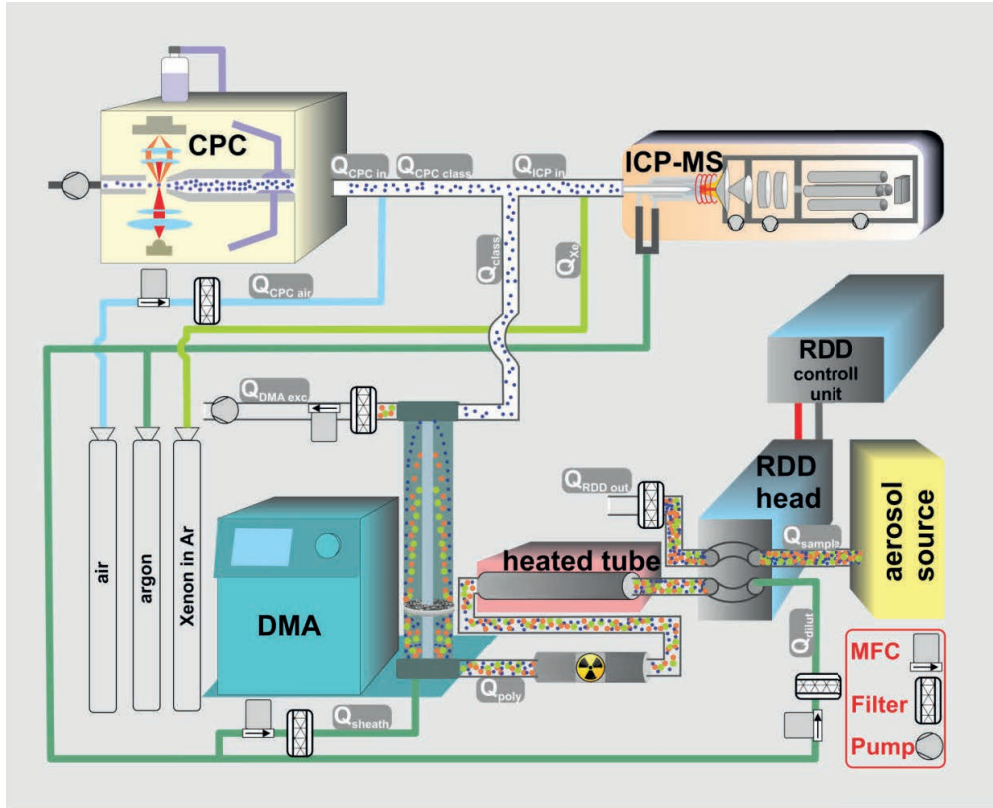


Figure 2.2-3 Coupling strategy for the different instrumental parts in RDD-SMPS-ICPMS setup. Nomenclature: Q_{sample} : flow from the aerosol generator; Q_{dilut} : RDD dilution argon flow; $Q_{\text{RDD out}}$: raw aerosol flow out of the RDD; Q_{poly} : flow of diluted polydisperse aerosol at the DMA inlet; Q_{sheath} : DMA sheath gas flow; Q_{class} : flow of classified aerosol at the DMA outlet; $Q_{\text{DMA exc}}$: DMA gas excess flow; $Q_{\text{CPC class}}$: fraction of Q_{class} guided into the CPC; $Q_{\text{CPC air}}$: additional air flow for the CPC; $Q_{\text{CPC in}}$: total flow entering the CPC; $Q_{\text{ICP in}}$: fraction of Q_{class} guided into the ICPMS; Q_{Xe} : xenon flow; MFC: mass flow controller.

The generated aerosol is transferred first to the RDD where thanks to the use of a mass flow controller (MFC) and a filter, e.g. a High-Efficiency Particulate Air filter (HEPA), a defined flow of particle-free dilution argon is used for the quenching and the dilution. Argon is used as dilution gas instead of air, because of the low air tolerance of the ICP-MS. An impactor with a cut-off diameter of 1 μm was added at the inlet of the RDD control unit to avoid further transport of larger particle. The diluted aerosol can be maintained at temperature as high as 350°C in the evaporation tube. It is advisable for safety reason to add another (HEPA) filter at the RDD outlet for the excess raw gas ($Q_{\text{RDD out}}$). The performance of all the filters in use can be checked from time to time by using the CPC. After passing through the radioactive source, the aerosol is finally introduced into the DMA where the particle size classification takes place. On one hand, another MFC in series with a filter were used to adjust the sheath gas flow (Q_{sheath}) introduced to the DMA, that will act as main gas stream in which the particles are selected. On the other hand, for adjusting the DMA excess gas flow ($Q_{\text{DMA exc}}$) a vacuum has to be applied using a pump in series with a filter and an MFC, at the DMA outlet. The classified aerosol at the DMA outlet is split in two fractions, where one is guided towards

the CPC and the other one towards the ICP-MS (Fig. 2.2-3). The flow split at the DMA outlet is done such that 30% of the aerosol is directed to the CPC, the other 70% to the ICP-MS. CPC actively aspirates a flow defined by a critical orifice and an external pump, which is about 1 L/min. CPC flow fraction of the classified aerosol ($Q_{\text{CPC class}}$) is tuned at preference by adding a particle-free air flow, i.e. the filtered air ($Q_{\text{CPC air}}$), with another MFC equipped with a upstream filter. As a result, the classified flow rate at the ICP inlet ($Q_{\text{ICP in}}$) is the difference between the flow rate at the DMA outlet (Q_{class}) and $Q_{\text{CPC class}}$.

2.2.2.2 Measurement protocol

Flow adjustment. To achieve a stable operation of the RDD-SMPS-ICP-MS setup, all the gas and aerosol flows should be adjusted carefully as described below. Nevertheless, before tuning the SMPS-ICP-MS parameters, the flows used for the aerosol sources must be set. In this section, an example is given of a set of parameter values for adjusting the RDD, SMPS and ICP-MS. Another set of parameters is possible; but the procedure will however remain the same. The flow abbreviations used are listed in the caption of Figure 2.2-3.

In the following steps the use of a primary flow calibrator (Giliblator-2, Sensidyne) is recommended, to measure the different gas and aerosol flows before starting every measurement:

- First set the argon sheath flow at the corresponding DMA inlet to 3 L/min.
- Set the temperature of the RDD heating block to 80 °C, and that of the evaporation tube to 350 °C. As soon as these temperatures are reached, set the dilution factor of the RDD to the desired value by adjusting the disk rotation speed manually. For instance, a 100% rotating speed corresponds to a dilution factor of 14.9.
- Adjust the MFC of the argon dilution flow manually in order to maintain Q_{sample} (at the RDD outlet) at 0.6 L/min. The ratio 0.6/3 of the sheath gas to the sample gas is chosen to cover a particle size ranging from about 14 to about 334 nm.
- Adjust $Q_{\text{DMA exc}}$ at the DMA outlet to maintain Q_{class} at 0.6 L/min (i.e. at the same value as Q_{poly} at the DMA inlet).
- Adjust the MFC of the filtered air at the CPC inlet, to set the amount of compressed air directed into the CPC to $Q_{\text{CPC air}} = 0.18$ L/min. This corresponds to 30% of Q_{class} .
- Measure $Q_{\text{ICP class}}$ at the ICP-MS inlet (e.g. with the flow calibrator). This should be 0.42 L/min, i.e. 70% of Q_{class} . Slight change of this flow can be corrected by fine-tuning the MFC of the DMA excess gas again.

SMPS software settings. The ambient temperature and pressure are used to calculate the dynamic viscosity and the mean free path of argon.[104] Once this two values are given as an input, the up and down scan durations of the DMA scanning cycle are set to 150 s and 30 s (i.e. 1 DMA cycle = 1 scan = 180 s). The DMA maximum voltage is limited to 4.5 kV to cover the PSD interval ranging from about 14 to about 334 nm. A voltage maximum of 10 kV is normally used in air-operated SMPS. Due to the lower dielectric strength of argon relative to that of air, the limit should be set

lower in this application, since otherwise electric arcing would occur, leading to instrument damage and signal errors.

ICP-MS settings. In order to introduce the dry aerosol directly into the ICP-MS, the conventional introduction system of liquid samples has to be removed. An additional conductive tube is added between the DMA outlet and the ICP-MS inlet by using a T connector. This tube is used for xenon (Xe), which is added to sample flow, to optimize the ICP-MS plasma prior to each measurement and to control the plasma stability during the measurement.

Table 2-1 Typical settings of the main ICP-MS settings used for the RDD-SMPS-ICP-MS measurement of aerosol.

Parameter	Value	To be tuned
Power	1350 W	yes
ICP-MS dilution gas (argon)	0.58 L min ⁻¹	Yes
Sampling depth	8 mm	Yes
Collision gas (ORS)	2 ml min ⁻¹	Yes (for the same set of measurements don't change this value after tuning it)
Integration time	0.2 s per isotope	Yes, if the ICP-MS time resolution should be changed
Xe flow	4 ml min ⁻¹	No (to keep the same ICP-MS sensitivity)

The Xe flow with a concentration of about 100 ppmv in an argon matrix is kept constant for all measurements (e.g. at 4 mL min⁻¹) to tune the other parameters in the ICP-MS software, including ICP dilution gas and sampling depth, to achieve a fixed Xe intensity. The main ICP-MS tuning parameters are listed in Table 2-1. The parameters to be tuned prior to each measurement are indicated in the last column.

2.2.2.3 Data analysis

The ICP-MS measures the ion intensity per unit time (unit: count per second, or cps) for each m/z. This intensity is proportional to the analyte mass. SMPS data represent the number-weighted PSD of classified aerosol (PSD_n) entering the DMA (number of particles × cm⁻³), based on the number concentrations determined by the CPC behind the DMA. To compare both ICP-MS and SMPS signals, the volume-weighted PSD (PSD_v) must be calculated.

The raw signal intensities versus time for each m/z from the ICP-MS data was exported, as well as the PSD_n – determined by the SMPS software – as a function of the particle diameter (dp). From the SMPS raw data, the particle diameter and the corresponding scanning time are derived in order to correlate the ICP-MS measurement time with the particle diameter. The SMPS software must consider that the aerosol flow at the DMA outlet is split, and only 30% of the classified particles

reach the CPC. This can be achieved by multiplying the counting efficiency values – stored in a separate table as type-specific CPC characteristics – by a factor of 0.3. Since the desired information is not primarily the particle concentration between RDD and DMA, but that at the RDD inlet, the measured concentrations are multiplied by the RDD dilution factor.

To calculate volume-weighted data from the original number-weighted SMPS data, the recorded concentrations of PSD_n is multiplied by the volume $V(dp)$ of the measured particles, assuming a spherical morphology.[51] The ICP-MS net signal is calculated by subtracting the background signal from the raw ion signal for each isotope. Then, the net signal is multiplied by the inverse single charge probability $1/p+1(dp)$ to get the corrected ICP intensity, which is approximately proportional to the concentration at the DMA inlet and hence at the RDD inlet (assuming no particle losses between RDD inlet and ICP-MS or CPC inlets). The probability of particles to carry one elemental positive charge is calculated by using the Wiedensohler approximation [105]. For the SMPS data processed by the SMPS software, the correction for this charge probability is normally implemented in the software. For a given SMPS scan, the SMPS particle concentration or the ICP-MS intensity is plotted as a function of particle diameter in an x-y diagram. In the case of a steady-state aerosol, the same type of diagram is used to present the concentration or intensity averaged over several scans. 2D surface or 3D diagrams are chosen to plot the SMPS concentration or ICP-MS intensity as functions of diameter and time. In the case of thermal processes, if a temperature program is used, the time can be substituted by the corresponding temperature values or shown as a separated curve with a secondary y-axis and linked x-axis. The calculations needed for ICPMS and SMPS data to make such plots can be automated by implementing macros in Excel or by using calculation software like MATLAB or Igor Pro, which allows obtaining robust final results in a short time.

2.2.3 Different aerosol sources coupled with RDD-SMPS-ICP-MS

The RDD-SMPS-ICP-MS setup was further coupled with all the aerosol sources enlisted in section 2.1.1 were tested:

- The aerosol generator was used to introduce a dried aerosol from a salt solution or a particle suspension into the RDD-SMP-ICP-Ms setup.
- The TGA was used to model analysis of emissions from thermal processes.
- The tubular furnace was employed in combination with the aerosol generator to study the effect of reducing and oxidizing atmosphere on the PSD of ZnO nanoparticles.

2.2.3.1 AG-RDD-SMPS-ICP-MS^{II}

The aerosol generator introduced in section 2.1.1.1 was used to generate a dried aerosol from the salt solution or the particle suspension. First, the suspension or solution was filled into the bottle and mounted on the aerosol generator. The compressed air valve of the aerosol generator was set slightly above 1 bar. In this case the provided gas was not air but argon, because of the low tolerance of ICP-

MS to air. The resulting aerosol flow was adjusted to be about 1 L min^{-1} behind the diffusion drier. Finally, the outlet of the drier was connected to the RDD inlet. The disk rotation speed was set to zero to acquire blank signals (e.g. for 2 scans or 6 min) and was then set the speed back to its original value to start the measurement.

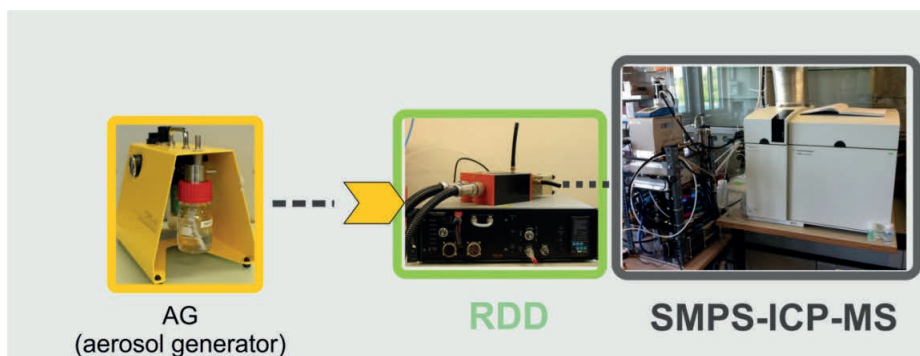


Figure 2.2-4 Schematic of the coupling between an aerosol generator and the RDD-SMPS-ICP-MS setup.

2.2.3.2 TGA-RDD-SMPS-ICP-MS^{II, III}

As an example for applying the RDD-SMPS-ICPMS in measuring emissions from thermal processes, a copper chloride (CuCl_2) sample was analyzed into a TGA. A desired temperature program was used to simulate the thermal process, with a steady-state temperature at 25°C for 18 min and a fast increase to reach the stable temperature of 450°C for other 15 minutes. An alumina crucible with maximum capacity of $700 \mu\text{l}$ was used to introduce 50 mg of CuCl_2 powder.

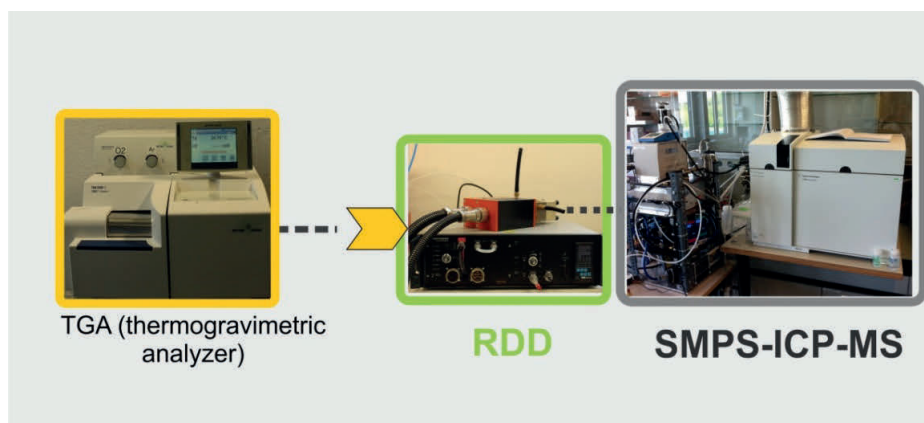


Figure 2.2-5 Schematic of the coupling between a TGA and RDD-SMPS-ICP-MS

Before starting the acquisition the flows through the TGA have to be carefully adjusted. The reactive gas (e.g. O_2) is mixed with argon to the appropriate ratio in order to prevent nucleation and condensation and it was adjusted to about 20 mL min^{-1} with an MFC. The flow of the protective gas (argon) was set instead to about 80 mL min^{-1} . At the TGA outlet, an argon flow of about 900 mL min^{-1} was added to get a total flow of about 1 L min^{-1} (i.e. the sum of the flows of O_2 , protective argon and

added argon). If the RDD pump is used, the MFC controlling the dilution Ar was adjusted to reach the required flow. The SMPS and ICP-MS acquisition time were set to cover the desired total duration of the aerosol measurement (e.g., for 10 SPMS scans, the ICP-MS acquisition time was set to at least 30 min). After setting the gas flows and the SMPS and the ICP-MS parameters, the two instruments were started manually at the same time. The SMPS and ICP-MS blank signals were acquired at 25 °C for 18 min (6 scans).

The same combination of instrument was also used also on ZnCl_2 powders and several metal oxide powders (i.e. ZnO , CuO , CdO , PbO), with a slight different configuration that the represented one in Figure 2.2-5. The ICP-MS was directly connected in series with the RDD instead of the SMPS to perform the calibration of the RDD-ICP-MS coupling, as it is explained in Ch. 5.

2.2.3.3 (AG)- Tubular furnace-RDD-SMPS-ICP-MS^{II}

As explained in section 2.2.2.1, the AG was used to generate ZnO dried particles from a prepared suspension. In order to study the effect of reducing and oxidizing atmosphere on the PSD of ZnO nanoparticles, a total flow of 1.5 L min^{-1} was introduced from the AG to the tubular furnace (Figure 2.2-6) by adding 50 mL min^{-1} flow of oxygen (or hydrogen) and additional dilution argon. At the outlet of the furnace, the aerosol was diluted with a mixture of Air/Ar, introduced into the RDD and sequentially to the SMPS-ICP-MS. A stream of ZnO dried particles was also generated and introduced in the tubular furnace during the thermal treatment of solid samples (e.g. sawdust and metal oxide/chlorides powders).

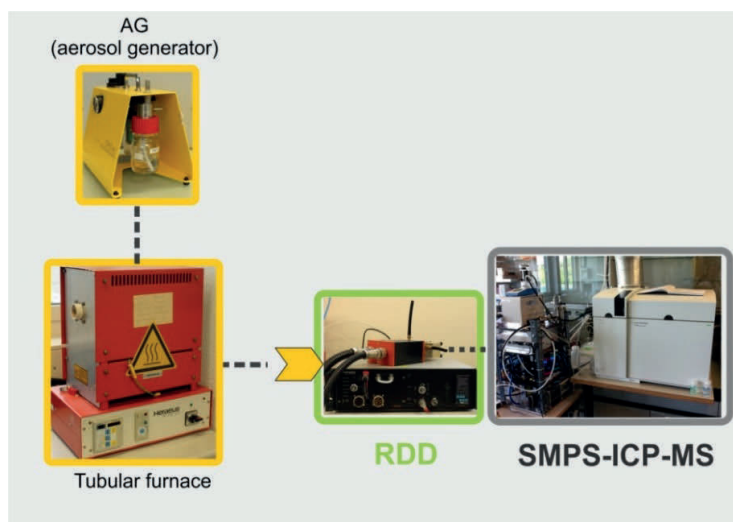


Figure 2.2-6 Schematic of the coupling among AG, tubular furnace and RDD-SMPS-ICP-MS

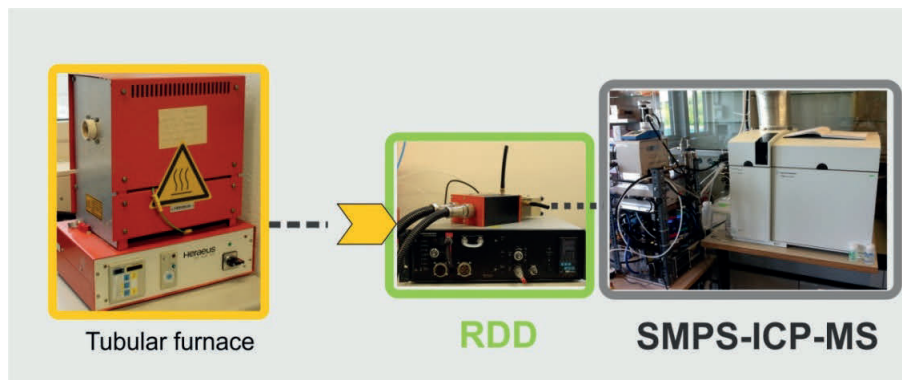


Figure 2.2-7 Schematic of the coupling between the tubular furnace and the RDD-SMPS-ICP-MS

For online measurements of nano-objects formed in combustion processes, only the tubular furnace was used to thermally treat the solid samples (i.e. sawdust, ZnO impregnated sawdust), as represented in the schematic in Figure 2.2-7.

2.3 Materials

2.3.1 Speciation study with GC-ICP-MS/FID ¹

2.3.1.1 Chemicals

Stock solutions with a mixture of linear and cyclic siloxane compounds were prepared using 2-propanol as solvent (20842.330, normapur, lot# 18A294016, VWR Chemicals) by adding single standards of hexamethyldisiloxane (L2, 101696070, lot # BCBQ3284V, $\geq 98.5\%$, Sigma-Aldrich), octamethyltrisiloxane (L3, 1002439965, lot # MKCC5212, $\geq 98\%$, Sigma-Aldrich), hexamethylcyclotrisiloxane (D3, 101600743, lot # STBF4369V, $\geq 98\%$, Sigma-Aldrich), octamethylcyclotetrasiloxane (D4, 101694668, lot # BCBP8413V, $\geq 98\%$, Sigma-Aldrich), decamethylcyclopentasiloxane (D5, 1001969542, lot # MKBR6099V, $\geq 97\%$, Sigma-Aldrich), dodecamethylcyclohexasiloxane (D6, 1002567912, lot # MKBT1945V, $\geq 95\%$, Sigma-Aldrich). The concentrations of the two stock solutions and the calibration standard solutions prepared are reported in tables A.1.1-1, A.1.1-2 and A.1.1-3 in Appendix A.

2.3.1.2 Samples

Using the LQ four samples were taken over a two-day period at a biogas production plant in Switzerland. At this plant, biogas is produced independently in three digesters. Two mesophilic digesters, operated at 42°C , process in total 45'000 tonnes/year of substrates containing manure as well as waste from the food industry. One thermophilic digester, operated at 55°C , processes 16'000 tonnes/year of green waste, food waste, and agricultural waste (including manure and crop products). The biogas produced at all three digesters is combined and passed through an activated carbon filter to remove H_2S . During the biogas sampling campaign, flowrates of sampled biogas from 830 to 1092 $\text{ml}_\text{N} \text{ min}^{-1}$ and liquid solvent flowrates from 0.7 to 1.7 ml min^{-1} were used, corresponding to gas-to-

liquid ratios of 492 to 1645, respectively. The choice of different values relies to some extent on fluctuations of pressure in the biogas stream that could not be controlled. Therefore, the gas-to-liquid values were adjusted accordingly to maintain comparable gas-to-liquid partitioning throughout the different measurements.

Two biogas samples *Manure1* and *Manure2* were taken at the outlet of each of the two mesophilic digesters using a gas-to-liquid ratio of 845 and 492, respectively. The other two samples *MixUntreated* and *MixTreated* were collected in the combined biogas flow from the three digesters, before and after the activated carbon filter, using a gas-to-liquid ratio of 1645 and 1361, respectively. For the same sampling position and conditions, two samples were measured in two replicates each. The samples were stored in a chilled and dark environment and analyzed in the week following the sampling campaign.

2.3.2 Preliminary studies with RDD-SMPS-ICP-MS ^{II}

2.3.2.1 Chemicals

A commercial zinc oxide nanopowder (5810MR, 1314-13-2, AUER-REMY), was used to prepare suspensions of ZnO NPs. The average particle size provided by the manufacturer was verified with SEM analysis. Characterizations and further specifications of the powder are reported in Appendix A in Figures A.2.1-1 and A.2.1-2 and Table A.2.1-1. For the colloidal stability of ZnO particles dispersion, a solution 0.1% wt of Poly Acrylic Acid (PAA, MW2000, 50% wt H₂O, electronic grade, 535931-100G, lot # 02115HIV, Sigma-Aldrich) was required.

2.3.2.2 Samples

For the first measurement, an aqueous sodium chloride (NaCl, Merck, for analysis EMSURE®, 7647-14-5, 106404) solution was prepared with a concentration of 200 µg/mL while for the second measurement a suspension 0.3% wt of zinc oxide (Suspension A) was prepared by dispersing 333.3 mg of the commercial powder in 100 g of dispersant solution. The second suspension with a concentration of 600 µg mL⁻¹ of ZnO (suspension B) was prepared by dilution of suspension A with the same dispersant solution, under constant magnetic stirring and ultrasonic bath for six minutes. Finally, for the thermal treatment experiments CuCl₂ (Merck, for analysis EMSURE®, 10125-13-0) and ZnO (Merck, reagent grade ≥ 99%, 8849.0100203, K16151449) powders were used.

2.3.3 RDD-SMPS-ICP-MS calibration strategy and resolving power in heterogeneous matrices ^{II, III}

The calibration of the setup RDD-SMPS-ICP-MS was performed using anhydrous ZnCl₂ (Sigma-Aldrich, reagent grade ≥98%, 793523-100G, lot # MKCC7426) and CdCl₂ powders (Fluka, reagent grade ≥ 99%, 20899, GA10523). ZnO (Merck, reagent grade ≥ 99%, 8849.0100203, lot # K16151449). The evaporation experiments included a mixture of several commercial powders: PbO (Fluka, reagent grade ≥ 99%, 15338, GA2053), CdO (Merck, reagent grade ≥ 99%, 2015.0100, 212 K14082415), CuO (Merck, reagent grade ≥ 99%, 1.02766.0100, TP995866930), ZnO (Merck, reagent grade ≥ 99%,

8849.0100203, K16151449) and $\text{CaCl}_2 \cdot 2\text{H}_2\text{O}$ (Merck, reagent grade $\geq 99\%$, 111TA106282). The samples were introduced into the TGA using an alumina crucible with a maximum capacity of 700 μL .

2.3.4 Combustion experiments ^{IV, V}

2.3.4.1 Chemicals

Nitric acid (HNO_3 , 65%, Z0346841519, 1.00441.1000, Merck) and hydrochloric acid HCl (30%, Z0344318516, 1.00318.1000, Merck), were used to dissolve the deposited material and to clean the liner and the quartz tube of the tubular furnace after each experiment. The resulting solutions were further diluted and analyzed by ICP-MS. Zn calibration solutions for analysis of the collected samples were prepared by the dilution of Zn standard solution 1000 $\mu\text{g ml}^{-1}$ (Merck, 1.19806.0100) with ultrapure water (MilliQ, 18.2 $\text{M}\Omega\text{-cm}$).

2.3.4.2 Samples

Beechwood sawdust. The samples of beech wood were collected in the forest area of Villigen in March 2012 and further characterized by Bahrle.[106] The multi-element analysis was performed in ICP-MS after microwave assisted acid digestion with HNO_3 . The results are reported in Appendix A, in Tables A.4.1-1 and A.4.1-2. Multi-element calibration solutions were prepared by dilution of a commercial multi-elemental standard solution (Bernd Kraft, 10931.2000, batch-no.: 1530569). Non-treated samples and samples impregnated with ZnO suspension were used for incineration experiments.

Beechwood sawdust impregnated with ZnO suspension. In order to obtain a synthetic nano-waste sample, 2 g of beech wood sawdust were impregnated with zinc oxide suspension A (0.3% wt), already presented in section 2.3.1.2. The sawdust samples were kept in contact with 15 ml of ZnO suspension for three hours under magnetic stirring. After a drying step of 90 minutes at 105°C in a thermobalance (PM100, LP-16, Mettler-Toledo), the samples were carefully removed from the Petri capsule. In every experiment, an amount of 400 mg of the prepared batch was transferred into a boat-shaped alumina crucible and introduced into the tubular furnace for the thermal treatment experiments.[107]

2.4 Additional off-line characterization techniques

The off-line techniques explained in this section were mainly used to characterize the ZnO suspension introduced in section 2.3.1.2 or to assess the size and morphology of the generated nanoparticles. The sampling of the size-selected nanoparticles using an in-house-built collection cell is also presented.

2.4.1 Nanozetasizer

The Zetasizer Nano series (Malvern) performs size measurements using Dynamic Light Scattering (DLS) (also known as PCS - Photon Correlation Spectroscopy) that measures Brownian motion and relates this to the size of the particles. The relationship between the size of a particle and its speed due to Brownian motion is defined in the Stokes-Einstein equation.

2.4.2 X-ray disc centrifuge

In the x-ray disc centrifuge (BI-XDC, Brookhaven) the X-rays absorption is proportional to mass-volume. Normally concentrated suspension are needed in order to have an accurate analysis, considering a reasonably quick duration time of the measurement (20 min) and a size range from 10 nm to 100 μm . With the use of Stokes' Law is possible to correlate the settling phenomena with the actual size of the particles.

2.4.3 Scanning Electron Microscopy (SEM) and Transmission Electron Microscopy (TEM)

Electron microscopy techniques, like Scanning Electron Microscopy (SEM) and Transmission Electron Microscopy (TEM), are very powerful tools for the characterization of a very wide range of materials. In SEM and TEM, characteristic of the sample related to its morphology, structure and composition can be analyzed from micrometer (μm) to nanometer (nm) and down to atomistic (\AA) scale. From the interaction of the electron beam with the sample and depending on the specific emission volumes within the sample, different types of signals are obtained. These signals include secondary electrons, backscattered electrons, transmitted electrons, diffracted electrons, characteristic X-rays, and other photons of various energies (shown also in Fig. 2.4-1). [54]

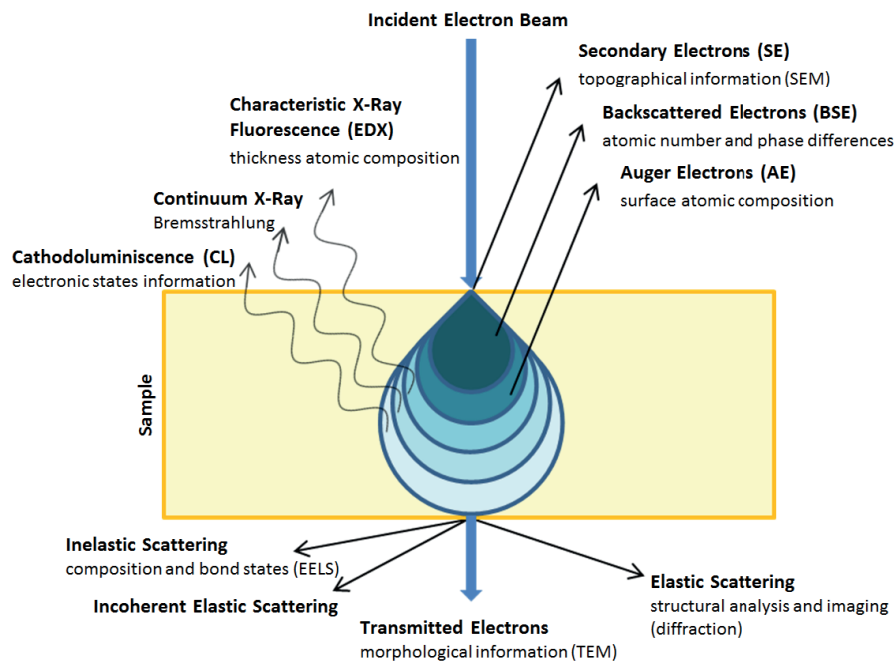


Figure 2.4-1 Schematic of the interaction between the electron beam and a sample. Adapted from reference [108]

Imaging in electron microscopy is mainly used to investigate the particle size and the morphology of the sample under analysis. In SEM, the secondary electrons and the backscattered electrons are mainly probed, while in TEM the transmitted electrons are used to obtain 3D-like and 2D-like imag-

es, respectively. Energy Dispersive X-ray Spectroscopy (EDXS) in either SEM or TEM samples the characteristic X-rays of the atoms in order to clarify the chemical composition of the specimen (e.g. qualitative and quantitative analysis of the composition of the sample). From the spatial distribution of the diffracted electrons in TEM (known as an electron diffraction pattern) useful information about the crystallographic structure of the material can be obtained. [108]

2.4.3.1 Sampling of size-selected nanoparticles using a collection cell

In order to determine exact morphology and size of the NPs generated during the experiments, a sampling technique was implemented for following TEM analysis. The size-selected particles from 13 to 340 nm were collected at the outlet of the DMA with an aspiration EM grid sampler, built in-house at PSI, which design was based on the MPS sampling system described by R'mili et al [109]. It is composed of two parts, the male and female connectors shown in Figure 2.4-2. An O-ring ensures the TEM grid in position once the two parts are closed. The aerosol flow is aspirated with a membrane pump from the Q_{class} at the outlet of the DMA, first through the female connector and then throughout the used TEM grid via the holes of its membrane to the male part connected to the inlet point of the pump, where the gas flow is controlled using a needle valve. The overall Q_{class} is splitted in two fractions with a Y-connector, since only 0.3 L min^{-1} is actually sampled, while the remaining 0.120 L min^{-1} is directed to the exhaust vent.



Figure 2.4-2 Picture representing the particle collection cell, the membrane pump used to guarantee a flow-through of 3 L min^{-1} , and the male and female connectors with the position of the TEM grid.

A commercial TEM grid “Quantifoil 1.2/1.3”, Cu 400 mesh was chosen, taking into account the following advantages:

- i. holes diameter, the smallest among the available products on the market to allow an efficient sampling;
- ii. high number of mesh (Figure 2.4-3 a), with the needed resistance to the gas flow to avoid damage of the carbon membrane under pressure.
- iii. well-defined structure (shape and size of the holes), that shows reduced standard deviation ($<10\%$) compared to a less homogenous one, such as the Holey type (Fig.2.4-3 b and c)

In the work presented by R'mili et al [109], the efficiency of deposition of different size-class of particles was compared between experimental results and a model that assume a similar behavior than in a flow-through porous membrane. The deposition mechanisms is influenced mainly by impaction for

particles above 30 nm (deposition on membrane surface), while surface diffusion is prevalent on particles below 30 nm (mainly collected on the holes border).[109]

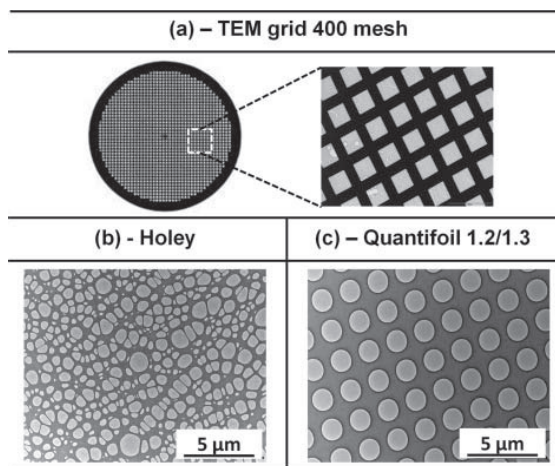


Figure 2.4-3 Examples of TEM porous grids with 400 mesh Cu grid (a) and carbon foil “Holey” (b) and a “Quantifoil” type (c). Figure adapted from reference [109].

The particles were filtered through the TEM grid after size-selection at the outlet of DMA from the tube normally directed to the ICP-MS, with a flow rate of 0.3 L min^{-1} (Figure 2.4-4). The particles were collected in separate replicates of the experiments during which the ICP-MS detection was not included. The samples were later analyzed with a JEOL JEM-2010 transmission electron microscope (200 kV, point resolution of 0.25 nm), to investigate particle size and morphology, while the chemical composition was clarified through the use of EDXS and electron diffraction pattern of the crystalline material (whenever possible).

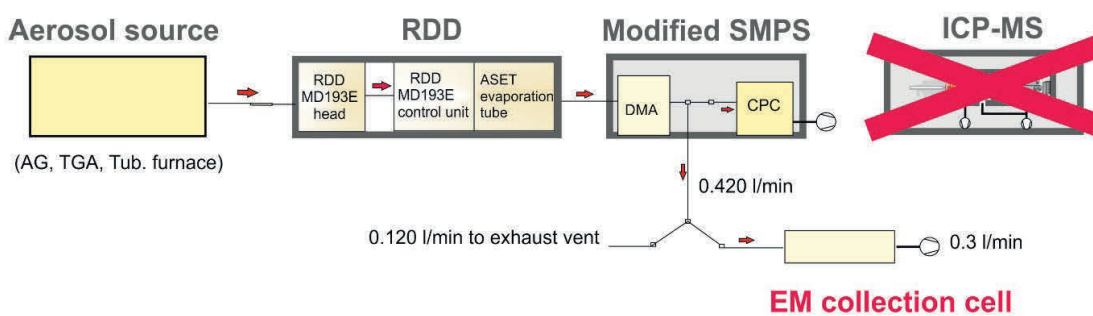
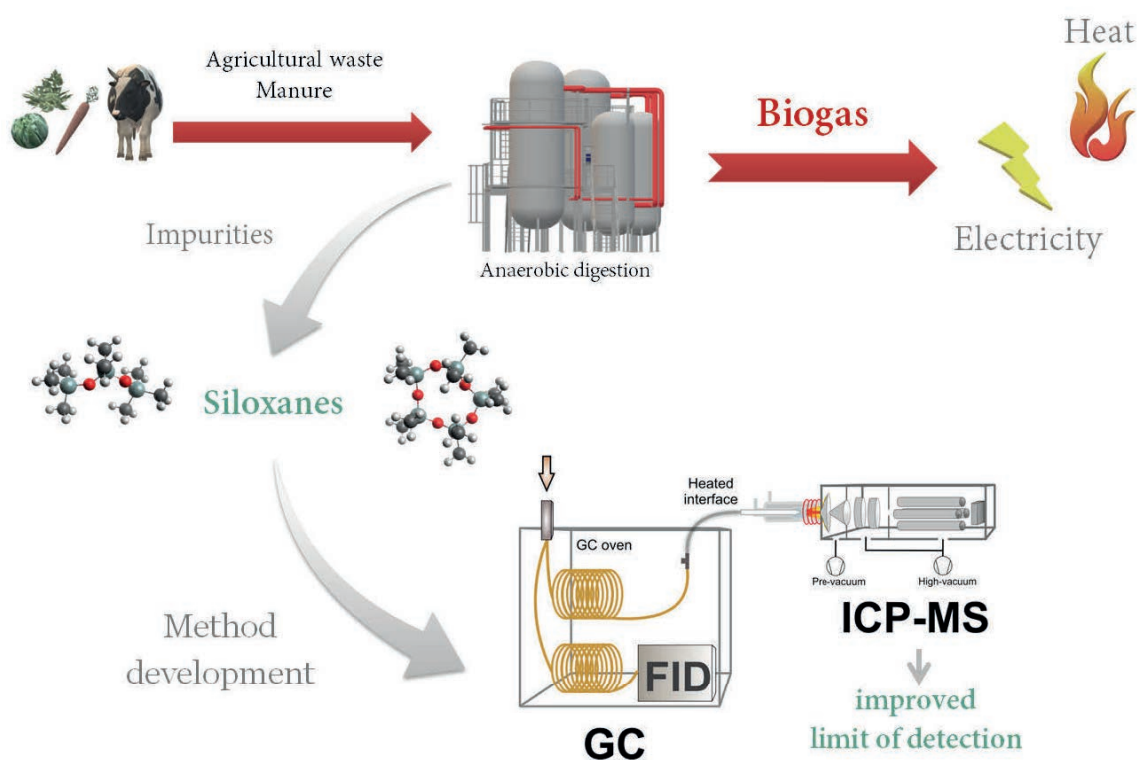


Figure 2.4-4 Schematic of the sampling point of size-selected particles with the collection cell. The scheme it is valid for all the different aerosol sources use in the frame of this dissertation.

Chapter 3 Speciation analysis with GC-ICP-MS/FID of siloxane compounds in biogas



Material from this chapter has been published in:

- (I) Debora Foppiano, Mohamed Tarik, Jörg Schneebeli, Adelaide Calbry- Muzyka, Serge Biollaz and Christian Ludwig, Siloxanes compounds in biogas from manure and agricultural waste: Method development and Speciation analysis with GC-ICP-MS/FID., **2018**, in peer-review.

The author carried out the method development and the speciation analysis with GC-ICP-MS, the biogas analysis done at the CPM group laboratories at Paul Scherrer Institut (PSI), the evaluation of the GC-FID method, the coordination of the research project, as well as the compilation of the first draft of the manuscript.

A novel method for the determination of linear and cyclic siloxane compounds (L2, L3, D3, D4, D5, and D6) in biogas was developed by combining gas chromatography (GC) with two different detectors running simultaneously, a FID and an ICP-MS. Using a continuous liquid quench sampling system biogas samples were collected, from a Swiss biogas production plant processing manure and agricultural wastes. Even if significant concentrations of siloxanes are normally linked to biogas from wastewater treatment plants (WWTP) or landfill gas, also manure and agricultural waste samples showed values in the range of $0.1 \text{ mg}_{\text{Si}} \text{ Nm}^{-3}$, which would already cause severe damage to appliances such as solid oxide fuel cells (SOFC). The GC-ICP-MS method showed very good linearities for all the investigated compounds (R^2 between 0.999 and 1.000). The limits of detection and quantification (LOD and LOQ) in the gas for cyclic compounds, such as D5, would vary upon the used sampling conditions and be approximately $0.002\text{-}0.004 \text{ mg}_{\text{Si}} \text{ Nm}^{-3}$ and $0.007\text{-}0.014 \text{ mg}_{\text{Si}} \text{ Nm}^{-3}$, respectively. These LOD and LOQ values satisfy the needs of new analytical methods with improved LODs to fulfill the EURAMET (the European Association of National Metrology Institutes) requirements, which fix recommended levels for Si total amounts between 0.1 and $0.3 \text{ mg}_{\text{Si}} \text{ Nm}^{-3}$. The method was evaluated with liquid standards prepared in the same solvent used for the sampling procedure; the global mean of recoveries for D5 was $99.9 \pm 0.8\%$, with very good intraday precision ($\text{RSD} \leq 5\%$). While GC-FID showed higher detection limits and matrix effects, it could still be suitable for an initial estimation of the siloxane compounds present in the biogas, at least for D5, by following some given suggestions in the computation. Moreover, the GC-FID analysis can provide useful information also on other classes of impurities contained in the biogas, such as volatile organic compounds (VOC).

3.1 Experimental and results

3.1.1 Method development for the speciation analysis of siloxanes

Initial efforts were needed in order to find the best combination of operating conditions for the instrumental arrangement. Different column flows and split ratios were tested to achieve the highest signal to background ratio and reproducible shapes of the chromatographic peaks. The He flow (2 ml min^{-1}) was set according to the suggestion given by an Agilent open-source software, which indicates the optimum value in the operated split ratio, temperature, and pressure of the inlet. The oven temperature program was first developed with GC-FID for a mixture of siloxane compounds. The initial temperature was defined based on the elution of the solvent and the low boiling compounds. The heating rate was set to $10^\circ\text{C min}^{-1}$ in order to achieve optimal separation of the compounds and avoid overlapped peaks. Unfortunately, the method resulted in long times of analysis for one sample only (1 hour, considering at least 2 replicates for each sample). With the further prospect of analyzing samples in parallel (or solely) with GC-ICP-MS, the program runtime was significantly reduced. The minimum time of analysis found to maintain a good resolution of the siloxanes peaks was approximately 12 minutes, with a heating rate of $20^\circ\text{C min}^{-1}$ from the initial temperature at

55°C to the maximum of 200°C. Furthermore, such a short program presents the major advantage of being suitable for online measurements (e.g. of breakthrough curves for catalysts or filters).

The main operating conditions of GC 7890A, autosampler 7693 A, FID, interface and 7700x ICP-MS after optimization are summarized in Table 3-1 (additional parameters for 7700x are reported in table A.1.1.2 in appendix A).

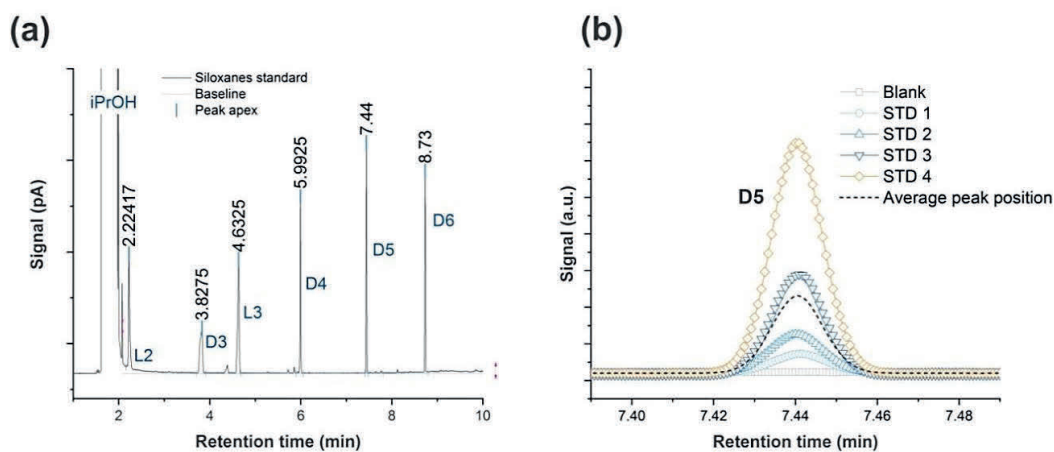
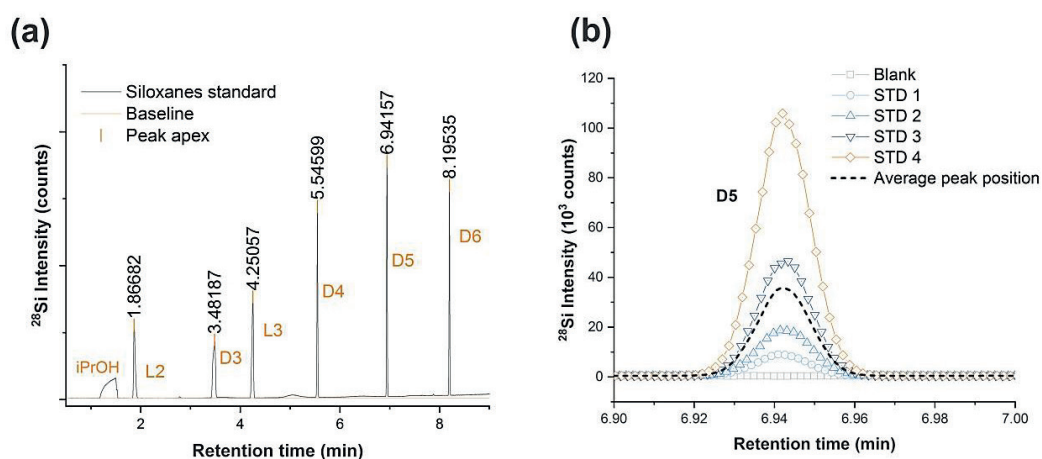
Table 3-1 Operating conditions for GC7890A, ALS 7693 A, FID detector, GC-ICP-MS interface, and 7700x ICP-MS

<i>Operating conditions</i>	<i>GC 7890A</i>
<i>Front inlet (ALS 7693 A)</i>	Syringe size: 10 µL; injection volume: 1.5 µL
<i>Split/splitless injector</i>	Split mode, split ratio:10; Temperature: 225°C
<i>Column flow</i>	2 ml min ⁻¹ He, constant flow mode
<i>Oven gradient</i>	55°C for 3 min, ramp 20°C min ⁻¹ till 200°C, constant max temperature for 2 min (total time= 12.25 min)
FID	
<i>Heater</i>	275°C
<i>Flows</i>	30 ml min ⁻¹ H ₂ ; 300 ml min ⁻¹ Air; 25ml min ⁻¹ make-up gas
GC-ICP-MS interface	
<i>Temperature</i>	Transfer line and ICP-MS injector tip: 250°C
<i>Flow transfer line</i>	432 ml min ⁻¹ (He GC, Ar/O ₂ , carrier Ar)
7700x ICP-MS	
<i>RF power</i>	1400W
<i>Sampling depth</i>	8 mm
<i>Ar carrier gas</i>	0.37 L min ⁻¹
<i>Ar/O₂ option gas</i>	5% (12 ml min ⁻¹ O ₂ in 60 ml min ⁻¹ Ar)
<i>Torch position</i>	H=0.8 mm; V=-0.3 mm

The retention times (RT) of each compound for both techniques is reported, instead, in Table 3-2, for the experiments in which, through the same inlet, two columns were connected to the detectors. The two set of RTs are quite similar, thanks to the fact that the same type of column is used and there is no big difference of pressure between the two detectors. Additionally, it can be noticed that the variations among the same RT are rather small, with RSD never higher than 0.4%. The clear separation of the compounds in the chromatograms and the stability of the RT over time are shown also in Figure 3.1-1 and 3.1-2.

Table 3-2 Retention time at peak apex for the compound identification with GC- FID and GC-ICP-MS.

Instrument	Retention times (min) \pm RSD%					
	<i>L2</i>	<i>D3</i>	<i>L3</i>	<i>D4</i>	<i>D5</i>	<i>D6</i>
GC-FID	2.224 \pm 0.1	3.828 \pm 0.1	4.632 \pm 0.1	5.992 \pm 0.1	7.44 \pm 0.3	8.73 \pm 0.2
GC-ICP-MS	1.867 \pm 0.4	3.48 \pm 0.4	4.251 \pm 0.1	5.546 \pm 0.05	6.942 \pm 0.02	8.195 \pm 0.02

**Figure 3.1-1** GC-FID: Retention time of siloxanes (a); RT shift over time and average peak position for D5 (b).**Figure 3.1-2** GC-ICP-MS: Retention time of Siloxanes (a); RT shift over time and average peak position for D5(b).

Regarding ICP-MS, the operating conditions were tuned using 4 ml min⁻¹ flow of Xe in Ar (100 ppm_v Xe in Argon) controlled by an MFC (mass flow controller) prior to the transfer line. The parameters were adjusted, first, to have the highest intensity level of ¹²⁴Xe (3 10⁵ cps) and lowest ²⁸Si background signal (3 10³ cps). Secondly, those optimized parameters were verified before every measurement in order to have similar intensities over time for ¹²⁴Xe intensity and ²⁸Si backgrounds. Figure 3.1-3 shows a quite constant evolution of those values among the 95% CI (confidence interval), over a two-months period.

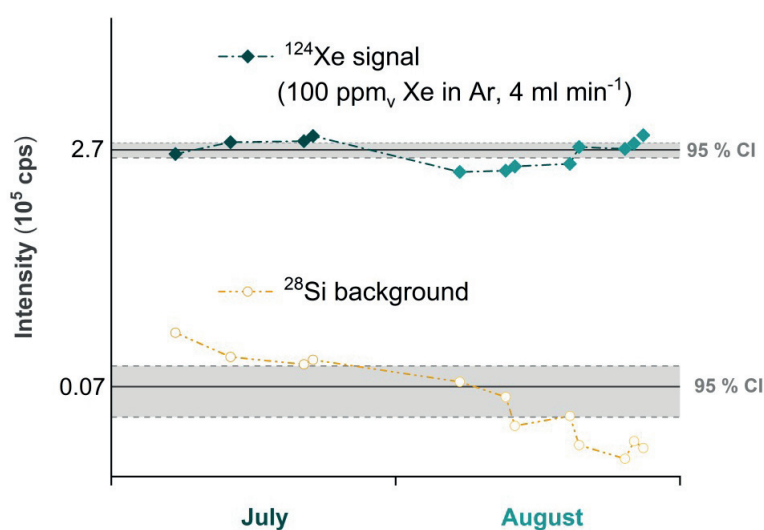


Figure 3.1-3 ¹²⁴Xe intensity and ²⁸Si backgrounds measured before each analysis, over 2 months. CI= confidence interval.

The possibility of mixing helium (He, known to reduce polyatomic interferences)[110] with hydrogen, (H₂, which selectively reduces isobaric interferences for ²⁸Si) [88] in the ORS was found to be crucial to achieving high sensitivities, lower LOD and LOQ (limit of quantification), and a constant background signal over time in GC-ICP-MS. Table 3-3 shows an example for D5, with two optimized conditions for different gas compositions in the ORS and one column connected to the GC inlet.

Table 3-3 Comparison between ²⁸Si sensitivities, LOD and LOQ calculated for D5 in GC-ICP-MS, using two different gas composition in ORS.

ORS gases flow	²⁸ Si Sensitivity	D5 LOD	D5 LOQ	R ²
(ml min ⁻¹)	(cps/ppb)	ppb _{Si} (ng ml ⁻¹)	ppb _{Si} (ng ml ⁻¹)	(linear fit)
He (2.4)	286.03	10.36	34.53	1.000
He (1.4), H ₂ (1)	532.91	3.63	12.10	1.000

The two calibration curves are reported also in Figure 3.1-4, while the concentrations of the stock can be found in table A.1.1.3 in appendix A.

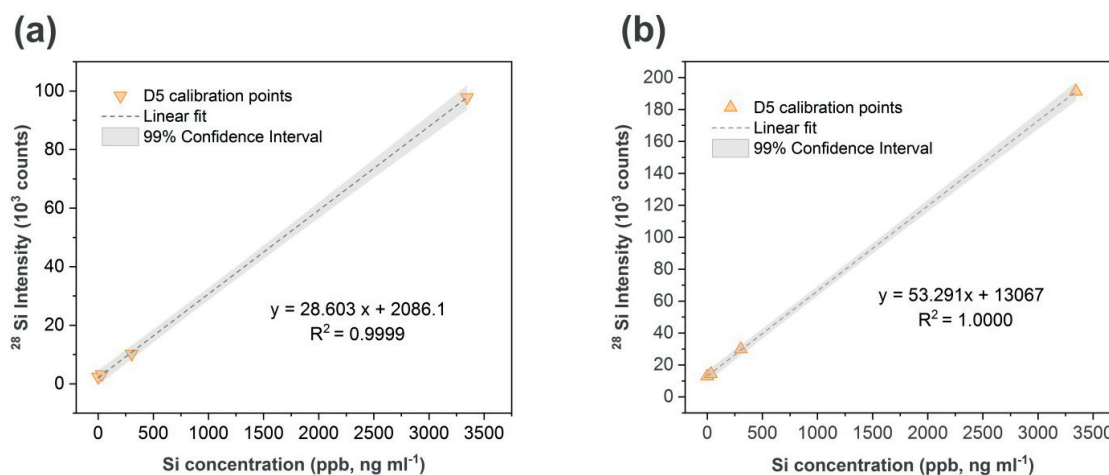


Figure 3.1-4 GC-ICP-MS calibration curve for D5, ORS gas flows optimization (GC inlet connected with one column only). ORS gas composition and flows: He 2.4 ml min⁻¹ (a); He 1.4 ml min⁻¹ and H₂ 1.0 ml min⁻¹ (b).

The sensitivity corresponds to S , the x coefficient in the linear equation of the calibration curve ($I = S \cdot c + I_0$), where x is also indicated as c, i.e. concentration. The LOD and LOQ are calculated as the ratio of 3 times and 10 times σ (the standard deviation of the blank, calculated over the integration window) and S. The reported concentrations are expressed as ng ml⁻¹ and refer to the liquid solution. Assuming the same experimental conditions of the sampling campaign, the LOD and LOQ of D5 in the gas would be approximately 0.002-0.004 mg_{Si} Nm⁻³ and 0.007-0.014 mg_{Si} Nm⁻³ for the case of He and H₂ mixture, respectively. Although those values, at least for D5, are in line with those reported for GC-MS[85], the main advantage of GC-ICP-MS resides in significantly reduced matrix effects, for which quantification by an external calibration is still accurate, while for GC-MS internal standards addition is often required to correct for significant systemic errors. [112]

The beneficial effect of the chosen gas composition in the ORS was tested for all siloxane compounds in GC-ICP-MS and the figures of merit are reported below in Table 3-4. The values of sensitivities are calculated after the split at the GC inlet. The measured ICP-MS intensities are, as expected, nearly the half for all compounds, which is consistent with the split (50:50). For the sake of comparison, we reported in Table A.1.1.4 in appendix A also the intensities measured when only one column is connected to the GC inlet.

The lack of certified reference material did not allow a classical method validation; on this matter, research programs involving several metrological institutes across European countries are currently aiming to provide reference materials for siloxane compounds in the gas phase.[113] However, the stability issues linked to some of the siloxanes and adhesion on canister or Tedlar bags walls are still

a challenging task.[114] Therefore, it was chosen to evaluate the method on liquid standards prepared in the same solvent used for the biogas sampling procedure. Throughout the analyses, standard solutions were measured every 5 samples. The global mean of recoveries for D5 was $99.9 \pm 0.8\%$, with very good intraday precision ($RSD \leq 5\%$). Moreover, a blank measurement was run every 5th sample, after checking the standards recovery, to ensure no memory effect or degradation of the column leading to false readings.

Table 3-4 ^{28}Si sensitivities, LOD, LOQ, R^2 and BEC (blank equivalent concentration) in GC-ICP-MS for siloxanes compounds analyzed, using two columns connected to the same inlet.

Siloxanes	^{28}Si Sensitivity (cps/ppb)	LOD ppb_{Si} (ng mL^{-1})	LOQ ppb_{Si} (ng mL^{-1})	R^2 (linear fit)	BEC ppb (ng mL^{-1})
<i>L2</i>	275.38	1.38	4.61	0.9998	16.76
<i>D3</i>	329.59	1.79	5.98	0.9992	23.57
<i>L3</i>	272.24	3.04	10.14	0.9999	15.29
<i>D4</i>	278.97	2.60	8.68	1.0000	12.38
<i>D5</i>	317.6	3.29	10.96	1.0000	20.89
<i>D6</i>	346.05	3.75	12.51	0.9999	22.54

In the case of FID, Figure 3.1-5 shows the usual range of concentration used to build a calibration curve from where the LOD and LOQ for D5 reported in Table 3-5 were calculated. More details on the peak area calculations were already provided in Chapter 2 (section 2.2.1.2).

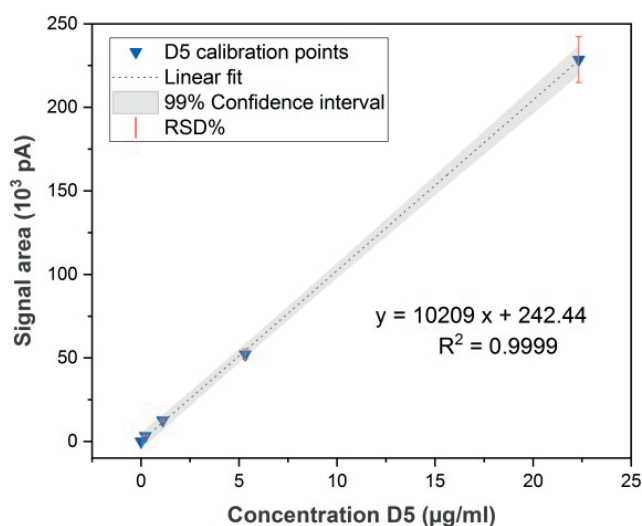
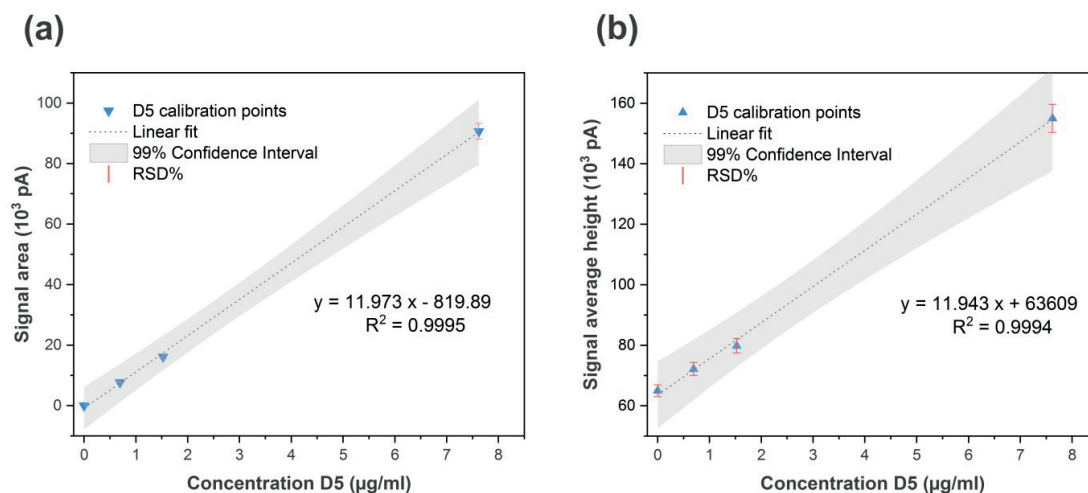


Figure 3.1-5 GC-FID calibration curves for D5 (one column only connected to GC inlet).

Table 3-5 RF (response factor), LOD, LOQ, R^2 (linear fit) in GC-FID for D5 (one column only connected from the inlet to the FID detector).

	Response factor (<i>area/amount</i>)	LOD <i>ppb_{Si}</i> (<i>ng mL⁻¹</i>)	LOQ <i>ppb_{Si}</i> (<i>ng mL⁻¹</i>)	R^2 (linear fit)
D5	9679.37	26.90	393.65	0.9999

Figure 3.1-6 shows the difference in sensitivity if the same calibration curve is calculated with *Method 1* or *Method 2*. The analysis and the interpolation of the samples can change quite substantially if the analyte peak is highly interfered. In this case an integration over 68 points could consider also the intensity assigned to neighbor peaks, resulting in an overestimation of the concentration. The figures of merit of GC-FID are also slightly different than for GC-ICP-MS. While in ICP-MS the sensitivity is the slope of the calibration curve, in FID the sensitivity is expressed as the response factor (RF), where RF is the ratio between area and amount of a certain compound. Different range of concentration will have then different RF; the interpolation is compiled by attributing the RF closer to the range of concentration expected. For better accuracy, the RF is normally an average RF calculated on 3 different replicates, at least.

**Figure 3.1-6** D5 calibration curves using GC-FID. (a) *Method 2*: peak area calculated as in GC software (n=68); (b) *Method 1*: peak area calculated as in ICP-MS software (n= 9).

The estimation of LOD (limit of detection) and LOQ (limit of quantification) implement the use of the signal to noise ratio (S/N) for a given calibration level. S/N below 10 means that the level is optimal for calculating the LOD, while S/N above 10 is suitable for LOQ calculations.

3.1.2 Simultaneous speciation analysis using GC-ICP-MS/FID

Manure and agricultural waste samples were analyzed by connecting the GC simultaneously with two detectors: ICP-MS and FID. The analysis was controlled mainly with the OPENLAB software, while the ICP-MS acquisitions were started with MassHunter. The calibration standards and biogas samples were introduced from the autosampler in the front inlet where the vaporization takes place, and they were split (50:50) between the two stationary columns. By running the two detectors simultaneously, the same conditions and stability of the samples were ensured. For each sampling conditions set, i.e. sampling point and gas-to-liquid ratio, two different samples were collected and each of them analyzed in two replicates. Figure 3.1-7 presents a comparison for both acquisitions on sample Manure1.

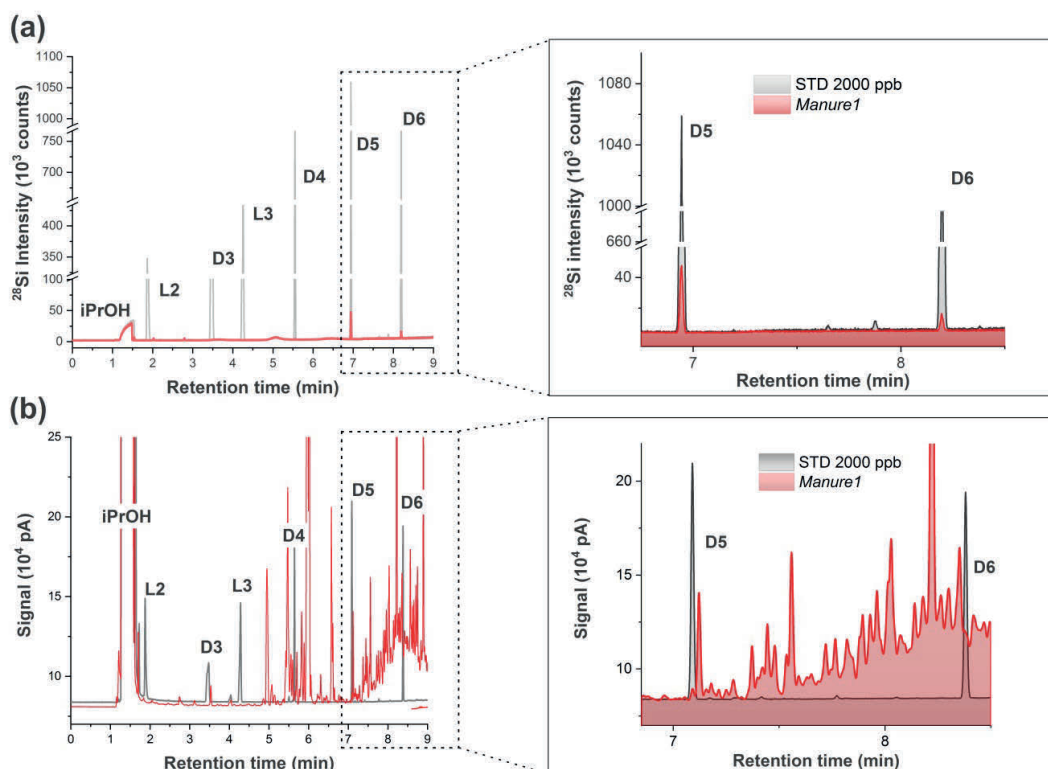


Figure 3.1-7 Assignment of the peaks to siloxane compounds in GC-ICP-MS based on ^{28}Si mass intensity (a) and GC-FID signal (b) for the sample *Manure1*. The grey lines show in both plots the profile and retention time of a multi-siloxane standard with a concentration of nearly 2 ppm_(l).

In the case of ICP-MS, only a few peaks present in the chromatogram do not have any analytical meaning linked to the siloxanes content, and their presence is consistent in the blank, the standard solutions and samples (Fig. S6 in SI). A high peak related to the solvent is visible due to the high carbon concentration. In fact, $^{12}\text{C}^{16}\text{O}^+$ is among the two main polyatomic interferences for ^{28}Si , together with $^{14}\text{N}_2^+$.^[115] The relatively low boiling temperature of the solvent is helpful to avoid co-elution with other compounds of interest, and the background remains almost constant for the

overall analysis. Only D5 and D6 are observed in GC-ICP-MS; the peaks (in Figure 3.1-7a) are above the thresholds and show good correlation in RT with the standard solution, resulting in concentrations above the LOQ, listed in Table 3-6.

Table 3-6 Siloxanes quantitative results in analyzed biogas samples; (*): each of them was sampled twice and two replicates for each sample were analyzed.

GC-ICP-MS	Si concentration in the liquid phase (ppb, ng ml ⁻¹) \pm RSD%		Si concentration in the biogas (mg _{Si} Nm ⁻³) \pm RSD%	
	<i>D5</i>	<i>D6</i>	<i>D5</i>	<i>D6</i>
Samples				
<i>MixUntreated</i> *	87.0 \pm 3.3	35.9 \pm 2.3	0.10 \pm 3.3	0.02 \pm 2.3
<i>MixTreated</i> *	\leq LOD	\leq LOD	\leq LOD	\leq LOD
<i>Manure1</i> *	126.0 \pm 0.7	52.8 \pm 1.7	0.15 \pm 0.7	0.03 \pm 1.7
<i>Manure 2</i> *	51.2 \pm 9.6	41.10 \pm 0.2	0.10 \pm 3.4	0.08 \pm 0.2

The FID analysis results in a much more complex chromatogram, due to the detection of numerous organic compounds present in the matrix. In the zoom-in of plot b (Fig.3.1-7), it can be seen that the presence of a neighbor peak with higher intensity could lead to unaccurate determination and quantification of D5. Nevertheless, its resolution is still possible, which is not the case for D6. Complementary analyses, later presented in this section, were carried out with another GC-FID instrument to gain more information on the class of compounds contained in each matrix. Table 3-7 shows how the two different integration *Methods 1* and *2* influence the final value of concentration. As explained in appendix A, the main difference between the two methods regards the number of integration points. During the analysis of samples, such as *Manure1*, the interpolation can change quite substantially if the analyte peak of D5 is highly interfered.

Table 3-7 Siloxanes quantitative results in analyzed biogas samples with GC-FID. (a) : calculated as in MassHunter (n=9); (b): calculated as in OPENLAB (n=68); (§): Si concentration refers to D5 only; (*): each of them was sampled twice and two replicates for each sample were analyzed.

GC-FID	Si concentration [§] in the liquid phase (ppb, ng ml ⁻¹) \pm RSD%		Si concentration [§] in the biogas (mg _{Si} Nm ⁻³) \pm RSD%	
	<i>Method 1</i> ^a	<i>Method 2</i> ^b	<i>Method 1</i> ^a	<i>Method 2</i> ^b
Samples				
<i>MixUntreated</i> *	212 \pm 2	2524 \pm 47.8	0.13 \pm 2	1.53 \pm 47.8
<i>MixTreated</i> *	\leq LOD	\leq LOD	\leq LOD	\leq LOD
<i>Manure1</i> *	154.2 \pm 21.8	2461.5 \pm 1.7	0.18 \pm 21.8	2.91 \pm 1.7
<i>Manure 2</i> *	54.9 \pm 37.4	2307.1 \pm 1.1	0.11 \pm 37.3	4.68 \pm 1.1

An integration over 68 points (*Method 2*) could consider, for instance, the intensity associated with neighbor peaks, leading to overestimation of the siloxanes concentration and consequently the Si concentration in the biogas. *Method 1*, instead, is generally affected by a higher uncertainty among different samples collected under the same conditions, because of the limited number of points considered for the integration.

3.1.3 Additional characterization of the biogas samples

Separate analyses in GC-FID revealed the complexity of the biogas matrix. Figure 3.1-8 and 3.1-9 show how a longer temperature program, with slower heating rate, makes it possible to resolve other organic compounds in the biogas, for instance, terpenes such as α -pinene and limonene, as well as the terpenoid para-cymene, all characteristic of biogas originating from food or green wastes.[116] Even though the determination of trace D5 is still possible, all of the samples present a complex pattern of unseparated peaks, which elutes at the same time of D6 (at retention times between 24 and 30 minutes). In this pattern, higher order alkanes (C13, C14) could be identified by GC-MS, as well as more complex branched hydrocarbons. It is also likely that other compounds such as ketones, alcohols, and sulfur- or nitrogen-containing compounds, could be contained in these biogas samples. Unfortunately, using methods such as GC-FID, which are not element-specific, not only silicon compounds but also other low-concentration compounds could be obscured by co-elution with trace hydrocarbons and not detected in the matrix. The advantage of GC-ICP-MS relies precisely on this point: by being an element-specific technique, the resolution of siloxanes peaks was proven to be always possible and rarely interfered, even with a reduced temperature program, hence an overall lower time of analysis.

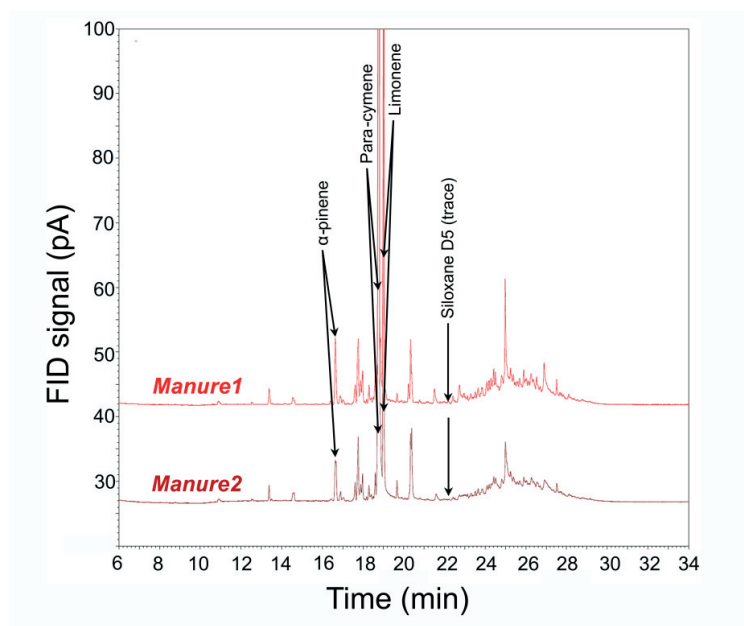


Figure 3.1-8 Manure1 and Manure2 samples analyzed in GC-FID and normalized by the gas-to-liquid ratio.

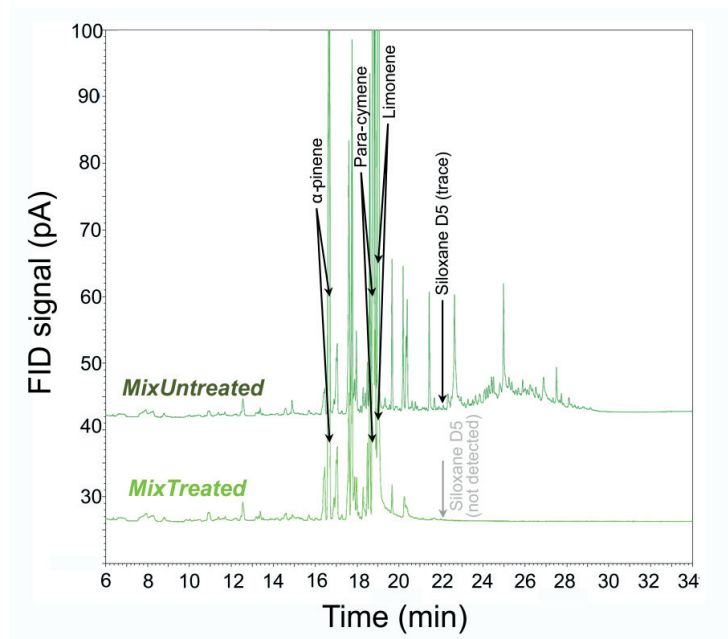
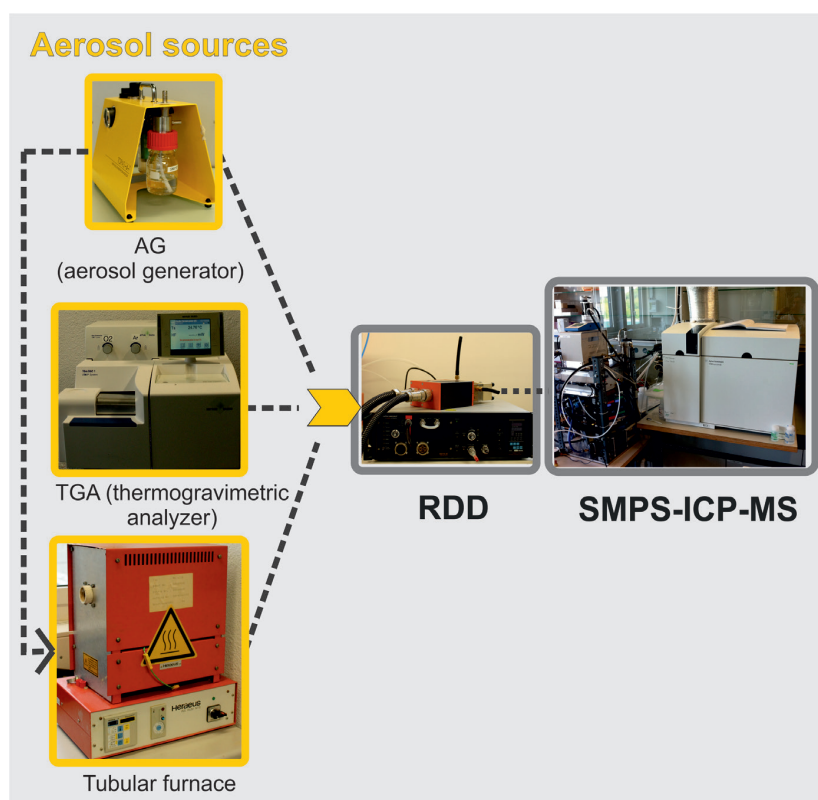


Figure 3.1-9 *MixUntreated* and *MixTreated* samples (before and after the activated carbon filter) analyzed in GC-FID.

Finally, Fig. 3.1-9 shows the effect of the use of filters or adsorption materials to reduce not only the concentration of siloxanes (confirmed by GC-ICP-MS) but also other impurities in the biogas. Among the most common filters, different types of activated carbons are by far ruling the market, even though recent studies suggested a good suitability of wood ashes or biochar and zeolites.[86,117–119] The chromatogram of the *MixTreated* sample appears consistently reduced in hydrocarbons fraction, especially of the compounds at higher retention times, which would generally trend towards having higher boiling points and thus a higher tendency to adsorb in activated carbons.

Chapter 4 Preliminary studies with RDD-SMPS-ICP-MS



Material from this chapter has been published in:

- (II) Mohamed Tarik, Debora Foppiano, Adrian Hess, and Christian Ludwig, A Practical Guide on Coupling a Scanning Mobility Particle Sizer and Inductively Coupled Plasma Mass Spectrometer (SMPS-ICPMS), *J. Vis. Exp.*, **2017**, (125), e55487, doi:10.3791/55487.
- (V) Debora Foppiano, Mohamed Tarik, Elisabeth Müller Gubler, and Christian Ludwig, Emissions of Secondary Formed Nano-Objects from the Combustion of Impregnated Wood. An Online Size-Resolved Elemental Investigation, *Environ. Sci. Technol.*, **2018**, 52, 895-903, (in supporting information for publication).

The NPs suspension preparation and characterization as well as the experiments on a salt solution, suspensions, and powders (except for the CuCl_2 powder experiment performed by M. Tarik) were planned and executed by D. Foppiano, who also took the lead in compiling the manuscript for the original publication (V).

4.1 Abstract

A large variety of analytical methods are available to characterize particles in aerosols and suspensions. The choice of the appropriate technique depends on the properties to be determined. In many fields, information about particle size and chemical composition are of great importance. While in aerosol techniques particle size distributions of gas-borne particles are determined online, their elemental composition is commonly analyzed offline after an appropriate sampling and preparation procedure. To obtain both types of information online and simultaneously, a hyphenated setup was recently developed, including a SMPS and an ICP-MS. This allows first to classify the particles with respect to their mobility diameter, and then to determine their number concentration and elemental composition in parallel. A RDD is used as the introduction system, giving more flexibility regarding the use of different aerosol sources. In this work, a practical guide is provided describing the different steps for establishing this instrumentation, and how to use this analysis tool. The versatility of this hyphenated technique is demonstrated in example measurements on three different aerosols generated out of a) a salt solution, b) a suspension, and c) emitted by a thermal process. An additional part regarding the ZnO suspension preparation, characterization and thermal behavior in different redox conditions are also reported.

4.2 Experimental and Results

The instruments and couplings used for these preliminary tests have been already described in Chapter 2, in the following session the results of the experiments on a salt solution, a suspension, and powders, and some details on the ZnO suspension preparation are given.

4.2.1 NaCl solution

Starting from an aqueous NaCl solution ($200\text{ }\mu\text{g mL}^{-1}$), an aerosol generator was used to produce a polydispersed aerosol (Fig. 4.2-1 a, b, and c). The ICP-MS and SMPS coupling was chosen to monitor simultaneously the particle size distribution (PSD) and the chemical composition of the generated aerosol. The signals from the two instruments did not show a substantial change with time, and the time-resolved signal of sodium correlates well to the PSDv(volume related PSD) during the entire measuring period. Since Na has a relatively high ICP-MS background signal, it results in a noisier signal than that recorded by the SMPS. The mode of the PSDn (number related PSD) lies at a lower particle diameter than that of the PSDv. Since the generated particles are NaCl particles, the behavior of the Cl signal is like that of Na and correlates well with the volume-related SMPS data (data not shown). The NaCl measurement is a simple example showing that a steady-state process can be controlled/monitored well with the coupled SMPS-ICP-MS system. This setup can also be used in such experiments as an online analytical tool to reveal the effects of different experimental parameters on the properties of the generated particles. Moreover, the example of NaCl shows that keeping the experimental conditions constant results in a steady state time-resolved signal.

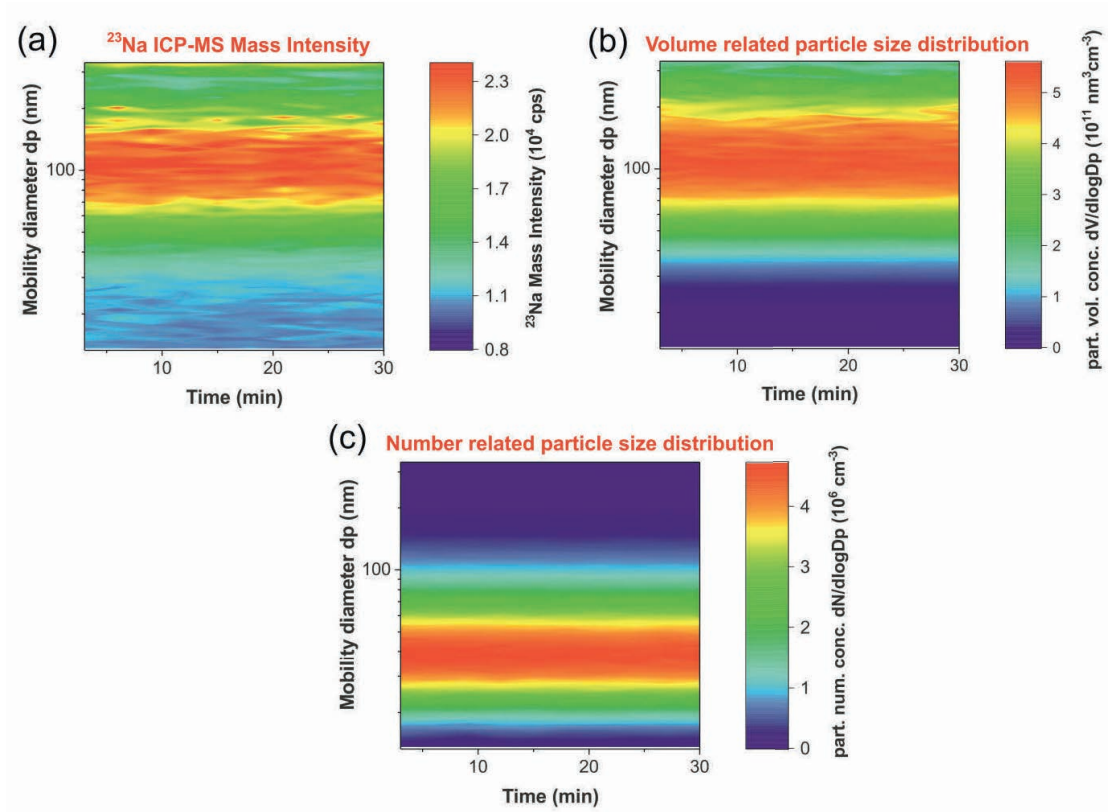


Figure 4.2-1. SMPS-ICP-MS data of the measurement of the NaCl solution. a) ICP-MS corrected signal of ^{23}Na . b) Volume related particle size distribution (PSDv). c) The corresponding number related particle size distribution (PSDn). The SMPS concentrations and ICP-MS intensities are plotted as functions of mobility diameter (dp) and time.

4.2.2 ZnO suspension

4.2.2.1 ZnO suspension preparation and offline characterization

For the suspension preparation a commercial powder of zinc oxide (AUER – REMY), was used. For the colloidal stability of ZnO particles dispersion, two main conditions are required and reported in literature, either particular pH conditions or the use of different ligands to control both steric and electrostatic forces between the nanoparticles. Among the different ligands used for that purpose, Poly Acrylic Acid (PAA) is shown to be one of the most efficient,[120] also in the case of synthesis of ZnO nanoparticles.[121] In our case, a solution of Poly Acrylic Acid (PAA) at 0.1% wt (pH~9), was used. The specifications provided by the company about the powder are reported in Appendix A (Table A.2.1-1).

A suspension 0.3% wt of zinc oxide (Suspension A) was prepared by mixing 333.3 mg of the commercial powder in 100 g of dispersant. The amount of nano-powder used was chosen, according to the minimum weight W_{\min} needed to have a representative sample. [122] A treatment with an ultrasonic horn was applied three times for two minutes, much more effective than bath immersion in terms of size reduction rate, minimum achievable size, and rate of sedimentation, for concentrated dispersions.[123] The second suspension with a concentration of 600 ppm of ZnO (suspension B) was

prepared by dilution of Suspension A with the same dispersant solution, under constant magnetic stirring. The homogenization included the use of an ultrasonic bath for 6 minutes, repeated twice. With the same procedure of suspension B, also another suspension with a ZnO concentration of 30 ppm was prepared (suspension C).

In collaboration with the advanced nanoparticle synthesis laboratory in our group (CPM at PSI), the suspensions were characterized with the use of two different instruments, a Malvern Zetasizer Nano series and a Brookhaven X-ray disc centrifuge (BI-XDC). The effective Zn concentration was also measured by ICP-MS in Suspension B and is reported in Appendix A in Table A.2.2-1. The table A.2.2-2 in Appendix A reports a mode of nearly 130 nm as result of the volume distribution measured with the Zetasizer. The X-ray disc centrifuge determination, instead, provides a volume distribution with a mean at nearly 200 nm (table A.2.2-3 in Appendix A), in good agreement with some bigger particles seen in SEM and TEM analyses (Figures A.2.1-1 and A.2.1-2).

4.2.2.2 RDD-SMPS-ICP-MS online characterization

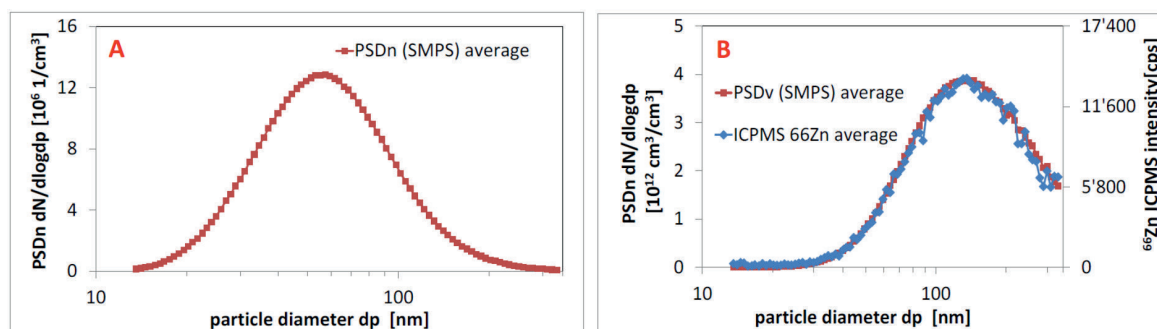


Figure 4.2-2. SMPS-ICPMS data of the ZnO suspension. A) Number-based PSD (PSDn), recorded by SMPS. B) The corresponding volume-based PSD (PSDv) and corrected ^{66}Zn signal, detected by ICPMS. The three signals are an average over 4 SMPS scans.

The RDD-SMPS-ICP-MS setup was used as a tool to measure online the particles generated from the ZnO suspension (Fig. 4.2-2). Assuming a morphology of spherical particles, the measurement with SMPS showed a mode around 130 nm, which is in good agreement with the measurement performed with the Zeta sizer nano series. As can be seen in Figure 4.2-2 a and b, the PSDv appears shifted towards larger particles when compared to PSDn, as seen for the NaCl measurement. Moreover, at large particle diameters, the ICP-MS intensity curve lies slightly below the curve detected by SMPS. SMPS measuring data are originally based on particle numbers, while ICP-MS intensities are proportional to the mass concentration. To compare the size-resolved signals, only the volume related PSD were considered by multiplying the size-resolved number concentrations by the calculated particle volume.[107]

4.2.2.3 Thermal treatment of ZnO suspension in oxidizing and reducing atmosphere

A thermal treatment on the ZnO suspension B ($600 \mu\text{g mL}^{-1}$) was performed in oxidizing and reducing atmosphere, by adding a flow of 50 mL min^{-1} of O_2 and H_2 , respectively. In the two different series of experiments, dried particles were injected into a tubular furnace, applying the thermal treatment also shown in Figure 4.2-3 (brown line), where, firstly, the SMPS and ICP-MS signals under oxidizing conditions are represented. The ^{66}Zn ICP-MS mass intensity (Fig. 4.2-3b) shows that in oxidizing conditions the particles containing Zn have a PSD in a size range between nearly 100 and 299 nm, with more or less constant intensity. Up to a temperature of 620°C , PAA (used to stabilize the suspension) contribute partially to the total PSD, most probably in the outer layer. As reported in a study measuring weight losses with TGA[121], is between 200 and 600°C that organic compound adsorbed on the nanoparticles surface, such as PAA, are removed. Indeed, at 728°C , the volume-based PSD measured matches perfectly the time-resolved ICP-MS signal of Zn (Fig. 4.2-3b), suggesting the complete removal of PAA particles.

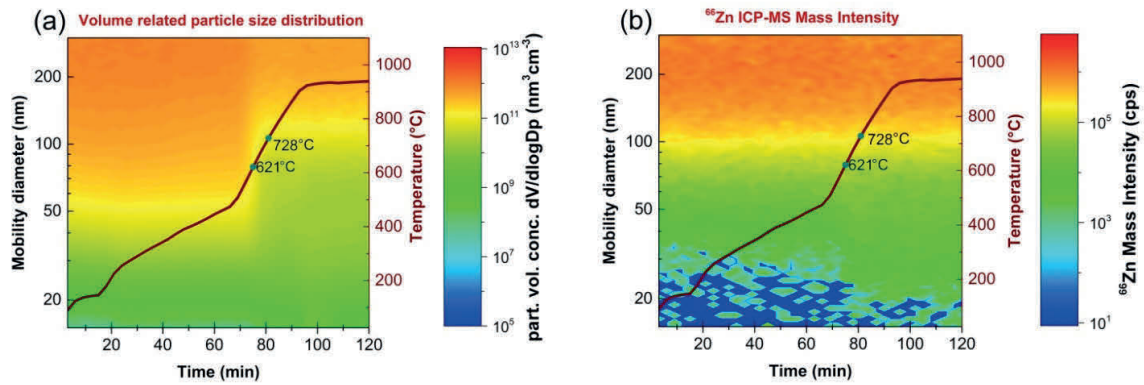


Figure 4.2-3 (a) Volume related particle size distribution of ZnO suspension, (b) ICP-MS mass intensity of ^{66}Zn , in presence of O_2 (50 mL min^{-1}).

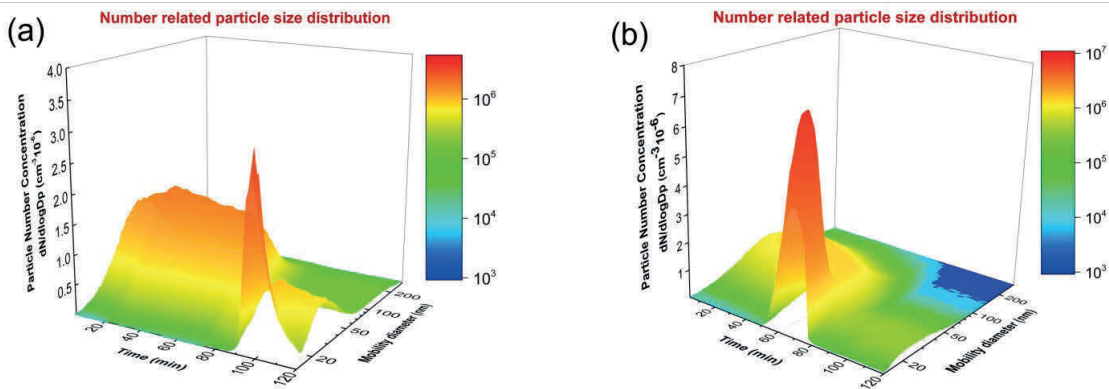


Figure 4.2-4 (a) 3d surface of number-related PSD of ZnO suspension, (b) 3d surface of number-related PSD of dispersant solution (Polyacrylic acid 0.1wt%).

Figure 4.2-4, reports a comparison between measurement on ZnO suspension and on PAA dispersant solution and shows that after approximately at 600°C, the contribution of PAA to the total particle size distribution is not relevant anymore, while a clear PSD is still measurable in the case of ZnO suspension. On the other hand, under reducing conditions and after a temperature of about 750°C, the concentration of Zn-containing particles decreases drastically to the background level at 840°C, as shown in Figure 4.2-5. A gray deposition on the quartz tube of the tubular furnace was noticed, suggesting agglomeration and condensation phenomena involving larger particles in the cold zone of the tube. The deposited material was washed out, dissolved and analyzed by ICP-MS. A Zn amount of 134.8 µg was found. The particle size distribution measured with the modified SMPS, operating in argon, was further confirmed with a reference instrument, a commercial air-operated SMPS from TSI. As it is shown in Figure 4.2-6, the two diagrams present a very similar PSD differing only slightly in term of concentration, due mainly to the different sensitivity of the two instruments.

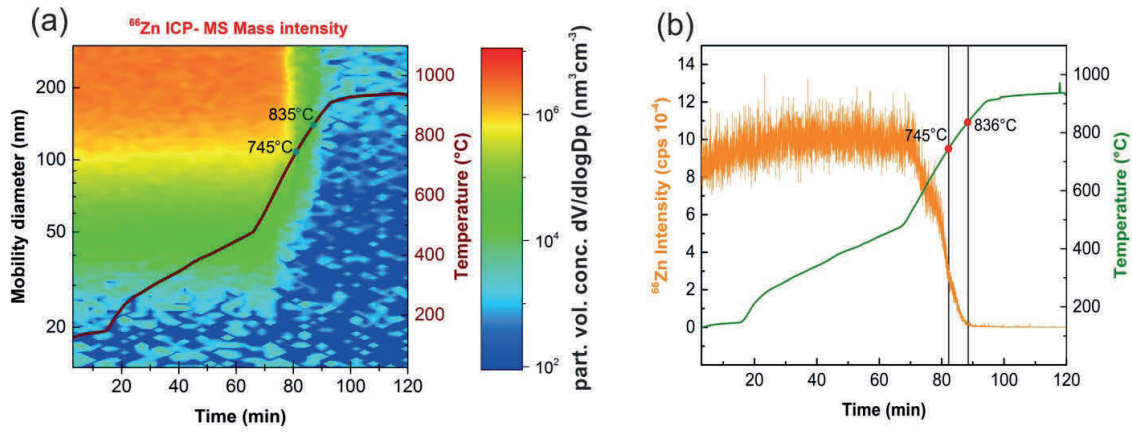


Figure 4.2-5 (a) ICP-MS Corrected and raw intensity of ^{66}Zn in reducing atmosphere of a size-classified particle with the use of SMPS, and (b) not size-classified particles (without the use of SMPS), respectively.

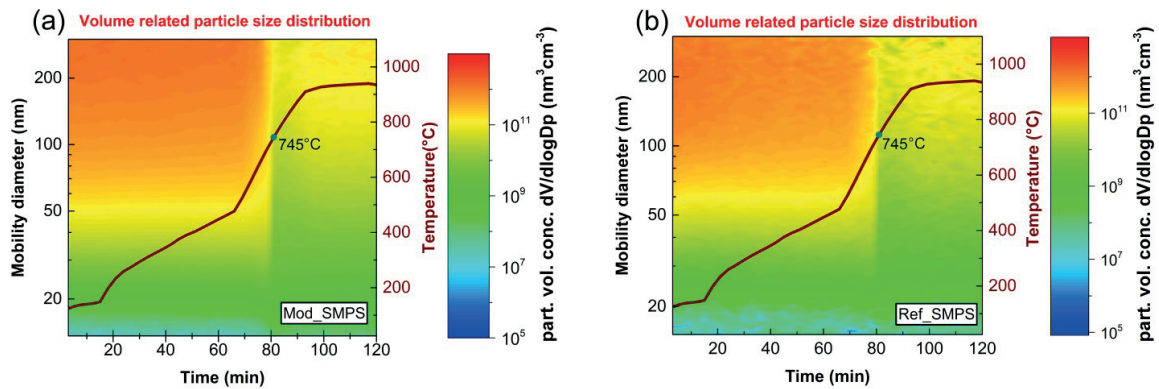


Figure 4.2-6 Volume related particle size distribution of ZnO suspension measured with the modified SMPS (Mod_SMPS) in-house build (a) and measured with a commercial SMPS (Ref_SMPS) from TSI company (b), in presence of H_2 (50 mL min⁻¹).

4.2.3 Powders thermal treatment

4.2.3.1 CuCl_2 powder thermal treatment

In this section, the results of the thermal treatment of a CuCl_2 sample by using the TGA are presented. Figure 4.2-7 shows the PSDn recorded for particles down to 20 nm at the beginning of the TGA heating (at about 21 min on time axis, i.e. at the beginning of the 7th SMPS scan). Subsequently, the particle concentration in PSDn reaches a steady state when the temperature is maintained constant and the particles cover a size range between 60 and 250 nm. A slight increase is observed in the particle size after the 11th SMPS scan (at about 30 min on time axis). Considering PSDv (Fig. 4.2-7b), the contribution of the different particle sizes is quite different from that of PSDn, and with the PSDv increasing significantly mainly between 150 and 330 nm. While the ICP-MS signal of Cu shown in Figure 4.2-7c correlates well with the PSDv.

Figures 4.2-7 d and e show the corrected and raw ^{35}Cl intensity during the up and down scans, respectively. After the starting point of the heating period, besides the intensity corresponding to particles of chlorine species, a constant Cl intensity covers the particle size range measured (in the time interval 18 to 33 min, i.e. from the 7th to the 11th SMPS scan). This is due to the evaporation of Cl gaseous species. The chlorine particulates are recorded in the same size range as copper, especially with a diameter above 150 nm. Another experiment using the same sample (CuCl_2) was performed without SMPS and by using only the TGA-RDD-ICP-MS setup. Here the ICP-MS signal of the non-classified aerosol particles was measured (Figure 4.2-7f). Similar to the case of SMPS-ICP-MS, an increase of both signals (Cl and Cu) in the last scans can be observed. In the examples presented, the correlation between the time-resolved ICP-MS signal of Cu and PSDv is obvious. For a mixed-source aerosol with different particles, the contribution of each element in the overall PSDv is determined by the ICP-MS signals. Therefore, the SMPS-ICP-MS setup allows monitoring changes in elemental and/or size concentration of the generated aerosol. For instance, the higher signal of PSDn in the CuCl_2 experiment (Fig. 4.2-7c) may be caused by the abrupt start of the heating process. While, the increase in SMPS and ICP-MS signals during the final scans can be explained by the change of the temperature gradient of the CuCl_2 sample with time, which changes the total amount of the material reaching the evaporation temperature. Finally, considering the SMPS output data, the concentration in PSDv is shifted towards larger particle size than in PSDn. This is because the signal is multiplied with the 3rd power of the particle diameter to convert PSDn to PSDv, resulting in a stronger weighting of large particles in the volume than in the number regime. On the other hand, the SMPS-ICP-MS combination allows not only to measure but also to distinguish between gas and particle species. Indeed, the part of the signal related to the PM can be easily distinguished from that of gaseous compounds, because the ICP-MS signal of the latter covers the entire size range and does not follow a distribution shape such as that of the signal related to particles. This is due to the fact that the SMPS scanning has no effect on gaseous species, and the ICP-MS measures the total intensity of a given isotope. This behavior is demonstrated by measuring Cl, which evaporates not only as particles but also as gaseous species (Fig. 4.2-7 d and e). Indeed, thermodynamic calculations showed

that under oxidizing conditions CuCl_2 is evaporated at about 450°C as Cl_2 gas and as condensable species CuCl_2 , Cu_3Cl_3 and Cu_4Cl_4 (data not shown).

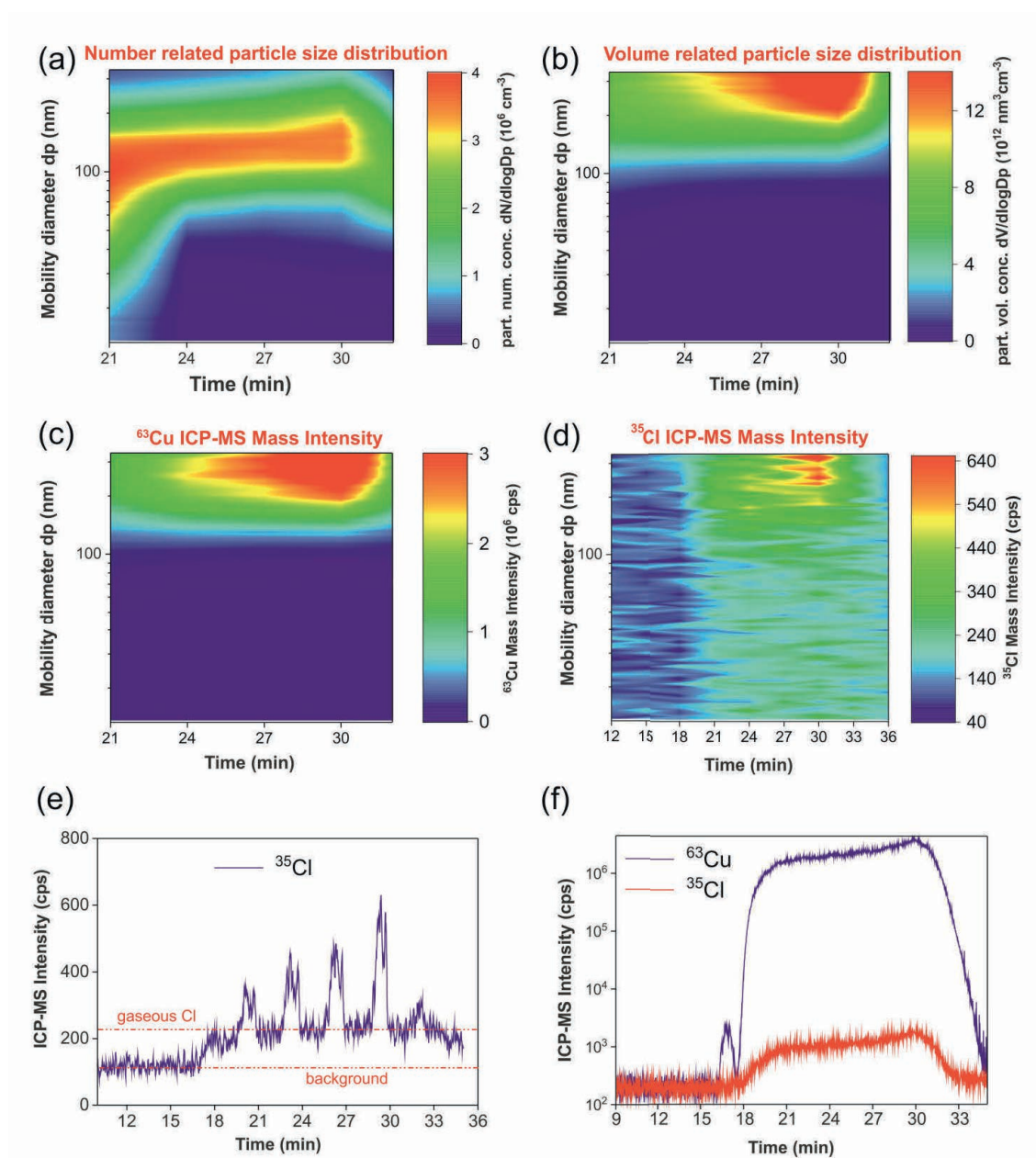


Figure 4.2-7 SMPS-ICPMS data from measuring CuCl_2 evaporation by using the TGA. (a) 2D plot of PSDn (b) 2D plot of PSDv. (c) 2D plot of ^{63}Cu ICPMS signal. (d) 2D plot of ^{35}Cl ICPMS signal. (e) Non-corrected raw ^{35}Cl ICPMS signal vs. time. (f) ICPMS signal of ^{63}Cu and ^{35}Cl recorded during thermal treatment of CuCl_2 by using TG-RDD-ICPMS setup (without SMPS). In both experiments (with and without SMPS) blank signals at 25°C are measured for about 18 min (6 SMPS scans), before starting and maintaining the heating period (for 15 min) at 450°C . The recording of SMPS-ICPMS signals was started at the same time as that of the TGA signals and was stopped 1 scan after switching it off (resulting in a total of 12 SMPS scans).

4.2.3.2 ZnO powder thermal treatment

The thermal treatment tests performed on the ZnO nanopowder under reducing atmosphere confirmed literature data, showing a change in morphology and chemical composition. Fine particles are detected by SMPS-ICP-MS measurement with a maximum concentration at about 823°C (Fig. 4.2-8). Part of the generated particles was lost as deposition on the liner and the quartz tube of the tubular furnace. This deposition was collected with HCl and milliQ water, in order to estimate the Zn concentration. A Zn content of approximately 26.2 mg was measured by ICP-MS, showing that nearly half of the starting amount of ZnO powder was lost in the cold zone of the tube.

In a second experiment repeated in the same conditions, the deposited material was collected using ethanol, and dispersed with an ultrasonic horn to be deposited on an Al stub for subsequent SEM-EDX analysis.

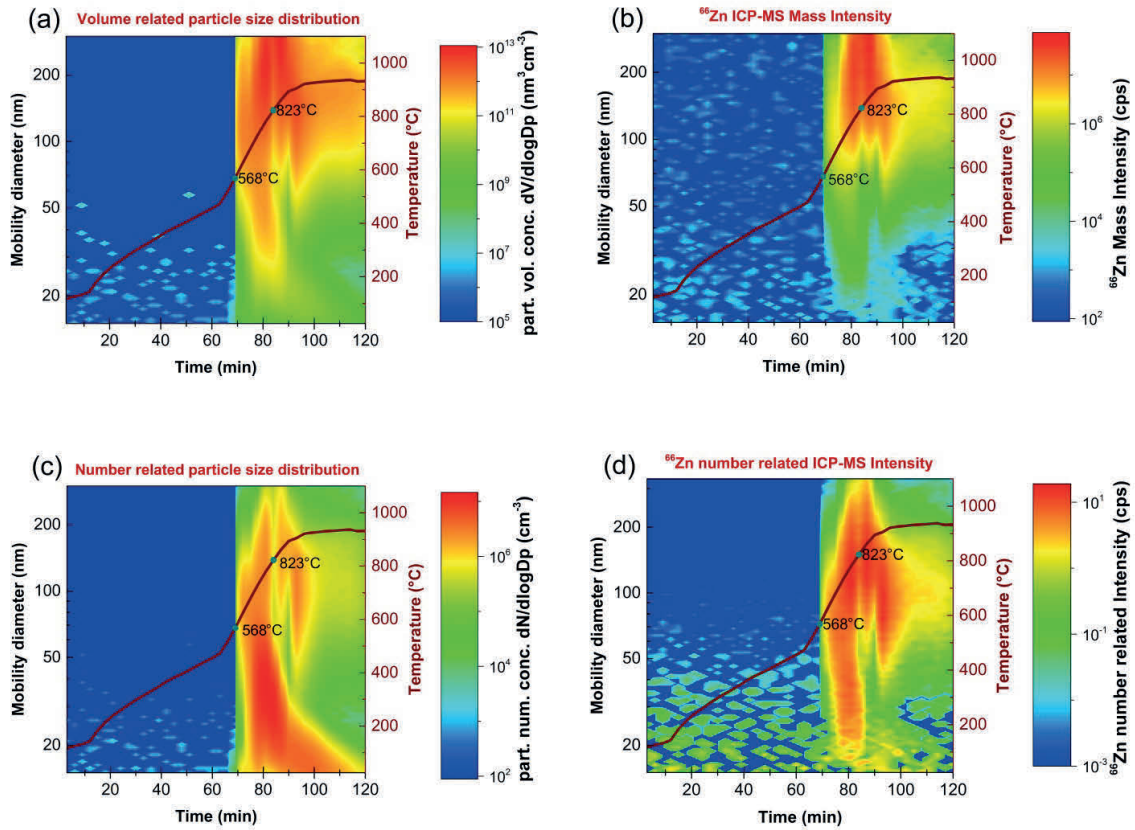


Figure 4.2-8 ZnO powder thermal treatment, in presence of H₂ (50 ml min⁻¹). (a) Volume-related PSD of ZnO powder, (b) corrected ICP-MS mass intensity of ⁶⁶Zn, (c) Number-related PSD, (d) number related ICP-MS intensity of ⁶⁶Zn.

The SEM and EDX analyses reported in Figure 4.2-9, show the presence of two different morphologies. The spectrum (b) corresponding to the hexagonal prismatic indicates only the presence of Zinc, while the spectrum (c), recorded for the flower-like type morphology, shows also a clear

oxygen signal, suggesting Zn metallic for the first and ZnO for the second one. A different analysis was performed on submicron particles collected in the flue gas after size-selection in the DMA. The TEM analysis shows a core-shell structure, proving the reduction of ZnO to Zn(g), followed by further condensation to smaller particles with an outer passivation layer of ZnO, as soon as temperature reaches a value lower than 830°C.

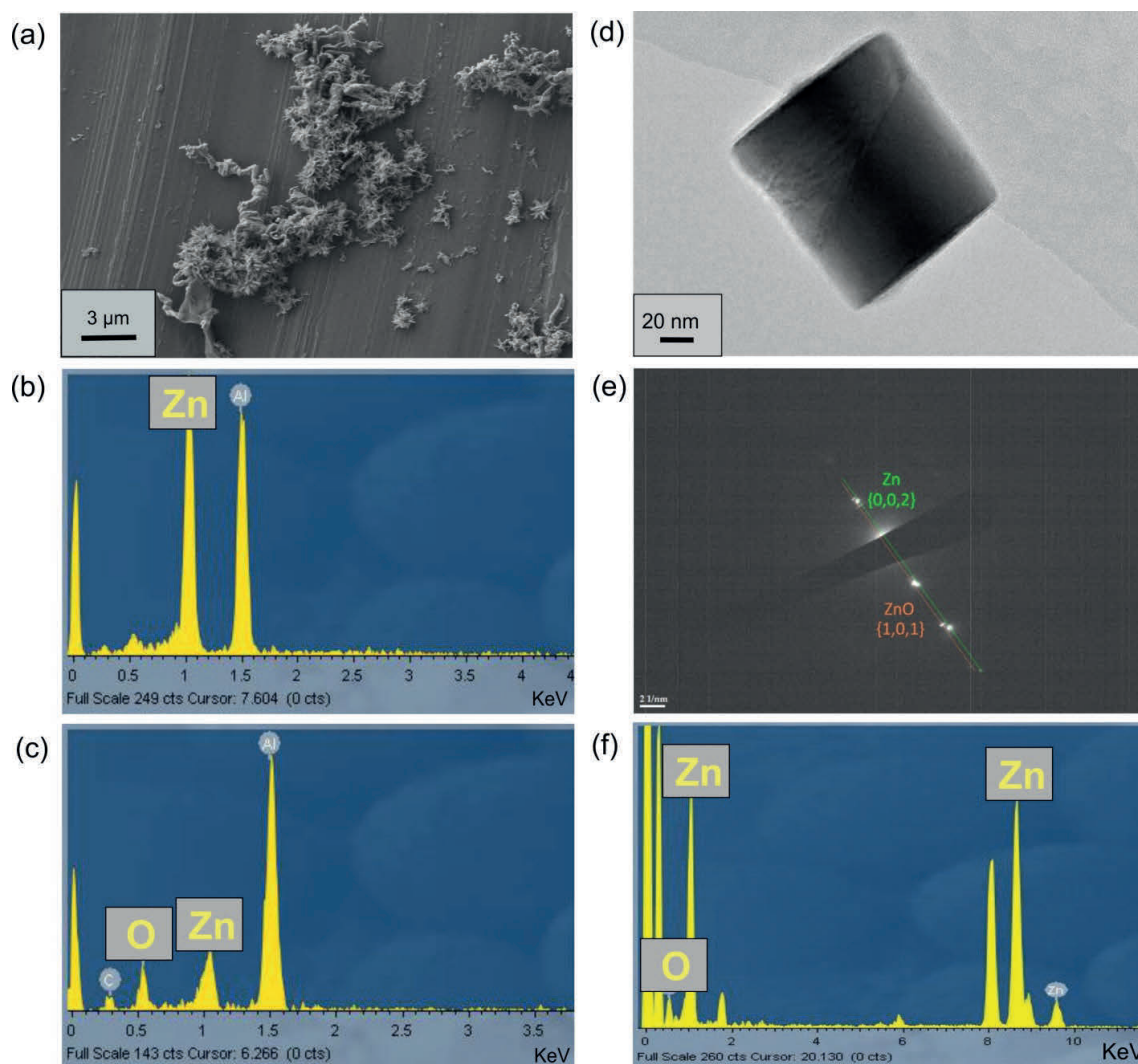
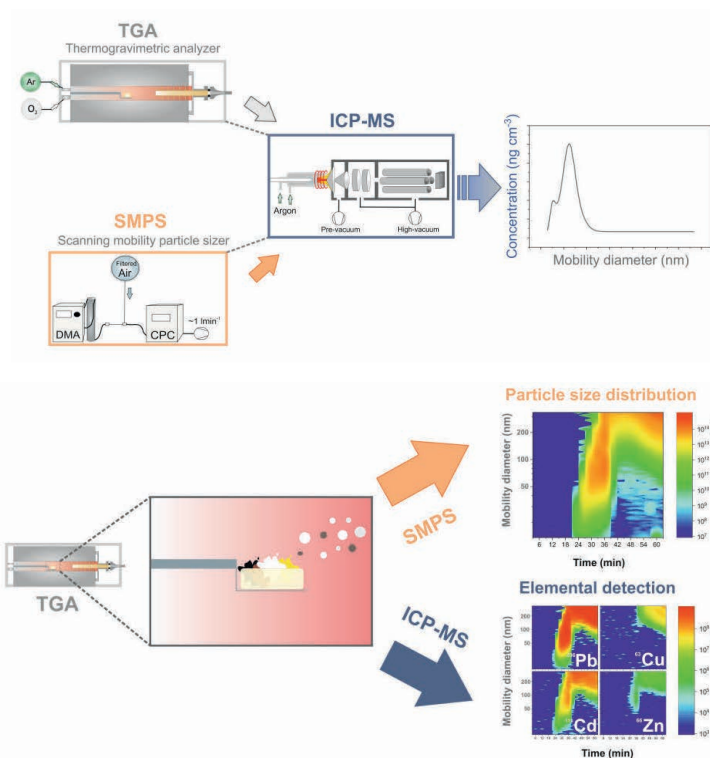


Figure 4.2-9 SEM micrograph of ZnO powder (a), after thermal treatment in presence of H₂ (50 ml min⁻¹); EDXS spectra of the prismatic hexagonal (b) and flower like type (c) morphology. TEM micrograph on size-selected particles collected at the outlet of the DMA(d), after thermal treatment in presence of H₂ (50 ml min⁻¹); corresponding indexation of electron diffraction pattern (e) and EDX spectrum (f).

Chapter 5 RDD-SMPS-ICP-MS calibration strategy and resolving power for heterogenous matrices



Material from this chapter has been published in:

- (III) Debora Foppiano, Mohamed Tarik, Elisabeth Müller Gubler, and Christian Ludwig, Combustion generated nanomaterials: online characterization *via* an ICP-MS based technique. Part I: calibration strategy with a TGA, *J. Anal. At. Spectrom.*, **2018**, 33, 1493-1499.
- (IV) Debora Foppiano, Mohamed Tarik, Elisabeth Müller Gubler, and Christian Ludwig, Combustion generated nanomaterials: online characterization *via* an ICP-MS based technique. Part II: resolving power for heterogenous matrices, *J. Anal. At. Spectrom.*, **2018**, 33, 1500-1505.

The author performed the experiments with the TGA and the RDD-SMPS-ICP-MS measurements, as well as the data treatment and evaluation, and took the lead in compiling the first draft of the manuscripts, resulting in the two publications listed above.

A calibration strategy for the hyphenated RDD-SMPS-ICP-MS setup is here presented. Evaporation experiments of ZnCl_2 powder were performed at four different temperatures, using a TGA as an aerosol source to correlate linearly the weight in loss of the TGA with the averaged ICP-MS intensities measured in transient mode. The calibration curve of Zn showed a good correlation factor ($R^2 = 0.9985$) and a sensitivity of $20.95 \cdot 10^3 \text{ counts ng}^{-1}$. The LoD (limit of detection) of the method was estimated to be $\sim 32 \text{ ng cm}^{-3}$, once the total dilution of the whole setup is considered. A second set of experiments was performed, where ZnO and $\text{CaCl}_2 \cdot 2\text{H}_2\text{O}$ powders were used as reactants to generate ZnCl_2 particles. The output data of the two instruments were treated and appropriately converted, to allow a direct and quantitative comparison between the performances of SMPS and ICP-MS. The ICP-MS signal of Zn was quantified by using the external calibration performed with the coupling of a TGA with an ICP-MS, while the SMPS volume data used two general assumptions, namely spherical morphology and bulk density of ZnCl_2 . Additional TEM analysis performed on the size-selected ZnCl_2 particles allowed to check their morphology. The proposed calibration strategy of the ICP-MS signals enables to evaluate the SMPS quantification procedure. Additionally, a mixture of several metal chlorides particles generated by the reaction of metal oxides (PbO , CdO , CuO , ZnO) with $\text{CaCl}_2 \cdot 2\text{H}_2\text{O}$ was considered in order to assess the resolving power of the technique in complex heterogeneous matrices.

5.1 Experimental section

5.1.1 Instrumentation

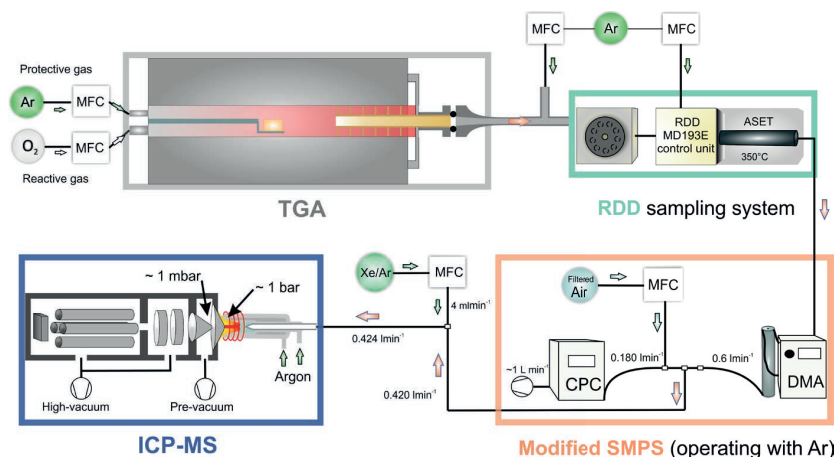


Figure 5.1-1 Setup scheme. TGA (thermogravimetric analyzer): aerosol source; RDD (rotating disc diluter): dilution and sampling system; SMPS (scanning mobility particle sizer): size-selection; ICP-MS (inductively coupled plasma mass spectrometry): elemental composition.

Figure 5.1-1 represents a schematic of the setup RDD-SMPS-ICP-MS. A thermogravimetric analyser is employed as an aerosol source, providing specific information about the weight loss of the sample meanwhile the particles are generated through evaporation of the initial amount. The protective and reactive gases were set to give a total of 100 mL min^{-1} , in some cases as a mixture of Ar/O_2 while in

others as Ar solely. Figure 5.1-1 represents the TGA configuration in real scale. The outgoing flow is accurately measured with a primary flow calibrator (Giliblator 2, Gillian, USA). An additional Argon flow of 230 mL min^{-1} was radially added at the outlet of the TGA and the RDD (Matter Aerosol, Switzerland) was employed as conditioning, dilution and sampling system to control the introduction into the analytical setup. The combined effect of the dilution at the outlet of the TGA and inside the RDD is acting efficiently as quench gas to minimize losses and prevent the agglomeration. The temperature of the RDD disk was kept to 120°C to avoid deposition on the cavities and the dilution Argon flow was set to 0.6 L min^{-1} . The aerosol flow is further directed to an evaporation tube set at 350°C in order to avoid condensation and agglomeration of the particles before introducing them into the in-house developed SMPS operating with Ar instead of Air.[124] Once the particles are size-selected the resulting flow is split in between the CPC and the ICP-MS (30:70). The CPC is counting the particles, while ICP-MS (Agilent 7700x) provides information on their elemental composition. An additional flow of 4 mL min^{-1} of Xe/Ar mixture (100 ppmv Xe in Ar from Carbegas, A1AW4RL, Saphir quality) was added at the ICP-MS inlet, in order to optimize the operating parameter of ICP-MS and to monitor any drift of the signal during the analysis.

5.1.2 Calibration experiment with ZnCl_2 powder

In order to calibrate the RDD-SMPS-ICP-MS system, i.e. to quantify the ICP-MS signal, evaporation experiments of ZnCl_2 powder were performed using a TGA as an aerosol source. As mentioned in the instrumental description, the gas flow inside the TGA was set to have a total flow of 100 mL min^{-1} of Ar (reactive gas: 46 mL min^{-1} ; protective gas 54 mL min^{-1}). An alumina crucible with 40 mg of ZnCl_2 anhydrous powder was placed in the furnace. In order to ensure a reproducible evaporation of particles over time, the sample was pre-treated at 330°C (the melting temperature) and a ZnCl_2 uniform layer was obtained on the crucible surface. The melting temperature was confirmed by previous experiments on ZnCl_2 powder at a constant heating rate of 5°C min^{-1} up to 600°C (see Fig. 5.1-2). Owing to evaporation behaviour observed in this experiment and the thermochemical calculations using HSC software (version 7.0 from Outotech)[125] reported in Figure 5.1-3, the TGA program for the calibration experiment was set as follow: the temperature was maintained constant at 330° , 410° , 430° and 450°C for 15 min each. The heating rate between these temperatures was set to 5°C min^{-1} (see Fig. A.3.1 in Appendix A).

Table 5-1 Operating conditions of the ICP-MS (Agilent 7700x)

Parameters	ICP-MS (Agilent 7700x)
Power	1350 W
Sampling depth	8 mm
Nebulizer gas	0.42 L min^{-1}
Dilution gas (Ar)	0.58 L min^{-1}
Xe/Ar (100 ppm v Xe in Ar)	4 mL min^{-1}
He (collision cell)	1.5 mL min^{-1}

Once the aerosol is generated from the TGA, it followed the path shown in Figure 5.1-1 and described in paragraph 5.1.1, except for the DMA which was by-passed using a conductive tube. Table 5-1 is summarizing the operating conditions used for ICP-MS during the experiments.

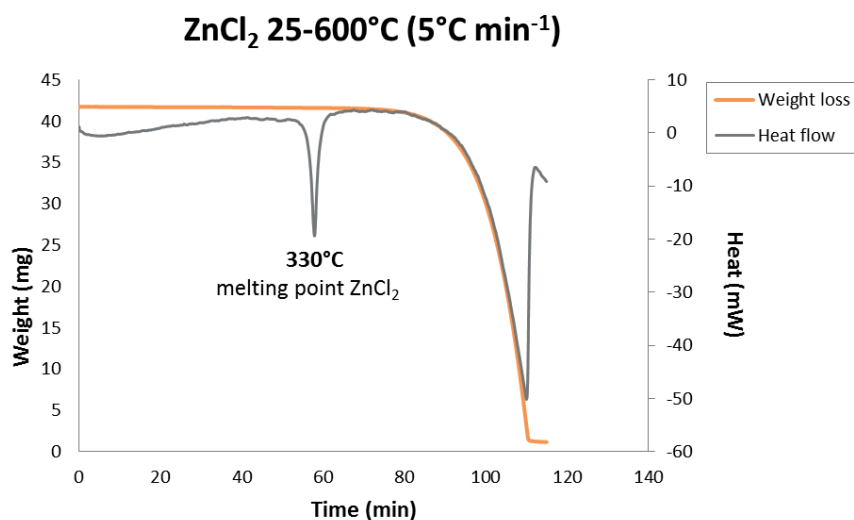


Figure 5.1-2 Evaporation studies on ZnCl₂ powder at constant heating rate (5°C min⁻¹) between 25-600 °C

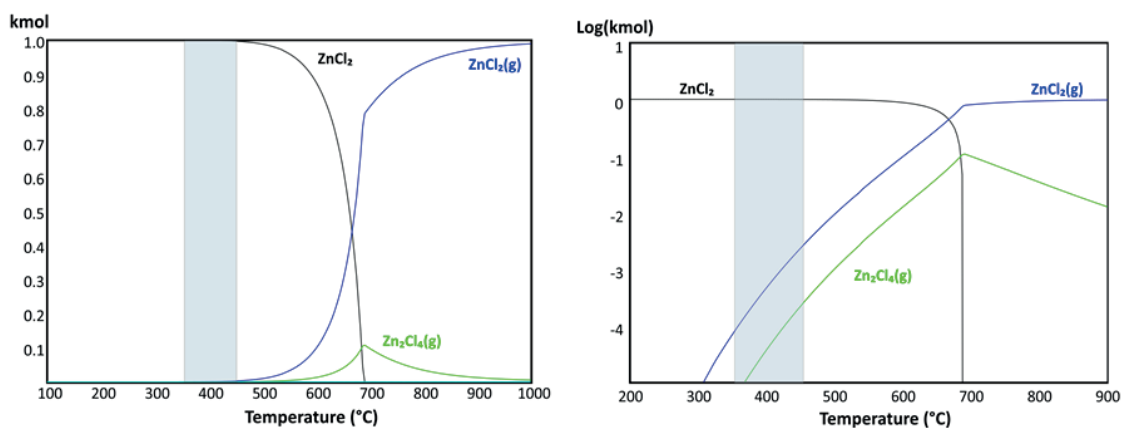


Figure 5.1-3 Thermochemical calculation on ZnCl₂ evaporation with HSC software. The grey area highlighted represents the range of temperatures investigated.

5.1.3 Calibration experiment with CdCl₂ powder

In order to quantify the ICP-MS signal of Cd and to calibrate the RDD-SMPS-ICP-MS system, evaporation experiments of CdCl₂ powder were performed using a TGA as an aerosol source. The total gas flow inside the TGA was set to 100 ml min⁻¹ (reactive gas O₂: 46 mL min⁻¹; protective gas Ar: 54 mL min⁻¹). An alumina crucible with nearly 40 mg of CdCl₂ anhydrous powder was placed in

the furnace. In order to identify the most suitable temperature range for our experiments, thermochemical calculations were performed with HSC software (Fig.A.3.2 in Appendix A). Consequently, the TGA program for the calibration experiment was set as follows: the temperature was maintained constant at 439°, 457°, 475°, 493° and 511°C for 15 min each. The heating rate between these temperatures was set to 5°C min⁻¹ (Fig. A.3.3 in Appendix A). The isotope ¹¹¹Cd was measured by using ICP-MS with an integration time of 0.2 s with the same operating conditions reported in Table 5.1-1.

5.1.4 ZnCl₂ particle analysis

ZnO and CaCl₂ · 2H₂O powders were used as reactants to generate ZnCl₂ particles. Previous thermochemical calculations with HSC software (Fig.5.1-4) allowed to predict the generated species and to choose the optimal range of temperature. A constant heating rate of 10°C min⁻¹ was set between 25°C and 850°C with an isothermal step at the last temperature for 20 minutes (see Fig. A.3.4 in Appendix A), using O₂ instead of Ar as a reactive gas, in the same ratio reported in the previous section. A mixture of 25 mg of ZnO and 60 mg of CaCl₂ · 2H₂O was introduced into the furnace and the generated aerosol was first diluted at the outlet of the TGA and in the RDD (total dilution DF = 108) and then introduced into the DMA. Using the ICP-MS, a transient signal of the isotope ⁶⁶Zn was acquired (integration time 0.2 s), while the CPC measured simultaneously the particle concentration of the size-selected particles. ¹²⁴Xe isotope was measured at the same time to control the plasma stability and to monitor any possible drift occurring during the experiment.

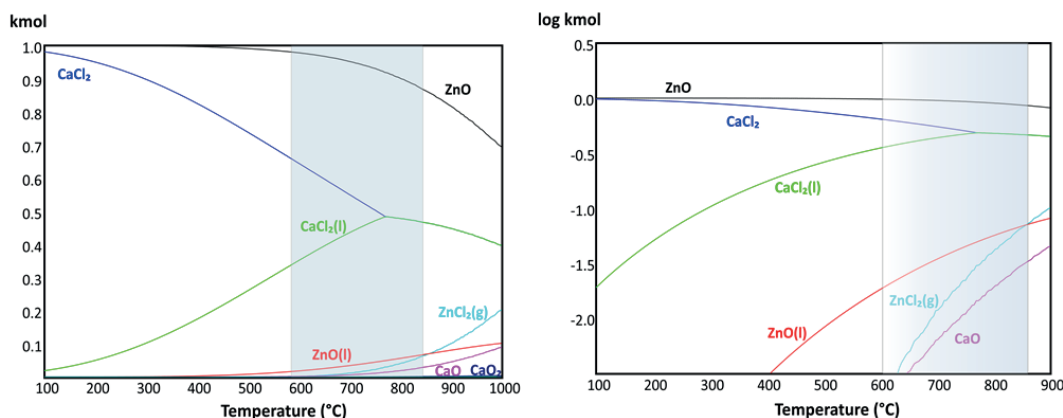


Figure 5.1-4 Thermochemical calculation on ZnO and CaCl₂ system with HSC software. The grey area highlighted represents the range of temperatures investigated.

5.1.5 Mixture of different metal chlorides particles analysis

PdO, CdO, CuO, ZnO, and CaCl₂ · 2H₂O powders were used as reactants to generate a mixture of different metal chlorides (PbCl₂, CdCl₂, CuCl₂ and ZnCl₂) particles. As a results of the thermochemical calculations with HSC software (Fig.5.1-5), the temperature was increased between

25°C and 850°C at a constant heating rate of 10°C min⁻¹, then an isothermal step at 850°C was maintained for 20 minutes (Fig. A.3.4 in appendix A), using O₂ as a reactive gas, in the same ratio reported above. A mixture of 25 mg of ZnO, 10 mg of PbO, 7 mg of CdO, 4 mg of CuO and 83 mg of CaCl₂ · 2H₂O was introduced into the furnace and the generated aerosol was initially diluted at the outlet of the TGA and in the RDD (total dilution factor: DF= 108) and later introduced into the DMA. Transient signals of the isotopes ²⁰⁶Pb, ¹¹¹Cd, ⁶³Cu, and ⁶⁶Zn were acquired (with an integration time of 0.2 s each) by ICP-MS, while the CPC was measuring concurrently the particle concentration of the size-selected particles.

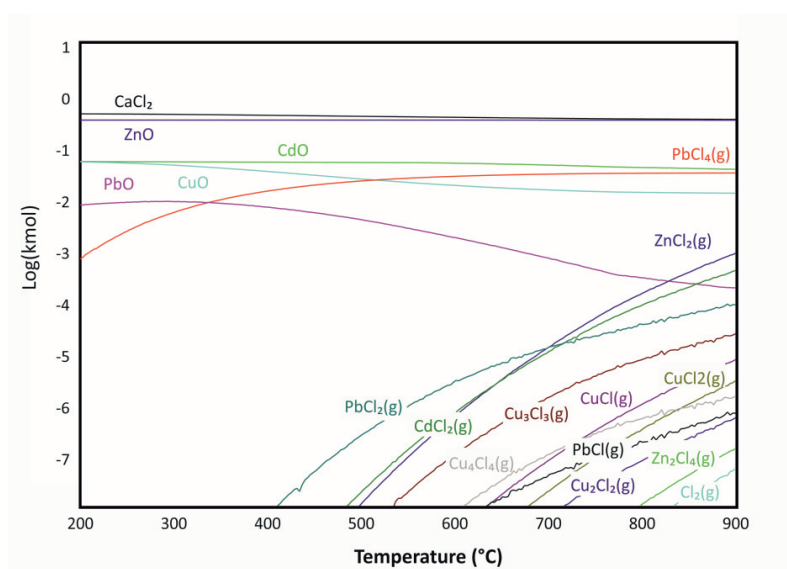


Figure 5.1-5 Thermochemical calculation on PbO, CdO, CuO and ZnO reactions with CaCl₂ with HSC software. The molar ratio resembles exactly the ones used in our experimental procedure.

5.1.6 TEM analysis: experimental procedure

Similar experiments, such as describe in section 5.1.4 and 5.1.5, were repeated to collect the size-selected particles on a TEM grid (Quantifoil R 1.2/1.3 Cu- 400 mesh, S143-3, PLANO GmbH) for following imaging and EDXS analysis. The particles were sampled with an aspiration EM grid sampler, following the specification already described in Chapter 2. The particular hygroscopic nature of the material was not allowing a direct exposure to air. Therefore, the sample was kept in Argon atmosphere, moved to a glove-box and introduced there into a special sample holder equipped with a sliding specimen protection cover (often used in the cryo-TEM analysis).

5.1.7 Data evaluation

Figure 5.1-6 illustrates the different steps of the developed ICP-MS calibration strategy using TGA and how to compare the data of the two different instruments (ICP-MS and SMPS). The SMPS is providing information on the mobility diameter of particles and their number concentration, while the ICP-MS is providing information about the intensity of a specific isotope as a function of time.

Since the instruments are synchronized, by comparison of acquisition time of SMPS and ICP-MS signals, these latter can be expressed as a function of the mobility diameter. The quantification concept includes different conversion processes for the two instruments which lead to a direct and quantitative comparison of SMPS and ICP-MS data. On one hand, the SMPS number-based data has to be transformed first into volume-related data by assuming spherical geometry of the particles (Fig. 5.1-6D). On the other hand, the possibility of a linear correlation between the signal of weight loss in the TGA and the intensity in ICP-MS (Fig. 5.1-6A) enables to perform an external calibration of the ICP-MS intensity and express it in mass concentration (Fig. 5.1-6C). The calibration curve can be obtained by plotting the average of the transient signal of ICP-MS collected at constant temperature and for 15 min as a function of the TGA weight loss rate (Fig 5.1-6B). In the case of a single compound measurement in which the chemical composition is known, namely “ZnCl₂” or “CdCl₂”, the SMPS signal can be also converted into ng cm⁻³ by using the density of the corresponding bulk material (Fig. 5.1-6E). The formula shown in Fig. 5.1-6 represents the relative variation of the resulting ICP-MS and SMPS quantified data and it is used to evaluate how the assumptions adopted are influencing the output of SMPS results.

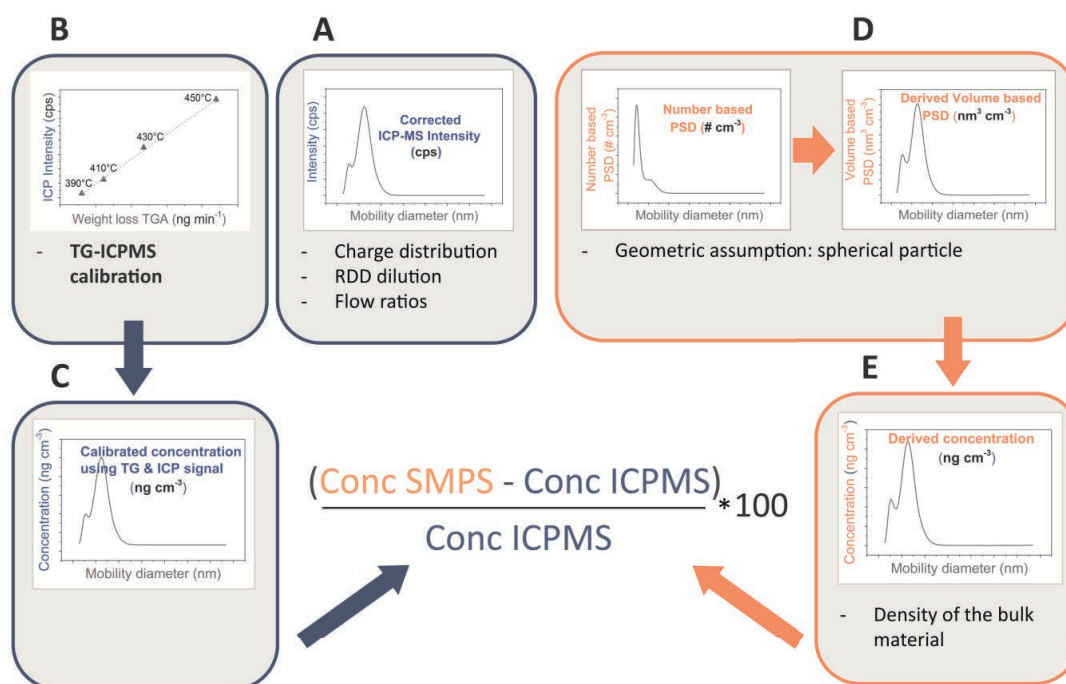


Figure 5.1-6 Data evaluation and calibration strategy TGA-ICP-MS

5.2 Results and discussion

5.2.1 ICP-MS calibration

The TG-ICP-MS calibration was obtained by correlating the weight loss rate of ZnCl_2 or CdCl_2 and the corresponding ICP-MS intensity measured at four different temperatures. Each point corresponds to an average of an ICP signal recorded during 15 min and taking into consideration the time needed to stabilize the TGA temperature. The calibration curve of Zn is plotted in Figure 5.2-1 as an example of linear correlation, while an example of quadratic fitting is reported for the Cd calibration is reported in appendix A in Figure A.3.5. In Fig. 5.2-1 is reported also the good correlation factor ($R^2 = 0.9985$) with a sensitivity of $349.1 \text{ cps min ng}^{-1}$ or $20.95 \cdot 10^3 \text{ counts ng}^{-1}$ (if the total dilution factor is taken into account). The RSD % (relative standard deviation) calculated for each averaged ICP-MS value is lower than 4% , represented here below as a blue error bar. The LOD of the method is estimated to be $\sim 32 \text{ ng cm}^{-3}$. Taking into account the total dilution of the whole setup (including RDD and the flow dilutions), the LOD at the ICP-MS inlet is $\sim 0.1 \text{ ng cm}^{-3}$. The linearity of the signal response would be affected at low evaporation rates and could lead to a calibration of the second order in this particular region. Therefore, the evaporation rates were carefully selected in such a way that only a linear response is considered and the interpolation is avoided at the extremes of the curve. This type of calibration was applied for the first time for ICP-OES signals by Ludwig et al.[67] However the reported method was developed merely for the elemental analysis of thermal-evaporated metals. The applications of TG-ICP-OES were mainly studies on waste incinerators facilities, thermal treatment of electronic scrap, and biomass for heavy metal separations.[15,126,127]

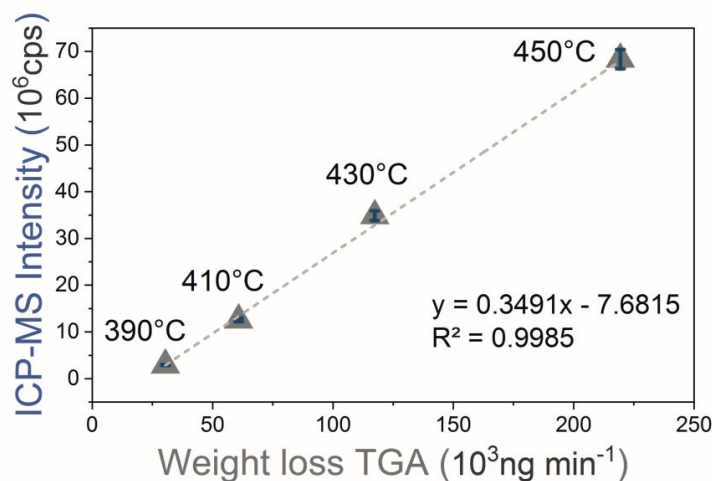


Figure 5.2-1 Calibration of the TG-ICP-MS for Zn; the dark lines on the grey triangle represent the RSD% for each point (RSD < 4%).

5.2.2 SMPS and ICP-MS data comparison

As mentioned above the measurement of one compound by ICP-MS and SMPS allows comparing directly the performance of these two instruments.

Fig. 5.2-2 represents the volume-related PSD (calculated from SMPS data) and the corrected ICP-MS mass intensity of ^{66}Zn , as a function of the mobility diameter. The contour plots are a sequence of several scans (3 min each) like the ones reported. Once combined all of the single scans linearly in time, the ICP-MS intensity or the PSD can be read in the contour plot with the colour scale, as a function of mobility diameter and time. The temperature is not shown in these diagrams; however, the time in the x-axis is proportional to the temperature which was increased with a constant rate of $5^{\circ}\text{C min}^{-1}$ from 25°C to 600°C . The two plots correlate well, except for a small increase in the concentration measured by SMPS for larger particles between 18 and 36 min, which were not observed by ICP-MS. This can be explained by the fact that unlike ICP-MS, which measured only Zn, SMPS analysis covered the overall particles generated during the reaction within the selected size range. The solid reaction between ZnO and $\text{CaCl}_2 \cdot 2\text{H}_2\text{O}$ is in fact generating not only ZnCl_2 but also H_2O particles, as soon as $\text{CaCl}_2 \cdot 2\text{H}_2\text{O}$ starts to melt and lose its hydration molecules. These plots can be expressed in the same unit as ng cm^{-3} using the calibration strategy already explained in the data evaluation paragraph. The ICP-MS signals of Zn was quantified by using the external calibration performed with TG-ICP-MS coupling, while the SMPS volume data used two general assumptions, namely spherical morphology and bulk density of ZnCl_2 .

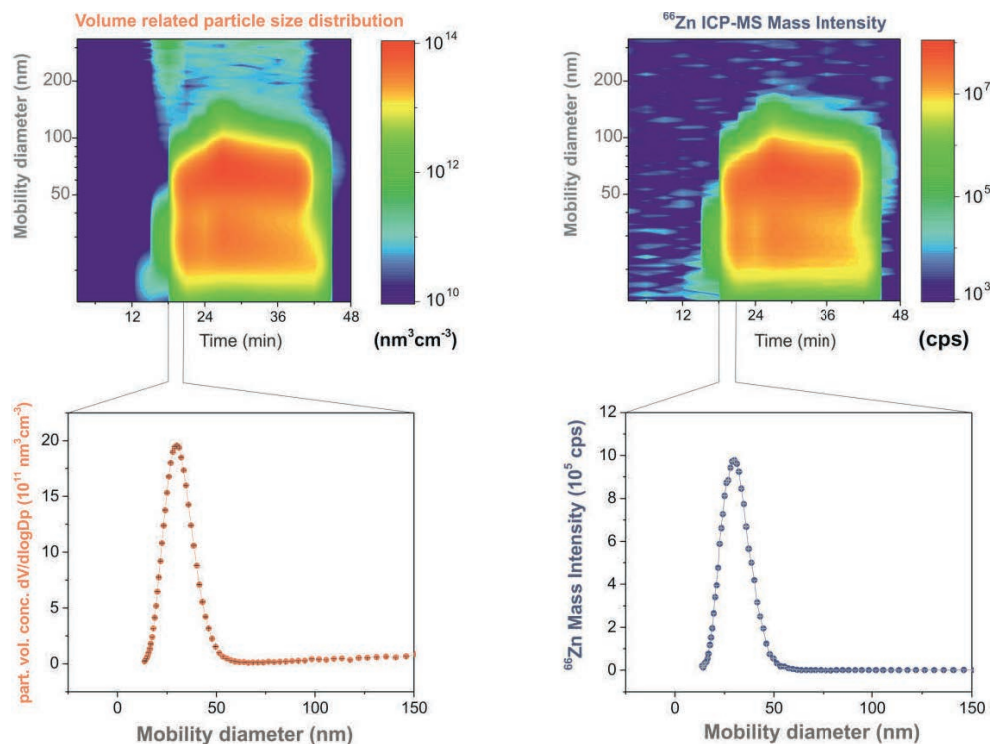


Figure 5.2-2 Volume-related particle size distribution and ^{66}Zn ICP-MS Intensity contour plots; examples below of a single scan in between 18 and 21 min of acquisition time.

The reproducibility of the analysis can be evaluated by comparing different replicates (Fig.A.3.6 in Appendix A presents an example of a repetitive analysis for the same sample in Fig.5.2-2, in the same operating conditions). The results show that the PSDs follow the same trend with an RSD for small particles (<20 nm) and bigger particles (>50 nm) of about 10%. The RDD-SMPS-ICP-MS setup is developed to accurately measure the particle size and concentration on a given sampling point (in this case the inlet of the RDD) independent of the combustion process and the behaviour of the particles along the pathways from the emission source to the sampling point. Provided that the parameters of the combustion process and the sampling conditions for a given sample are the same, the reproducibility of the particle concentration and the mobility diameter are defined by the ICP-MS and SMPS performances, respectively. The uncertainty budget of the overall setup can be estimated by considering the uncertainty contribution of each instrument. Previous studies demonstrated that the uncertainty of SMPS sizing is usually $\leq 2\%$, [128] while the uncertainty for ICP-MS signals lies below 5%. [129] The TEM analysis performed on ZnCl_2 particles, allowed to check the morphology of the size-selected particles, which was found to be spherical. Additionally, the EDX analysis confirmed the elemental composition of the sampled particles as ZnCl_2 (Fig.5.2-3). In Figure 5.2-4 the quantified SMPS and ICP-MS data are presented in the same unit (ng cm^{-3}).

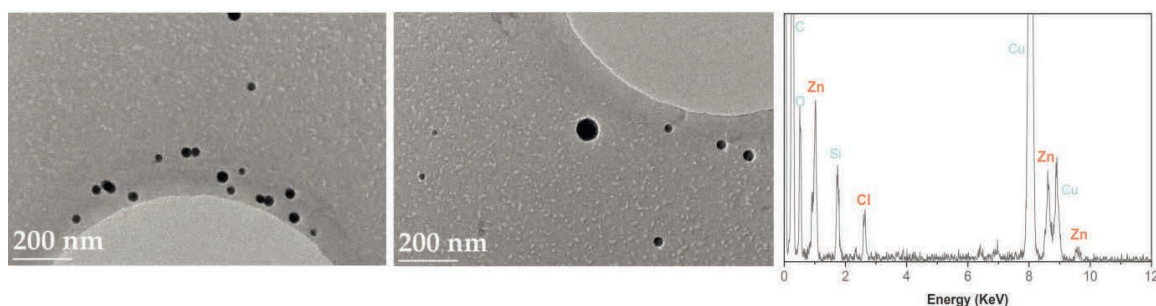


Figure 5.2-3 TEM analysis showing spherical morphology; EDX analysis confirmed the elemental composition of ZnCl_2 particles.

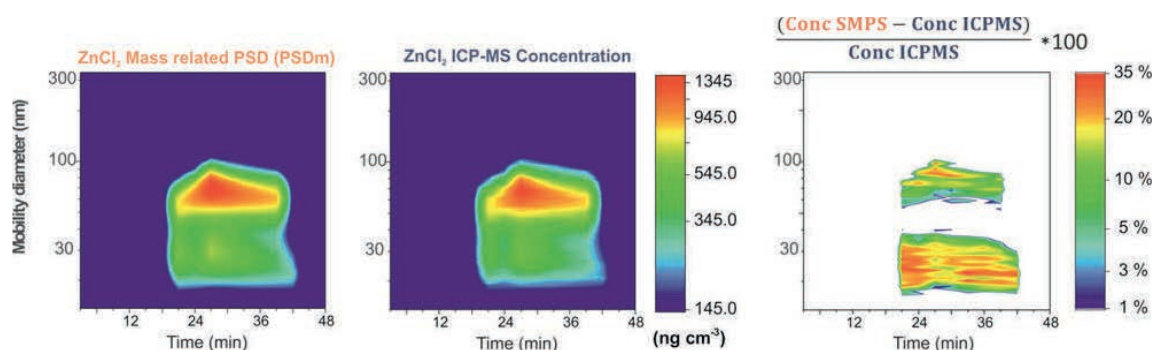


Figure 5.2-4 ZnCl_2 mass related PSD, ZnCl_2 ICP-MS concentration and SMPS-ICPMS data relative difference (%).

At first sight, a good correlation can be noticed regarding the ZnCl_2 concentration values for both instruments. However, an accurate comparison can be made only when the relative difference (in %) between the two sets of data is calculated, using the formula shown in paragraph 5.1-6, which considers only the positive values of the difference.

Small variations ($<1\%$) between the two instruments depends mostly on SMPS overestimations of the concentration compared to ICP-MS. In order to better understand this observation, a small discussion on the detection limit of the two instruments is needed. Regarding SMPS, the performances in the analyses are defined based on the cut-off diameter (depending on the DMA unit) and the dynamic range (depending on the CPC unit). The cut-off is the lowest value of mobility diameter that in our operating conditions can be determined, which is 13 nm (until a maximum value of 300 nm). The dynamic range is defined as the operation range in which SMPS is providing reliable results in terms of concentration, which for our instrument is in between 0 and $2 \cdot 10^4$ particles cm^{-3} . This means that any particle introduced into the CPC (lying in the dynamic range) is generating a response in concentration, even the particles generated from the released hydration molecules during ZnO and $\text{CaCl}_2 \cdot 2\text{H}_2\text{O}$ reaction. The ICP-MS, instead, is sensitive specifically to the mass/charge ratio selected (^{66}Zn in this case) and the quantification is linked to the LOD of the method.

Significant variations of SMPS data from ICP-MS are considered from 1% to 30% and are clearly visible in colour scale in Fig.5.2-4, in particular for larger particles above 100 nm and for smaller particles between 13 and 40 nm. Those differences can be explained as deviations from the two main assumptions used for SMPS data treatment. Larger particles, for instance, present a deviation from spherical geometry due to agglomeration phenomena. While, for smaller particles the use of the effective density would be more accurate than the bulk density. Particles can have a very different value of density depending on their size and asphericity. Thus, it is relevant to introduce also the concept of dynamic shape factor (DSF), from which the effective density can be derived. Hinds defined the DSF as the ratio of the drag force on an aspherical particle to the drag force on a spherical particle with a volume equivalent diameter d_{ve} . [8] Furthermore, Zelenyuk extensively reported how the equivalent volume diameter can be linked to both mobility diameter (db) and aerodynamic diameter (dva). In particular for spherical particles, the DSF is normally 1 and the effective density is proportional to the ratio between dva and db . However, the DSF can vary a lot depending on particle size, pressure and particle alignment in electric or aerodynamic flow fields and most of all as a function of asphericity, because of which the value of DSF is usually larger than 1. [130] So far the use of different aerosol instruments in tandem made possible to measure the two different parameter dva and db simultaneously or sequentially, in order to derive properties like DSF and effective density. In literature are reported different coupling which includes mainly DMA or SMPS for the mobility diameter and lots of other variations for dva , such as APM (aerosol particle mass) classifiers, impactors, AAC (aerodynamic aerosol classifier), mass spectrometers and aerosol mass spectrometers. [131–133] In this case, it was not possible to define the exact value of effective density of the smaller particles since the particle size is laying beyond the usual cut-off limits of

instruments employed for the determination of the aerodynamic diameter, but it is confirmed to be lower than the bulk density.

5.2.3 Mixture of different metal chlorides particles analysis

To assess the resolution power of the technique, a complex mixture of several metal chlorides particles generated by the reaction of metal oxides (PbO, CdO, CuO, ZnO) with $\text{CaCl}_2 \cdot 2\text{H}_2\text{O}$ was considered. The first purpose of these experiments was to distinguish the single contribution of each element in the overall particle size distribution (PSD). Although SMPS is performing the size-selection and providing information about the particle size, the volume-related concentration obtained (Fig. 5.2-5A) refers only to the overall amount of particles generated during the process. As a result of the time synchronization between the two instruments, the ICP-MS intensities can be also expressed as a function of particle size and, therefore, it is possible to determine the single-element contribution to the overall PSD. For instance, as can be seen in Fig. 5.2-5B, the signal relative to ^{206}Pb resembles quite closely the PSD measured in SMPS and results in a much higher intensity compared to all the other elements, i.e. the emission of particles containing Pb cover all PSD measured by SMPS. Furthermore, ^{111}Cd and ^{66}Zn follow the same emission pattern as Pb, even though the related intensity is lower. In the case of ^{63}Cu , instead, the evaporation occurred later on at a higher temperature, with a consistent contribution to the PSD only in the fraction of larger particles above 150 nm. The morphology and the particle size were analyzed also with TEM (transmission electron microscopy) in order to confirm the SMPS results (Fig. A.3.7 in Appendix A).

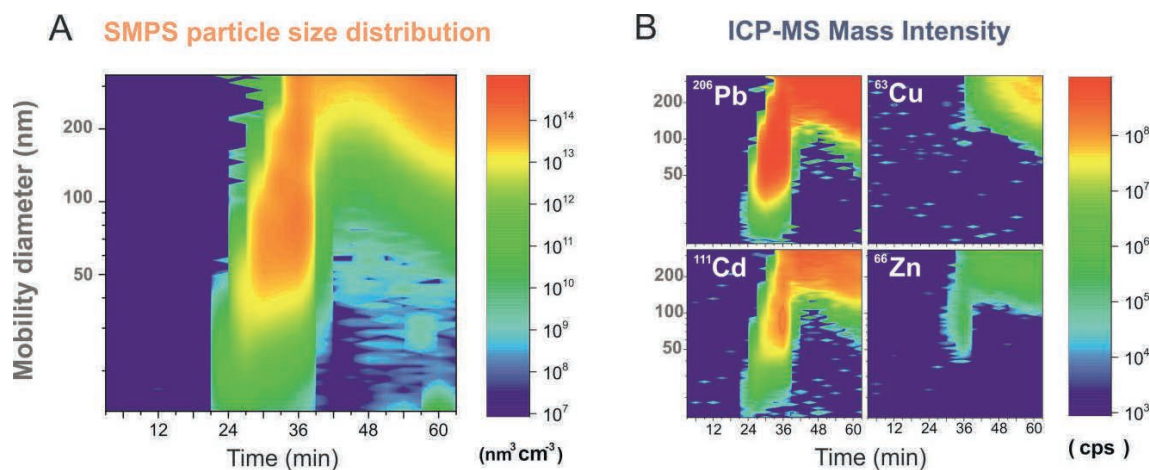


Figure 5.2-5 (A): SMPS particle size volume distribution of the overall amount of particles generated; (B): ICP-MS intensities of ^{206}Pb , ^{63}Cu , ^{111}Cd , ^{66}Zn (same scale of intensities for all of them).

The second purpose of these experiments regarded the quantification of metals content emitted over time. Firstly, it was calculated that $272 \mu\text{g min}^{-1}$ ($\text{RSD}\%=0.7$) of the initial sample was released over time with a total loss of $17.1009 \pm 0.0017 \text{ mg}$ during the overall analysis, as can be seen in Figure 5.4-6. Secondly, the contribution of two of the metals in the overall PSD was determined.

In section 5.2.2 it was already shown how the ^{66}Zn ICP-MS signal could be quantified and expressed in ng cm^{-3} , thanks to the calibration strategy by coupling ICP-MS with a TGA. As mentioned in the paragraph 5.1.3, we performed this type of calibration also for ^{111}Cd (shown in Fig.A.3.5) and used those two calibration curves to quantify the metal emissions during the evaporation experiment with the mixture of metal chlorides. In summary, as Fig. 5.2-7 is showing, not only elemental detection is performed with high resolving power but also the determination of the mass contribution of a specific element in the overall PSD is possible.

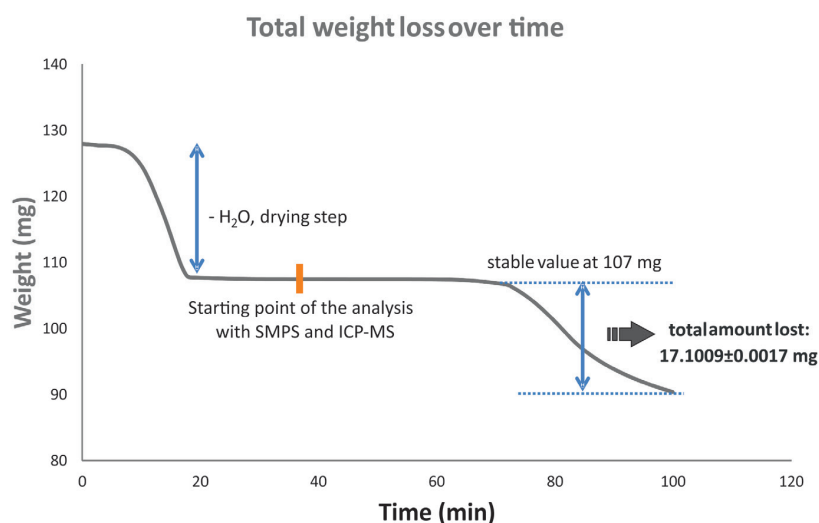


Figure 5.2-6 Total weight loss over time during experiment with PbO , CdO , CuO , ZnO and $\text{CaCl}_2(\text{H}_2\text{O})_2$ powders. The time scale reported in this plot is not corresponding to the one shown in Fig. 5.2-5, the measurement with SMPS and ICP-MS was started once stabilization of the sample weight was reached (indicated in the plot with an orange line).

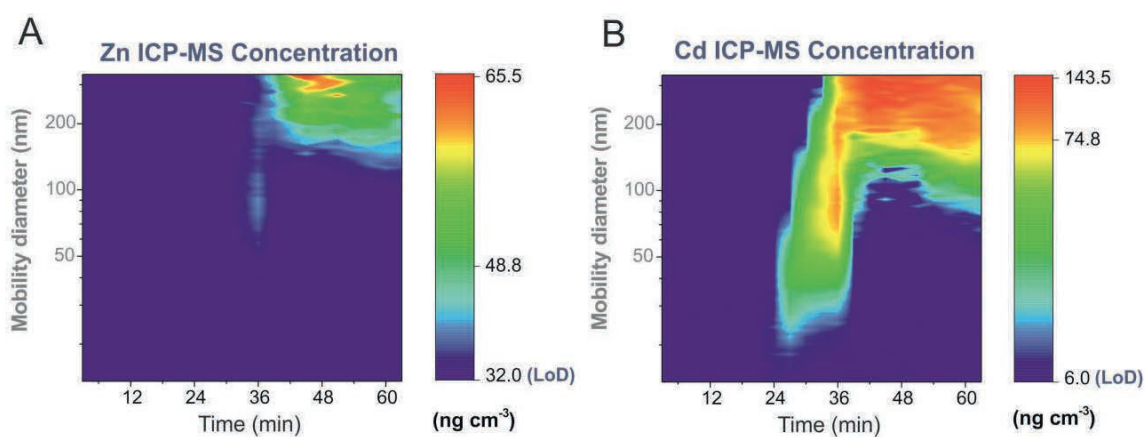
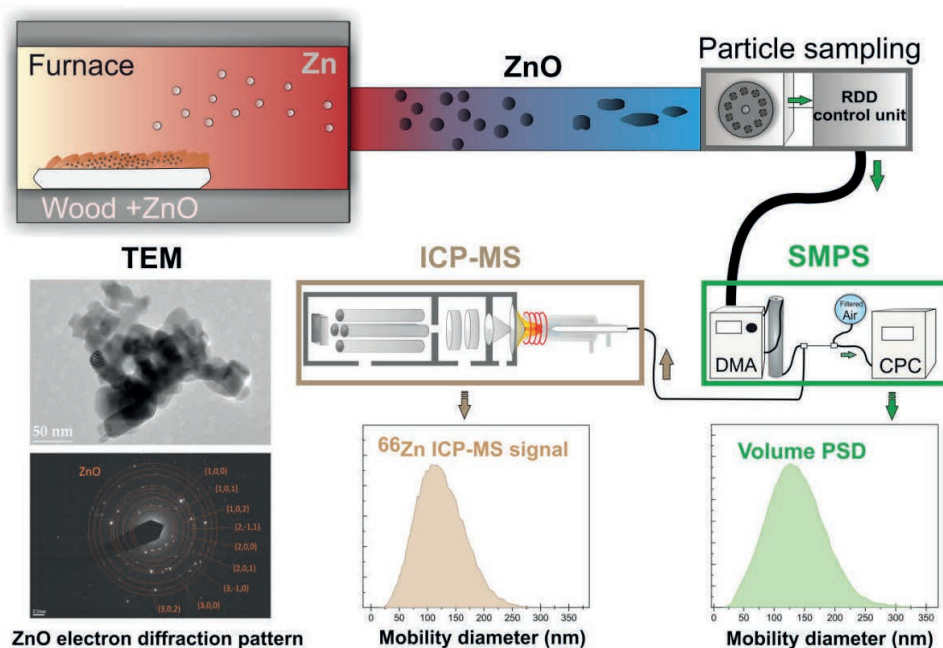


Figure 5.2-7 Zn (A) and Cd (B) concentration obtained by extrapolation from TGA-ICP-MS calibration

The results of this analytical method are promising and it can be applied for different applications. For instance, to study thermochemical and kinetical properties, as the evaporation rate of high boiling point metal compounds. In previous attempts by Ludwig et al.,[23,66] only the elemental composition was acquired, whereas the SMPS-ICP-MS setup can help to obtain size-resolved and elemental information at the same time. On the other hand, characterization of flame-synthesized particles and inorganic particles detection from diesel engines or combustion emissions might be as well interesting as other applications for the RDD-SMPS-ICP-MS system, since the concentration levels are high and often requires an extensive dilution.

Chapter 6 Emissions of secondary formed nano-objects from the combustion of impregnated wood



Material from this chapter has been published in:

- (IV) Debora Foppiano, Mohamed Tarik, Elisabeth Müller Gubler, and Christian Ludwig, Combustion generated nanomaterials: online characterization *via* an ICP-MS based technique. Part II: resolving power for heterogenous matrices, *J. Anal. At. Spectrom.*, **2018**, 33, 1500-1505.
- (V) Debora Foppiano, Mohamed Tarik, Elisabeth Müller Gubler, and Christian Ludwig, Emissions of Secondary Formed Nano-Objects from the Combustion of Impregnated Wood. An Online Size-Resolved Elemental Investigation, *Environ. Sci. Technol.*, **2018**, 52, 895-903.

The author performed incineration experiments and the RDD-SMPS-ICP-MS measurements, as well as the indexation of the electron diffraction pattern, the data treatment and evaluation, and took the lead in compiling the first draft of the manuscripts, resulting in the two publications listed above.

The release of secondary nano-objects formed during waste combustion processes is becoming a matter of concern, considering their known toxicity and the fact that the 100% efficiency of filtering systems is not always ensured. An increased cytotoxicity and genotoxicity on human peripheral blood lymphocytes is known particularly in the case of ZnO, which is often contained in paints and waterproof agents, heading to a relevant quantity present in the waste wood material. In this study, the behavior of ZnO nanoparticles during wood combustion and the effect of the reduction potential of generated carbon species on the release of secondarily formed ZnO-containing nano-objects were investigated. By hyphenating a modified scanning mobility particle sizer (SMPS) and inductively coupled mass spectrometry (ICP-MS), it was possible to obtain simultaneously size-resolved and chemical information on the emitted nanoparticles. Through the established correlation between SMPS and ICP-MS signals, Zn-containing particles were efficiently resolved from the combustion generated particles and the Zn content estimated thanks to the calibration strategy coupling a TGA with the RDD-SMPS-ICP-MS. Transmission electron microscopy (TEM) and energy-dispersive X-ray spectroscopy (EDXS) on size-selected particles confirmed the SMPS and ICP-MS data. The use of electron diffraction allowed determining the structure of the crystalline materials as hexagonal ZnO. A possible mechanism of reduction of ZnO to Zn and further reformation as secondary nano-objects is proposed.

6.1 Experimental section

6.1.1 Instrumental arrangement

The experimental setup consisted of a tubular furnace, used as a lab-scale incinerator (Heraeus, RE 1.1), connected to the SMPS-ICP-MS, together with a rotating disk diluter (RDD) equipped with a heating tube as the introduction system. A detailed description of RDD-SMPS-ICP-MS coupling strategy and instruments specifications was already presented in chapter 2, 4, and 5.[68,134]

Several mass flow controllers (MFC) were used to precisely adjust the flows. The different flows up- and downstream the tubular furnace were verified by a standard primary flow calibrator (Gilibrator-2, Sensidyne) at the beginning of every measurement.

Figure 6.1-1 shows a drawing of the experimental setup. The argon-borne particles were generated starting from a ZnO suspension by the aerosol generator by applying a relative gas pressure at the inlet of the nebulizer of approximately 1 bar. The aerosol was then passed through the silica gel dryer at ambient pressure, to reduce the relative humidity. A total flow of 1.5 L min^{-1} was introduced into the tubular furnace by adding 50 mL min^{-1} flow of oxygen (or hydrogen) and additional argon to the aerosol generated flow. In order to avoid losses due to electrostatic deposition in the system, all the instruments were connected using electrically conductive tubes. At the outlet of the furnace, the aerosol is diluted with a mixture of air/Ar and introduced into the RDD.

The RDD consists of a dilution head and a control unit. The dilution argon flow provided to the dilution head has to be defined by an MFC, because it determines also the flow rate of the diluted aerosol directed to the DMA. Only the RDD connected to the modified SMPS was also equipped

with an evaporation tube, operated at 350°C in all experiments. The SMPS is operated such as a size range between 13 and 300 nm is covered. A second SMPS instrument (TSI) was used as a reference, operated with a separate RDD, as shown in Figure 6.1-1. The classified aerosol leaving the DMA was split between the CPC and the ICP-MS with a ratio 3:7. A flow of 4 mL min⁻¹ of a mixture of xenon in argon (Xe 100 ppm_v), precisely adjusted with an MFC, was added to the monodisperse aerosol flow directed into the ICP-MS. This allowed a proper tuning of ICP-MS parameters before each measurement to obtain high sensitivity based on the recorded signal of ¹²⁴Xe, and an eventual plasma drift could, therefore, be monitored during the overall analysis.

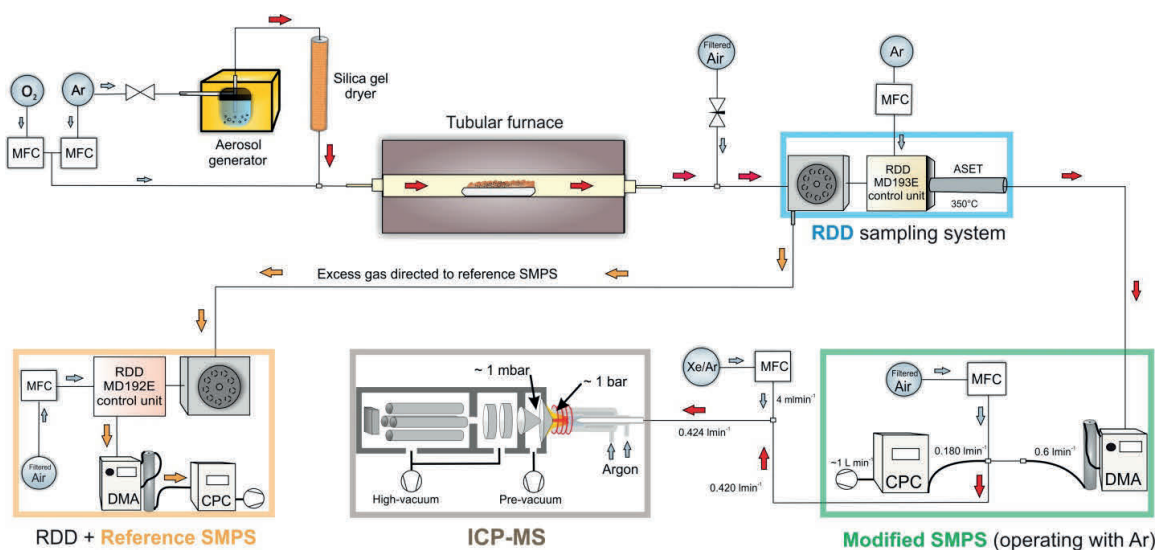


Figure 6.1-1 Flow concept of the thermal treatment and the SMPS-ICPMS setup. The red arrows show the main path of the measurement, while orange arrows show the parallel measurement with a reference SMPS. The different gases provided to the system are instead indicated as light-blue arrows. Legend: MFC = mass flow controller, RDD = rotating disc diluter, ASET = evaporation tube, SMPS = scanning mobility particle sizer, DMA = differential mobility analyzer, CPC = condensation particle counter, ICP-MS = inductively coupled plasma mass spectrometry.

6.1.2 Temperature program of the lab-scale incinerator

In order to determine the optimal dilution ratio for the generated emissions and to protect the instrument's detectors, a first temperature program was performed with a constant heating rate between 200 and 500°C. In details, the program (Fig. 6.1-2a) consisted of a first drying step at a constant temperature for 10 minutes, after which the temperature was increased fast up to nearly 220°C and from there a constant heating rate of 5° min⁻¹ was applied for 50 min. At nearly 500°C the heating rate was increased from 5° min⁻¹ to 20° min⁻¹ until nearly 910°C was reached. The final temperature was then kept constant for 20 minutes.

A standard incineration procedure was later applied to simulate the combustion processes in an industrial plant (Fig. 6.1-2b), consisting of a drying step, a fast pyrolysis from 300 to 900°C, a combustion at 900°C and an afterburning from 900 to 400°C. The different temperatures reported in the Fig. 6.1-2 are the real temperature measured with a thermocouple inside the quartz tube (gray

line, $T_{\text{profile sample}}$) and with another thermocouple outside the alumina shield giving the temperature provided by the furnace (green line, $T_{\text{profile furnace}}$). The acquisitions of both SMPS and ICP-MS signals were started simultaneously when a temperature of 105°C was reached inside the tubular furnace in the case of the first temperature program. For the incineration program lasting only 24 min, the measurements were started simultaneously with the furnace's temperature program, but the RDD channel was opened only for combustion and afterburning steps, 6 min after the start.

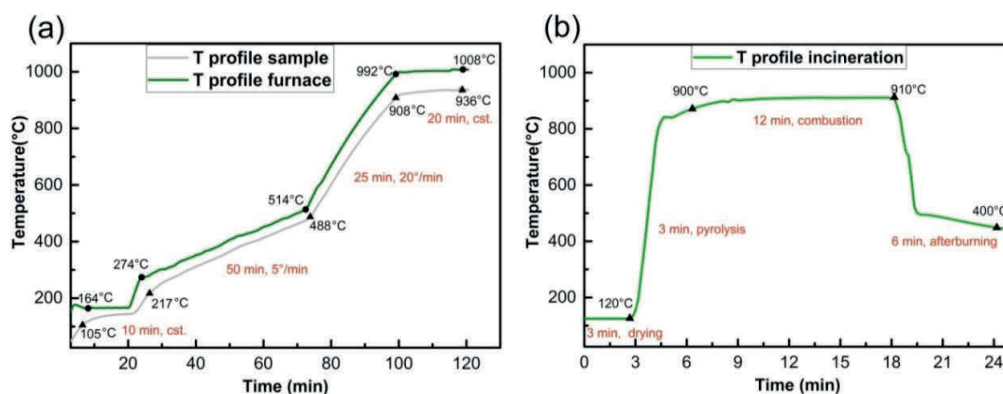


Figure 6.1-2 Temperature program applied to the sample introduced inside the tubular furnace (a); gray line: temperature T_{in} measured with a thermocouple inside the tubular furnace, close to the sample; green line: temperature T_{out} measured in the outer part of the tubular furnace, outside the alumina shield. Temperature profile of a standard incineration procedure in a larger incinerator (b).

6.1.3 Size-selected particles collection and sample preparation for TEM

The size-selected particles from 13 to 340 nm were collected at the outlet of the DMA, using an aspiration EM grid sampler[109] (detail view and schematic sampling point reported in the Chapter 2). The particles were filtered through a TEM grid (Quantifoil R 1.2/1.3 Cu 400 mesh) from the tube normally directed to the ICP-MS at the outlet of DMA, with a flow rate of 0.3 L min⁻¹ by using a membrane pump. The particles were collected in separate replicates of the experiments reported in the Result and Discussion for which the ICP-MS detection was not included. The samples were later analyzed with a JEOL JEM-2010 transmission electron microscope (200 kV, point resolution of 0.25 nm), to investigate particle size and morphology. The chemical composition was clarified through the use of EDXS and electron diffraction pattern of the crystalline material.

6.2 Results and discussion

6.2.1 ZnO injected particles during sawdust thermal treatment

A brief subsection is firstly reported on beech sawdust thermal treatment only, in order to carefully evaluate the contribution of the particles generated by sawdust incineration and the ZnO particles produced with the aerosol generator and additionally injected into the tubular furnace,.

6.2.1.1 Beech sawdust thermal treatment

The beech sawdust incineration experiments were performed under oxidizing conditions (O_2 50 mL min^{-1}) in a lab scale incinerator, following the temperature program reported in Figure 6.1-2. The highest concentration of particles (shown in Fig. 6.2-1a) was measured between 280 and 380°C, due to carbonaceous particles emission. This observation is in accordance with previous TGA studies, reporting the decomposition of hemicellulose, cellulose, and lignin at temperatures around 230-380°C, followed by cellulose pyrolysis up to nearly 480°C.[135] In this range of temperatures the hemicellulose and lignin fractions of the wood (60% of the sample) are converted mainly to aerosol or gas (CO , CO_2 , H_2O , etc.).

Even if a clear particle formation event can be measured in SMPS, no clear corresponding distribution can be seen in the ICP-MS contour plot. Figure 6.2-1b shows instead that the mass intensity of ^{13}C covers almost constantly the overall range of particles from approximately 280 till 630°C. This means that in the size range considered the contribution of the gaseous compound to the overall signal of carbon is significantly higher than that of the classified particles. This observation could be also a consequence of the use of the heating tube in the RDD, which is kept at 350°C to have maximum transport efficiency and could prevent coagulations phenomena (which would generate agglomerates probably above our maximum value of 300 nm).

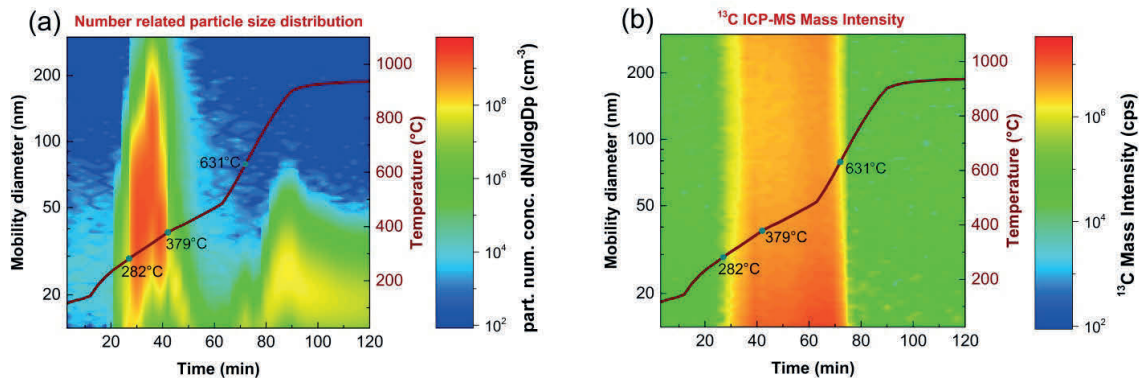


Figure 6.2-1 Number related PSD of sawdust during thermal treatment (a) and ICP-MS mass intensity of ^{13}C (b).

6.2.1.2 Injection of ZnO particles during sawdust thermal treatment

Dried ZnO particles generated with the use of an aerosol generator were constantly injected into the lab-scale incinerator during the thermal treatment of beech sawdust, such as the one described in the section above. The particle size distribution and the intensity of ^{66}Zn were measured with SMPS-ICP-MS. Figure 6.2-2b shows the particle-size-related ICP-MS intensity covering a 100-290 nm size range, with intensity more or less constant during the total time of analysis. The contribution of Zn in the overall PSD was efficiently resolved through the established correlation between ICP-MS and SMPS

shown in the previous chapters. As shown in Figure 6.2-2c, the raw signal of the ICP-MS follows the size selection applied in the SMPS, for which particles with the same mobility diameter will reach the ICP at a specific DMA voltage. By increasing the voltage the next size class is selected. This iterative process allows for a corresponding signal between each size class and ICP-MS intensity over a time range of 150 s (up scan), followed by a fast down scan from high to low voltage, in order to start the next up scan.

The size range of particle-size-related ICP-MS intensity is confirmed by preliminary studies performed in the same conditions on the ZnO suspension alone, which showed a broad distribution ranging from 50 nm up to 290 nm, with a higher intensity between 100 and 290 nm (Fig. 4.2-3 in Chapter 4).

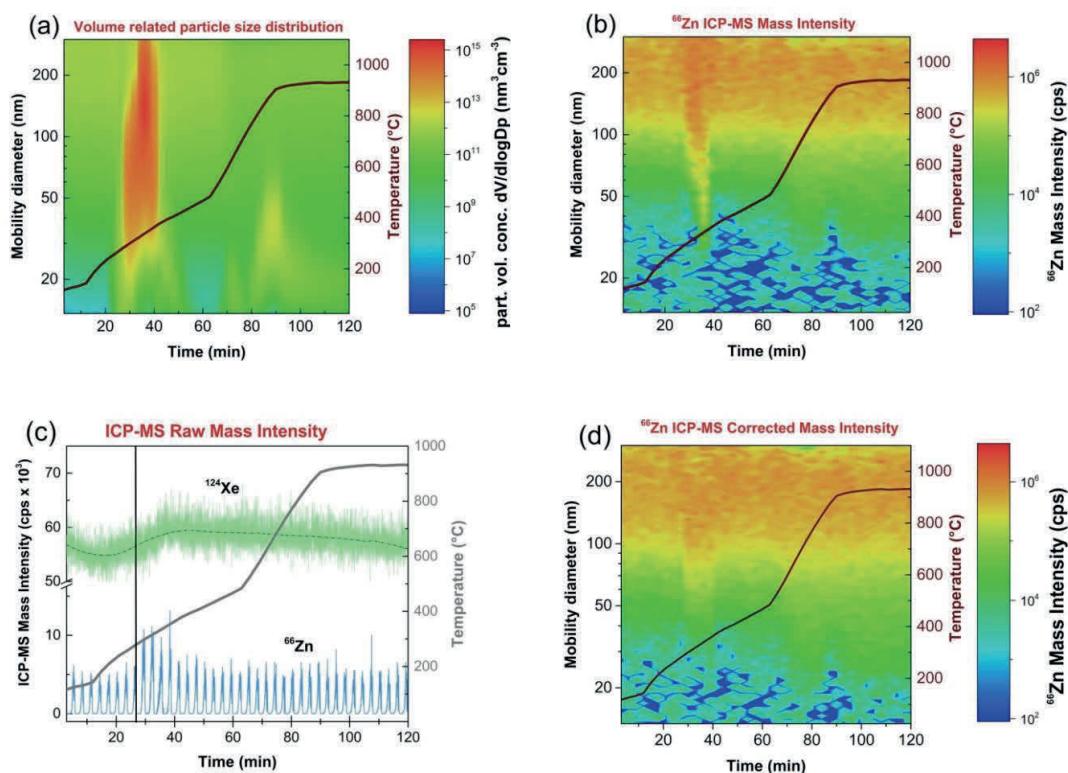


Figure 6.2-2 2D plot of the volume-related PSD of combusted sawdust and injected ZnO particles (a) and the size-related ICP-MS intensity of ⁶⁶Zn (b). Raw ICP-MS intensity for ⁶⁶Zn and ¹²⁴Xe (c) showing increasing intensity from the black line; size-related ICP-MS intensity of ⁶⁶Zn (d) corrected proportionally to the ¹²⁴Xe signal.

The experiments on sawdust only showed a maximum in the particle concentration within 280 and 380°C (Fig.6.2-1a). In correspondence precisely with this temperature interval, an unexpected increased intensity in the ⁶⁶Zn ICP-MS signal and a decrease in the mobility diameter were detected for the injected ZnO particles (Figure 6.2-2b). This behavior may have two possible explanations. First, through the combustion, the concentration of C increased resulting in an increased ionization efficiency of the plasma and then in higher sensitivity of the different elements present in the plasma, including Zn. Fliegel et al. reported how carbon addition is consistently improving sensitivity for all

elements from Li to Bi by the use of a mixed gas plasma with methane addition.[136] This seems to be confirmed by the corresponding increase in the ^{124}Xe signal, in this particular time frame with respect to the overall analysis (Figure 6.2-2c). Second, alterations of the ZnO particles could occur due to the reducing potential of the carbon compound generated by the sawdust combustion, resulting in a decrease of the particle size diameter in comparison to the size of the injected particles. This hypothesis is not confirmed by TEM analysis on the size-selected particles collected during this time frame (SMPS scan from 30 to 40 min in Fig.6.2-2c). Figure 6.2-3b shows that not only the particle size is comparable but also the morphology is consistent with the one analyzed for the ZnO powder (Figure 6.2-3a), that is, the carbon generated atmosphere is not having a relevant effect on the ZnO nanoparticles but only on the corresponding ICP-MS signal intensities, at this specific temperature interval. Therefore, the particle-size-related ICP-MS signal was corrected proportionally to the drift registered for the ^{124}Xe signal (Figure 6.2-2d).

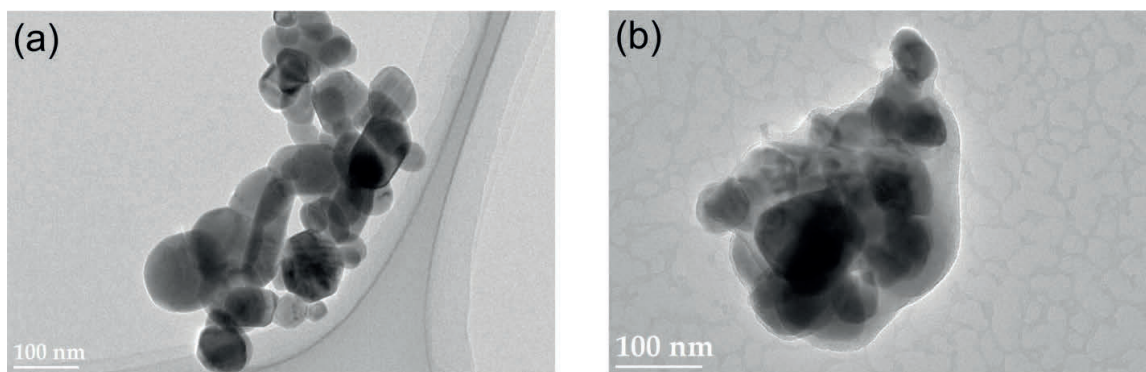


Figure 6.2-3 TEM micrograph on ZnO commercial nanopowder dispersed in ethanol (a); TEM micrograph on injected ZnO particles, which were collected after thermal treatment at about 340°C during the sawdust combustion (b) and after size selection through the DMA.

6.2.2 ZnO impregnated sawdust thermal treatment

As a nanowaste model, a sample of ZnO-impregnated sawdust was investigated to monitor submicron particles release during thermal treatment, applying the same conditions of the previously presented experiment (in excess of oxygen and with the same temperature profile). For the ^{66}Zn only a few peaks were detectable in ICP-MS (Figure 6.2-4b), which can be most probably due to physical transport of some ZnO particles.

Nevertheless, ZnO contained in the sawdust is to a great extent retained in the bottom ashes. These results might be explained by the fact that ZnO is very stable at the oxidizing conditions up to high temperatures.[137] Although carbothermal reduction of ZnO is a process commonly used in metallurgical extraction,[138] this reaction cannot be taken into consideration as a possible scenario, since elemental C and CO (g) generated by decomposition of carbon species occur before reaching the temperature at which ZnO can be reduced (at about 500°C in case of excess H_2 , as shown in Figure 4.2-8 in Chapter 4). On the other hand, the investigation of the behavior of the ZnO

nanopowder under reducing atmosphere (excess of H_2 in an argon atmosphere) confirmed the evaporation of $Zn(g)$ and the change in morphology and chemical composition of the reformed Zn -containing particles. At nearly $800^\circ C$, the maximum in intensity is detected by SMPS-ICP-MS (Figure 4.2-8 in Chapter 4). TEM analysis and electron diffraction patterns of the size-selected particles collected at the DMA outlet suggest a core-shell structure with an inner Zn core and an outer passivation layer generated by reoxidation of Zn surface (Figure 6.2-5b below and Figure 4.2-9 d-f in Chapter 4). In this experiment, a substantial deposition on the quartz tube was observed, either as a white or gray film, in different areas of the tube. Figure 6.2-5a shows the presence of Zn in two different morphologies, a lamellar one and a flower-like type, most probably associated with ZnO . The Zn deposited in the form of lamellar or hexagonal prismatic crystals, probably where the temperature in the quartz tube dropped from 600 to $400^\circ C$, as reported in previous experiments by Weidenkaff.[139] Further characterizations were already reported and commented in Chapter 4 (Figure 4.2-8 b-c).

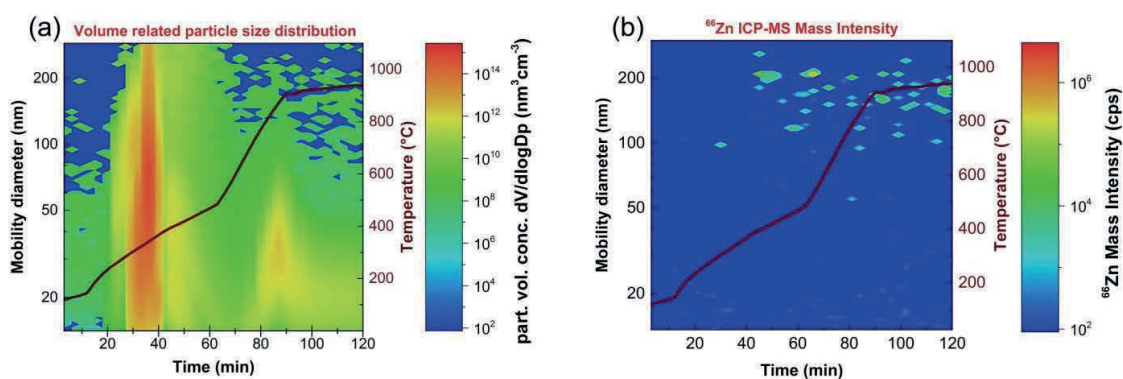


Figure 6.2-4 Volume-related PSD of ZnO -impregnated sawdust (a) and ICP-MS mass intensity of ^{66}Zn (b), in presence of O_2 (50 mL min^{-1}). Temperature profile (brown line) with a constant heating rate ($5^\circ C\text{ min}^{-1}$) between 200 and $500^\circ C$.

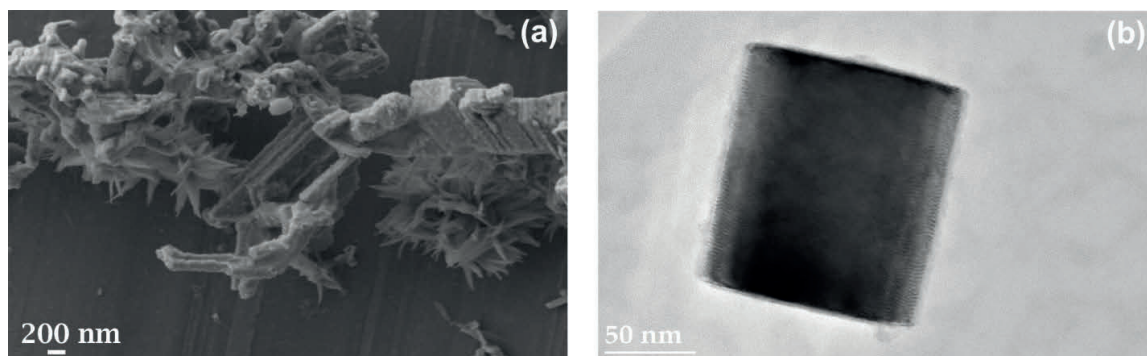


Figure 6.2-5 SEM micrograph of ZnO powder (a), after thermal treatment in presence of H_2 (50 mL min^{-1}); TEM micrograph of size-selected particles collected at the outlet of the DMA(b), after thermal treatment in presence of H_2 (50 mL min^{-1}).

6.2.3 ZnO impregnated sawdust incineration

Another sample from the same batch of ZnO-impregnated sawdust was used for a standard incineration experiment. According to the similarity laws described by Wochele et al.,[140] the typical 100 min program of a municipal solid waste incinerator was reduced to 24 min for a lab-scale incinerator (brown line in Fig. 6.2-6), in order to observe the complete conversion of carbon compound to CO₂. The eventual release of ZnO particles at these particular conditions is investigated by RDD-SMPS-ICP-MS. In opposition to the previous experiments (Fig.6.2-4), a clear PSD ranging from 50 to 240 nm was obtained for Zn-containing particles, as reported in Figure 6.2-6b. Additionally, what stands out in Figure 6.2-6 is the good correlation between the shape of volume-related PSD and ⁶⁶Zn ICP-MS mass intensity. These results indicate that with this temperature program applied, an effective reduction occurs. As suggested in the previous section, reduction of ZnO by C or CO is a quite known process that leads to the formation of Zn.

However, the main limitation from the SMPS-ICP-MS measurement presented in Figure 6.2-6 is that the submicron particles emitted during combustion can be only related to generally Zn-containing particles, without having specific information on the molecular composition and morphology. Therefore, the size-selected particles contributing to the intensity measured in Figure 6.2-6b were collected at the outlet of the DMA through aspiration EM sampler and further characterized with TEM.

First of all, the intercorrelation between PSD measured with TEM and SMPS appears clear. The size distribution is confirmed in a range of smaller particles of 20 nm to the statistically significant presence of 50, 70, and 85 nm particles, together with bigger agglomerate with an aerodynamic diameter up to around 240 nm probably formed in the cold zone of the quartz tube or during particle collection.

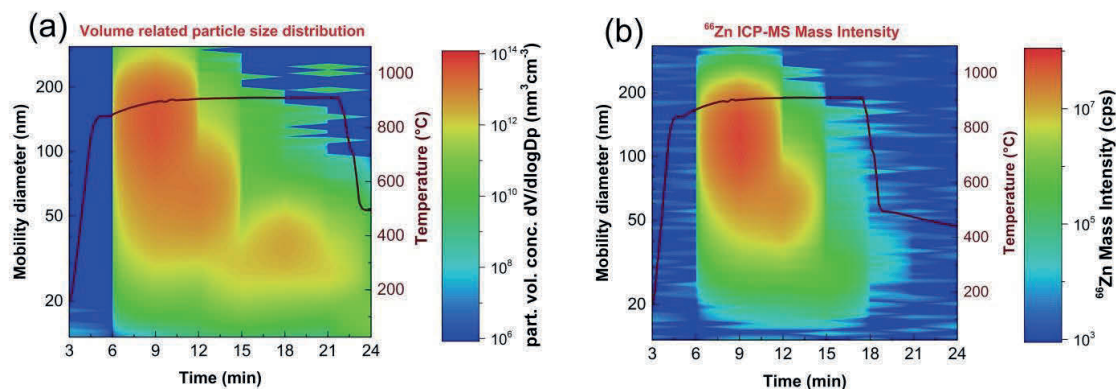


Figure 6.2-6 Volume related particle size distribution of ZnO-impregnated sawdust (a) and ICP-MS mass intensity of ⁶⁶Zn (b), in presence of O₂ (50 mL min⁻¹). Temperature profile (brown line) lasting only 24 min: drying step, fast pyrolysis from 300 to 900°C, combustion at 900°C, and afterburning from 900 to 400°C. Measurements started simultaneously with the furnace's temperature program, but the RDD channel opened only for combustion and afterburning steps, 6 min after the start.

In the following subsection is suggested a mechanism of reduction and further re-oxidation to give ZnO as the final product. Thermochemical calculations supporting this hypothesis are additionally reported in Appendix A (Fig. A.4.4-1 and A.4.4-2).

6.2.3.1 ZnO reduction and further re-oxidation

If solid carbon or CO_(g) is present at high temperatures, a reduction of ZnO can occur following the reactions written below:



The gas ratio, as soon as zinc vapor is formed, is expressed as:

$$p_{\text{CO}_2}/p_{\text{CO}} = K/p_{\text{Zn}} \quad (3)$$

Where K is the equilibrium constant and p is the partial pressure of the indicated compound. Since the partial pressures of Zn, CO, and CO₂ are stoichiometrically related, only one degree of freedom is defined, either temperature or pressure. Ellingham diagram shows the thermochemical dependency of various oxides on the log of pCO₂/pCO plotted vs (1/T).

For instance, at p_{Zn} = 1 atm intersection between the curve of liquid zinc and plotted pCO₂/pCO ratio take place at 907°C, where equilibrium between liquid and gaseous Zn is reached.[138]

Depending on the relative pressure of Zn and CO, the dew point of Zn will shift to lower or higher temperatures, assuming much lower CO₂ pressure, since complete conversion is expected at the end of the 24 min program. Thermochemical calculations performed with HSC software show the reduction of ZnO by mainly CO from nearly 600°C (Fig. B.4.4-2), considering for the input molar ratio the high excess of C contain in the feedstock compared to the concentration of impregnated Zn. In presence of H₂O, the water-gas-shift reaction (WGSR) can occur:



which is exothermic only for temperature below 700°C and tends to shift to reactants as temperature increases. Therefore, reduction of ZnO could take place also through reaction with H₂, despite the fact that C has been proved as a stronger reducing agent for temperatures above 660 °C.[24]

Without the use of a proper quenching, re-oxidation of Zn was observed at a temperature below 840°C.[139,141] Thus, during cooling in the cold zone of the quartz tube, the Zn generated is oxidized again to ZnO by either CO₂ or H₂O vapor before applying an efficient dilution to prevent further agglomeration

6.2.4 ZnO nano-object from impregnated wood combustion: estimation of Zn content in emissions

This section describes the estimation of Zn content in emissions during the incineration of impregnated wood. State-of-the art methods for the determination of metals emissions from stationary sources (such as Method 29, from the Environmental Protection Agency)[142] often include the use of quartz fibre filters for PM and impinger bottles for gaseous emissions, with following offline analysis with ICP-OES (inductively coupled plasma emission spectroscopy), ICP-MS or CV-AAS (cold vapour atomic absorption spectroscopy). Most of the studies on wood combustion emissions presents a similar approach regarding the PM elemental analysis, with collection of the particles onto analytical filters and subsequent ICP-MS analysis, while the size distribution is often determined with SMPS or FMPS (fast mobility particle sizer) and ELPI (electrical low-pressure impactor) or HRLPI (high-resolution low-pressure cascade impactor). Other offline methods to assess the concentration of trace metal in aerosol samples are XRF (X-ray fluorescence) or PIXE (proton-induced X-ray emission).[143–145] Some exceptions were although including an online strategy, such as trace metal analysis on soot particles by SP-AMS(soot-particle aerosol mass spectrometer)[56] or organic emissions determination by SPI-ToF-AMS (single-photon ionization time-of-flight mass spectrometry).[146] Those methods require anyway an extensive data treatment and availability of molecular fragmentation tables.

For all the above reasons, the quantification of Zn was here performed using the calibration strategy coupling a TGA to the RDD-SMPS-ICP-MS setup already described in Chapter 5. Although a matrix-matched calibration might deliver more accurate quantification. [72] no substantial matrix effects were expected, due to the high dilution applied. Indeed, the monitoring of the plasma stability through ^{124}Xe signal, acquired during the whole experiments, confirmed this supposition. As described before in section 6.2.3, most of the Zn-containing particles were emitted after the fast pyrolysis and during the combustion at 900°C. Fig. 6.2-9 shows on the right side the ICP-MS intensities measured as a function of the mobility diameter and time (a) and the corresponding Zn concentrations on the left side (b), which lies all well beyond the LoD of the method.

Assuming that the entire Zn concentration hereby measured can be referred to ZnO nano-objects, this latter can be expressed also as volume-related concentration using the density of bulk ZnO (Fig. 6.2-9d). Apart from knowing the effective density would lead to more accurate results,[147] the quantification of the volume concentration of ZnO is succeeded. Moreover, possible incongruences due to geometrical factors are bypassed by gathering the ZnO volume-related PSD from the Zn concentration measured in ICP-MS.

The ZnO nanoparticles presented morphology rather similar to a nano-rod than a sphere. Those deviations from the spherical geometry could lead to significant changes in particle mobility diameter. Nevertheless, the range of voltages applied and the low electric field caused in this case a random orientation of the particles, without any preferential particle alignment during the size-selection into the DMA. [130,148] As a result of Fig. 6.2.4 c and d comparison, it can be concluded that the volume concentration of ZnO can be tracked and discriminated from the total PSD even

though it gives in a very small contribution. This observation is consistent with the studies of Elssasser and Leavy, who both reported how a higher ratio of organic matter is generated during each stage of wood combustion in comparison with the inorganic fraction.[57,149]

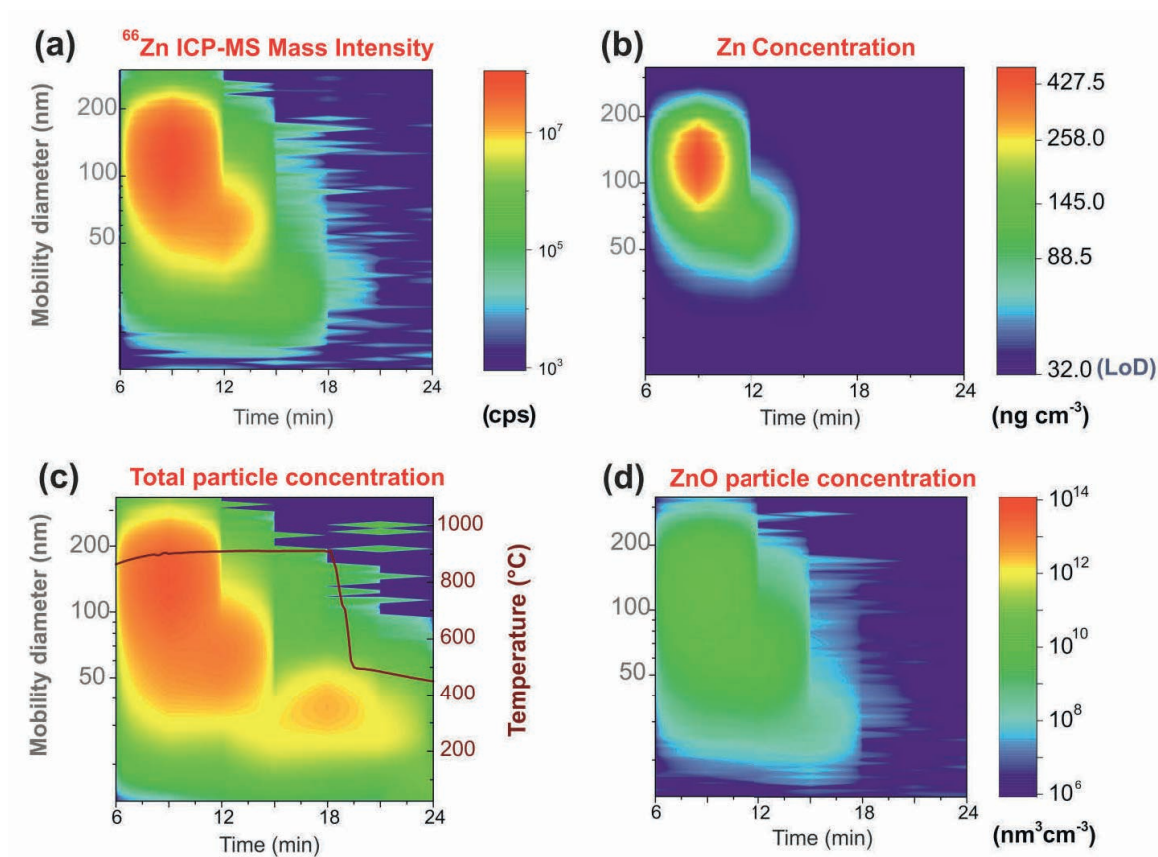
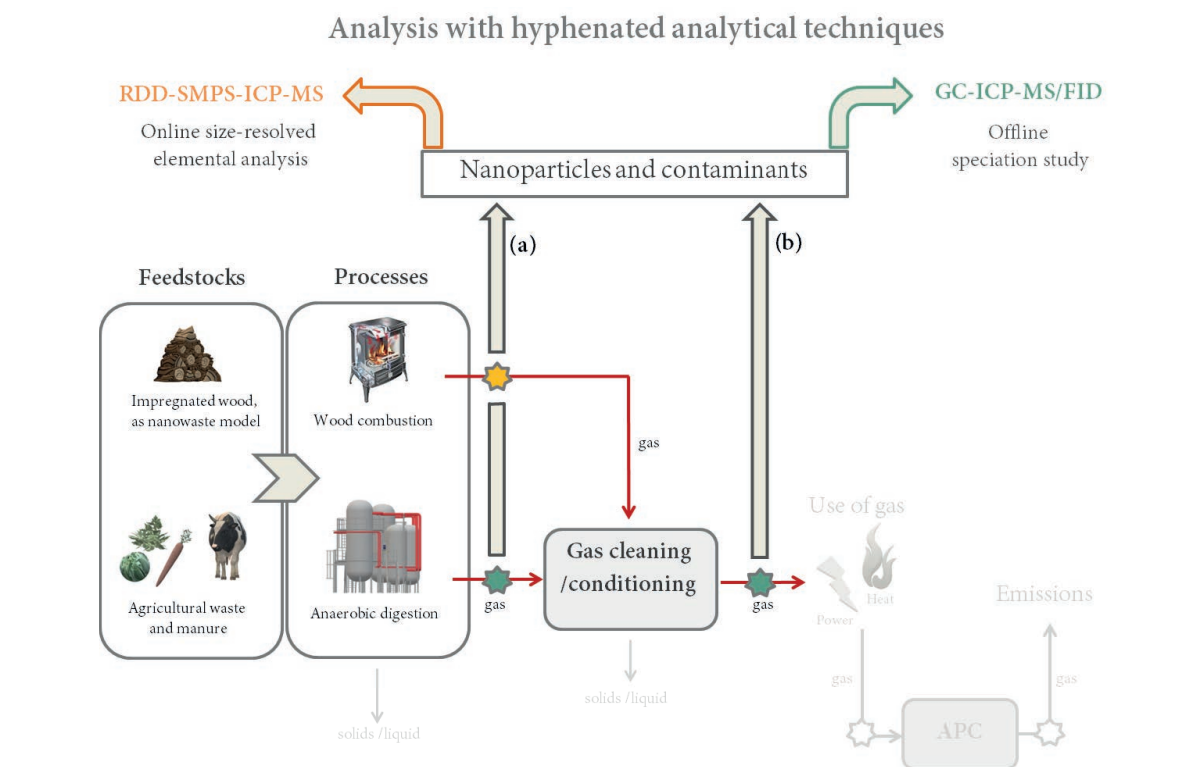


Figure 6.2-9 (a) ICP-MS measured intensities for ^{66}Zn , (b) calculated concentration of Zn, (c) volume distribution of the total amount of particles generated, (d) volume distribution of ZnO only. The right colour scale ($\text{nm}^3\text{cm}^{-3}$) is valid for both plots (c) and (d).

6.2.5 Wood fly ashes

Elled et al. detected a bimodal PSD for wood fly ashes with submicron and micrometer ranges, respectively. The first PSD mode (submicron particles) is attributed to inorganic matter, while the second one derives from fragmentation of mineral and char.[137] The formation of ash particles and aggregates has been previously shown to occur for condensation of organic material or inorganic vapors on the generated ZnO particles. Alkali salts are generally found on the surface of these newly formed particles if efficient combustion occurs.[26] Since we focus in our experiments principally on the first peak of this bimodal distribution, only smaller inorganic particles were detected, while bigger agglomerates of organic carbon are directed to the excess gas during DMA selection.

Chapter 7 Concluding remarks and outlook



Material from this chapter has been partially published in :

- (I) Debora Foppiano, Mohamed Tarik, Jörg Schneebeli, Adelaide Calbry- Muzyka, Serge Biollaz and Christian Ludwig, Siloxanes compounds in biogas from manure and agricultural waste: Method development and Speciation analysis with GC-ICP-MS/FID., **2018**, in peer-review.
- (II) Mohamed Tarik, Debora Foppiano, Adrian Hess, and Christian Ludwig, A Practical Guide on Coupling a Scanning Mobility Particle Sizer and Inductively Coupled Plasma Mass Spectrometer (SMPS-ICPMS), *J. Vis. Exp.*, **2017**, (125), e55487, doi:10.3791/55487.
- (III) Debora Foppiano, Mohamed Tarik, Elisabeth Müller Gubler, and Christian Ludwig, Combustion generated nanomaterials: online characterization via an ICP-MS-based technique. Part I: calibration strategy with a TGA, *J. Anal. At. Spectrom.*, **2018**, 33, 1493-1499.
- (IV) Debora Foppiano, Mohamed Tarik, Elisabeth Müller Gubler, and Christian Ludwig, Combustion generated nanomaterials: online characterization via an ICP-MS-based technique. Part II: resolving power for heterogenous matrices, *J. Anal. At. Spectrom.*, **2018**, 33, 1500-1505.
- (V) Debora Foppiano, Mohamed Tarik, Elisabeth Müller Gubler, and Christian Ludwig, Emissions of Secondary Formed Nano-Objects from the Combustion of Impregnated Wood. An Online Size-Resolved Elemental Investigation, *Environ. Sci. Technol.*, **2018**, 52, 895-903.

This chapter reports on the main findings and gives concluding remarks of this doctoral thesis. The importance of hyphenated techniques was highlighted for waste treatment and bioenergy processes. The combination among different analytical techniques was proven to be successful for determining the presence and the fate of nanoparticles and contaminants generated during waste treatment and biogas production processes, respectively. Concluding remarks on two main scientific questions of this thesis are presented separately in the following sections, together with a possible outlook for future developments. Finally, general conclusion are reported at the end of this chapter. The superscript notation in roman numbers indicate the original publications on which a particular section of this chapter is based and they are reported with their full bibliographic reference on the first page of this chapter.

7.1 Speciation of siloxanes in biogas production process ^I

A successful speciation analysis of siloxane compounds in biogas was achieved by coupling a GC with two detectors (FID and ICP-MS) running simultaneously. The parallel analyses with GC-ICP-MS are particularly recommended to meet the requirements of new European regulations (lower detection limits).[43] Siloxane concentration in biogas from manure and agricultural waste was proven to be lower than in the case of wastewater treatment plant (WWTP) biogas, where the concentration of D5 can reach up to 10 mg Nm⁻³. [114] The sample MixUntreated (collected before adsorption on activated carbon) shows concentrations around 0.1 mg_{Si} Nm⁻³, which are enough to degrade the performance of SOFCs or to cause microturbines damages in the long run. However, samples of biogas treated by an activated carbon filter did not contain Si in concentrations above 0.002-0.004 mg_{Si} Nm⁻³. Regardless of the good efficiency of the adsorption material, it is good practice to monitor the concentration in the treated fraction after a certain number of hours to verify when regeneration of the filter is needed.

A major advantage resides in the continuous liquid quench system used in the sampling campaign that allows performances comparable with other techniques but improved time-resolution. Considering the wide-spread use in analysis laboratories, the GC-FID is here suggested for preliminary estimations, even in case of field measurements. Nevertheless, certain precautions are needed in the data treatment, since it was here established that GC-FID overestimates the concentration of siloxanes in the analysed samples. Thanks to the comparison between concentrations simultaneously determined with GC-FID and GC-ICP-MS, it was demonstrated that, in case of highly interfered peaks, the integration with a lower number of points around the peak apex might be affected by higher uncertainty but is, in any case, suggested to achieve an estimation closer to the real value of concentration. Hence, it is less precise but more accurate than considering an extended number of points through the integration window (from the baseline). After an initial assessment with GC-FID, accurate and precise determinations can be achieved by analyzing the samples with the developed GC-ICP-MS method.

7.1.1 Outlook

For future development, the integration in the GC of a SCD -sulfur chemiluminescence- detector, species-specific for sulfur compounds, would provide additional benefits for the simultaneous determination of sulfur compounds, one of the major classes of impurities in biogas. Furthermore, even lower limit of detections could be reached by using a GC-ICP-MS/MS strategy that includes the use of a triple quadrupole as an analyzer. The principle can be summarized as a selection of the mass of interest in the first quadrupole, a mass-shift applied in the second quadrupole either to the isobaric interferences or the analyte by reaction with a gas and after that the selection of the mass to charge ratio of interest in the third quadrupole. The instrument was proven to be successful for the detection of heteroatom in different applications, such as environmental, clinical, life science, nuclear, and semiconductor materials characterization.[150,151]

7.2 Fate of NPs during combustion of impregnated wood, used as a model nano-waste ^{III, IV, V}

Compared with the state-of-the-art analytical methods for aerosols characterization, such as particle sizers, the RDD-SMPS-ICP-MS combination is not only able to simultaneously acquire chemical and size information, but the time-resolved ICP-MS signals also allow the determination of each element's contribution in the overall PSD. However, only particles with a diameter below 400 nm can be measured by the current argon-operated SMPS-ICP-MS. Furthermore, for a complete characterization of aerosol particles, other offline techniques are needed to determine other properties, including the morphology and the molecular structure.

The calibration strategy of RDD-SMPS-ICP-MS and the comparison between SMPS and ICP-MS performances were presented. Thanks to the coupling between a TGA and the RDD-ICP-MS, it was possible not only to obtain qualitative information about the size-classes and elemental composition but also to express the concentration for the elements of interest in ng cm^{-3} . Owing to the presented TGA calibration concept, a more accurate quantification than that of SMPS was achieved, in the case of analysis of a single compound (i.e. ZnCl_2). Even though the SMPS is essential to perform the size-selection, it was here observed that the mass concentration derived from the SMPS number concentration can be biased by the deviations from the two main assumptions adopted in the data treatment. Deviations from the spherical geometry and the bulk density can lead, indeed, to a relative difference between the two instruments up to 30%. Moreover, the use of SMPS solely allows neither speciation studies nor quantification in case of mixtures analyses, which make in this respect the quantification method using TGA very promising. In the second part of this study, we proved also the resolving power of the technique in a complex matrix, such as a mixture of different metal chlorides. However, especially for heterogeneous samples, it is suggested that in the future a matrix-matched calibration approach would be used, which could better take into account also matrix effects and reduce the calibration time. In conclusion, the coupling of TGA with ICP-MS and the successful calibration strategy applied were crucial to obtain reliable information about their concentration, in addition to their PSD and elemental composition.

The current data highlight the importance of determining the fate of nano-objects during thermal treatment processes. Although the work presented by Walser et al. might suggest the entrapment in the bottom ashes and APC residues of most of the nanoparticles (CeO_2) injected in a waste incinerator,[15] that case is not considering metal nanoparticles and non-nano particulate metals in waste which may reform as incidental nanoparticles.[17] As explained by Roes et al. secondary nano-objects might be formed depending on the conditions present in the incinerator. Moreover, in the case of particle size below 100 nm, a complete removal from flue gas is not ensured.[18]

This study confirms the presence of incidental ZnO nano-objects in the fine particles fraction upon combustion of a nanowaste model, with dimensions also below 100 nm detected by the use of an online analytical technique. Moreover, this finding proves the possibility of formation of secondary nano-objects that can decompose and reform as new species.. Due to the demonstrated toxicity of ZnO,[152–154] a particular attention should be addressed to emissions by small and medium scale plants below 1 MW, in which efficient filtering systems are not always implemented. Therefore, new experiments with larger burners, and in particular, tests on particle removal are suggested.

The majority of the studies on emission from stationary sources includes mainly off-line analyses with separated online PSD measurement and offline elemental composition determination, whereas for online studies AMS related techniques are primarily reported in the literature. The RDD-SMPS-ICP-MS system is extremely useful for detecting metal particles even among complex mixtures including a size and time-resolved acquisition with a faster data treatment, without needing extensive molecular databases. The use of complementary techniques is nevertheless advisable to collect information regarding the chemical speciation, further transformations occurring in the gas and the morphology of the particles emitted.

7.2.1 Outlook

In the measurement protocol, two critical points can be identified. The first point regards the consideration of multiple particle charges, which is not yet implemented in the data evaluation procedure for ICP-MS. While the single-charge correction gives a good correlation between SMPS and ICP-MS data when measuring small particles (up to 200 nm), correction for multiple charges on large particles should be established and implemented to improve the quality of the resulting information for particles above 200 nm. Another explanation of this effect could be that the larger particles are not completely decomposed and ionized in the plasma. The second critical point is the choice of the appropriate RDD dilution factor. Indeed, like in the analysis of liquid samples, the ICP-MS intensity level of the different isotopes depends on the corresponding sensitivity. The Cu signal, for example, is about three orders of magnitude higher than that of Cl. Therefore, an appropriate value of the aerosol dilution must be set considering the ICP-MS sensitivity of the measured elements. This might present a limitation of multi-element analysis for aerosols, either for the determination of light elements for which the sensitivity is low and the difference to that of metals and heavy metals is significant or for the determination of different elements in the sample if their concentration varies in a relative large range (e.g. from ppb to %) . However, the aerosol dilution

value can be changed during the same experiment, if the process of aerosol generation is known. For example, the dilution factor can be lowered during the phase in which a low particle amount is generated. Nevertheless, feeding highly particle-loaded aerosols into the DMA should be avoided to protect the CPC and the ICP-MS instrumentation. In summary, depending on the sampled aerosol, a compromise between RDD dilution, matrix loading, and ICP-MS sensitivity of the isotopes of interest should be found. Even though the time resolution of the SMPS-ICP-MS setup is limited by the SMPS scan duration, which is usually chosen in the range of a few minutes, the time resolution can still be enhanced for a fixed or narrow range of particles size.

For thermal treatment processes, a TGA can be used as a quantification tool [66]. This aspect was particularly developed in chapter 5, where the quantification method for the overall setup is described. The quantification of liquids or suspensions, instead, can be easily made using appropriate standard solutions.

Another point of improvement could be the design of a recirculation concept for argon, operating the DMA with air and exchanging this to argon (e.g. by means of a gas exchange device)[155], which would allow the use of higher DMA voltage and hence to enhance the measured particle range. Another solution to increase the particle range would include the use of a standard air-operating SMPS and a microwave inductively coupled atmospheric-pressure plasma (MICAP) operating with nitrogen instead of argon, [156–158] which not only means perfect suitability with the aerosol upcoming from the SMPS but also reduced costs and relative compact design, which can make it a good alternative for fast monitoring in field measurements.

Finally, automating the setting of the different parameters and merging the needs of SMPS and ICP-MS into a single concept, regarding the operating condition, would reduce substantially the steps of the measurement protocol. These steps help to make the SMPS-ICP-MS a powerful online setup for quantitative or qualitative analyses of different kinds of aerosols generated from liquid solutions, suspensions, or emission sources.

7.3 Final remarks

The combination among different analytical techniques was proven to be successful for determining the presence and the fate of nanoparticles and contaminants generated during nano-waste treatment and biogas production processes, respectively.

First, the performances of GC-ICP-MS and GC-FID were compared for speciation study of siloxane compounds in biogas production processes. Even though the two techniques have been singularly reported in literature, the novelty was here represented by their simultaneous operation and by the application chosen, for which a method development was required. Moreover, this analytical arrangement has the potential to be a valuable candidate to reach lower detection limit for Si, in the frame of different appliances such as SOFC, where even concentrations in the ppb range are enough to cause damages to the cells.

Moving from a relatively renowned example of hyphenated techniques, the use of RDD-SMPS-ICP-MS is suggested for the online measurement of gas-borne nanoparticles emitted during thermal

processes. The instrument had been developed in the CPM group during the four years previous to the start of this thesis. Despite an initial validation already proposed, further preliminary studies were needed to assess the performances of this hyphenated technique for combustion processes. In particular, the combustion of wood containing nano-materials was considered to evaluate the effect of redox conditions on the release of primary and secondary nanoparticles from nano-waste. The RDD-SMPS-ICP-MS setup was initially combined with different aerosol sources to evaluate weaknesses and points for improvements. One of the major improvements achieved was the use of the TGA, among the different aerosol sources employed in this thesis, as a powerful tool for quantifying the ICP-MS intensities of the detected metal elements. A tubular furnace, instead, was employed as a lab-scale incinerator to study ZnO-impregnated wood, as a model of nano-waste, during combustion experiments. The main focus was to verify the release of incidental nanoparticles, which are defined as the nanoparticles potentially generated in the flue gas by evaporation and further condensation of metal compounds. The reducing conditions generated through the decomposition of the wood proved to have an effect on heavy metals thermochemical behaviour, such as that of Zn, which is known to be redox-sensitive, i.e. it exhibits different volatility depending on the redox conditions. Therefore, thanks to the online size-resolved elemental analysis with RDD-SMPS-ICP-MS the presence of secondary formed ZnO-nano-objects was detected in waste combustion gases. Moreover, the successful calibration of the setup with a TGA could finally lead also to the determination of their concentration. The employment of hyphenated techniques was crucial not only to determine the presence of compounds of interest but also to understand complex thermochemical behaviour during the studied processes. This acquired knowledge is fundamental in order to ultimately understand and control the fate of nano-objects and support the development of environmentally sound and clean bioenergy and waste treatment technologies.

Bibliography

- [1] Obama, B. The irreversible momentum of clean energy. *Science* (80-.). **2017**, 355 (6321), 126–129.
- [2] Kröcher, O. SCCER BIOSWEET - The Swiss competence center for energy research on bioenergy. *Chimia (Aarau)*. **2015**, 69 (10), 2015.
- [3] Wochele, J.; Ludwig, C.; Stucki, S. The problem with Waste. In *Municipal Solid Waste Management*; Springer: New York, Berlin, Heidelberg, 2003; pp 2–3.
- [4] Obernberger, I.; Brunner, T.; Bärnthaler, G. Chemical properties of solid biofuels-significance and impact. *Biomass and Bioenergy* **2006**, 30 (11), 973–982.
- [5] de Wild, P. J.; Uil, H. den; Reith, J. H.; Kiel, J. H. A.; Heeres, H. J. Biomass valorisation by staged degasification. A new pyrolysis-based thermochemical conversion option to produce value-added chemicals from lignocellulosic biomass. *J. Anal. Appl. Pyrolysis* **2009**, 85 (1–2), 124–133.
- [6] Lanzerstorfer, C. Chemical composition and physical properties of filter fly ashes from eight grate-fired biomass combustion plants. *J. Environ. Sci. (China)* **2015**, 30, 191–197.
- [7] Nzihou, A.; Stanmore, B. The fate of heavy metals during combustion and gasification of contaminated biomass-A brief review. *Journal of Hazardous Materials*. 2013, pp 56–66.
- [8] Hinds, W. C. *Aerosol Technology*, 2nd editio.; John Wiley and Sons, New York, 1999.
- [9] Araujo, J. A.; Nel, A. E. Particulate matter and atherosclerosis: Role of particle size, composition and oxidative stress. *Part. Fibre Toxicol.* **2009**, 6, 1–19.
- [10] ISO - International Organization for Standardization. ISO/TS 80004-2, <https://www.iso.org/obp/ui/#iso:std:iso:ts:80004:-2:ed-1:v1:en> (visited on 02.12.2018).
- [11] Laden, F.; Schwartz, J.; Speizer, F. E.; Dockery, D. W. Reduction in fine particulate air pollution and mortality: Extended follow-up of the Harvard Six Cities Study. *Am. J. Respir. Crit. Care Med.* **2006**, 173 (6), 667–672.
- [12] Limbach, L. K.; Li, Y.; Grass, R. N.; Brunner, T. J.; Hintermann, M. A.; Muller, M.; Gunther, D.; Stark, W. J. Oxide Nanoparticle Uptake in Human Lung Fibroblasts: Effects of Particle Size, Agglomeration, and Diffusion at Low Concentrations. *Environ. Sci. Technol.* **2005**, 39 (23), 9370–9376.
- [13] Dandley, E. C.; Taylor, A. J.; Duke, K. S.; Ihrie, M. D.; Shipkowski, K. A.; Parsons, G. N.; Bonner, J. C. Atomic layer deposition coating of carbon nanotubes with zinc oxide causes

- acute phase immune responses in human monocytes in vitro and in mice after pulmonary exposure. *Part. Fibre Toxicol.* **2015**, *13* (1), 29.
- [14] Sanderson, P.; Delgado-Saborit, J. M.; Harrison, R. M. A review of chemical and physical characterisation of atmospheric metallic nanoparticles. *Atmos. Environ.* **2014**, *94*, 353–365.
- [15] Walser, T.; Limbach, L. K.; Brogioli, R.; Erismann, E.; Flamigni, L.; Hattendorf, B.; Juchli, M.; Krumeich, F.; Ludwig, C.; Prikopsky, K.; et al. Persistence of engineered nanoparticles in a municipal solid-waste incineration plant. *Nat. Nanotechnol.* **2012**, *7* (8), 520–524.
- [16] Buha, J.; Mueller, N.; Nowack, B.; Ulrich, A.; Losert, S.; Wang, J. Physical and chemical characterization of fly ashes from swiss waste incineration plants and determination of the ash fraction in the nanometer range. *Environ. Sci. Technol.* **2014**, *48* (9), 4765–4773.
- [17] Wiesner, M. R.; Plata, D. L. Environmental, health and safety issues: Incinerator filters nanoparticles. *Nat. Nanotechnol.* **2012**, *7* (8), 487–488.
- [18] Roes, L.; Patel, M. K.; Worrell, E.; Ludwig, C. Preliminary evaluation of risks related to waste incineration of polymer nanocomposites. *Sci. Total Environ.* **2012**, *417–418*, 76–86.
- [19] Johnson, D. R. Nanometer-sized emissions from municipal waste incinerators: A qualitative risk assessment. *J. Hazard. Mater.* **2016**, *320*, 67–79.
- [20] Stucki, S.; Jakob, A. Thermal treatment of incinerator fly ash: Factors influencing the evaporation of ZnCl₂. *Waste Manag.* **1997**, *17* (4), 231–236.
- [21] Merdzan, V.; Domingos, R. F.; Monteiro, C. E.; Hadioui, M.; Wilkinson, K. J. The effects of different coatings on zinc oxide nanoparticles and their influence on dissolution and bioaccumulation by the green alga, *C. reinhardtii*. *Sci. Total Environ.* **2014**, *488–489* (1), 316–324.
- [22] Osmond, M. J.; McCall, M. J. Zinc oxide nanoparticles in modern sunscreens: An analysis of potential exposure and hazard. *Nanotoxicology* **2010**, *4* (1), 15–41.
- [23] Ludwig, C.; Lutz, H.; Wochele, J.; Stucki, S. Studying the evaporation behavior of heavy metals by thermo-desorption spectrometry. *Anal. Bioanal. Chem.* **2001**, *371* (8), 1057–1062.
- [24] Jakob, A.; Stucki, S.; Kuhn, P. Evaporation of Heavy Metals during the Heat Treatment of Municipal Solid Waste Incinerator Fly Ash. *Environ. Sci. Technol.* **1995**, *29* (9), 2429–2436.
- [25] Wellinger, M.; Wochele, J.; Biollaz, S. M. A.; Ludwig, C. Online elemental analysis of process gases with ICP-OES: A case study on waste wood combustion. *Waste Manag.* **2012**, *32* (10), 1843–1852.
- [26] Tissari, J.; Sippula, O.; Torvela, T.; Lamberg, H.; Leskinen, J.; Karhunen, T.; Paukkunen, S.; Hirvonen, M. R.; Jokiniemi, J. Zinc nanoparticle formation and physicochemical properties in wood combustion - Experiments with zinc-doped pellets in a small-scale boiler. *Fuel* **2015**, *143*, 404–413.

-
- [27] Scarlat, N.; Dallemand, J. F.; Fahl, F. Biogas: Developments and perspectives in Europe. *Renew. Energy* **2018**, *129*, 457–472.
- [28] Verbeeck, K.; Buelens, L. C.; Galvita, V. V.; Marin, G. B.; Van Geem, K. M.; Rabaey, K. Upgrading the value of anaerobic digestion via chemical production from grid injected biomethane. *Energy Environ. Sci.* **2018**, *11* (7), 1788–1802.
- [29] Davidsson; Bernstad Saraiva, A.; Magnusson, N.; Bissmont, M. Technical evaluation of a tank-connected food waste disposer system for biogas production and nutrient recovery. *Waste Manag.* **2017**, *65*, 153–158.
- [30] Abdul Aziz, N. I. H.; Hanafiah, M. M.; Mohamed Ali, M. Y. Sustainable biogas production from agrowaste and effluents – A promising step for small-scale industry income. *Renew. Energy* **2018**, *132*, 363–369.
- [31] Bak, C. u.; Lim, C. J.; Lee, J. G.; Kim, Y. D.; Kim, W. S. Removal of sulfur compounds and siloxanes by physical and chemical sorption. *Sep. Purif. Technol.* **2018**, *209* (March 2018), 542–549.
- [32] Arnold, M. VTT RESEARCH NOTES 2496 Reduction and monitoring of biogas trace compounds. *Survivability* **2006**, *25*.
- [33] Rocha, F.; Homem, V.; Castro-Jiménez, J.; Ratola, N. Marine vegetation analysis for the determination of volatile methylsiloxanes in coastal areas. *Sci. Total Environ.* **2018**, *650*, 2364–2373.
- [34] Lanzini, A.; Madi, H.; Chiodo, V.; Papurello, D.; Maisano, S.; Santarelli, M.; Van herle, J. Dealing with fuel contaminants in biogas-fed solid oxide fuel cell (SOFC) and molten carbonate fuel cell (MCFC) plants: Degradation of catalytic and electro-catalytic active surfaces and related gas purification methods. *Progress in Energy and Combustion Science.* 2017, pp 150–188.
- [35] Madi, H.; Diethelm, S.; Poitel, S.; Ludwig, C.; Van herle, J. Damage of siloxanes on Ni-YSZ anode supported SOFC operated on hydrogen and bio-syngas. *Fuel Cells* **2015**, *15* (5), 718–727.
- [36] Madi, H. Investigations into the Effects of Biofuel Contaminants on Solid Oxide Fuel Cells, EPFL, 2016.
- [37] Madi, H.; Lanzini, A.; Diethelm, S.; Papurello, D.; Van Herle, J.; Lualdi, M.; Gutzon Larsen, J.; Santarelli, M. Solid oxide fuel cell anode degradation by the effect of siloxanes. *J. Power Sources* **2015**, *279*, 460–471.
- [38] Ruiling, G.; Shikun, C.; Zifu, L. Research progress of siloxane removal from biogas. *Int. J. Agric. Biol. Eng.* **2017**, *10* (1), 30–39.
- [39] Gersen, S.; Visser, P.; van Essen, M.; Brown, M.; Lewis, A.; Levinsky, H. Impact of silica deposition on the performance of gas-fired domestic appliances caused by the combustion of siloxanes in the fuel. *Renew. Energy* **2018**, *132*, 575–586.

-
- [40] Mojsiewicz-Pieńkowska, K.; Krenczkowska, D. Evolution of consciousness of exposure to siloxanes—review of publications. *Chemosphere*. 2018, pp 204–217.
- [41] Dungey, S. Identification of potential PBT/vPvB substances under the European REACH Regulation (EC) No. 1907/2006. **2014**, No. 1907.
- [42] ECHA, 2015. Annex XV Restriction Report Proposal for a Restriction: Octamethylcyclotetrasiloxane D4 and Decamethylcyclopentasiloxane D5. Environment Canada, 2009. Proposed Risk Management Approach for Cyclo- tetrasiloxane, Cyclopentasiloxane. No. June 2015.
- [43] EURAMET, Metrology for Biogas, 2017. *EMRP project ENG54, 2014-2017*, https://www.euramet.org/Media/docs/EMRP/JRP/JRP_Summaries_2013/Energy_JRPs/ENG54_Publishable_JRP_Summary.pdf; 2017.
- [44] Chen, B. T.; Crow, D. J. Use of an aerodynamic particle sizer as a real-time monitor in generation of ideal solid aerosol. *J. Aerosol Sci.* **1986**, *17* (6), 963–972.
- [45] Intra, P.; Tippayawong, N. An overview of differential mobility analyzers for size classification of nanometer-sized aerosol particles. *Songklanakarin J. Sci. Technol.* **2008**, *30* (2), 243–256.
- [46] Masayuki, I.; Takahashi, K. Measurement of Aerosol particles by dynamic light Scattering-I. Effect of non-gaussian concentration fluctuation in real time photon correlation spectroscopy. *J. Aerosol Sci.* **1991**, *22* (7), 815–822.
- [47] Burtscher, H. Physical characterization of particulate emissions from diesel engines: A review. *Journal of Aerosol Science*. 2005, pp 896–932.
- [48] Hagendorfer, H.; Lorenz, C.; Kaegi, R.; Sinnet, B.; Gehrig, R.; Goetz, N. V.; Scheringer, M.; Ludwig, C.; Ulrich, A. Size-fractionated characterization and quantification of nanoparticle release rates from a consumer spray product containing engineered nanoparticles. *J. Nanoparticle Res.* **2010**, *12* (7), 2481–2494.
- [49] Cernuschi, S.; Giugliano, M.; Ozgen, S.; Consonni, S. Number concentration and chemical composition of ultrafine and nanoparticles from WTE (waste to energy) plants. *Sci. Total Environ.* **2012**, *420*, 319–326.
- [50] Petrović, V. S.; Janković, S. P.; Tomić, M. V.; Jovanović, Z. S.; Knežević, D. M. The possibilities for measurement and characterization of diesel engine fine particles - A review. *Thermal Science*. 2011, pp 915–938.
- [51] Flagan, R. C. Differential mobility analysis of aerosols: A tutorial. *KONA Powder Part. J.* **2008**, *26*, 254–268.
- [52] Salgueiro-González, N.; López de Alda, M. J.; Muniategui-Lorenzo, S.; Prada-Rodríguez, D.; Barceló, D. Analysis and occurrence of endocrine-disrupting chemicals in airborne particles. *TrAC - Trends Anal. Chem.* **2015**, *66*, 45–52.
- [53] Pröfrock, D.; Prange, A. Inductively coupled plasma-mass spectrometry (ICP-MS) for

- quantitative analysis in environmental and life sciences: A review of challenges, solutions, and trends. *Appl. Spectrosc.* **2012**, *66* (8), 843–868.
- [54] Pease, R. F. W. *Significant advances in scanning electron microscopes (1965-2007)*; Elsevier Masson SAS, 2008; Vol. 150.
- [55] Kawamoto, N.; Tang, D. M.; Wei, X.; Wang, X.; Mitome, M.; Bando, Y.; Golberg, D. Transmission electron microscope as an ultimate tool for nanomaterial property studies. *J. Electron Microsc.* (Tokyo). **2013**, *62* (1), 157–175.
- [56] Carbone, S.; Onasch, T.; Saarikoski, S.; Timonen, H.; Saarnio, K.; Sueper, D.; Rönkkö, T.; Pirjola, L.; Häyrinen, A.; Worsnop, D.; et al. Characterization of trace metals on soot aerosol particles with the SP-AMS: Detection and quantification. *Atmos. Meas. Tech.* **2015**, *8* (11), 4803–4815.
- [57] Leavey, A.; Patel, S.; Martinez, R.; Mitroo, D.; Fortenberry, C.; Walker, M.; Williams, B.; Biswas, P. Organic and inorganic speciation of particulate matter formed during different combustion phases in an improved cookstove. *Environ. Res.* **2017**, *158*, 33–42.
- [58] Krystek, P.; Ulrich, A.; Garcia, C. C.; Manohar, S.; Ritsema, R. Application of plasma spectrometry for the analysis of engineered nanoparticles in suspensions and products. *J. Anal. At. Spectrom.* **2011**, *26* (9), 1701–1721.
- [59] Pace, H. E.; Rogers, N. J.; Jarolimek, C.; Coleman, V. A.; Higgins, C. P.; Ranville, J. F. Determining transport efficiency for the purpose of counting and sizing nanoparticles via single particle inductively coupled plasma mass spectrometry. *Anal. Chem.* **2011**, *83* (24), 9361–9369.
- [60] Laborda, F.; Jiménez-Lamana, J.; Bolea, E.; Castillo, J. R. Selective identification, characterization and determination of dissolved silver(i) and silver nanoparticles based on single particle detection by inductively coupled plasma mass spectrometry. *J. Anal. At. Spectrom.* **2011**, *26* (7), 1362–1371.
- [61] Liu, L.; He, B.; Liu, Q.; Yun, Z.; Yan, X.; Long, Y.; Jiang, G. Identification and accurate size characterization of nanoparticles in complex media. *Angew. Chemie - Int. Ed.* **2014**, *53* (52), 14476–14479.
- [62] Li, L.; Stoiber, M.; Wimmer, A.; Xu, Z.; Lindenblatt, C.; Helmreich, B.; Schuster, M. To What Extent Can Full-Scale Wastewater Treatment Plant Effluent Influence the Occurrence of Silver-Based Nanoparticles in Surface Waters? *Environ. Sci. Technol.* **2016**, *50* (12), 6327–6333.
- [63] Mozhayeva, D.; Strenge, I.; Engelhard, C. Implementation of Online Preconcentration and Microsecond Time Resolution to Capillary Electrophoresis Single Particle Inductively Coupled Plasma Mass Spectrometry (CE-SP-ICP-MS) and Its Application in Silver Nanoparticle Analysis. *Anal. Chem.* **2017**, *89* (13), 7152–7159.
- [64] Weber, A. P.; Baltensperger, U.; Gäggler, H. W.; Tobler, L.; Keil, R.; Schimdt-Ott, A.

- Simultaneous in-situ measurements of mass, surface and mobility diameter of silver agglomerates. *J. Aerosol Sci.* **1991**, *22* (5), 257–260.
- [65] Hess, A.; Tarik, M.; Losert, S.; Ilari, G.; Ludwig, C. Measuring air borne nanoparticles for characterizing hyphenated RDD-SMPS-ICPMS instrumentation. *J. Aerosol Sci.* **2016**, *92*, 130–141.
- [66] Ludwig, C.; Wochele, J.; Jörimann, U. Measuring evaporation rates of metal compounds from solid samples. *Anal. Chem.* **2007**, *79* (7), 2992–2996.
- [67] Ludwig, C.; Schuler, A. J.; Wochele, J.; Stucki, S. Measuring heavy metals by quantitative thermal vaporization. *Water Sci. Technol.* **2000**, *42* (7–8), 209–216.
- [68] Hess, A.; Tarik, M.; Foppiano, D.; Edinger, P.; Ludwig, C. Online Size and Element Analysis of Aerosol Particles Released from Thermal Treatment of Wood Samples Impregnated with Different Salts. *Energy and Fuels* **2016**, *30* (5).
- [69] Reed, R. B.; Higgins, C. P.; Westerhoff, P.; Tadjiki, S.; Ranville, J. F. Overcoming challenges in analysis of polydisperse metal-containing nanoparticles by single particle inductively coupled plasma mass spectrometry. *J. Anal. At. Spectrom.* **2012**, *27* (7), 1093.
- [70] Streng, I.; Engelhard, C. Capabilities of fast data acquisition with microsecond time resolution in inductively coupled plasma mass spectrometry and identification of signal artifacts from millisecond dwell times during detection of single gold nanoparticles. *J. Anal. At. Spectrom.* **2016**, *31* (1), 135–144.
- [71] Gschwind, S.; Flamigni, L.; Koch, J.; Borovinskaya, O.; Groh, S.; Niemax, K.; Günther, D. Capabilities of inductively coupled plasma mass spectrometry for the detection of nanoparticles carried by monodisperse microdroplets. *J. Anal. At. Spectrom.* **2011**, *26* (6), 1166.
- [72] Gschwind, S.; Hagendorfer, H.; Frick, D. A.; Günther, D. Mass Quantification of Nanoparticles by Single Droplet Calibration Using Inductively Coupled Plasma Mass Spectrometry. *Anal. Chem.* **2013**, *85*, 5875–5883.
- [73] Borovinskaya, O.; Hattendorf, B.; Tanner, M.; Gschwind, S.; Günther, D. A prototype of a new inductively coupled plasma time-of-flight mass spectrometer providing temporally resolved, multi-element detection of short signals generated by single particles and droplets. *J. Anal. At. Spectrom.* **2013**, *28* (2), 226–233.
- [74] Borovinskaya, O.; Gschwind, S.; Hattendorf, B.; Tanner, M.; Günther, D. Simultaneous mass quantification of nanoparticles of different composition in a mixture by microdroplet generator-ICPTOFMS. *Anal. Chem.* **2014**, *86* (16), 8142–8148.
- [75] Meermann, B.; Laborda, F. Analysis of nanomaterials by field-flow fractionation and single particle ICP-MS. *J. Anal. At. Spectrom.* **2015**, *30* (6), 1226–1228.
- [76] Motellier, S.; Pelissier, N.; Mattei, J. G. Contribution of single particle inductively coupled plasma mass spectrometry and asymmetrical flow field-flow fractionation for the

- characterization of silver nanosuspensions. Comparison with other sizing techniques. *J. Anal. At. Spectrom.* **2017**, *32* (7), 1348–1358.
- [77] Hadioui, M.; Merdzan, V.; Wilkinson, K. J. Detection and Characterization of ZnO Nanoparticles in Surface and Waste Waters Using Single Particle ICPMS. *Environ. Sci. Technol.* **2015**, *49* (10), 6141–6148.
- [78] Montaña, M. D.; Olesik, J. W.; Barber, A. G.; Challis, K.; Ranville, J. F. Single Particle ICP-MS: Advances toward routine analysis of nanomaterials. *Analytical and Bioanalytical Chemistry*. 2016, pp 5053–5074.
- [79] Lee, S.; Bi, X.; Reed, R. B.; Ranville, J. F.; Herckes, P.; Westerhoff, P. Nanoparticle size detection limits by single particle ICP-MS for 40 elements. *Environ. Sci. Technol.* **2014**, *48* (17), 10291–10300.
- [80] Salcedo, D.; Laskin, A.; Shutthanandan, V.; Jimenez, J. L. Feasibility of the detection of trace elements in particulate matter using online high-resolution aerosol mass spectrometry. *Aerosol Sci. Technol.* **2012**, *46* (11), 1187–1200.
- [81] Streibel, T.; Schnelle-Kreis, J.; Czech, H.; Harndorf, H.; Jakobi, G.; Jokiniemi, J.; Karg, E.; Lintelmann, J.; Matuschek, G.; Michalke, B.; et al. Aerosol emissions of a ship diesel engine operated with diesel fuel or heavy fuel oil. *Environ. Sci. Pollut. Res.* **2016**, 1–16.
- [82] Czech, H.; Sippula, O.; Kortelainen, M.; Tissari, J.; Radischat, C.; Passig, J.; Streibel, T.; Jokiniemi, J.; Zimmermann, R. On-line analysis of organic emissions from residential wood combustion with single-photon ionisation time-of-flight mass spectrometry (SPI-TOFMS). *Fuel* **2016**, *177*, 334–342.
- [83] Arrhenius, K.; Brown, A. S.; van der Veen, A. M. H. Suitability of different containers for the sampling and storage of biogas and biomethane for the determination of the trace-level impurities - A review. *Anal. Chim. Acta* **2016**, *902*, 22–32.
- [84] Cortada, C.; Dos Reis, L. C.; Vidal, L.; Llorca, J.; Canals, A. Determination of cyclic and linear siloxanes in wastewater samples by ultrasound-assisted dispersive liquid-liquid microextraction followed by gas chromatography-mass spectrometry. *Talanta* **2014**, *120*, 191–197.
- [85] Piechota, G.; Buczkowski, R. Development of chromatographic methods by using direct-sampling procedure for the quantification of cyclic and linear volatile methylsiloxanes in biogas as perspective for application in online systems. *Int. J. Environ. Anal. Chem.* **2014**, *94* (8), 837–851.
- [86] Vagenknechtová, A.; Ciahotný, K.; Vrbová, V. Siloxanes removal from biogas using activated carbon. *Acta Polytech.* **2017**, *57* (2), 131–138.
- [87] Easter, R. N.; Caruso, J. A.; Vonderheide, A. P. Recent developments and novel applications in GC-ICPMS. *J. Anal. At. Spectrom.* **2010**, *25* (4), 493–502.
- [88] Agilent Technologies. *GC-ICP-MS Helps Solve Biogas Usage Problem With Low Detection*

Limits for Siloxanes; 2008.

- [89] Schweigkofler, M.; Niessner, R. Determination of siloxanes and VOC in landfill gas and sewage gas by canister sampling and GC-MS/AES analysis. *Environ. Sci. Technol.* **1999**, *33* (20), 3680–3685.
- [90] Papurello, D.; Schuhfried, E.; Lanzini, A.; Romano, A.; Cappellin, L.; Märk, T. D.; Silvestri, S.; Biasioli, F. Influence of co-vapors on biogas filtration for fuel cells monitored with PTR-MS (Proton Transfer Reaction-Mass Spectrometry). *Fuel Process. Technol.* **2014**, *118*, 133–140.
- [91] Papurello, D.; Silvestri, S.; Tomasi, L.; Belcari, I.; Biasioli, F.; Santarelli, M. Biowaste for SOFCs. In *Energy Procedia*; 2016; Vol. 101, pp 424–431.
- [92] Papurello, D.; Tomasi, L.; Silvestri, S.; Belcari, I.; Santarelli, M.; Smeacetto, F.; Biasioli, F. Biogas trace compound removal with ashes using proton transfer reaction time-of-flight mass spectrometry as innovative detection tool. *Fuel Process. Technol.* **2016**, *145*, 62–75.
- [93] Hepburn, C. A.; Vale, P.; Brown, A. S.; Simms, N. J.; McAdam, E. J. Development of on-line FTIR spectroscopy for siloxane detection in biogas to enhance carbon contactor management. *Talanta* **2015**, *141*, 128–136.
- [94] Kajolinna, T.; Aakko-Saksa, P.; Roine, J.; Käll, L. Efficiency testing of three biogas siloxane removal systems in the presence of D5, D6, limonene and toluene. *Fuel Processing Technology*. 2015, pp 242–247.
- [95] Bottom, R. Principles and Applications of Thermal Analysis, Ch.3. In *Principles and Applications of Thermal Analysis*; Gabbott, P., Ed.; Blackwell Publishing Ltd, 2008; pp 88–118.
- [96] Kaufman Rechulski, M. D.; Schneebeli, J.; Geiger, S.; Schildhauer, T. J.; Biollaz, S. M. A.; Ludwig, C. Liquid-quench sampling system for the analysis of gas streams from biomass gasification processes. part 2: Sampling condensable compounds. *Energy and Fuels* **2012**, *26* (10), 6358–6365.
- [97] Kaufman Rechulski, M. D.; Schneebeli, J.; Geiger, S.; Schildhauer, T. J.; Biollaz, S. M. A.; Ludwig, C. Liquid-quench sampling system for the analysis of gas streams from biomass gasification processes. part 1: Sampling noncondensable compounds. *Energy and Fuels* **2012**, *26* (12), 7308–7315.
- [98] Hill, S. J.; Fisher, A.; Batey, J. H.; Prohaska, T.; Horstwood, M.; Nowell, G.; Goenaga-Infante, H.; Eiden C, G.; Hunter, K.; Stresau, D.; et al. *Inductively Coupled Plasma- Mass Spectrometry (ICP-MS)*; Nelms, S. M., Ed.; Blackwell Publishing Ltd., 2013.
- [99] Gerdes, K.; Carter, K. E. Calibration strategy for semi-quantitative direct gas analysis using inductively coupled plasma mass spectrometry. *Spectrochim. Acta - Part B At. Spectrosc.* **2011**, *66* (9–10), 712–725.
- [100] Edinger, P.; Tarik, M.; Hess, A.; Testino, A.; Ludwig, C. Online Detection of Selenium and Its Retention in Reducing Gasification Atmosphere. *Energy and Fuels* **2016**, *30* (2), 1237–1247.

-
- [101] Skoog, D. A.; Holler, F. J.; Crouch, S. R. "Gas Chromatography" (Ch.27). In *Principle of Instrumental Analysis*; Thomson Brooks/Cole, a part of The Thomson Corporation., 2000; pp 788–811.
- [102] Bouyssiere, B.; Baco, F.; Savary, L.; Lobinski, R. Speciation analysis for mercury in gas condensates by capillary gas chromatography with inductively coupled plasma mass spectrometric detection. *J Chromatogr A* **2002**, *976* (1–2), 431–439.
- [103] Hess, A.; Tarik, M.; Ludwig, C. A hyphenated SMPS–ICPMS coupling setup: Size-resolved element specific analysis of airborne nanoparticles. *J. Aerosol Sci.* **2015**, *88*, 109–118.
- [104] Kulkarni, P.; Baron, P. A.; Willeke, K. "Fundamentals of Single Particle Transport" (Ch.2). In *Aerosol Measurement: Principles, Techniques, and Applications*; Kulkarni, P., Baron, P. A., Willeke, K., Eds.; WILEY, 2011; pp 15–30.
- [105] Wiedensohler, A. An approximation of the bipolar charge distribution for particles in the submicron range. *J. Aerosol Sci.* **1988**, *19* (1), 387–389.
- [106] Bährle, C. Formation, Structure, and Reactivity of Organic Radicals in Lignin and its Depolymerization Products, ETH Zurich, 2016.
- [107] Hess, A.; Tarik, M.; Foppiano, D.; Edinger, P.; Ludwig, C. Online Size and Element Analysis of Aerosol Particles Released from Thermal Treatment of Wood Samples Impregnated with Different Salts. *Energy and Fuels* **2016**, *30* (5), 4072–4084.
- [108] Datye, A. K.; Hansen, P. L.; Helveg, S. "Electron Microscopy and Diffraction." In *Handbook of Heterogeneous Catalysis*; Wiley-VCH GmbH & Co KGaA, 2008.
- [109] R' mili, B.; Le Bihan, O. L. C.; Dutouquet, C.; Aguerre-Charriol, O.; Frejafon, E. Particle Sampling by TEM Grid Filtration. *Aerosol Sci. Technol.* **2013**, *47* (7), 767–775.
- [110] Freije-Carrelo, L.; Moldovan, M.; García Alonso, J. I.; Thanh Vo, T. D.; Encinar, J. R. Instrumental Setup for Simultaneous Total and Speciation Analysis of Volatile Arsenic Compounds in Gas and Liquefied Gas Samples. *Anal. Chem.* **2017**, *89* (11), 5719–5724.
- [111] Bianco, C.; Kezic, S.; Visser, M. J.; Pluut, O.; Adami, G.; Krystek, P. Pilot study on the identification of silver in skin layers and urine after dermal exposure to a functionalized textile. *Talanta* **2015**, *136*, 23–28.
- [112] Xu, L.; Shi, Y.; Cai, Y. Occurrence and fate of volatile siloxanes in a municipal Wastewater Treatment Plant of Beijing, China. *Water Res.* **2013**, *47* (2), 715–724.
- [113] van der Veen, A. M. H.; Brown, A. S.; Li, J.; Murugan, A.; Heinonen, M.; Haloua, F.; Arrhenius, K. Measurement requirements for biogas specifications. *17th Int. Congr. Metrol.* **2015**, *6*, 08006.
- [114] Arrhenius, K.; Yaghooby, H.; Rosell, L.; Bükér, O.; Culleton, L.; Bartlett, S.; Murugan, A.; Brewer, P.; Li, J.; van der Veen, A. M. H.; et al. Suitability of vessels and adsorbents for the short-term storage of biogas/biomethane for the determination of impurities – Siloxanes, sulfur

- compounds, halogenated hydrocarbons, BTEX. *Biomass and Bioenergy* **2017**, *105*, 127–135.
- [115] May, T. W.; Wiedmeyer, R. H. A table of polyatomic interferences in ICP-MS. *At. Spectrosc.* **1998**, *19* (5), 150–155.
- [116] Kumar, A.; Alaimo, C. P.; Horowitz, R.; Mitloehner, F. M.; Kleeman, M. J.; Green, P. G. Volatile organic compound emissions from green waste composting: Characterization and ozone formation. *Atmos. Environ.* **2011**, *45* (10), 1841–1848.
- [117] Papurello, D.; Tomasi, L.; Silvestri, S.; Santarelli, M. Evaluation of the Wheeler-Jonas parameters for biogas trace compounds removal with activated carbons. *Fuel Process. Technol.* **2016**, *152*, 93–101.
- [118] Papurello, D.; Boschetti, A.; Silvestri, S.; Khomenko, I.; Biasioli, F. Real-time monitoring of removal of trace compounds with PTR-MS: Biochar experimental investigation. *Renew. Energy* **2018**, *125*, 344–355.
- [119] Cabrera-Codony, A.; Georgi, A.; Gonzalez-Olmos, R.; Valdés, H.; Martín, M. J. Zeolites as recyclable adsorbents/catalysts for biogas upgrading: Removal of octamethylcyclotetrasiloxane. *Chem. Eng. J.* **2017**, *307*, 820–827.
- [120] Kwon, D.; Park, J.; Park, J.; Choi, S. Y.; Yoon, T. H. Effects of surface-modifying ligands on the colloidal stability of ZnO nanoparticle dispersions in in vitro cytotoxicity test media. *Int. J. Nanomedicine* **2014**, *9*, 57–65.
- [121] Aimable, A.; Buscaglia, M. T.; Buscaglia, V.; Bowen, P. Polymer-assisted precipitation of ZnO nanoparticles with narrow particle size distribution. *J. Eur. Ceram. Soc.* **2010**, *30* (2), 591–598.
- [122] Allen, T. *Particle Size Measurement*; Chapman & Hall, 1997.
- [123] Chung, S. J.; Leonard, J. P.; Nettleship, I.; Lee, J. K.; Soong, Y.; Martello, D. V.; Chyu, M. K. Characterization of ZnO nanoparticle suspension in water: Effectiveness of ultrasonic dispersion. *Powder Technol.* **2009**, *194* (1–2), 75–80.
- [124] Losert, S.; Hess, A.; Ilari, G.; von Goetz, N.; Hungerbuehler, K. Online characterization of nano-aerosols released by commercial spray products using SMPS–ICPMS coupling. *J. Nanoparticle Res.* **2015**, *17* (7), 293.
- [125] Roine, A. Outokumpu HSC Chemistry for Windows: Chemical Reaction and Equilibrium Software with Extensive Thermochemical Database. *User's Guid.* **2002**, No. version 5.
- [126] Scharnhorst, W.; Ludwig, C.; Wochele, J.; Jolliet, O. Heavy metal partitioning from electronic scrap during thermal End-of-Life treatment. *Sci. Total Environ.* **2007**, *373* (2–3), 576–584.
- [127] Stolzenburg, M. R.; McMurry, P. H. Method to assess performance of scanning mobility particle sizer (SMPS) instruments and software. *Aerosol Sci. Technol.* **2018**, *52* (6), 1–5.
- [128] Barwick, V. J.; Ellison, S. L. R.; Fairman, B. Estimation of uncertainties in ICP-MS analysis:

- A practical methodology. *Anal. Chim. Acta* **1999**, *394* (2–3), 281–291.
- [129] Keller, C.; Ludwig, C.; Davoli, F.; Wochele, J. Thermal treatment of metal-enriched biomass produced from heavy metal phytoextraction. *Environ. Sci. Technol.* **2005**, *39* (9), 3359–3367.
- [130] Zelenyuk, A.; Cai, Y.; Imre, D. From Agglomerates of Spheres to Irregularly Shaped Particles: Determination of Dynamic Shape Factors from Measurements of Mobility and Vacuum Aerodynamic Diameters. *Aerosol Sci. Technol.* **2006**, *40* (3), 197–217.
- [131] Tavakoli, F.; Olfert, J. S. Determination of particle mass, effective density, mass-mobility exponent, and dynamic shape factor using an aerodynamic aerosol classifier and a differential mobility analyzer in tandem. *J. Aerosol Sci.* **2014**, *75*, 35–42.
- [132] Hillemann, L.; Babick, F.; Stintz, M. Measurement of the dynamic shape factor using APM and SMPS in parallel. In *Procedia Engineering*; 2015; Vol. 102, pp 1177–1182.
- [133] Slowik, J. G.; Stainken, K.; Davidovits, P.; Williams, L. R.; Jayne, J. T.; Kolb, C. E.; Worsnop, D. R.; Rudich, Y.; DeCarlo, P. F.; Jimenez, J. L. Particle morphology and density characterization by combined mobility and aerodynamic diameter measurements. Part 2: Application to combustion-generated soot aerosols as a function of fuel equivalence ratio. *Aerosol Sci. Technol.* **2004**, *38* (12), 1206–1222.
- [134] Tarik, M.; Foppiano, D.; Hess, A.; Ludwig, C. A Practical Guide on Coupling a Scanning Mobility Sizer and Inductively Coupled Plasma Mass Spectrometer (SMPS-ICPMS). *J. Vis. Exp.* **2017**, *125* (e55487), 1–9.
- [135] Tancredi, N.; Gabús, M.; Yoshida, M. I.; Suárez, A. C. Thermal studies of wood impregnated with ZnCl₂. *European Journal of Wood and Wood Products*. 2016, pp 1–6.
- [136] Fliegel, D.; Frei, C.; Fontaine, G.; Hu, Z.; Gao, S.; Günther, D. Sensitivity improvement in laser ablation inductively coupled plasma mass spectrometry achieved using a methane/argon and methanol/water/argon mixed gas plasma. *Analyst* **2011**, *136* (23), 4857–5092.
- [137] Elled, A. L.; Åmand, L. E.; Eskilsson, D. Fate of zinc during combustion of demolition wood in a fluidized bed boiler. *Energy and Fuels* **2008**, *22* (3), 1519–1526.
- [138] Shamsuddin, M. *Physical Chemistry of Metallurgical Processes*; 2016; Vol. 44.
- [139] Weidenkaff, A.; Steinfeld, A.; Wokaun, A.; Auer, P. O.; Eichler, B.; Reller, A. Direct solar thermal dissociation of zinc oxide: condensation and crystallization of zinc in the presence of oxygen. *Sol. Energy* **1999**, *65* (1), 59–69.
- [140] Wochele, J.; Ludwig, C.; Stucki, S. Heavy metal volatilization during MSW incineration. In *Municipal Solid Waste Management*; Springer: New York, Berlin, Heidelberg, 2003; pp 211–220.
- [141] Weibel, D.; Jovanovic, Z. R.; Gálvez, E.; Steinfeld, A. Mechanism of Zn particle oxidation by H₂O and CO₂ in the presence of ZnO. *Chem. Mater.* **2014**, *26* (22), 6486–6495.

- [142] (EPA), E. P. A. "Method 29-Determination of metals emission from stationary sources", <https://www.epa.gov/emc/method-29-metals-emissions-stationary-sources>.
- [143] Arffman, A.; Yli-Ojanperä, J.; Kalliokoski, J.; Harra, J.; Pirjola, L.; Karjalainen, P.; Rönkkö, T.; Keskinen, J. High-resolution low-pressure cascade impactor. *J. Aerosol Sci.* **2014**, *78*, 97–109.
- [144] Savolahti, M.; Karvosenoja, N.; Tissari, J.; Kupiainen, K.; Sippula, O.; Jokiniemi, J. Black carbon and fine particle emissions in Finnish residential wood combustion: Emission projections, reduction measures and the impact of combustion practices. *Atmos. Environ.* **2016**, *140*, 495–505.
- [145] Sippula, O.; Lamberg, H.; Leskinen, J.; Tissari, J.; Jokiniemi, J. Emissions and ash behavior in a 500kW pellet boiler operated with various blends of woody biomass and peat. *Fuel* **2017**, *202*, 144–153.
- [146] Czech, H.; Pieber, S. M.; Tiitta, P.; Sippula, O.; Kortelainen, M.; Lamberg, H.; Grigonyte, J.; Streibel, T.; Prévot, A. S. H.; Jokiniemi, J.; et al. Time-resolved analysis of primary volatile emissions and secondary aerosol formation potential from a small-scale pellet boiler. *Atmos. Environ.* **2017**, *158*, 236–245.
- [147] Foppiano, D.; Tarik, M.; Gubler Müller, E.; Ludwig, C. Combustion generated nanomaterials: online characterization via an ICP-MS based technique. Part I: calibration strategy with a TGA. *J. Anal. At. Spectrom.* **2018**, *33* (9), 1493–1499.
- [148] Zelenyuk, A.; Imre, D. On the Effect of Particle Alignment in the DMA. *Aerosol Sci. Technol.* **2007**, *41* (2), 112–124.
- [149] Elsasser, M.; Busch, C.; Orasche, J.; Schön, C.; Hartmann, H.; Schnelle-Kreis, J.; Zimmermann, R. Dynamic changes of the aerosol composition and concentration during different burning phases of wood combustion. *Energy and Fuels* **2013**, *27* (8), 4959–4968.
- [150] Vanhaecke, F. AGILENT 8800 ICP-QQQ APPLICATION HANDBOOK. **2015**.
- [151] Nelson, J.; Hopfer, H.; Silva, F.; Wilbur, S.; Chen, J.; Shiota Ozawa, K.; Wylie, P. L. Evaluation of GC-ICP-MS/MS as a new strategy for specific heteroatom detection of phosphorus, sulfur, and chlorine determination in foods. *J. Agric. Food Chem.* **2015**, *63* (18), 4478–4483.
- [152] Sliwinska, A.; Kwiatkowski, D.; Czarny, P.; Milczarek, J.; Toma, M.; Korycinska, A.; Szymraj, J.; Sliwinski, T. Genotoxicity and cytotoxicity of ZnO and Al₂O₃ nanoparticles. *Toxicol. Mech. Methods* **2015**, *25* (3), 176–183.
- [153] Uski, O.; Jalava, P. I.; Happonen, M. S.; Torvela, T.; Leskinen, J.; Mäki-Paakkanen, J.; Tissari, J.; Sippula, O.; Lamberg, H.; Jokiniemi, J.; et al. Effect of fuel zinc content on toxicological responses of particulate matter from pellet combustion in vitro. *Sci. Total Environ.* **2015**, *511*, 331–340.
- [154] Sharma, V.; Anderson, D.; Dhawan, A. Zinc oxide nanoparticles induce oxidative DNA

- damage and ROS-triggered mitochondria mediated apoptosis in human liver cells (HepG2). *Apoptosis* **2012**, *17* (8), 852–870.
- [155] Kovacs, R.; Nishiguchi, K.; Utani, K.; Günther, D. Development of direct atmospheric sampling for laser ablation-inductively coupled plasma-mass spectrometry. *J. Anal. At. Spectrom.* **2010**, *25* (2), 142–147.
- [156] Schild, M.; Gundlach-Graham, A.; Menon, A.; Jevtic, J.; Pikelja, V.; Tanner, M.; Hattendorf, B.; Günther, D. Replacing the Argon ICP: Nitrogen Microwave Inductively Coupled Atmospheric-Pressure Plasma (MICAP) for Mass Spectrometry. *Anal. Chem.* **2018**, *90*, 13443–13450.
- [157] Thaler, K. M.; Schwartz, A. J.; Haisch, C.; Niessner, R.; Hieftje, G. M. Preliminary survey of matrix effects in the Microwave-sustained, Inductively Coupled Atmospheric-pressure Plasma (MICAP). *Talanta* **2018**, *180*, 25–31.
- [158] Schwartz, A. J.; Cheung, Y.; Jevtic, J.; Pikelja, V.; Menon, A.; Ray, S. J.; Hieftje, G. M. New inductively coupled plasma for atomic spectrometry: the microwave-sustained, inductively coupled, atmospheric-pressure plasma (MICAP). *J. Anal. At. Spectrom.* **2016**, 1–10.

Appendix A Additional data sets

A.1 Siloxanes in biogas

A.1.1 Stock and standard solution concentrations

Table A.1.1-1 Stock solution 1: Si and single compound concentrations.

	Concentration (ppm, $\mu\text{g ml}^{-1}$)	Si concentration (ppm, $\mu\text{g ml}^{-1}$)
L2	452	156.25
L3	508	180.81
D3	416	157.41
D4	456	171.96
D5	508	191.70
D6	420	158.56

Table A.1.1-2 Stock solution 2: Si and single compound concentrations.

	Concentration (ppm, $\mu\text{g ml}^{-1}$)	Si concentration (ppm, $\mu\text{g ml}^{-1}$)
L2	6.78	2.34
L3	7.62	2.71
D3	6.24	2.36
D4	6.84	2.58
D5	7.62	2.88
D6	6.30	2.38

Table A.1.1-3 Standards solutions: Si concentrations.

Standards	Si concentrations (ppb, ng ml^{-1})					
	<i>L2</i>	<i>D3</i>	<i>L3</i>	<i>D4</i>	<i>D5</i>	<i>D6</i>
<i>STD 1</i>	213.06	246.56	214.64	234.49	261.41	216.22
<i>STD 2</i>	468.74	542.44	472.22	515.88	575.09	475.69
<i>STD 3</i>	1171.85	1356.10	1180.54	1289.70	1437.74	1189.21
<i>STD 4</i>	2343.70	2712.20	2361.08	2579.39	2875.47	2378.43

A.1.2 7700x ICP-MS (Agilent Technologies) additional operating conditions

Table A.1.2 7700x ICP-MS (Agilent Technologies) additional operating conditions

<i>Operating conditions</i>	<i>Voltage (V)</i>
<i>Extraction lens 1</i>	0.0
<i>Extraction lens 2</i>	-195.0
<i>Omega bias lens</i>	-80.0
<i>Omega lens</i>	10.2
<i>Cell entrance lens</i>	-40.0
<i>Cell exit lens</i>	-60.0
<i>Deflect lens</i>	2.0
<i>Plate bias lens</i>	-55.0
<i>RF matching</i>	1.39

A.1.3 D5 stock solutions and calibration standards for gas composition optimization in ORS

Table A.1.3 Stock solutions and calibration standards: Si and D5 concentrations

Stock and standard solutions	D5 concentration	Si concentration
	<i>(ppm, $\mu\text{g ml}^{-1}$)</i>	<i>(ppm, $\mu\text{g ml}^{-1}$)</i>
STOCK 1	436	164.52
STOCK 2	4.207	3.344
	<i>(ppb, ng ml^{-1})</i>	<i>(ppb, ng ml^{-1})</i>
STD 1	87.76	33.12
STD 2	805.80	304.08
STD 3	8863.88	3344.86

A.1.4 GC-ICP-MS figures of merit when only one column is connected to the GC inlet

Table A.1.4 ^{28}Si sensitivities, LoD, LoQ, R^2 and BEC in GC-ICP-MS for siloxanes compounds analyzed, using one column connected to the GC inlet.

Siloxanes	^{28}Si Sensitivity <i>(cps/ppb)</i>	LoD <i>ppb_{Si} (ng ml^{-1})</i>	LoQ <i>ppb_{Si} (ng ml^{-1})</i>	R^2 <i>(linear fit)</i>	BEC <i>ppb (ng ml^{-1})</i>
L2	391.81	2.349	7.829	0.9999	3.894
D3	460.17	1.566	5.200	1.0000	12.794
L3	454.95	0.613	2.043	0.9999	1.455
D4	466.22	4.916	16.387	0.9998	12.510
D5	480.75	4.002	13.340	0.9997	12.978
D6	509.70	4.636	15.452	1.0000	28.366

A.2 Preliminary studies with RDD-SMPS-ICP-MS

A.2.1 Zinc oxide nanopowder characterization

SEM analysis on a small amount of powder added in ethanol (Sigma-Aldrich, pure grade 99.9%) and finely dispersed applying an ultrasonic treatment with an ultrasonic horn (2 times for 2 minutes). In figure S1 (a) an overview of the ZnO particles morphology is shown. The sample appears to be homogeneously distributed and the particles size varies from 40 nm to a maximum of 300 nm. The XRD measurement (Fig. A2.1-1 b) confirmed the hexagonal structure provided by the manufacturer. The measurement was repeated also by using Transmission Electron Microscopy, together with the electron diffraction pattern confirming the results already shown with SEM.

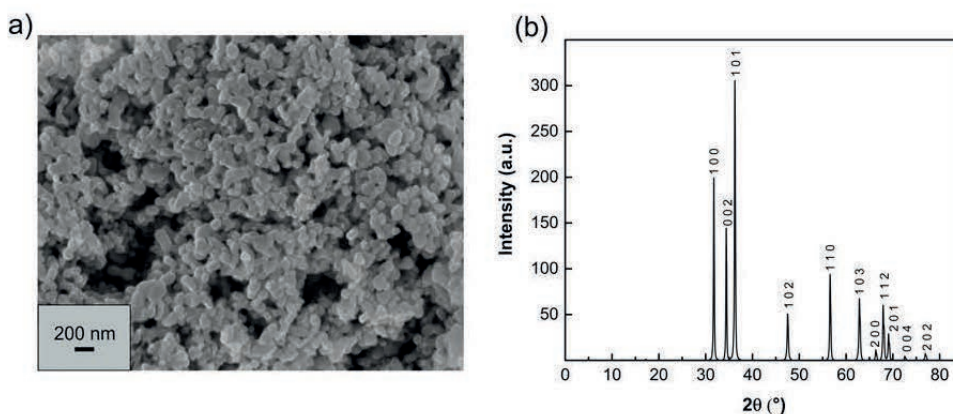


Figure A.2.1-1 SEM micrograph of ZnO nanopowder, showing nearly spherical morphology (a) and XRD pattern of ZnO commercial powder (b).

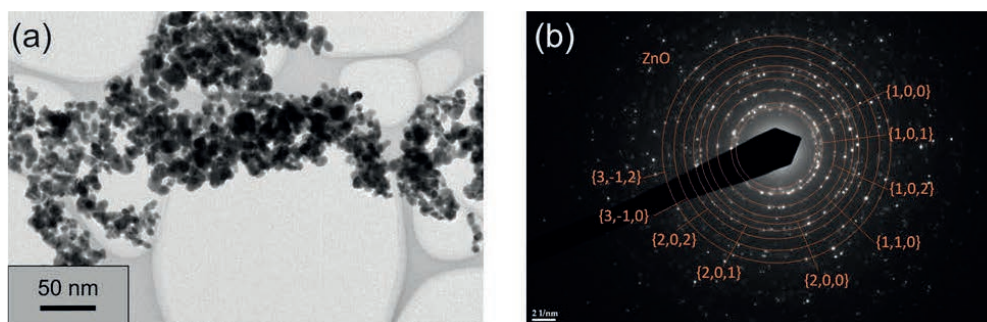


Figure A.2.1-2 TEM micrograph of ZnO powder, showing nearly spherical morphology (a) and indexation of electron diffraction pattern of ZnO commercial powder (b).

Table A.2.1-1 Zinc oxide powder specifications, provided by the manufacturer (AUER-REMY)

<i>Purity</i>	<i>Average particle size</i>	<i>Specific surface area</i>	<i>Morphology</i>	<i>Crystallographic structure</i>
99.5%	20 nm	50 m ² /g	Nearly spherical	Hexagonal

A.2.2 ZnO suspension characterization

A.2.2.1 ZnO suspension analysis by ICP-MS

Table A.2.2-1. ICP-MS analysis on ZnO suspension. LOD: limit of detection; LOQ: limit of quantification (of the method) including the dilution (for these samples the dilution was about 2.0×10^4 mL/g)

<i>Sample name</i>	<i>Zn conc ppm</i>	<i>RSD %</i>
ZnO suspension (600 ppm)	556.9	1.72
Method LOQ %	0.4	
ICP LoD ng mL ⁻¹	0.006	

A.2.2.2 Zetasizer Nano series

Table A.2.2-2. Malvern Zeta sizer nano series characterization on ZnO suspension; Material RI:2.00, Dispersant RI: 1.330, material absorption: 0.010

<i>Sample name</i>	<i>Size d50 (nm)</i>	<i>Temperature(°C)</i>
ZnO_PAA0.1%wt-pH9 1	131.9	25
ZnO_PAA0.1%wt-pH9 2	132.3	25
ZnO_PAA0.1%wt-pH9 3	128	25

ZnO suspension (B) and blank (dispersant solution) filtered with a membrane filter, pore size 0.45 μm and then measured by Zeta sizer Nano series.

A.2.2.3 XDC-BI measurement

Table A.2.2-3 Brookhaven BI-XDC characterization on ZnO suspension

<i>Sample name</i>	<i>Size d50 (μm)</i>	<i>Mean (μm)</i>	<i>Std. deviation (μm)</i>	<i>Mode (μm)</i>
ZnO_1.8%wt_1	0.217	0.233	0.130	0.182
ZnO_1.8%wt_1	0.204	0.222	0.105	0.184

Analysis on a concentrated suspension (1.8% ZnO)

A.3 RDD-SMPS-ICP-MS calibration strategy and resolving power for heterogenous matrices

A.3.1 TGA temperature program during ZnCl_2 calibration experiment

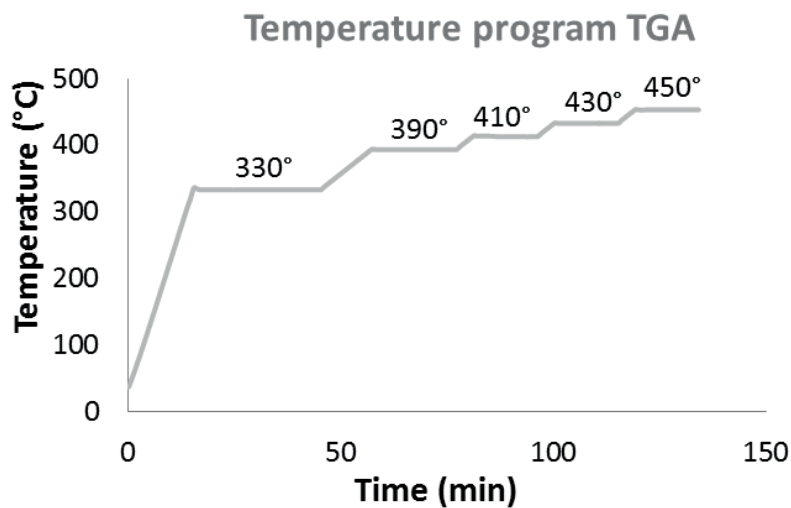


Figure A.3.1 Temperature program TGA during experiment with ZnCl_2 powder

A.3.2 HSC thermochemical calculation on CdCl_2

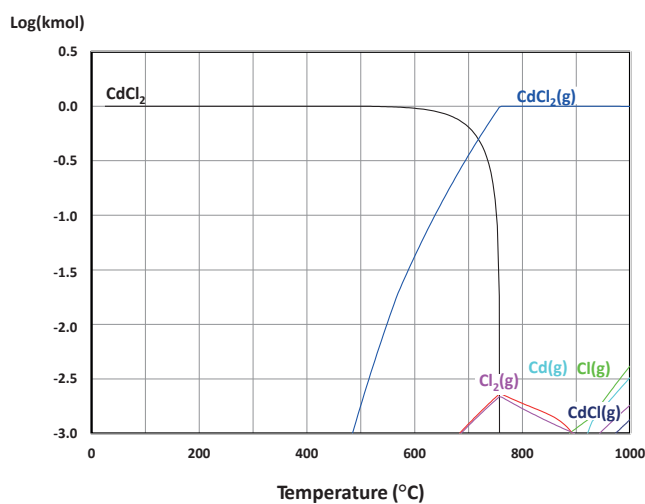


Figure A.3.2 Thermochemical calculation on CdCl_2 evaporation with HSC software.

A.3.3 TGA temperature program during CdCl_2 calibration experiment

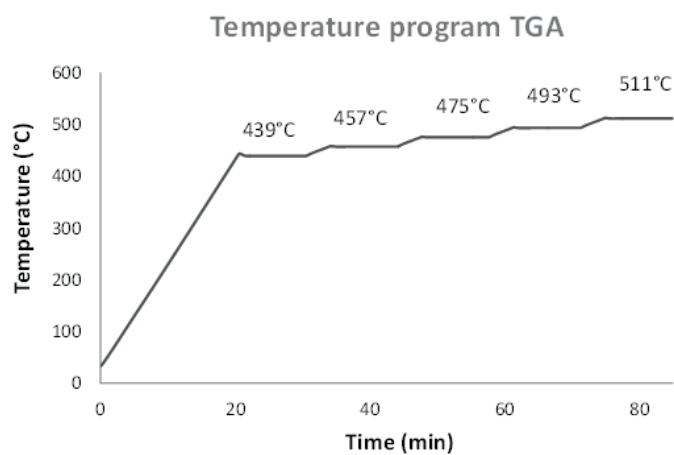


Figure A.3.3 Temperature program TGA during experiment with CdCl_2 experiments.

A.3.4 TGA temperature program during metal oxides and $\text{CaCl}_2 \cdot 2\text{H}_2\text{O}$ experiments

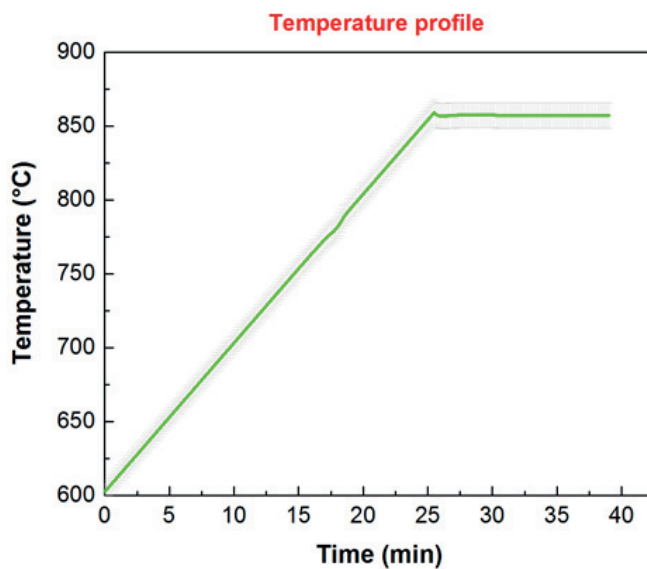


Figure A.3.4 Temperature program TGA during experiment with PbO , CdO , CuO , ZnO and $\text{CaCl}_2(\text{H}_2\text{O})_2$ powders

A.3.5 CdCl₂ calibration curve

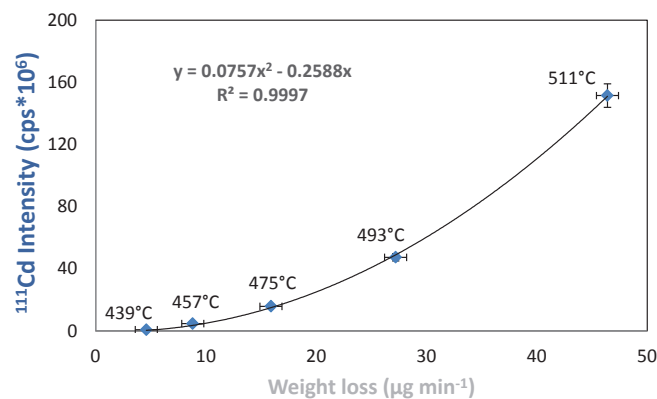


Figure A.3.5 CdCl₂ second order calibration curve, used for the determination of Cd concentration in the experiments with PbO, CdO, CuO, ZnO and CaCl₂(H₂O)₂. The RSD% associated with each point is ≤5%

A.3.6 Reproducibility of analysis for ZnO and CaCl₂·2H₂O experiment

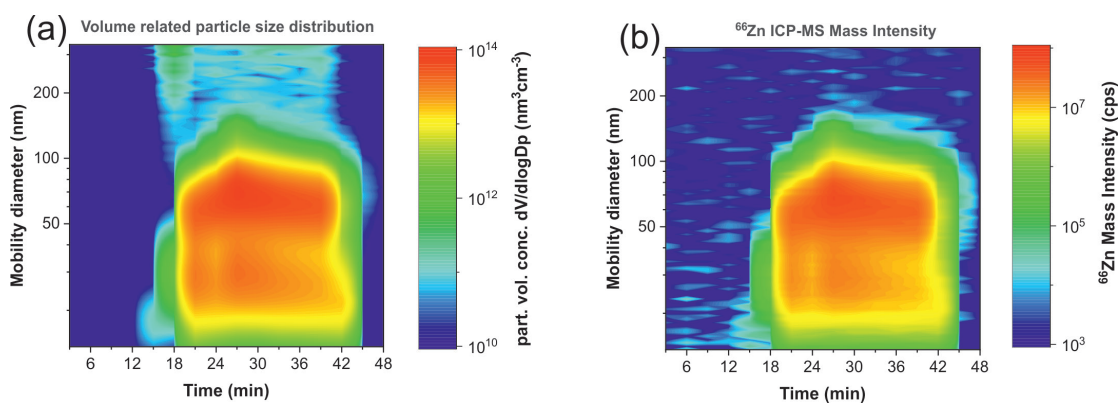


Figure A.3.6 Volume-related size distribution and ⁶⁶Zn ICP-MS Intensity contour plots of a repetitive analysis with the same operating conditions like the sample in Fig.4. The results show that the PSDs follow the same trend with an RSD for small particles (<20 nm) and bigger particles (>50 nm) of about 10%.

A.3.7 TEM analysis on Mixed oxide powders and CaCl₂·2H₂O experiment

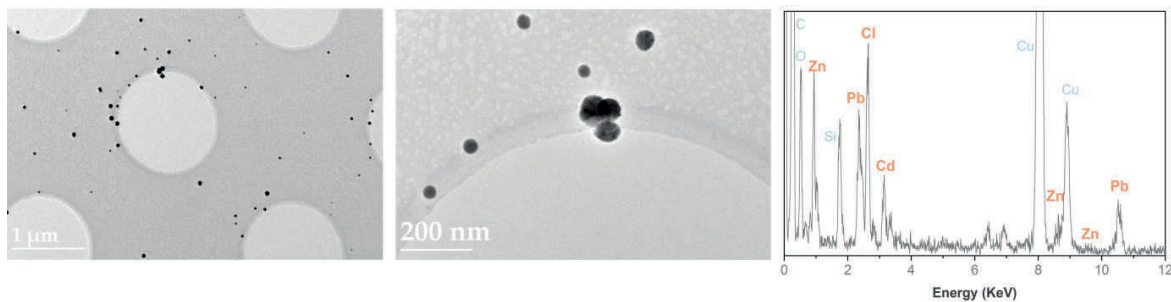


Figure A.3.7 TEM micrographs and EDX analysis on size-selected particles generated during experiment with PbO, CdO, CuO, ZnO and CaCl₂(H₂O)₂ powders.

A.4 Emissions of secondary formed nano-objects from the combustion of impregnated wood

A.4.1 Sawdust multi-element analysis in ICP-MS

Microwave assisted acid digestion of three different samples from the same batch of beech wood saw dust (dilution with solution 1% HNO_3), further analyzed by ICP-MS. The resulting composition is listed in the table below in a concentration range of % for main components and concentration range down to ppm(mg kg^{-1}) for trace element.

Table A.4.1-1 ICP-MS elemental analysis on beech wood saw dust.

	<i>Sawdust 1</i>		<i>Sawdust 2</i>		<i>Sawdust 3</i>		<i>Average</i>
	Conc %	RSD%	Conc %	RSD%	Conc %	RSD %	Conc %
K	0.133	0.6	0.134	0.5	0.131	1.5	0.133
Ca	0.0517	0.4	0.0527	1.1	0.0523	2.1	0.0522
Mg	0.0148	0.8	0.0148	0.7	0.0146	1.4	0.0147
P	0.0145	1.4	0.0145	1.1	0.0136	0.6	0.0142

Table A.4.1-2 ICP-MS elemental analysis on beech wood saw dust.

	<i>Sawdust 1</i>		<i>Sawdust 2</i>		<i>Sawdust 3</i>		<i>Average</i>
	Conc. [mg kg^{-1}]	RSD%	Conc. [mg kg^{-1}]	RSD%	Conc. [mg kg^{-1}]	RSD%	Conc. [mg kg^{-1}]
Mn	5.291	0.5	5.246	0.9	5.056	1.4	5.198
Fe	4.565	0.9	5.054	0.4	4.641	2.3	4.753
Na	2.759	0.3	1.839	2.3	1.542	0.9	2.047
Cu	1.179	0.4	1.160	0.9	1.178	0.6	1.172
Zn	1.118	4.7	1.068	3.0	1.081	1.6	1.089
Pb	0.497	1.1	0.161	1.1	0.108	5.2	0.255
Cr	0.135	2.1	0.132	3.6	0.125	6.3	0.131

A.4.2 ZnO impregnated sawdust multi-element analysis in ICP-MS

Table A.4.2 ICP-MS elemental analysis on beech wood sawdust impregnated with ZnO suspension. LOD: limit of detection; LOQ: limit of quantification (of the method) including the dilution (for these samples the dilution was about 6×10^5 ml/g)

Sample Name	<i>Zn</i>	
	Conc. %	RSD %
Saw dust_1	1.64	0.42
Saw dust_2	1.48	1.37
Saw dust_3	1.35	1.80
Average	1.49	
method LOQ %	0.01	
ICP LOD ng/ml	0.07	

A.4.3 Efficiency of sawdust impregnation with ZnO nanopowder

Table A.4.3 The efficiency of impregnation calculated on expected value (assuming 100% efficiency) and real concentration measured with ICP-MS.

<i>Zn conc. expected (%)</i>	<i>Zn conc. measured (%)</i>	<i>Efficiency %</i>
1.81	1.49±0.14	82.32

A.4.4 Thermochemical calculations

The input concentrations are based on real ratios between C and Zn in impregnated wood. The algorithm used for calculation is based on minimum Gibbs energies output.

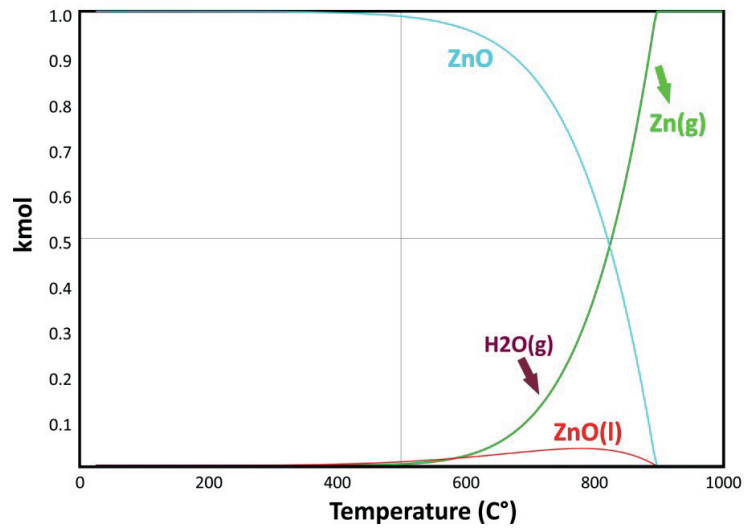


Figure A.4.4-1. Thermochemical calculations with HSC software, initial concentrations: ZnO (1 kmol), H₂ (10 kmol)

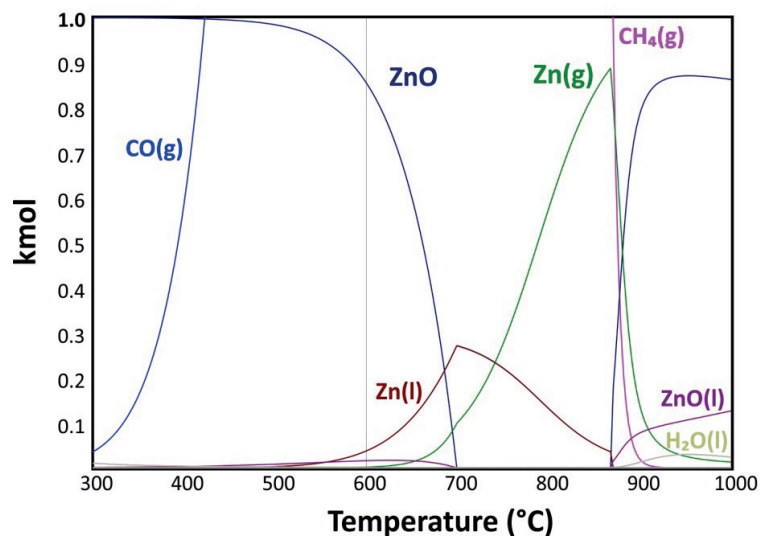


Figure A.4.4-2. Thermochemical calculations with HSC software, initial concentration considering real ratio existing between C and Zn in the impregnated wood: ZnO (1 kmol), CO and H₂ in excess (175 kmol).

Appendix B Co-authorship

“Online Size and Element Analysis of Aerosol Particles Released from Thermal Treatment of Wood Samples Impregnated with Different Salts”



The first eight months of this thesis were mainly focused on training over the coupling SMPS-ICP-MS and on supporting the activities related to the study of particles released from thermal treatment of wood samples (impregnated with different salts). In the frame of this collaboration, the author (Debora Foppiano) took over the task of ICP-MS measurements of metals contained in sawdust, the sample impregnation and preparation, and the experimental part of flow calibrations and optimization of the instruments parameters.

Reprinted with permission from *Energy and Fuels*, **2016**, 30, 4072–4084. Copyright 2016 American Chemical Society.

Online Size and Element Analysis of Aerosol Particles Released from Thermal Treatment of Wood Samples Impregnated with Different Salts

Adrian Hess,^{*,†,‡} Mohamed Tarik,[†] Debora Foppiano,^{†,‡} Philip Edinger,^{†,‡} and Christian Ludwig^{*,†,‡}

[†]Bioenergy and Catalysis Laboratory (LBK), Energy and Environment Research Division (ENE), Paul Scherrer Institut (PSI), CH 5232 Villigen PSI, Switzerland

[‡]Environmental Engineering Institute (IIE), School of Architecture, Civil and Environmental Engineering (ENAC), École Polytechnique Fédérale de Lausanne (EPFL), CH 1015 Lausanne, Switzerland

Supporting Information

ABSTRACT: Thus far, the elemental characterization of particles in energy conversion process gases and emissions has conventionally either been performed offline or information on the particle size has not been available. Such processes include combustion in engines or thermal treatments of renewable and fossil fuels for heat and power generation. One established physical aerosol measurement instrument is the scanning mobility particle sizer (SMPS), providing size distribution and concentration of gas-borne particles online, with temporal resolutions of a few minutes or even less. However, a far greater wealth of information can be gained by combining the opportunities of the SMPS with those of an inductively coupled plasma mass spectrometer (ICPMS), which enables the determination of the elemental composition of an introduced sample with low detection limits and a wide dynamic measuring range, and those of a rotating disk diluter (RDD), used as a sample introduction interface, making the setup independent of a defined aerosol source flow. We have recently presented such an instrumental setup, which is used now for online measurements on particulate sodium, chlorine, potassium, and copper, in aerosols emitted by differently impregnated wood samples, heated in a thermogravimetric analyzer (TGA). The TGA allows controlling the temperature, oxygen content, and gas flows in the furnace and is used for generating model aerosols to study the influence of different fuel treatments on the emissions during the combustion process. The ability of RDD–SMPS–ICPMS to discriminate between several elements contained in specific particle size classes between 13 and 340 nm at different times in the aerosol emitted by a thermal process is demonstrated.

INTRODUCTION

Emissions from biomass incineration and other thermal processes can be seen as aerosols, consisting of a gas mixture and gas-borne particles. Particles in the sub-micrometer size range are usually formed by condensation of evaporated matter in a supersaturated environment. In a highly supersaturated atmosphere, such particles can be formed in the absence of condensation nuclei, but the more common formation mechanism is particle growth around existing nuclei.¹ Such effects occur inside a flame and after combustion processes, when the temperature decreases and supersaturation is achieved. The assessment of particulate emissions usually includes chemical analysis of the overall aerosol or filtered gases, and the number or mass concentration and size distribution of the gas-borne nanoparticles are determined. Information on the major gaseous compounds and also on the elemental composition of such process emissions can be obtained online. Likewise, particle size distributions (PSDs) can be measured with time resolutions in the range of a few minutes or even less,^{2,3} e.g., using a scanning mobility particle sizer (SMPS).⁴ The aerosol mass spectrometer (AMS) is an aerosol characterization equipment providing both physical and chemical information simultaneously. Introduced particles are decomposed on a hot (600 °C) tungsten surface, and the resulting gas molecules are ionized by electron impact, classified

for their mass-to-charge ratio (m/z), and finally counted. This technique enables the detection of organic compounds, their fragments, and some inorganic salts in gas-borne particles even below 100 nm^{5,6} but does not offer element information on the investigated particles.

Several groups have been investigating the effects of different parameters on the release of alkali metals and other elements from the incineration of biomass or fossil fuels.^{7,8} Different elements in process aerosols have been analyzed by inductively coupled plasma optical emission spectrometry (ICPOES).⁹ Measurements by SMPS have been combined with chemical gas and offline particle analysis,¹⁰ and larger particles in industrial emissions have been analyzed offline by ion chromatography and inductively coupled plasma mass spectrometry (ICPMS).¹¹ Besides, particulate emissions from zinc (Zn)-impregnated wood pellets were investigated regarding the Zn content in the fraction of fine particles below 1 μm ,¹² but up to now, such information was not available for narrow particle size fractions and with temporal resolutions in the range of a few minutes.

Received: January 23, 2016

Revised: March 14, 2016



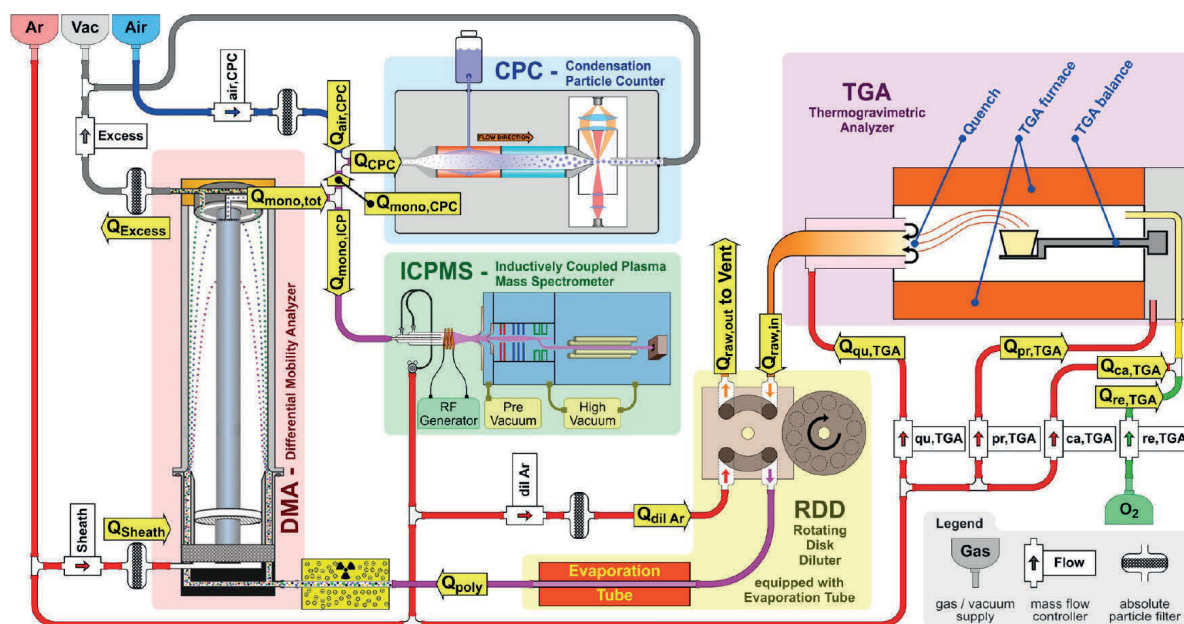


Figure 1. Experimental TGA–RDD–SMPS–ICPMS setup, with all flows indicated. $Q_{\text{raw,in}}$ raw aerosol flow from the TGA to the RDD; $Q_{\text{raw,out}}$ raw aerosol flow released by the RDD; $Q_{\text{dil Ar}}$ dilution argon flow in the RDD; Q_{poly} diluted polydisperse aerosol provided to the DMA by the RDD; Q_{sheath} sheath argon flow; Q_{excess} excess gas flow at the DMA outlet; $Q_{\text{mono,tot}}$ total monodisperse flow at the DMA outlet; Q_{CPC} total flow in the condensation particle counter (CPC); $Q_{\text{air,CPC}}$ air flow to reduce the monodisperse aerosol fraction consumed by the CPC; $Q_{\text{mono,CPC}}$ and $Q_{\text{mono,ICP}}$ CPC and ICPMS fractions of monodisperse aerosol flow; $Q_{\text{qu,TGA}}$ quench gas flow in the TGA interface; $Q_{\text{pr,TGA}}$ protective gas flow in the TGA balance mechanics; $Q_{\text{ca,TGA}}$ gas flow to carry the generated aerosol out of the TGA furnace; and $Q_{\text{re,TGA}}$ reactive gas flow, i.e., O_2 provided to the sample to enable controlled combustion of the wood sample (DMA scheme adapted from the scanning mobility particle sizer brochure of TSI, available at www.tsi.com).

Because introduced matter is decomposed into elemental ions in the inductively coupled plasma at 5000–10 000 °C, ICPMS can provide information on the elemental composition of any sample, dissolved in aqueous acid solutions,¹³ and has been established in recent years for the characterization of even single solid particles in the nanometer size range, suspended in liquids.^{14,15} However, element information specifically on the composition of gas-borne nanoparticles emitted by thermal processes is traditionally obtained offline,¹⁶ especially with the focus on the elemental composition of distinct particle size fractions.¹⁷ Such procedures include particle sampling, sample preparation, and offline analysis¹⁸ and are, therefore, time-consuming and entail the risk of sample contamination and other alterations. Moreover, the results of such analyses usually represent longer measuring periods and do not provide time-resolved information.

Recently, an instrumental setup was presented by Hess et al., consisting of a rotating disk diluter (RDD), SMPS, and ICPMS.^{19,20} A first application was the assessment of engineered nanoparticles (ENPs) in aerosols from commercial spray products.²¹ In the present work, the RDD–SMPS–ICPMS arrangement was equipped with an evaporation tube (ET) to eliminate volatile particle fractions and focus on solid particles and connected to a thermogravimetric analyzer (TGA), wherein a wood pellet was treated thermally with controlled combustion parameters, such as the temperature, oxygen (O_2) content, and other gas flows in the atmosphere surrounding the fuel sample. Using the RDD–SMPS–ICPMS setup, the emitted aerosols were analyzed online, with respect to the PSD and the size-resolved elemental particle

composition, with a temporal resolution of 3 min. Differently impregnated wood samples underwent a thermal treatment and were analyzed in this arrangement to investigate the influence of these impregnations on the formed aerosol particles.

EXPERIMENTAL SECTION

Instrumental Arrangement. A TGA (TGA/STDA851e from Mettler Toledo) had earlier been equipped by Ludwig et al. with a gas quench, named condensation interface (CI), to immediately cool and dilute the aerosol released by the TGA sample, to prevent further condensation and particle agglomeration, and to preserve the aerosol for subsequent analysis.²² This TGA was connected to the RDD–SMPS–ICPMS instrumentation, which was similar to the recently described setup,^{19,20} except for the ICPMS instrument (7700 instead 8800 QQQ from Agilent) and the RDD, which was further equipped with an ET (ASET15-1 from Matter Aerosol), to bring volatile components of the diluted aerosol into the gas phase, like it is required, e.g., for measuring particulate emissions of internal combustion engines, according to the regulation of the Swiss Association for Standardization (SNV)²³ or following the European Particle Measurement Programme (PMP).²⁴ The whole arrangement is sketched in Figure 1.

Gas Flows. All gas flows were maintained by mass flow controllers (MFCs) and verified with a primary flow calibrator (Gilibrator-2 from Sensidyne). To apply oxidizing conditions to the sample pellet, O_2 was used as reactive gas in the TGA, with a flow of $Q_{\text{re,TGA}} = 18 \text{ mL min}^{-1}$. Argon flows served as the sample carrier gas, $Q_{\text{ca,TGA}} = 63 \text{ mL min}^{-1}$, as the protective gas to prevent sample aerosol and reactive gas entering the balance chamber, $Q_{\text{pr,TGA}} = 22 \text{ mL min}^{-1}$, and as the quench gas in the CI, $Q_{\text{qu,TGA}}$, which was set such that a total flow of 1.0 L min^{-1} resulted at the outlet of the TGA quench interface. The sum of these gas flows was complemented by the gas and particles

Table 1. Fuel Samples Used for All Experiments

sample name	batch weight (g) ^a	first salt	second salt	pellet weight (mg) ^b
natural	no batch	no sawdust treatment, no salts added		199.8
H ₂ O	2.0	water treatment, without salts added		200.4
KCl	2.0	28.6 mg KCl		200.9
CuSO ₄	2.0	23.9 mg CuSO ₄ ·5H ₂ O		201.2
CuCl ₂	2.0	16.2 mg CuCl ₂ ·2H ₂ O		200.0
CuSO ₄ -KCl	2.0	24.2 mg CuSO ₄ ·5H ₂ O	28.9 mg KCl	200.9

^aAmount of sawdust that underwent impregnation or water treatment. ^bWeight of the pellet that was finally used for the experiment.

generated in the furnace and provided as raw aerosol flow to the RDD head, $Q_{\text{raw,in}} \approx 1.0 \text{ L min}^{-1}$. Because this flow was well-defined, the raw aerosol pump of the RDD, which would normally maintain $Q_{\text{raw,out}}$ and $Q_{\text{raw,in}} = Q_{\text{raw,out}}$ was not used and, therefore, disconnected.

Argon was also used as sheath gas in the differential mobility analyzer (DMA). To cover the range of larger particles, a low sheath gas flow was set, $Q_{\text{sheath}} = 3.00 \text{ L min}^{-1}$. Although the ideal ratio between sample and sheath gas flows of the used DMA type would be 1:10, an increased polydisperse aerosol inlet flow was set, $Q_{\text{poly}} = 0.60 \text{ L min}^{-1}$, to reduce the residence time in the aerosol lines and to increase the CPC and ICPMS signals. The monodisperse flow at the DMA outlet was set equal, $Q_{\text{mono,tot}} = Q_{\text{poly}} = 0.60 \text{ L min}^{-1}$. A 30% fraction of this flow was consumed by the CPC, $Q_{\text{mono,CPC}} = 0.18 \text{ L min}^{-1}$, the remaining 70% portion was directed to the ICPMS, $Q_{\text{mono,ICP}} = 0.42 \text{ L min}^{-1}$. The flow adjustment procedure has been published earlier¹⁹ and is described in the [Supporting Information](#).

Instrument Settings. After introduction of a sample into the TGA at room temperature, a drying period of 10 min at 105 °C was applied as the first step of the TGA program. The temperature was then increased, with a constant heating rate of 5 °C min⁻¹, to 950 °C. This final temperature was kept for 30 min; therefore, the total experiment duration was 209 min. The RDD diluter head temperature was set to $T_{\text{RDD}} = 80 \text{ °C}$. After a pre-experiment, performed without ET, large sedimented particles and sticky droplets had been observed on the impactor, installed at the inlet of the reference SMPS. To focus on the primarily emitted solid particles, volatile particle compounds were then vaporized in the ET at $T_{\text{ET}} = 350 \text{ °C}$ and no such staining was found on the impactor after the experiments performed with this arrangement. The RDD dilution factor was set to the technically possible minimum under argon operation, $DF_{\text{RDD}} = 18.1$. The DMA voltage was scanned between 10 V and 4.5 kV, covering the particle size range between 13.3 and 340 nm. The RF power to induce the plasma at the ICPMS inlet was set to 1350 W; the sampling depth was 8 mm; and 0.58 L_N min⁻¹ argon was added to the plasma torch as dilution gas.

A non-treated natural sawdust sample was digested in acid and conventionally analyzed by ICPMS to identify the chemical elements potentially contained in the later emitted aerosols. Sodium (Na), magnesium (Mg), potassium (K), and a trace of copper (Cu) were found. The detected concentrations are listed in the [Supporting Information](#). ¹³C, ²³Na, ³⁵Cl, ³⁷Cl, ³⁹K, ⁶³Cu, and ⁶⁵Cu were monitored in the first experiment, when a pellet from natural sawdust was treated in the TGA. In addition, ³⁴S was screened in all other measurements. To consider the high carbon concentration in the generated aerosol, the integration time of m/z 13 was 0.05 s and those of all other m/z values were 0.25 s each.

The probability of particles to carry one elemental charge has to be known for calculating the particle concentration at the SMPS inlet from the values measured behind the DMA. In the aerosol neutralizer at the DMA inlet, a known equilibrium state of these particles is attained,²⁵ which can be calculated using the Wiedensohler approximation based on several coefficients,²⁶ depending upon the particle carrier gas.^{27,28} Adapted calculation coefficients were used to consider that the particle carrier gas was argon with less than 0.1% O₂ when passing the aerosol neutralizer.²⁹

Sample Preparation. The first presented experiment was performed with natural beech wood sawdust. For each of the following experiments, a batch of 2 g of sawdust was either

impregnated with a salt solution or treated with pure water. Because Cu is widely used in plant protection agents, two cupric salts were selected for impregnating the sawdust to compare the Cu release during the thermal treatment. These salts were copper sulfate (CuSO₄) and copper chloride (CuCl₂). To see whether or not additional chlorine (Cl) would affect the Cu release, two more impregnations were applied to further sawdust batches, one with only potassium chloride (KCl) and the other with both CuSO₄ and KCl. Finally, a sample was treated with pure water, to verify that the observed changes were caused by the addition of the salts and not as a result of osmotic effects during the impregnation.

A typical value for the Cu concentration in Swiss urban waste wood is 30 ppm,³⁰ and a first pre-experiment was performed with a wood pellet, impregnated with CuSO₄ to achieve this concentration. With this configuration, no particulate Cu release was detected. To see whether the Cu signal was missing as a result of limitations of the instrumentation or the thermal behavior of the fuel sample, the CuSO₄ concentration was increased, resulting in a Cu concentration of 0.3%.

On the basis of previous studies, Cu is expected to evaporate as chloride (e.g., CuCl₂).³¹ Considering the stoichiometry of the chloride formation, the KCl amount in the respecting solutions was dosed to provide Cl in excess, namely, Cl/Cu = 4:1 (mol). The salt solutions, used for impregnating the sawdust batches, are described in the [Supporting Information](#).

For each experiment with treated sawdust, the desired salt amount was dissolved in 15 mL of ultrapure water. The salt solution or pure water was added to 2 g of sawdust in a beaker, later closed with paraffin film. The mixture was stirred with a magnetic stirrer for 4 h at room temperature and then poured into a glass dish. Residues in the beaker were rinsed with 3 mL of ultrapure water and added to the sawdust slurry. The sample was heated in a drying oven for 90 min at 105 °C. The dried sawdust was then stirred manually, using a spatula, and the residues at the bottom and wall of the dish were carefully scraped off and mixed with the sawdust.

To prepare the sample fuel pellets, a stainless-steel die (P0808 from msscientific) with a diameter of 10 mm was filled with 200 mg of sawdust. The port at the bottom of the die was connected to a vacuum pump, and a force of 60 kN was applied to the stamp for 60 s to form each pellet. The pressed pellets with a diameter of 10 mm and a thickness of roughly 2.5 mm were again weighted. The sawdust batches, their treatments, and the masses of the pellets, which were finally used in the experiments, are listed in [Table 1](#).

The residues, remaining in the TGA crucibles after the experiments with the natural and impregnated samples, were acid-digested, and the same elements were conventionally analyzed by ICPMS, as had been measured by the coupled instrumentation. These measuring results are provided in the [Supporting Information](#).

Weight Information Obtained by the TGA. The weight recorded by the TGA balance right after the 10 min drying period at $T_{\text{TGA}} = 105 \text{ °C}$, W_{105} , was considered as the start weight of each sample undergoing the thermal treatment. For all samples, the remaining weights at $T_{\text{TGA}} = 500 \text{ °C}$ and at the end of the experiment at $T_{\text{TGA}} = 950 \text{ °C}$, $W_{500,\{\text{sample}\}}$ and $W_{950,\{\text{sample}\}}$, were read from the TGA data and the relative weight fractions at those temperatures were calculated.

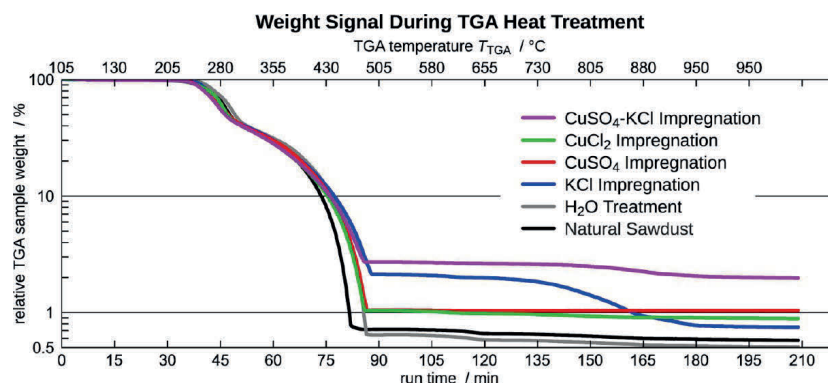


Figure 2. TGA signal recorded during the thermal treatment of all wood sawdust pellets. Lower and upper x axes: Experiment run time and TGA temperature, respectively. The sample weight is logarithmically scaled, to represent also the weight loss in the second part of the experiment. The curves are normalized, considering the weight after the initial 10 min drying period to be 100%.

$$RW_{T,\{sample\}} = \frac{W_{T,\{sample\}}}{W_{105,\{sample\}}}$$

The differences of the relative weights of all treated samples at these temperatures were compared to those of the natural sample to recognize the influence of the treatments on the behavior during the thermal process.

$$\Delta W_{T,\{sample\}} = RW_{T,\{sample\}} - RW_{T,natural}$$

RESULTS AND DISCUSSION

TGA Data. The signals recorded during the TGA experiments are plotted in Figure 2. The lower x axis indicates the experiment run time, the top x axis indicates the corresponding TGA temperature. The sample weight is logarithmically scaled at the y axis. In all experiments, about 60% of the dried wood sample was converted to gas or aerosol between 38 and 52 min after the start of the experiment, when the temperature was increasing from $T_{TGA} = 235$ to 310 °C. These were probably the hemicellulose and lignin fractions of the wood.³² After 85 min (480 °C), also the cellulose fraction was oxidized and about 0.7% of the initial weight of the natural sample was left. Obviously, the water treatment or subsequent drying step was influencing the behavior of the fuel samples between 300 and 500 °C, and the weight loss of the treated samples was slightly retarded in comparison to that of the natural sample. After 89 min (500 °C), the combustion of the organic fraction was accomplished and a stable state was reached in all experiments.

The remaining relative weight fractions of all pellets at 500 °C (89 min) and 950 °C (209 min), $RW_{T,\{sample\}}$, are listed in Table 2 as well as their differences to those of the natural fuel sample, $\Delta W_{T,\{sample\}}$.

$\Delta W_{500,KCl}$ was very close to the added KCl amount in the impregnation. Most of this surplus was released later, at temperatures above 500 °C. The values of $\Delta W_{500,CuSO_4}$ and $\Delta W_{500,CuCl_2}$ match the Cu amount in the impregnations well. However, the $CuCl_2$ sample lost further weight at higher temperatures, such as the natural sample, while the weight of the $CuSO_4$ sample remained constant.

In the experiment with the $CuSO_4$ -KCl-impregnated sample, $\Delta W_{500,CuSO_4-KCl}$ was higher than the sum of $\Delta W_{500,CuSO_4}$ and $\Delta W_{500,KCl}$, and the weight loss in the second period was lower than that of the KCl sample. This possibly

Table 2. Residues of All Fuel Pellet Samples at 500 and 950 °C

	$RW_{500} (\%)^a$	$RW_{950} (\%)^b$	$\Delta W_{500} (\%)^c$	$\Delta W_{950} (\%)^d$
natural	0.72	0.58		
H ₂ O	0.64	0.51	−0.08	−0.07
KCl	2.12	0.75	1.41	0.17
CuSO ₄	1.05	1.05	0.33	0.47
CuCl ₂	1.04	0.89	0.33	0.31
CuSO ₄ -KCl	2.71	1.98	1.99	1.40

^a RW_{500} = weight fraction remaining in the TGA after 89 min, at 500 °C, relative to the start weight of the dried sample after the initial 10 min period at 105 °C. ^b RW_{950} = final residue after experiment completion. ^c ΔW_{500} = difference between the remaining fraction of each impregnated fuel sample after 89 min (500 °C) compared to the natural pellet. ^d ΔW_{950} = difference between the final residue of the impregnated and natural fuel samples.

indicates that $CuSO_4$ was reacting with KCl and forming other stable species, such as K_2SO_4 , leading to a reduced weight loss. This appears to be consistent with the observation that, in the final period at constant 950 °C, the loss per time of the $CuSO_4$ -KCl sample was about twice as high as that of the other samples, because these secondary species might evaporate at higher temperatures. The observed values with the water-treated sample were very similar to those measured with the natural sample.

SMPS-ICPMS Signals. To correlate the data from SMPS and ICPMS and to visualize the development of both the volume-weighted PSD, determined by SMPS, and the distribution of the different elements on particle size fractions, measured by ICPMS, a self-written MATLAB code was used to create color map diagrams. The run time and TGA temperature are indicated on the lower and upper x axes. The particle diameter is logarithmically scaled on the y axis. The area, span by the x and y axes, is filled with colors, representing the particle concentrations or ICPMS mass intensities, related to specific particle size fractions and the experiment run time or TGA temperature. The colors are logarithmically scaled, as indicated by the scale bar at the right of the diagram area.

Natural Wood. The first particle emissions from the natural sample were observed after about 30 min, at temperatures above 200 °C, as seen in Figure 3, representing the development of the PSD during the TGA experiment. At about 280 °C, particle volume concentrations of up to

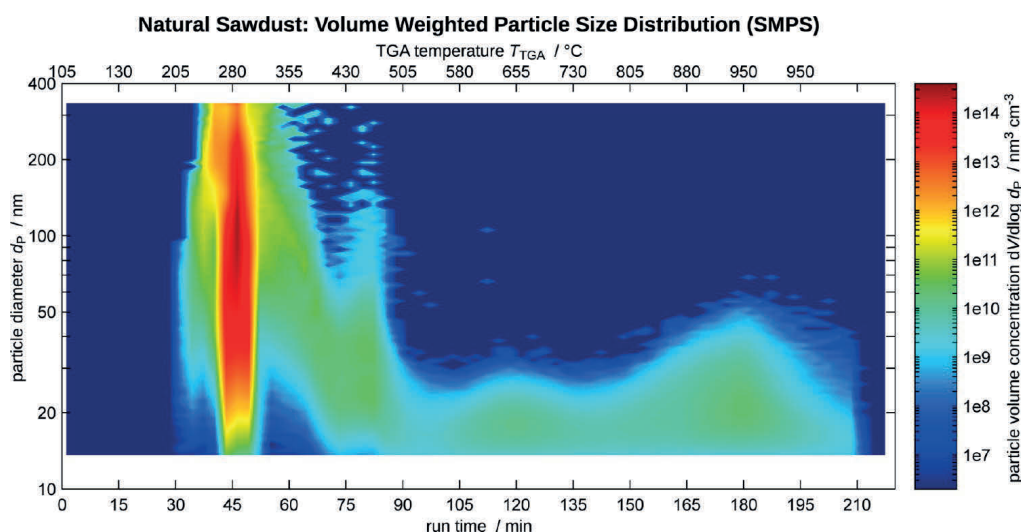


Figure 3. Development of the volume-weighted PSD of aerosol particles, emitted by the pellet, pressed from natural sawdust, during the TGA experiment, measured by SMPS. Lower and upper x axes: run time and TGA temperature, respectively. Diagram y axis: logarithmically scaled particle diameter. The colors represent the logarithmically scaled particle volume concentrations, as indicated on the color bar on the right side.

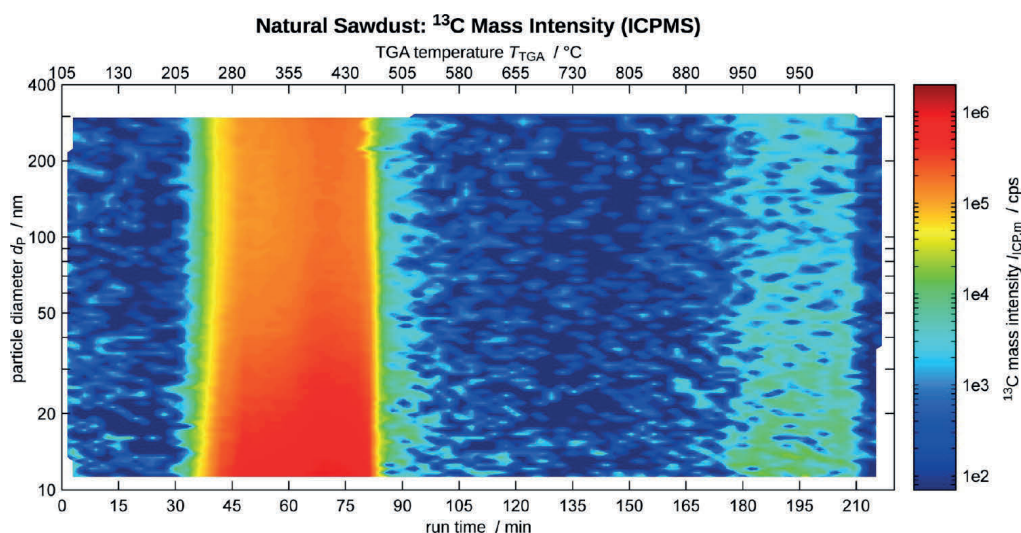


Figure 4. Particle-size-related ICPMS mass intensity on m/z 13, given in cps. The data are presented the same way as the volume-weighted PSD measured by SMPS and enable a qualitative observation of the carbon release during the TGA experiment with the pellet from natural sawdust.

$3 \times 10^{14} \text{ nm}^3 \text{ cm}^{-3}$ were observed at about 100 nm in the $dV/d \log d_p$ representation. In this temperature range, the TGA had recorded the highest sample weight decrease. Another increased particle release was observed at about 460 °C, when the combustion of the organic fraction was almost completed (Figure 2). However, these particle volume concentrations were about 4 orders of magnitude lower than those at 280 °C, and the mode of this size distribution was at about 30 nm. At 655 °C and when the final 950 °C was reached, particle concentrations in the same order of magnitude were detected, with modes around 20 nm.

In a similar manner, the time- and particle-size-resolved ICPMS mass intensity of the carbon isotope ^{13}C is displayed in Figure 4. Very high carbon concentrations were found between

35 and 85 min, at temperatures between 230 and 480 °C, when the TGA also had recorded the highest weight decrease, during the combustion of the organic wood fraction. The measured concentrations are nearly constant over the whole particle size range, indicating that the intensity mainly arose from gaseous and not particulate carbon, because otherwise, certain particle diameters would be emphasized. A gradual decrease from 10^6 counts per second (cps) at 13 nm to about 2×10^5 cps at 100 nm appears in the diagram because a signal is visualized which was converted to correctly reflect particulate element mass concentrations, and not the raw or net ICPMS intensity. The correction factor used for this conversion considers the probability of particles to carry one elemental charge and is a size-dependent particle property.

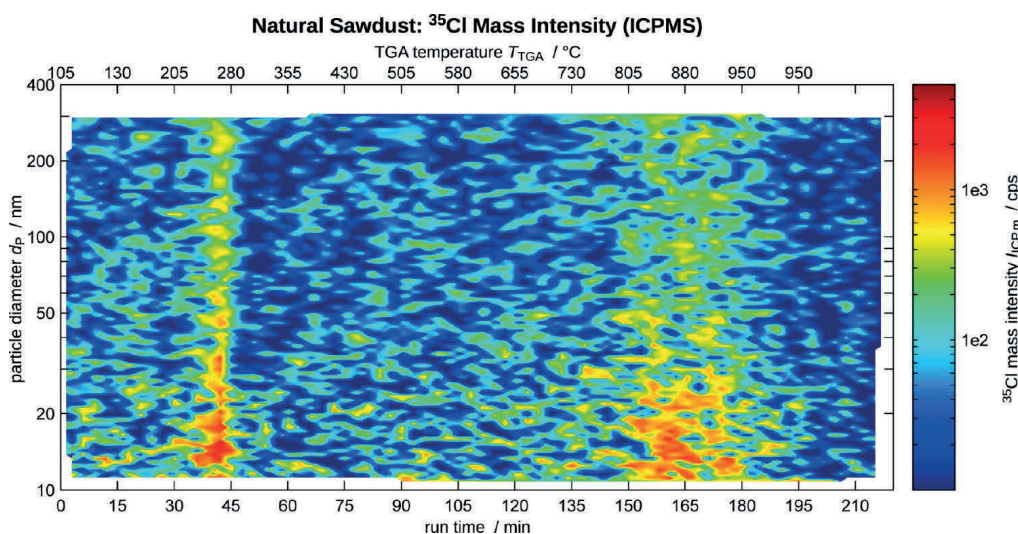


Figure 5. Particle-size-related ICPMS mass intensity on m/z 35, given in cps, representing the Cl release during the TGA experiment with the pellet from natural sawdust.

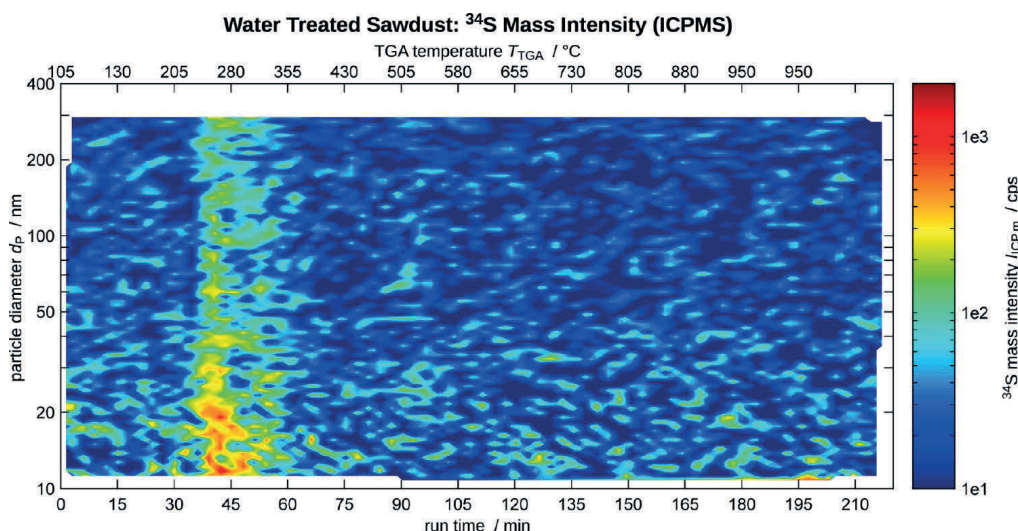


Figure 6. Particle-size-related ICPMS mass intensity on m/z 34, given in cps, representing the Cl release during the TGA experiment with the pellet from water-treated sawdust.

The particulate carbon fraction in this period would have been higher if no ET had been used to convert volatile matter into the gas phase, and volatile particles far above the classifying range of the DMA were expected. However, the ET allowed focusing on solid particles, and hardly reproducible effects, such as uncontrolled particle growth as a result of condensation were avoided. The weak ^{13}C signal at 950 °C had also been observed in the blank measurement and, hence, did not originate from the sample itself but from carbonaceous impurities in the TGA furnace.

The sample weight loss rate determined by the TGA at 280 °C was about $\dot{m}_{\text{wood}} = 10 \text{ mg min}^{-1}$. As an approximation, the stoichiometric wood composition was assumed to be $\text{CH}_{1.4}\text{O}_{0.7}$.³³ With the molar masses of C, H, and O, $M_{\text{C}} = 12 \text{ g}$

mol^{-1} , $M_{\text{H}} = 1 \text{ g mol}^{-1}$, and $M_{\text{O}} = 16 \text{ g mol}^{-1}$, the carbon release in this period can be estimated.

$$\begin{aligned} \dot{m}_{\text{C}} &= \frac{M_{\text{C}}}{M_{\text{CH}_{1.4}\text{O}_{0.7}}} \times \dot{m}_{\text{wood}} \\ &= \frac{12}{12 + 1.4 \times 1 + 0.7 \times 16} \times 10 \text{ mg min}^{-1} = 0.49 \text{ mg min}^{-1} \end{aligned}$$

The integrated particle volume concentration measured at the same time by the SMPS was $c_{\text{part,V}} = 1.2 \times 10^{14} \text{ nm}^3 \text{ cm}^{-3}$. With the total aerosol flow, $Q_{\text{raw,in}} \approx 1.0 \text{ L min}^{-1} = 10^3 \text{ cm}^3 \text{ min}^{-1}$, the particulate volume flow, $\dot{V}_{\text{part}} = 1.2 \times 10^{17} \text{ nm}^3 \text{ min}^{-1}$, can be estimated. With an assumed particle density, $\rho_{\text{part}} = 1 \text{ g cm}^{-3} = 10^{-18} \text{ mg nm}^{-3}$, the particulate mass flow is estimated to be in the order of $\dot{m}_{\text{part}} = 0.12 \text{ mg min}^{-1}$, which is 2.5% of the total carbon mass. Only about 10% of all particles were classified in

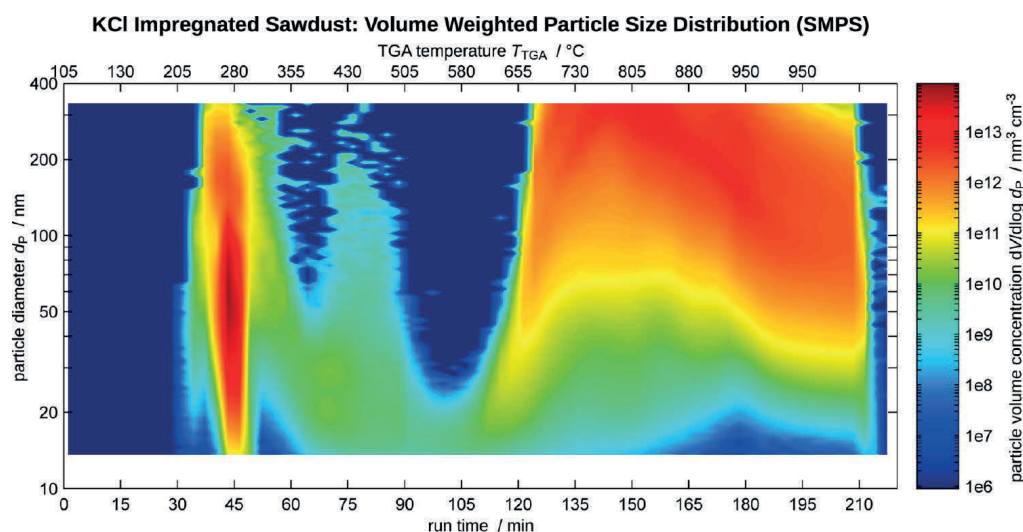


Figure 7. Development of the volume-weighted PSD of aerosol particles, emitted by the pellet from KCl-impregnated sawdust.

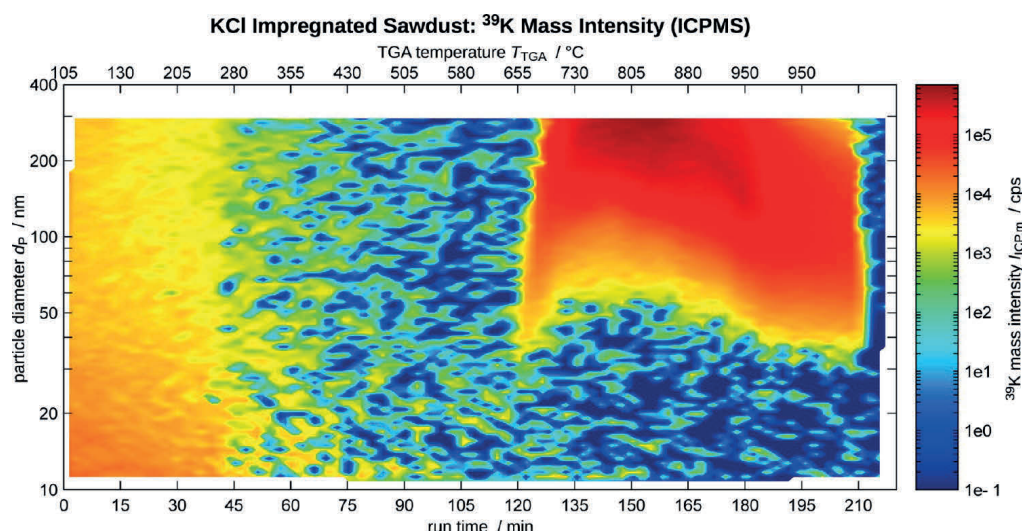


Figure 8. Particle-size-related ICPMS mass intensity on m/z 39, given in cps, representing the Cl release during the TGA experiment with the KCl-impregnated sample.

the DMA as a result of the probability of particles to carry one elemental charge, i.e., the probability to be correctly classified in the SMPS,²⁵ and only a narrow fraction of the remaining particles was passing the DMA at a particular time as a result of the size-scanning procedure. Therefore, the contribution of the classified particles to the total ^{13}C intensity was far below the standard deviation of the ICPMS background signal. This calculation is based on a number of assumptions and rough estimations. However, it explains why no carbon intensity could be allocated to particles, because the signal was dominated by gaseous carbon.

Figure 5 shows the visualization of the ^{35}Cl signal. Increased m/z 35 intensities were measured at about 260 °C, when the combustion process started, and above 805 °C for about 30 min. Because these enhanced Cl concentrations also span the whole particle size range, they can again be allocated to

gaseous emissions. There is a certain probability that these m/z 35 intensities were due to interferences, e.g., from carbonaceous compounds generated by the wood incineration and the plasma-surrounding atmosphere, such as $^{16}\text{C}^{18}\text{C}^1\text{H}$.³⁴ Because, for this case, a similarly wide pattern as in the ^{13}C map (Figure 4) would be expected, it appears more likely that indeed Cl was emitted at the beginning of the main combustion period. Together with some hydrogen released by the wood decomposition, it might have formed HCl and passed through the SMPS as a gas. The enhanced intensity between 800 and 950 °C is not clearly explained. Neither K nor Na emissions were detected in this experiment; therefore, this signal is not related to KCl or NaCl. The m/z 35 intensity could represent another gaseous compound containing Cl or be caused by an interference.

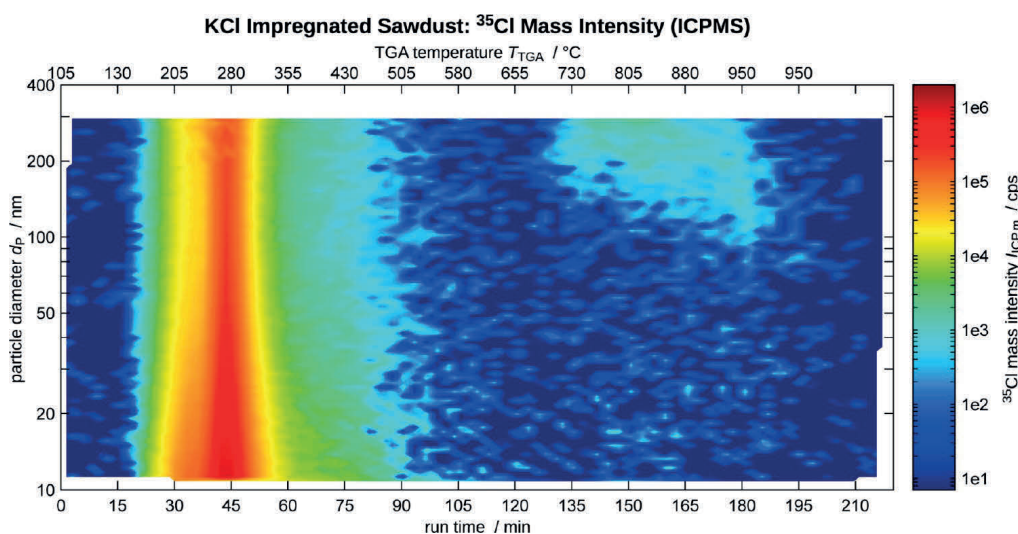


Figure 9. Particle-size-related ICPMS mass intensity on m/z 35, given in cps, representing the Cl release during the TGA experiment with the KCl-impregnated sample.

On the Na, K, and Cu maps, no enhanced intensities were observed during the experiment with the natural wood (data not shown). In a real combustion situation, where the fuel usually does not experience a constant heating rate but is rapidly heated and combusted, Na and K would probably be released together with Cl, as salts. However, in the TGA experiment presented here, Cl was released at lower temperatures and not available for later formation of salt particles.

Water Treatment. No obvious differences were observed between the SMPS and ICPMS signals from analyzing the emissions from the water-treated sawdust pellet to those of the natural sample, except the ^{13}C intensity, which lasted about 6 min longer, corresponding to the TGA signal. Therefore, no diagrams from this experiment are shown, except the ^{34}S map, which is shown in Figure 6, because no S information was available from the first experiment. Weak m/z 34 intensity of gaseous matter was recorded in the beginning of the main combustion period, between about 250 and 350 °C. These signals might have arisen from S, but it cannot be excluded that they were partially caused by polyatomic oxygen and nitrogen interferences.

KCl Impregnation. The time-dependent volume-weighted PSD, measured by the SMPS during the heat treatment of the KCl-impregnated sawdust pellet, is visualized in Figure 7. In the period with the highest particle emissions, around 280 °C, the mode of the PSD was about 50 nm, while it had been close to 100 nm in the experiment with the natural sawdust (Figure 3). The most obvious difference between the SMPS signals of these two experiments was found above 655 °C, where concentrations between 10^{12} and 10^{13} $\text{nm}^3 \text{ cm}^{-3}$ in the $dV/d \log d_p$ representation were measured with the modes of the size distribution first increasing from about 50 to above 300 nm and then returning to about 150 nm, at 950 °C. Unlike in the experiment with the pellet from natural sawdust, no PSDs with modes around 20 nm were found. Possibly, the primarily generated particles were in the same size range, but as a result of their much higher concentration, they rapidly disappeared by agglomeration, forming bigger particles.

While no particulate K emissions above the background level had been observed in the experiment with the natural sample, the ^{39}K map of the KCl-impregnated sample in Figure 8 shows an obvious time and size correlation to the SMPS signal in the temperature range above 650 °C. Thus, the RDD–SMPS–ICPMS instrumentation reveals that the detected SMPS particles are K compounds. Because no distinct particle diameters are emphasized below 400 °C, it can be excluded that the enhanced intensities on m/z 39 in this period were caused by particulate matter. Again, the intensity is slightly amplified at small particle diameters as a result of the correction for the single-particle charge probability. The enhanced signal did probably not arise from K. It could be a polyatomic interference, e.g., from $^{38}\text{Ar}^1\text{H}^+$, arising from water released in this period, or it might be caused by contaminations at the ICPMS inlet, dissipating during the first hour of operation.

Over a wide range, the KCl quantum in the fuel sample was stable. This was verified using thermodynamic equilibrium calculation software (HSC 7.1 from Outotec, data not shown). At moderate temperatures, KCl can only decompose if complex mechanisms enable the release of Cl (e.g., as HCl) and more stable K species are formed. The ^{35}Cl map in Figure 9 shows both gaseous and particulate Cl in the same diagram. Gaseous Cl was detected around 280 °C. This was probably HCl, formed by Cl^- ions from the impregnation and H^+ ions released in terms of the wood decomposition. The ^{35}Cl signal decreased to the background level after 90 min when the first weight decrease was accomplished, as seen in the TGA curve of the KCl-impregnated sample (Figure 2). In the same temperature and size range as K, particulate Cl was detected. At 805 °C, ^{35}Cl intensities above 2×10^3 cps were recorded, when those of ^{39}K were around 7×10^5 cps. Because usually 2–3 orders of magnitude are between the ICPMS sensitivities on these elements, it seems reasonable that the K and Cl intensities were caused by particles with a significant KCl content.

When particulate K was detected, also Na was found, with different concentrations but a similar distribution over the particle size range, as recognized in the ^{23}Na map in Figure 10.

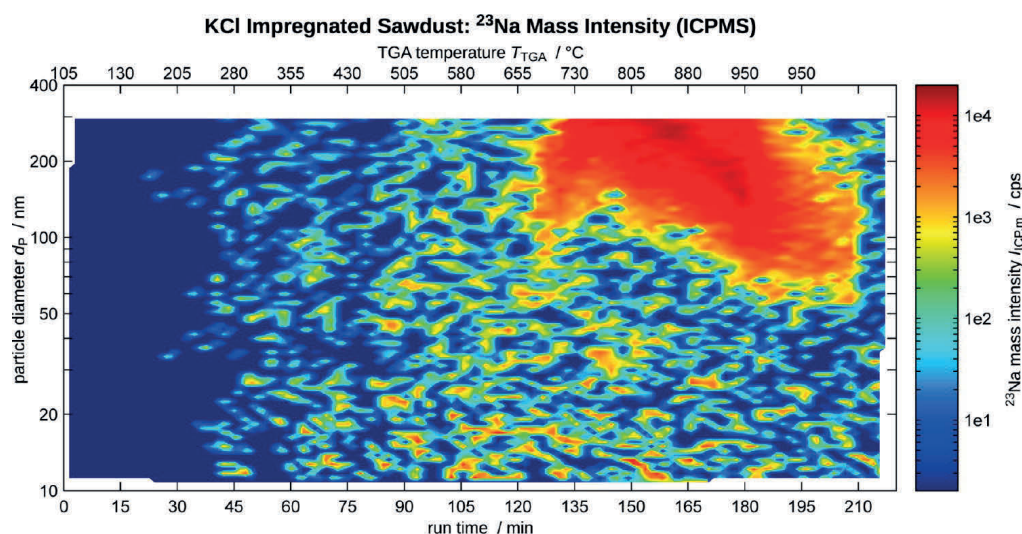


Figure 10. Particle-size-related ICPMS mass intensity on m/z 23, given in cps, representing the Cl release during the TGA experiment with the KCl-impregnated sample.

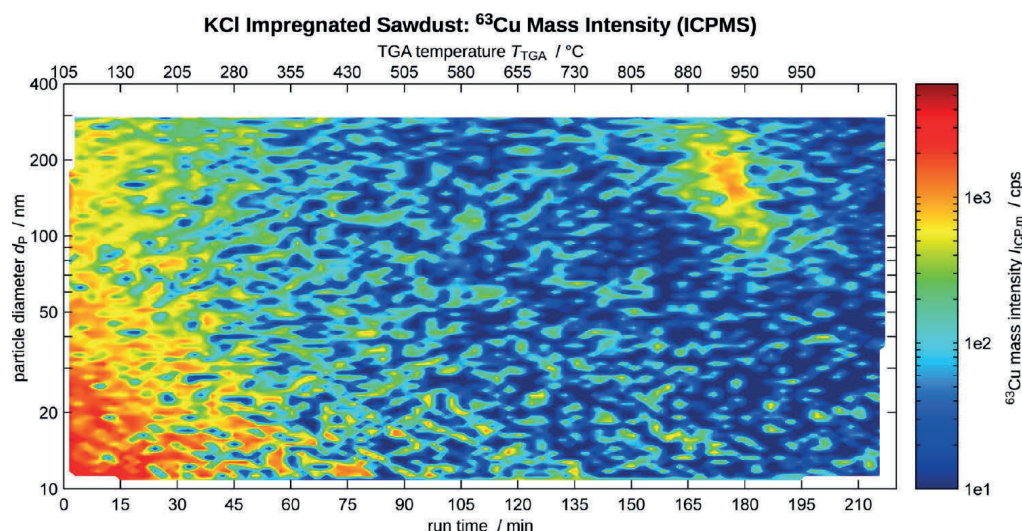


Figure 11. Particle-size-related ICPMS mass intensity on m/z 63, given in cps, representing the Cl release during the TGA experiment with the KCl-impregnated sample.

Such emissions were not observed in the experiment with the natural sample. Because Na had been found in the wet chemistry analysis of the wood sawdust but was not contained in the KCl impregnation, it appears that the naturally present Na^+ ions in the wood and the K^+ ions were competing for the additional Cl^- ions in the KCl impregnation, resulting in a considerable formation and release of particulate NaCl. The RDD–SMPS–ICPMS combination was able to show that ^{23}Na , ^{35}Cl , and ^{39}K were contained in the same particle size fractions. Because these signals coincide well regarding their distribution in the relevant size classes, they were probably not induced by separate NaCl and KCl particles but both salts were contained in the same particles.

In the period with the highest particulate Na, K, and Cl emissions, also an increase of the ^{63}Cu signal was detected on

the same particle diameters, as shown in Figure 11. A similar signal was neither recorded during the experiments with non-impregnated wood samples nor during the blank measurement, performed before the KCl experiment. The KCl impregnation seems to have provoked a release of Cu, contained in the natural wood, which had also been detected in the wet chemistry analysis of the sawdust.

The ^{13}C map was similar to that of the natural sample, except that the release of gaseous carbon during the main combustion period was about 6 min longer, as observed with the water-treated sample. Also, the ^{34}S map was not affected by the KCl impregnation (diagrams not shown).

CuSO_4 Impregnation and CuCl_2 Impregnation. During the treatment of the CuSO_4 -impregnated sample, the carbon-emitting period was longer, corresponding to the TGA signal.

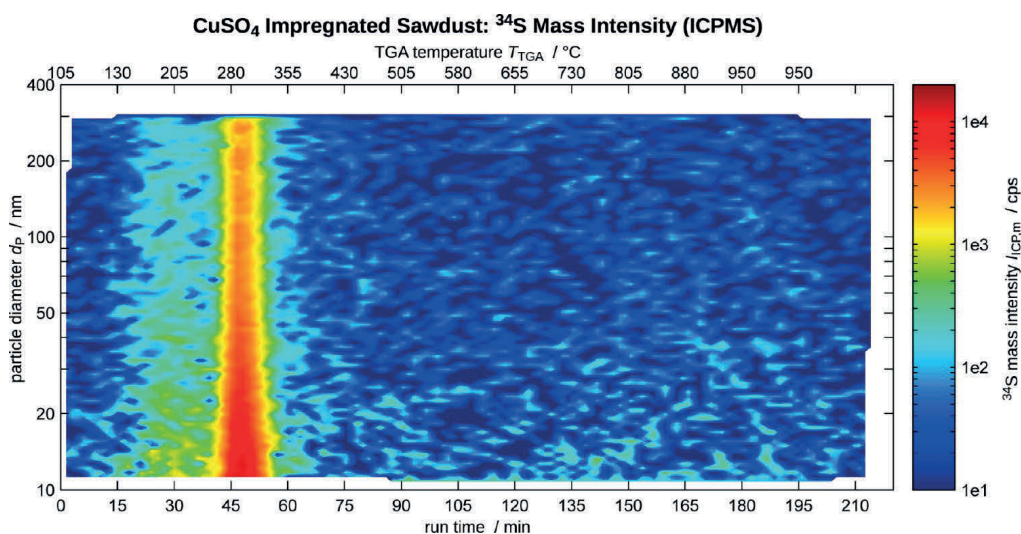


Figure 12. Particle-size-related ICPMS mass intensity on m/z 34, given in cps, representing the Cl release during the TGA experiment with the CuSO_4 -impregnated sample.

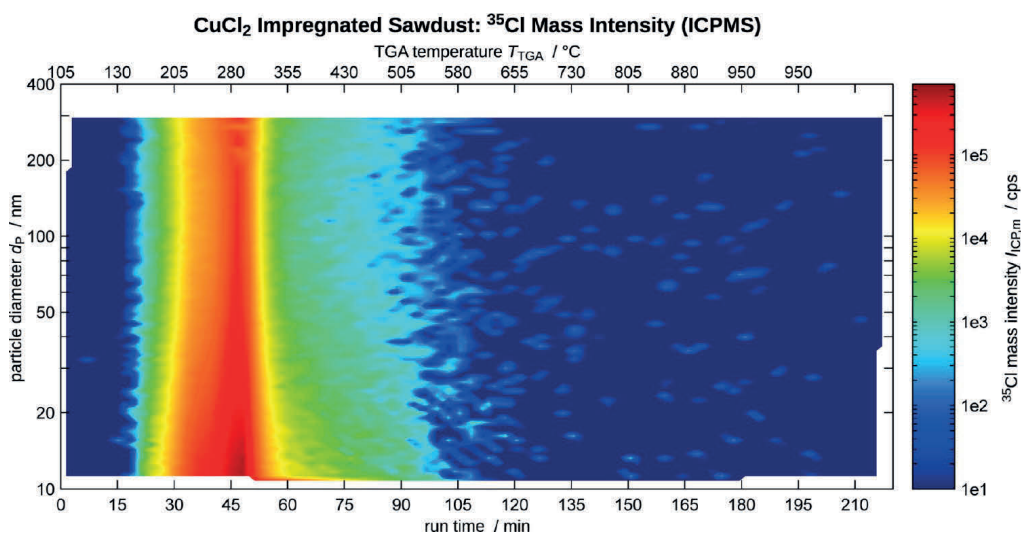


Figure 13. Particle-size-related ICPMS mass intensity on m/z 35, given in cps, representing the Cl release during the TGA experiment with the CuCl_2 -impregnated sample.

No Cu release was detected, and the only obvious difference to the experiment with the natural sample was that a gaseous S compound was found in the first combustion period around 280 °C, as shown in Figure 12. In the heating period below 250 °C, most of the water, including the hydration water of $\text{CuSO}_4 \cdot 5\text{H}_2\text{O}$, was evaporated. Under oxidizing conditions, CuSO_4 is thermodynamically stable below 400 °C. However, HSC calculations were made to check whether the formation of gaseous sulfur compounds was feasible under these conditions. They confirmed that sulfur dioxide (SO_2) can be formed under slightly reducing conditions (see Figure S1 of the Supporting Information) and hydrogen sulfide (H_2S) can immediately arise under highly reducing conditions (see Figure S2 of the Supporting Information). It seems that locally reducing

conditions were obtained during the prompt combustion of wood, possibly resulting in the formation of H_2S .

Below 500 °C, similar gaseous Cl emissions were measured from the CuCl_2 - as from the KCl-impregnated sample. In the HSC calculation, it was confirmed that Cl_2 and HCl species are stable under oxidizing conditions above 200 °C (see Figure S3 of the Supporting Information). Probably, most Cl was released in the period below 500 °C as HCl, and no Cl was later available to form chlorides. Hence, no Cl-containing particles were detected at high temperatures, as shown in Figure 13.

No particulate Cu was detected during both experiments with the CuSO_4 - and CuCl_2 -impregnated samples. Also, the other signals were similar to those recorded during the experiment with the natural sample and, hence, are not shown.

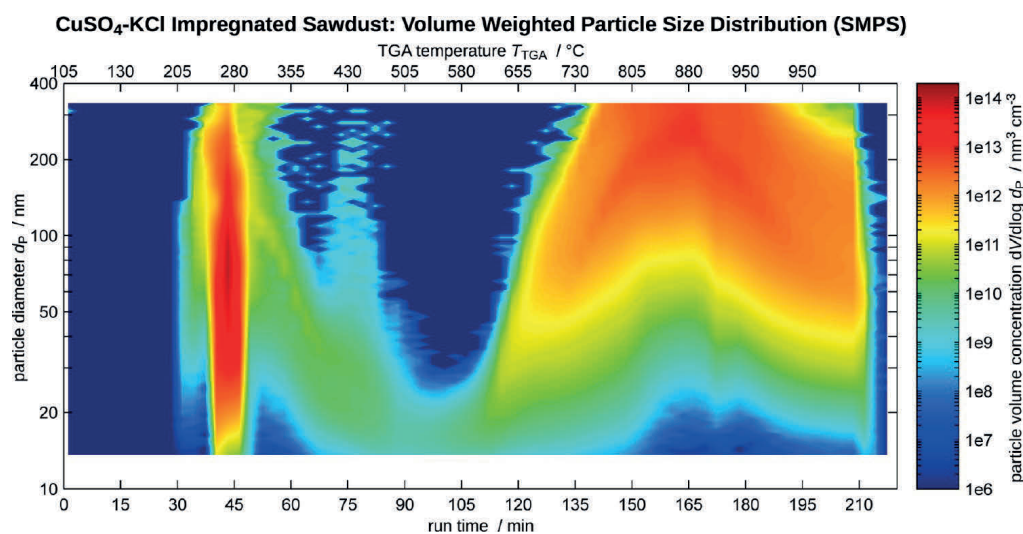


Figure 14. Development of the volume-weighted PSD of aerosol particles, emitted by the pellet from CuSO₄–KCl-impregnated sawdust.

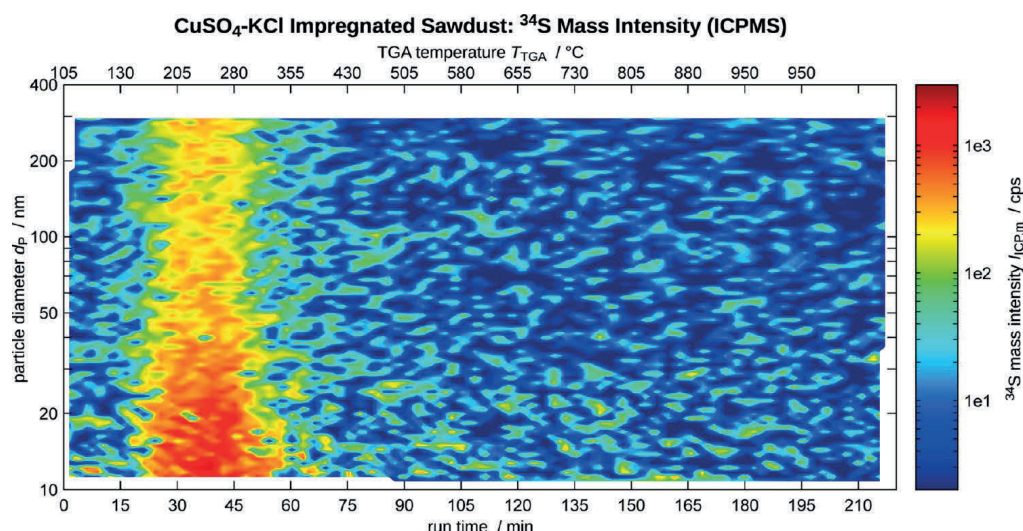


Figure 15. Particle-size-related ICPMS mass intensity on m/z 34, given in cps, representing the Cl release during the TGA experiment with the CuSO₄–KCl-impregnated sample.

CuSO₄–KCl Impregnation. The PSD map recorded by the SMPS during the heat treatment of the CuSO₄–KCl-impregnated sample is shown in Figure 14. In comparison to the KCl sample, the PSD between 600 and 800 °C was narrower and less particles above 100 nm were measured. This is consistent with the TGA signals, where a stronger weight decrease was observed in this period from the KCl- than from the CuSO₄–KCl-impregnated sample, because possibly CuSO₄ and KCl were reacting to other stable species, resulting in reduced evaporation. At 880 °C and above, the particle concentrations were in the same order of magnitude, when the weight loss rates were also similar. The relation of the K, Na, and Cl maps to the PSD map was very similar to that observed with the KCl sample. These diagrams are provided in Figures S4–S6 of the Supporting Information.

When the CuSO₄–KCl-impregnated sample was treated in the TGA, gaseous S was emitted between 200 and 300 °C. Unlike those from the sample with only CuSO₄ impregnation, these emissions were spread uniformly over the period when the temperature was increasing from 160 to 310 °C, as seen in the ³⁴S map in Figure 15. Similar to the case with the CuSO₄-impregnated sample, S species are supposed to arise under reducing conditions. Possibly, SO₂ was continuously formed (Figure S1 of the Supporting Information) in this experiment, while the more rapid H₂S formation mechanism (Figure S2 of the Supporting Information) was taking place with the CuSO₄ sample. This could explain the difference between the S signals below 350 °C in Figures 12 and 15.

Even the ⁶³Cu map was not remarkably different from that of the KCl experiment, although the sample contained Cu with a very high concentration of 0.3%. Hence, Cu seems to feature a

very low tendency to be evaporated in such a thermal process, if no Cl is available to form cupric chlorides. The ^{63}Cu map is shown in Figure S7 of the Supporting Information.

CONCLUSION

In the TGA, the O_2 content and furnace temperature can be controlled, which allows repeating a defined thermal treatment with differently impregnated fuel samples and studying the influence of these treatments on the combustion process. Coupling this equipment to the RDD–SMPS–ICPMS particle analyzing instrumentation enables simultaneous size-resolved online measurement of the elemental composition of gaseous and particulate emissions, depending upon fuel properties and TGA parameters.

Short SMPS scan durations in the range of a few minutes allow the generation of particle concentration maps, representing the time- and size-resolved particle concentration during such an experiment. Similar element maps, generated from the measured ICPMS intensities of a number of elements, with the same time and similar size resolution as the SMPS data, representing time- and size-resolved elemental composition of gas-borne particles in the nanometer size range, allow visually distinguishing between the gaseous and particulate nature of the detected elements.

The instrumentation was able to show that the KCl impregnation facilitated the release of particles containing Cu, which was originally present in the natural wood. Even very high concentrations of cupric salts in the wood sawdust impregnation did not lead to a substantial additional Cu release in terms of the applied heat treatment. Obviously, the addition of KCl has led to the formation of Na- and Cu-containing particles, confirming that adding Cl to the fuel provokes the release of alkali and heavy metals.

Future applications of the RDD–SMPS–ICPMS setup will include investigations of process gases, released by impregnated and real waste samples, which can undergo different heat treatments in the TGA, laboratory-scale furnace, or other thermal reactors.

ICPMS sensitivities may be determined for different particulate elements and SMPS–ICPMS operating conditions and collected in a database. This would allow not only allocating certain elements to distinct particle size fractions but also determining their concentrations in those particles.

ASSOCIATED CONTENT

Supporting Information

The Supporting Information is available free of charge on the ACS Publications website at DOI: 10.1021/acs.energy-fuels.6b00174.

Calculations of the salt amounts added to the impregnation solutions, flow adjustment procedure during instrument startup, analysis of the wood sawdust and residues from the TGA experiments, thermodynamic equilibrium calculations for verifying the formation of S and Cl species, and element maps from the TGA experiment with the CuSO_4 –KCl-impregnated sample (PDF)

AUTHOR INFORMATION

Corresponding Authors

*E-mail: hessa@alumni.ethz.ch.

*E-mail: christian.ludwig@psi.ch.

Notes

The authors declare no competing financial interest.

ACKNOWLEDGMENTS

Financial support was obtained from the Competence Center for Materials Science and Technology (CCMX, Project NanoAir), the Swiss National Science Foundation (Project 139136), the Swiss Nanoscience Institute (Argovia, Project NanoFil), and the Commission for Technology and Innovation (SCCER BIOSWEET). The authors thank Albert Schuler for his support in terms of maintaining and operating the TGA, Dominik Gschwend for his help to improve the data-processing code, and Alfred Wiedensohler (TROPOS) for providing the coefficients to calculate the charge probabilities of argon-borne particles.

REFERENCES

- (1) Hinds, W. C. Physical and Chemical Processes in Aerosol Systems. In *Aerosol Measurement*; Kulkarni, P., Baron, P. A., Willeke, K., Eds.; John Wiley & Sons, Inc.: Hoboken, NJ, 2011; pp 31–40, DOI: 10.1002/9781118001684.ch3.
- (2) Part, F.; Zecha, G.; Causon, T.; Sinner, E. K.; Huber-Humer, M. Current limitations and challenges in nanowaste detection, characterization and monitoring. *Waste Manage.* **2015**, *43*, 407–420.
- (3) Zhang, J. F.; Morawska, L. Combustion sources of particles: 2. Emission factors and measurement methods. *Chemosphere* **2002**, *49* (9), 1059–1074.
- (4) Wang, S. C.; Flagan, R. C. Scanning Electrical Mobility Spectrometer. *Aerosol Sci. Technol.* **1990**, *13* (2), 230–240.
- (5) Heringa, M. F.; DeCarlo, P. F.; Chirico, R.; Lauber, A.; Doberer, A.; Good, J.; Nussbaumer, T.; Keller, A.; Burtscher, H.; Richard, A.; Miljevic, B.; Prevot, A. S. H.; Baltensperger, U. Time-resolved characterization of primary emissions from residential wood combustion appliances. *Environ. Sci. Technol.* **2012**, *46* (20), 11418–11425.
- (6) Pratt, K. A.; Prather, K. A. Mass spectrometry of atmospheric aerosols - Recent developments and applications. Part II: On-line mass spectrometry techniques. *Mass Spectrom. Rev.* **2012**, *31* (1), 17–48.
- (7) Kowalski, T.; Ludwig, C.; Wokaun, A. Qualitative evaluation of alkali release during the pyrolysis of biomass. *Energy Fuels* **2007**, *21* (5), 3017–3022.
- (8) Blasing, M.; Muller, M. Investigations on the influence of steam on the release of sodium, potassium, chlorine, and sulphur species during high temperature gasification of coal. *Fuel* **2012**, *94* (1), 137–143.
- (9) Wellinger, M.; Wochele, J.; Biollaz, S. M. A.; Ludwig, C. Online elemental analysis of process gases with ICP-OES: A case study on waste wood combustion. *Waste Manage.* **2012**, *32* (10), 1843–1852.
- (10) Yang, J. J.; Gebremedhin, A.; Strand, M. Characterization of particles and inorganic vapors through high-temperature extraction in a biomass-fired grate boiler. *Energy Fuels* **2013**, *27* (10), S915–S922.
- (11) Taiwo, A. M.; Beddows, D. C. S.; Shi, Z. B.; Harrison, R. M. Mass and number size distributions of particulate matter components: Comparison of an industrial site and an urban background site. *Sci. Total Environ.* **2014**, *475*, 29–38.
- (12) Tissari, J.; Sippula, O.; Torvela, T.; Lamberg, H.; Leskinen, J.; Karhunen, T.; Paukkunen, S.; Hirvonen, M. R.; Jokiniemi, J. Zinc nanoparticle formation and physicochemical properties in wood combustion - Experiments with zinc-doped pellets in a small-scale boiler. *Fuel* **2015**, *143*, 404–413.
- (13) Solomon, P. A.; Fraser, M. P.; Herckes, P. Methods for chemical analysis of atmospheric aerosols. In *Aerosol Measurement*; Kulkarni, P., Baron, P. A., Willeke, K., Eds.; John Wiley & Sons, Inc.: Hoboken, NJ, 2011; pp 153–177, DOI: 10.1002/9781118001684.ch9.
- (14) Lee, S.; Bi, X. Y.; Reed, R. B.; Ranville, J. F.; Herckes, P.; Westerhoff, P. Nanoparticle size detection limits by single particle

ICP-MS for 40 elements. *Environ. Sci. Technol.* **2014**, *48* (17), 10291–10300.

(15) Mitrano, D. M.; Dasilva, Y. A. R.; Nowack, B. Effect of variations of washing solution chemistry on nanomaterial physicochemical changes in the laundry cycle. *Environ. Sci. Technol.* **2015**, *49* (16), 9665–9673.

(16) Vicente, E. D.; Duarte, M. A.; Calvo, A. I.; Nunes, T. F.; Tarelho, L. A. C.; Custodio, D.; Colombi, C.; Gianelle, V.; Sanchez de la Campa, A.; Alves, C. A. Influence of operating conditions on chemical composition of particulate matter emissions from residential combustion. *Atmos. Res.* **2015**, *166*, 92–100.

(17) Hagendorfer, H.; Lorenz, C.; Kaegi, R.; Sinnet, B.; Gehrig, R.; Goetz, N. V.; Scheringer, M.; Ludwig, C.; Ulrich, A. Size-fractionated characterization and quantification of nanoparticle release rates from a consumer spray product containing engineered nanoparticles. *J. Nanopart. Res.* **2010**, *12* (7), 2481–2494.

(18) Buha, J.; Mueller, N.; Nowack, B.; Ulrich, A.; Losert, S.; Wang, J. Physical and chemical characterization of fly ashes from swiss waste incineration plants and determination of the ash fraction in the nanometer range. *Environ. Sci. Technol.* **2014**, *48* (9), 4765–4773.

(19) Hess, A.; Tarik, M.; Ludwig, C. A hyphenated SMPS-ICPMS coupling setup: Size-resolved element specific analysis of airborne nanoparticles. *J. Aerosol Sci.* **2015**, *88*, 109–118.

(20) Hess, A.; Tarik, M.; Losert, S.; Ilari, G.; Ludwig, C. Measuring air borne nanoparticles for characterizing hyphenated RDD-SMPS-ICPMS instrumentation. *J. Aerosol Sci.* **2016**, *92*, 130–141.

(21) Losert, S.; Hess, A.; Ilari, G.; von Goetz, N.; Hungerbuehler, K. Online characterization of nano-aerosols released by commercial spray products using SMPS-ICPMS coupling. *J. Nanopart. Res.* **2015**, *17* (7), 293.

(22) Ludwig, C.; Wochele, J.; Jörimann, U. Measuring evaporation rates of metal compounds from solid samples. *Anal. Chem.* **2007**, *79* (7), 2992–2996.

(23) Swiss Association for Standardization, SNV. SN277206, *Internal Combustion Engines—Exhaust Gas After-treatment—Particle Filter Systems—Testing Method*; SNV: Winterthur, Switzerland, 2011.

(24) Giechaskiel, B.; Dilara, P.; Sandbach, E.; Andersson, J. Particle measurement programme (PMP) light-duty inter-laboratory exercise: Comparison of different particle number measurement systems. *Meas. Sci. Technol.* **2008**, *19* (9), 095401.

(25) Flagan, R. C. Differential mobility analysis of aerosols: A tutorial. *KONA* **2008**, *26*, 254–268.

(26) Wiedensohler, A. An approximation of the bipolar charge distribution for particles in the submicron size range. *J. Aerosol Sci.* **1988**, *19* (3), 387–389.

(27) Wiedensohler, A.; Fissan, H. J. Bipolar charge distributions of aerosol particles in high-purity argon and nitrogen. *Aerosol Sci. Technol.* **1991**, *14* (3), 358–364.

(28) Stober, J.; Schleicher, B.; Burtscher, H. Bipolar diffusion charging of particles in noble-gases. *Aerosol Sci. Technol.* **1991**, *14* (1), 66–73.

(29) Wiedensohler, A. Dissertation: Die bipolare Diffusionsaufladung von Partikeln in chemisch trägen Reinstgasen. Ph.D. Thesis, Universität Gesamthochschule Duisburg, Duisburg, Germany, 1989.

(30) Hasler, P.; Nussbaumer, T.; Bühler, R. *Vergasung von belasteten Brennstoffen zu Synthesegas*; Bundesamt für Energiewirtschaft: Bern, Switzerland, 1995.

(31) Jakob, A.; Stucki, S.; Struis, R. Complete heavy metal removal from fly ash by heat treatment: Influence of chlorides on evaporation rates. *Environ. Sci. Technol.* **1996**, *30* (11), 3275–3283.

(32) Babrauskas, V. Ignition of wood: A review of the state of the art. *Journal of Fire Protection Engineering* **2002**, *12* (3), 163–189.

(33) Behrendt, F.; Neubauer, Y.; Oevermann, M.; Wilmes, B.; Zobel, N. Direct Liquefaction of Biomass. *Chem. Eng. Technol.* **2008**, *31* (5), 667–677.

(34) May, T. W.; Wiedmeyer, R. H. A table of polyatomic interferences in ICP-MS. *Atom. Spectrosc.* **1998**, *19* (5), 150–155.

List of figures

Figure 1.1-1	Fuels and value-added chemicals in staged degasification.	3
Figure 1.1-2	Schematic of a moving grate furnace [4]	5
Figure 1.1-3	Schematic of ash formation from biomass during combustion, adapted from reference [7].....	5
Figure 1.1-4	Main classes of atmospheric particles; the major formation and growth mechanisms are also reported The four main modes are shown for particles with different particles size: nucleation, Aitken, accumulation and coarse mode for ambient particles. V = volume, Dp = particle diameter. [9]	6
Figure 1.1-5	Schematic of unintentionally produced nanomaterials or so-called incidental nanoparticles (INPs) in a waste incinerator.....	7
Figure 1.2-1	Graphical concept summarizing goals and scope of the thesis.	10
Figure 2.1-1	Schematic of aerosol generator ATM 221 representing the nozzle working principle. Courtesy of Topas GmbH (Germany).....	18
Figure 2.1-2	Schematic of the TGA/DCS 1. Courtesy of Mettler Toledo (CH).....	19
Figure 2.1-3	Rotating disc diluter (RDD) working principle side views. Courtesy of Testo GmbH (Germany).....	20
Figure 2.1-4	Schematic of the liquid quench sampling system, adapted from reference[96]. A, in the case of this dissertation, indicates not a synthetic gas mixture but biogas sampled in in a methane production plant.....	21
Figure 2.2-1	Schematic of the experimental setup combining GC-FID and GC-ICP-MS, each connected to a separate column from the same inlet (split 50:50). Legend: GC = gas chromatographer; FID = flame ionization detector; MFC = mass flow controller; ICP-MS= inductively coupled plasma mass spectrometry.	24
Figure 2.2-2	Integration methods used for the measured ²⁸ Si peak of D5 (siloxane compound).	25
Figure 2.2-3	Coupling strategy for the different instrumental parts in RDD-SMPS-ICPMS setup. Nomenclature: Q _{sample} : flow from the aerosol generator; Q _{dilut} : RDD dilution argon flow, Q _{RDD out} : raw aerosol flow out of the RDD; Q _{poly} : flow of diluted polydisperse aerosol at the DMA inlet; Q _{sheath} : DMA	

	sheath gas flow; Q_{class} : flow of classified aerosol at the DMA outlet; $Q_{\text{DMA exc}}$: DMA gas excess flow; $Q_{\text{CPC class}}$: fraction of Q_{class} guided into the CPC; $Q_{\text{CPC air}}$: additional air flow for the CPC; $Q_{\text{CPC in}}$: total flow entering the CPC; $Q_{\text{ICP in}}$: fraction of Q_{class} guided into the ICPMS; Q_{Xe} : xenon flow; MFC: mass flow controller.....	26
Figure 2.2-4	Schematic of the coupling between an aerosol generator and the RDD-SMPS-ICP-MS setup.	30
Figure 2.2-5	Schematic of the coupling between a TGA and RDD-SMPS-ICP-MS	30
Figure 2.2-6	Schematic of the coupling among AG, tubular furnace and RDD-SMPS- ICP-MS	30
Figure 2.2-7	Schematic of the coupling between the tubular furnace and the RDD-SMPS- ICP-MS	32
Figure 2.4-1	Schematic of the interaction between the electron beam and a sample. Adapted from reference [108]	35
Figure 2.4-2	Picture representing the particle collection cell, the membrane pump used to guarantee a flow-through of 3L min^{-1} , and the male and female connectors with the position of the TEM grid.	36
Figure 2.4-3	Examples of TEM porous grids with 400 mesh Cu grid (a) and carbon foil “Holey” (b) and a “Quantifoil” type (c). Figure adapted from reference[109]. ..	37
Figure 2.4-4	Schematic of the sampling point of size-selected particles with the collection cell. The scheme it is valid for all the different aerosol sources use in the frame of this dissertation.	37
Figure 3.1-1	GC-FID: Retention time of siloxanes (a); RT shift over time and average peak position for D5 (b).....	42
Figure 3.1-2	GC-ICP-MS: Retention time of Siloxanes (a); RT shift over time and average peak position for D5(b).	42
Figure 3.1-3	^{124}Xe intensity and ^{28}Si backgrounds measured before each analysis, over 2 months. CI= confidence interval.....	43
Figure 3.1-4	GC-ICP-MS calibration curve for D5, ORS gas flows optimization (GC inlet connected with one column only). ORS gas composition and flows: He 2.4 ml min^{-1} (a); He 1.4 ml min^{-1} and H_2 1.0 ml min^{-1} (b).....	44
Figure 3.1-5	GC-FID calibration curves for D5 (one column only connected to GC inlet)..	45
Figure 3.1-6	D5 calibration curves using GC-FID. (a) Method 2: peak area calculated as in GC software (n=68); (b) Method 1: peak area calculated as in ICP-MS software (n= 9).	46

Figure 3.1-7	Assignment of the peaks to siloxane compounds in GC-ICP-MS based on ^{28}Si mass intensity (a) and GC-FID signal (b) for the sample <i>Manure1</i> . The grey lines show in both plots the profile and retention time of a multi-siloxane standard with a concentration of nearly 2 ppm _(l)	47
Figure 3.1-8	<i>Manure1</i> and <i>Manure2</i> samples analyzed in GC-FID and normalized by the gas-to-liquid ratio.....	49
Figure 3.1-9	<i>MixUntreated</i> and <i>MixTreated</i> samples (before and after the activated carbon filter) analyzed in GC-FID.	50
Figure 4.2-1	SMPS-ICP-MS data of the measurement of the NaCl solution. a) ICP-MS corrected signal of ^{23}Na . b) Volume related particle size distribution (PSD _v). c) The corresponding number related particle size distribution (PSD _n). The SMPS concentrations and ICP-MS intensities are plotted as functions of mobility diameter (dp) and time.	53
Figure 4.2-2	SMPS-ICPMS data of the ZnO suspension. A) Number-based PSD (PSD _n), recorded by SMPS. B) The corresponding volume-based PSD (PSD _v) and corrected ^{66}Zn signal, detected by ICPMS. The three signals are an average over 4 SMPS scans.....	54
Figure 4.2-3	(a) Volume related particle size distribution of ZnO suspension, (b) ICP-MS mass intensity of ^{66}Zn , in presence of O_2 (50 mL min ⁻¹)	55
Figure 4.2-4	(a) 3d surface of number-related PSD of ZnO suspension, (b) 3d surface of number-related PSD of dispersant solution (Polyacrylic acid 0.1wt%).....	55
Figure 4.2-5	(a) ICP-MS Corrected and raw intensity of ^{66}Zn in reducing atmosphere of a size-classified particle with the use of SMPS, and (b) not size-classified particles (without the use of SMPS), respectively.....	56
Figure 4.2-6	Volume related particle size distribution of ZnO suspension measured with the modified SMPS (Mod_SMPS) in-house build (a) and measured with a commercial SMPS (Ref_SMPS) from TSI company (b), in presence of H_2 (50 mL min ⁻¹).	56
Figure 4.2-7	SMPS-ICPMS data from measuring CuCl_2 evaporation by using the TGA. (a) 2D plot of PSD _n (b) 2D plot of PSD _v . (c) 2D plot of ^{63}Cu ICP-MS signal. (d) 2D plot of ^{35}Cl ICPMS signal. (e) Non-corrected raw ^{35}Cl ICPMS signal vs. time. (f) ICPMS signal of ^{65}Cu and ^{35}Cl recorded during thermal treatment of CuCl_2 by using TG-RDD-ICPMS setup (without SMPS). In both experiments (with and without SMPS) blank signals at 25°C are measured for about 18 min (6 SMPS scans), before starting and maintaining the heating period (for 15 min) at 450°C. The recording of SMPS-ICP-MS signals was started at the same time as that of the TGA signals and was stopped 1 scan after switching it off (resulting in a total of 12 SMPS scans).....	58

Figure 4.2-8	ZnO powder thermal treatment, in presence of H ₂ (50 ml min ⁻¹). (a) Volume-related PSD of ZnO powder, (b) corrected ICP-MS mass intensity of ⁶⁶ Zn, (c) Number-related PSD, (d) number related ICP-MS intensity of ⁶⁶ Zn.....	59
Figure 4.2-9	SEM micrograph of ZnO powder (a), after thermal treatment in presence of H ₂ (50 ml min ⁻¹); EDXS spectra of the prismatic hexagonal (b) and flower like type (c) morphology. TEM micrograph on size-selected particles collected at the outlet of the DMA(d), after thermal treatment in presence of H ₂ (50 ml min ⁻¹); corresponding indexation of electron diffraction pattern (e) and EDX spectrum (f).....	60
Figure 5.1-1	Setup scheme. TGA (thermogravimetric analyzer): aerosol source; RDD (rotating disc diluter): dilution and sampling system; SMPS (scanning mobility particle sizer): size-selection; ICP-MS (inductively coupled plasma mass spectrometry): elemental composition.	62
Figure 5.1-2	Evaporation studies on ZnCl ₂ powder at constant heating rate (5°C min ⁻¹) between 25-600 °C.....	64
Figure 5.1-3	Thermochemical calculation on ZnCl ₂ evaporation with HSC software. The grey area highlighted represents the range of temperatures investigated. ..	64
Figure 5.1-4	Thermochemical calculation on ZnO and CaCl ₂ system with HSC software. The grey area highlighted represents the range of temperatures investigated. ..	65
Figure 5.1-5	Thermochemical calculation on PbO, CdO, CuO and ZnO reactions with CaCl ₂ with HSC software. The molar ratio resembles exactly the ones used in our experimental procedure.	66
Figure 5.1-6	Data evaluation and calibration strategy TGA-ICP-MS	67
Figure 5.2-1	Calibration of the TG-ICP-MS for Zn; the dark lines on the grey triangle represent the RSD% for each point (RSD < 4%).	68
Figure 5.2-2	Volume-related particle size distribution and ⁶⁶ Zn ICP-MS Intensity contour plots; examples below of a single scan in between 18 and 21 min of acquisition time.....	69
Figure 5.2-3	TEM analysis showing spherical morphology; EDX analysis confirmed the elemental composition of ZnCl ₂ particles.	70
Figure 5.2-4	ZnCl ₂ mass related PSD, ZnCl ₂ ICP-MS concentration and SMPS-ICP-MS data relative difference (%).	70
Figure 5.2-5	(A): SMPS particle size volume distribution of the overall amount of particles generated; (B): ICP-MS intensities of ²⁰⁶ Pb, ⁶³ Cu, ¹¹¹ Cd, ⁶⁶ Zn (same scale of intensities for all of them).	72
Figure 5.2-6	Total weight loss over time during experiment with PbO, CdO, CuO, ZnO and CaCl ₂ (H ₂ O) ₂ powders. The time scale reported in this plot is not corresponding to the one shown in Fig. 5.2-5, the measurement with SMPS and ICP-MS was started once stabilization of the sample weight was reached (indicated in the plot with an orange line).	73

Figure 5.2-7	Zn (A) and Cd (B) concentration obtained by extrapolation from TGA-ICP-MS calibration.....	73
Figure 6.1-1	Flow concept of the thermal treatment and the SMPS-ICPMS setup. The red arrows show the main path of the measurement, while orange arrows show the parallel measurement with a reference SMPS. The different gases provided to the system are instead indicated as light-blue arrows. Legend: MFC = mass flow controller, RDD = rotating disc diluter, ASET =evaporation tube, SMPS = scanning mobility particle sizer, DMA =differential mobility analyzer, CPC =condensation particle counter, ICP-MS= inductively coupled plasma mass spectrometry.....	77
Figure 6.1-2	Temperature program applied to the sample introduced inside the tubular furnace (a); gray line: temperature T_{in} measured with a thermocouple inside the tubular furnace, close to the sample; green line: temperature T_{out} measured in the outer part of the tubular furnace, outside the alumina shield. Temperature profile of a standard incineration procedure in a larger incinerator (b).....	78
Figure 6.2-1	Number related PSD of sawdust during thermal treatment (a) and ICP-MS mass intensity of ^{13}C (b).	79
Figure 6.2-2	2D plot of the volume-related PSD of combusted sawdust and injected ZnO particles (a) and the size-related ICP-MS intensity of ^{66}Zn (b). Raw ICP-MS intensity for ^{66}Zn and ^{124}Xe (c) showing increasing intensity from the black line; size-related ICP-MS intensity of ^{66}Zn (d) corrected proportionally to the ^{124}Xe signal.	80
Figure 6.2-3	TEM micrograph on ZnO commercial nanopowder dispersed in ethanol (a); TEM micrograph on injected ZnO particles, which were collected after thermal treatment at about 340°C during the sawdust combustion (b) and after size selection through the DMA.....	81
Figure 6.2-4	Volume-related PSD of ZnO-impregnated sawdust (a) and ICP-MS mass intensity of ^{66}Zn (b), in presence of O_2 (50 mL min^{-1}). Temperature profile (brown line) with a constant heating rate (5°C min^{-1}) between 200 and 500°C	82
Figure 6.2-5	SEM micrograph of ZnO powder (a), after thermal treatment in presence of H_2 (50 ml min^{-1}); TEM micrograph of size-selected particles collected at the outlet of the DMA(b), after thermal treatment in presence of H_2 (50 ml min^{-1}).	82
Figure 6.2-6	Volume related particle size distribution of ZnO-impregnated sawdust (a) and ICP-MS mass intensity of ^{66}Zn (b), in presence of O_2 (50 mL min^{-1}). Temperature profile (brown line) lasting only 24 min: drying step, fast	

	pyrolysis from 300 to 900°C, combustion at 900°C, and afterburning from 900 to 400°C. Measurements started simultaneously with the furnace's temperature program, but the RDD channel opened only for combustion and afterburning steps, 6 min after the start.	83
Figure 6.2-7	TEM micrograph (a), indexation of electron diffraction pattern (b), and EDX spectrum (c) on size-selected particles collected after the DMA.	84
Figure 6.2-8	TEM micrographs of agglomerated particles (a) and (c); indexation of electron diffraction patterns corresponding to selected area in orange (b) (d)...	84
Figure 6.2-9	(a) ICP-MS measured intensities for ^{66}Zn , (b) calculated concentration of (b) Zn, (c) volume distribution of the total amount of particles generated, (d) volume distribution of ZnO only. The right colour scale ($\text{nm}^3\text{cm}^{-3}$) is valid for both plots (c) and (d).	87
Fig. A.2.1-1	SEM micrograph of ZnO nanopowder, showing nearly spherical morphology (a) and XRD pattern of ZnO commercial powder (b).	111
Fig. A.2.1-2	TEM micrograph of ZnO powder, showing nearly spherical morphology (a) and indexation of electron diffraction pattern of ZnO commercial powder (b)..	111
Figure A.3.1	Temperature program TGA during experiment with ZnCl_2 powder.....	113
Figure A.3.2	Thermochemical calculation on CdCl_2 evaporation with HSC software.....	113
Figure A.3.3	Temperature program TGA during experiment with CdCl_2 experiments.....	114
Figure A.3.4	Temperature program TGA during experiment with PbO, CdO, CuO, ZnO and $\text{CaCl}_2(\text{H}_2\text{O})_2$ powders....	114
Figure A.3.5	CdCl_2 second order calibration curve, used for the determination of Cd concentration in the experiments with PbO, CdO, CuO, ZnO and $\text{CaCl}_2(\text{H}_2\text{O})_2$. The RSD% associated with each point is $\leq 5\%$	115
Figure A.3.6	Volume-related size distribution and ^{66}Zn ICP-MS Intensity contour plots of a repetitive analysis with the same operating conditions like the sample in Fig.4. The results show that the PSDs follow the same trend with an RSD for small particles (<20 nm) and bigger particles (>50 nm) of about 10%.....	115
Figure A.3.7	TEM micrographs and EDX analysis on size-selected particles generated during experiment with PbO, CdO, CuO, ZnO and $\text{CaCl}_2(\text{H}_2\text{O})_2$ powders.....	115
Fig. A4.4-1	Thermochemical calculations with HSC software, initial concentrations: ZnO (1 kmol), H_2 (10 kmol).....	118
Fig. A4.4-2	Thermochemical calculations with HSC software, initial concentration considering real ratio existing between C and Zn in the impregnated wood: ZnO (1 kmol), CO and H_2 in excess (175 kmol).....	118

List of tables

Table 2-2	Typical settings of the main ICP-MS settings used for the RDD-SMPS-ICP-MS measurement of aerosol.....	28
Table 3-1	Operating conditions for GC7890A, ALS 7693 A, FID detector, GC-ICP-MS interface, and 7700x ICP-MS.....	41
Table 3-2	Retention time at peak apex for the compound identification with GC- FID and GC-ICP-MS.....	42
Table 3-3	Comparison between ^{28}Si sensitivities, LOD and LOQ calculated for D5 in GC-ICP-MS, using two different gas composition in ORS.....	43
Table 3-4	^{28}Si sensitivities, LOD, LOQ, R^2 and BEC (blank equivalent concentration) in GC-ICP-MS for siloxanes compounds analyzed, using two columns connected to the same inlet.....	45
Table 3-5	RF (response factor), LOD, LOQ, R^2 (linear fit) in GC-FID for D5 (one column only connected from the inlet to the FID detector).....	46
Table 3-6	Siloxanes quantitative results in analyzed biogas samples; (*): each of them was sampled twice and two replicates for each sample were analyzed.....	48
Table 3-7	Siloxanes quantitative results in analyzed biogas samples with GC-FID. (a) : calculated as in MassHunter (n= 9); (b): calculated as in OPENLAB (n=68); (§): Si concentration refers to D5 only; (*): each of them was sampled twice and two replicates for each sample were analyzed.....	48
Table 5-1	Operating conditions of the ICP-MS (Agilent 7700x).....	65
Table A.1.1-1	Stock solution 1: Si and single compound concentrations.....	109
Table A.1.1-2	Stock solution 2: Si and single compound concentrations.....	109
Table A.1.1-3	Standards solutions: Si concentrations.....	109
Table A.1.2	7700x ICP-MS (Agilent Technologies) additional operating conditions.....	110
Table A1.3	Stock solutions and calibration standards: Si and D5 concentrations.....	110
Table A.1.4	^{28}Si sensitivities, LoD, LoQ, R^2 and BEC in GC-ICP-MS for siloxanes compounds analyzed, using one column connected to the GC inlet.....	110
Table A.2.1-1	Zinc oxide powder specifications, provided by the manufacturer (AUER-REMY).....	111

Table A.2.2-1	ICP-MS analysis on ZnO suspension. LOD: limit of detection; LOQ: limit of quantification (of the method) including the dilution (for these samples the dilution was about $2.0 \cdot 10^4$ mL/g).....	112
Table A.2.2-2	Malvern Zeta sizer nano series characterization on ZnO suspension; Material RI:2.00, Dispersant RI: 1.330, material absorption: 0.010... ..	112
Table A.2.2-3	Brookhaven BI-XDC characterization on ZnO suspension.....	112
Table A.4.1-1	ICP-MS elemental analysis on beech wood saw dust.....	116
Table A.4.1-2	ICP-MS elemental analysis on beech wood saw dust.....	116
Table A.4.2	ICP-MS elemental analysis on beech wood sawdust impregnated with ZnO suspension. LOD: limit of detection; LOQ: limit of quantification (of the method) including the dilution (for these samples the dilution was about $6 \cdot 10^5$ ml/g).....	117
Table A.4.3	The efficiency of impregnation calculated on expected value (assuming 100% efficiency) and real concentration measured with ICP-MS.....	117

List of publications

First author journal articles

- Debora Foppiano, Mohamed Tarik, Jörg Schneebeil, Adelaide Calbry- Muzyka, Serge Biollaz and Christian Ludwig, Siloxane compounds in biogas from manure and agricultural waste: method development and speciation analysis with GC-ICP-MS and GC-FID., **2018**, in peer-review.
- Debora Foppiano, Mohamed Tarik, Elisabeth Müller Gubler, and Christian Ludwig, Combustion generated nanomaterials: online characterization via an ICP-MS-based technique. Part I: calibration strategy with a TGA, *J. Anal. At. Spectrom.*, **2018**, 33, 1493-1499.
- Debora Foppiano, Mohamed Tarik, Elisabeth Müller Gubler, and Christian Ludwig, Combustion generated nanomaterials: online characterization via an ICP-MS-based technique. Part II: resolving power for heterogenous matrices, *J. Anal. At. Spectrom.*, **2018**, 33, 1500-1505.
- Debora Foppiano, Mohamed Tarik, Elisabeth Müller Gubler, and Christian Ludwig, Emissions of Secondary Formed Nano-Objects from the Combustion of Impregnated Wood. An Online Size-Resolved Elemental Investigation, *Environ. Sci. Technol.*, **2018**, 52, 895-903

Co-author journal articles

- Adrian Hess, Mohamed Tarik, Debora Foppiano, Philip Edinger, and Christian Ludwig. Online Size and Element Analysis of Aerosol Particles Released from Thermal Treatment of Wood Samples Impregnated with Different Salts. *Energy and Fuels*, **2016**, 30, 4072–4084.
- Mohamed Tarik, Debora Foppiano, Adrian Hess, and Christian Ludwig. A Practical Guide on Coupling a Scanning Mobility Sizer and Inductively Coupled Plasma Mass Spectrometer (SMPS-ICPMS). *J. Vis. Exp. (JoVE)*, **2017**, 125, e55487, doi:10.3791/55487.
- Patrick Steiger, Renaud Delmell, Debora Foppiano, Lorenz Holzer, Andre Heel, Maarten Nachtegaal, Oliver Kröcher and Davide Ferri. Stable Ni particles through structural reversibility in La-Fe-Ni perovskite type metal oxide catalysts. *ChemSusChem*, **2017**, 10 (11), 2505-2517.

Debora Foppiano

Curriculum vitae



debora.foppiano@psi.ch
foppiano.debora@gmail.com



Zürcherstrasse 43, 5400 Baden (CH)



orcid.org/0000-0003-3263-3569
SCOPUS Author ID: 7189444826



<https://www.linkedin.com/in/debora-foppiano-a2ab13176/>



EDUCATION

Ph.D in Civil and Environmental Engineering
EPFL (École polytechnique fédérale de Lausanne)- CH
Paul Scherrer Institute (5232 Villigen PSI, Switzerland)



March 2015 - ongoing

- Dissertation: Hyphenated Analytical Techniques for Studying the Speciation and Fate of Contaminants and Nanoparticles in Waste Treatment and Bioenergy Processes

Thesis director: Prof. Christian Ludvig, Co-director: Dr. Mohamed Tarik

M.Sc. in Chemical Sciences

Università degli Studi di Genova –IT-
110/110 cum laude



Oct. 2010 – Dec. 2012

- Thesis: Determination of Arsenic, Cadmium, Cobalt, Chromium, Nickel, and Lead in Cosmetic Face-Powders

Advisors: Dr. Carmela Ianni (UniGe); Dr. Marco Grotti (UniGe); Dr. Cristina Capelli (A.R.P.A.L.)

B.Sc. in Chemistry and Chemical Technologies

Università degli Studi di Genova –IT-
105/110



Oct. 2007 – Nov. 2010

- Thesis: Ionic and gas chromatography analysis on natural and drinking waters

Tutor: Dr. Enrico Raffo (IREN); Advisor: Dr. Nadia Parodi (UniGe)

WORK EXPERIENCE

Research Assistant (Part'Aera – Environment and climate change project)

A.R.P.A.L (Regional Environment Protection Agency),
Via Zunini 1- 17100 Savona (IT)



May 2014 – January 2015

- Determination of trace metals in waters, soils, waste waters, atmospheric particulate matter (PM 10 and PM 2,5)
- ICP-MS with DRC, ICP-OES, ET-AAS, HG-AAS
- Sample preparation with microwave digestion and solid phase extraction (SPE)

Analytical Chemist

A.R.P.A.L (Regional Environment Protection Agency),
Via Zunini 1- 17100 Savona (IT)



March 2013 – March 2014

- Determination of trace metals in waters, soils, waste waters, atmospheric particulate matter (PM 10) organotin compounds (TBT, DBT, TPhT, MBT) in sea waters
- ICP-MS with DRC, ICP-OES, ET-AAS, HG-AAS

INTERNSHIPS

A.R.P.A.L (Regional Environment Protection Agency)

Via Bombrini 8 – 16149 Genova (IT)



November 2011 – August 2012 (M.Sc. Thesis project)

IREN Group (Organic micro pollutants laboratory)

Via Piacenza 54 – 16138 Genova (IT)



May 2010 – August 2010 (250 hours)

Languages

English: proficient user

Italian: mother tongue

Spanish: independent user

French: basic user

German: basic user



License

Qualified Chemist



June 2013 - Università degli Studi di Genova –IT-

Competences

Technical. Expertize in the following analytical techniques: ICP-MS, ICP-OES, ET-AAS, HG-AAS, GC, HPLC, SMPS, TGA.

Managerial. Capacity of autonomously planning projects and delivery times; marked propensity to work cooperatively in project teams

IT. Microsoft Office™ tools (Excel, Word; Power Point), COREL Draw (technical drawings), data treatment (Origin, Excel), bibliography manager software (Mendeley Desktop) and instruments workstations.

Science. Scientific reading and writing, literature search.

PUBLICATIONS

- Foppiano, D.; Tarik, M.; Müller Gubler, E.; Ludwig, C. *Environ. Sci. Technol.* **2018**, 52 (2), 895–903.
- Foppiano, D.; Tarik, M.; Gubler Müller, E.; Ludwig, C. *J. Anal. At. Spectrom.* **2018**, 33 (9), 1500–1505.
- Foppiano, D.; Tarik, M.; Gubler Müller, E.; Ludwig, C. *J. Anal. At. Spectrom.* **2018**, 33 (9), 1493–1499
- Steiger, P., Delmelle, R., Foppiano, D., Holzer, L., Heel, A., Nachtegaal, M., Ferri, D. *ChemSusChem*, **2017**, 10 (11), 2505–2517.
- Tarik, M.; Foppiano, D.; Hess, A.; Ludwig, C. *J. Vis. Exp.*, **2017**, No. June, 1–9.
- Hess, A., Tarik, M., Foppiano, D., Edinger, P. and Ludwig, C. *Energy and Fuels*, **2016**, 30, 4072–4084.
- Capelli, C., Foppiano, D., Venturelli, G., Carlini, E., Magi, E., Ianni, C. *Analytical Letters*, **2014**, 47(7), 1201–1209,
- Lasagna, C., Raffo, E., Foppiano, D. *Journal of Biological Research*, **2011**, 84 (1)

Courses

- Project management: basic element for project controlling (PSI Akademie, 8 lessons) 📅 2018
- Design of experiments (EPFL) 📅 2017
- Academic writing for doctoral students (Centre de langues EPFL) 📅 2017
- Combining Structural & Analytical Investigations of Matter at the Micro-, Nano and Atomic Scale- (CCMX-EPFL) 📅 2016
- Aerosol I: Physical and chemical principles (ETHZ) 📅 2016
- Powder Characterization and Dispersion (CCMX -EPFL) 📅 2015

PARTICIPATION IN EVENTS

- D. Foppiano, M. Tarik, E. Müller, C. Ludwig. *Oral presentation* at **2018** Winter Conference on Plasma Spectrochemistry, January 2018, Amelia Island, Florida (USA)
- Participation as *Volunteer* in supporting scientific sessions during WRF **2017** (World Resource Forum), Geneva, (CH)
- D. Foppiano, M. Tarik, E. Müller, A. Hess, C. Ludwig. *Poster* at EAC **2017** (European Aerosol Conference), Zürich (CH).
- D. Foppiano, M. Tarik, C. Ludwig. *Poster* at EAC **2016** (European Aerosol Conference), Tours (FR).
- D. Foppiano, M. Tarik, E. Müller, A. Hess, C. Ludwig. *Poster* at 20th ETH Conference on Combustion Generated Nanoparticles **2016**, Zürich (CH).
- A. Hess, M. Tarik, D. Foppiano, C. Ludwig. *Poster* at CCMX Annual Meeting **2015**, Bern.
- D. Foppiano, C. Tiberiade, *oral communication* at Perkin Elmer Knowledge program **2014**, Genova (IT).

Honors and Awards

- **Travel award**, Scholarship for the attendance of 2018 Winter Conference on Plasma Spectrochemistry, January 2018, Amelia Island, Florida (USA)
- A. Hess, M. Tarik, D. Foppiano, C. Ludwig. *Poster* at CCMX Annual Meeting **2015**, Bern. This poster got one of 3 equivalent *best poster awards of the CCMX Annual Meeting*.

Affiliations (Scientific)

- Consiglio Nazionale dei Chimici (CNC)
(Italian Chemical Society)
📅 May 2014

